ENGINEERING EVALUATION OF POST-LIQUEFACTION RESIDUAL STRENGTH

(VOLUME 1: MAIN TEXT)

by

Joseph P. Weber, Raymond B. Seed, Robb E. S. Moss, Juan M. Pestana,
Chukwuebuka Nweke, Tonguc T. Deger and Khaled Chowdhury

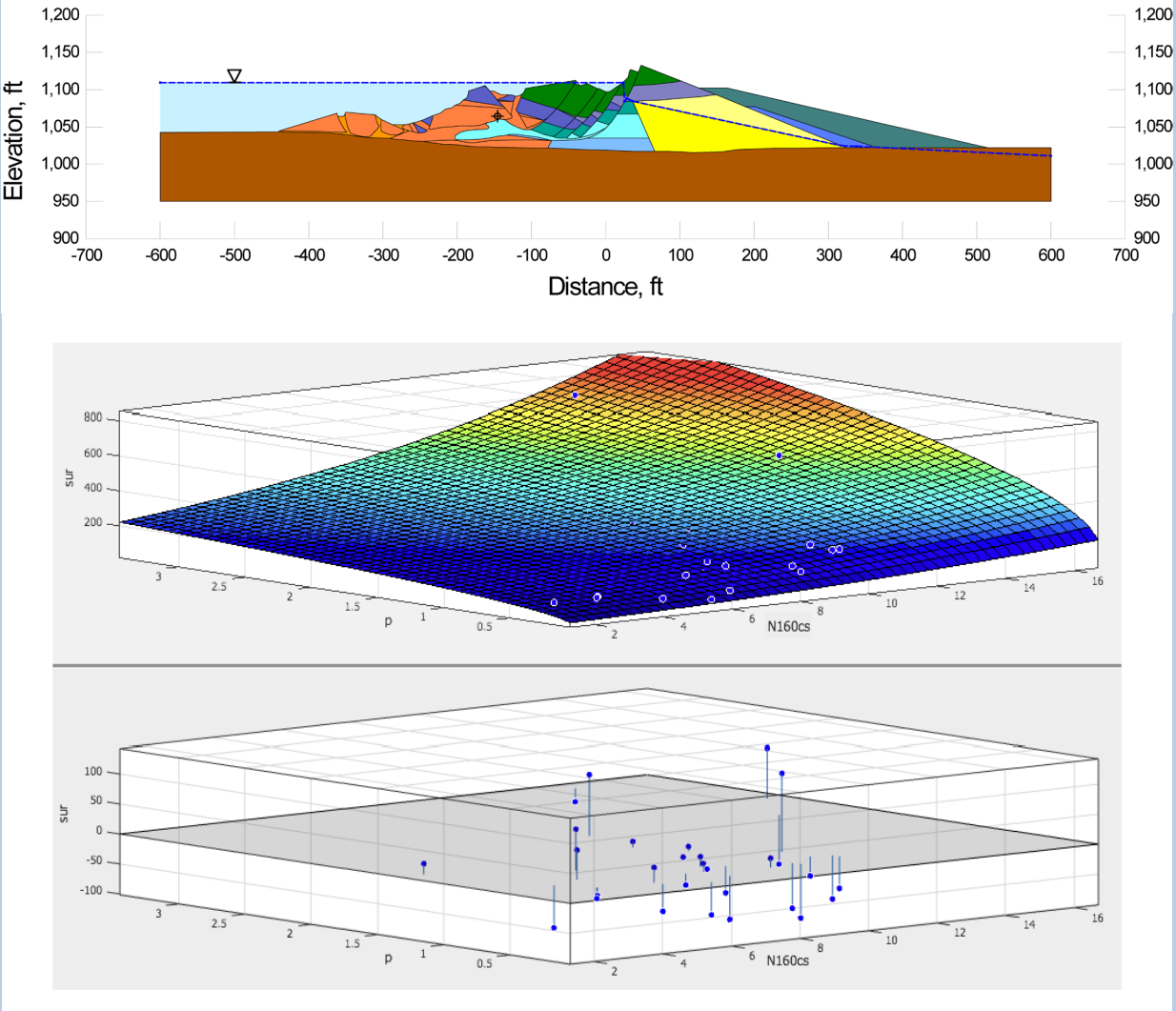

Geotechnical Research Report No. UCB/GT/22-01
Department of Civil and Environmental Engineering
University of California at Berkeley

August 2022

ENGINEERING EVALUATION OF POST-LIQUEFACTION RESIDUAL STRENGTH

(VOLUME 1: MAIN TEXT)

by

Joseph P. Weber, Raymond B. Seed, Robb E. S. Moss, Juan M. Pestana,
Chukwuebuka Nweke, Tonguc T. Deger and Khaled Chowdhury

Geotechnical Research Report No. UCB/GT/22-01

Department of Civil and Environmental Engineering
University of California
Berkeley, California

August 2022

ACKNOWLEDGEMENTS

This research was supported by the U.S. Nuclear Regulatory Commission (NRC) under Grant No. NRC-04-10-128, and this support is gratefully acknowledged. A number of technical experts provided valuable advice and consultation during the course of these studies, and these were Dr. Les Harder (HDR, Inc.), Dr. David Gillette (U.S. Bureau of Reclamation), Dr. Peter Robertson (Gregg Drilling and Testing, Inc.), Prof. Les Youd (Brigham Young University) and Prof. Kyle Rollins (Brigham Young University). Their valuable assistance and advice is gratefully acknowledged.

FORWARD

This research report incorporates a number of revisions and/or changes from the earlier report of Weber et al. (2015). These changes largely reflect the performance of additional Bayesian regressions to further improve the overall predictive relationship for evaluation of post-liquefaction residual strength (S_r) as a function of (1) initial effective overburden stress ($\sigma'_{v,i}$) and (2) normalized and corrected Standard Penetration Test (SPT) resistance ($N_{1,60,CS}$). The predictive relationship in this updated research report is an improved relationship, but the changes from the previous relationship are relatively modest. The updated relationship predicts slightly higher values of S_r across the full ranges of $\sigma'_{v,i}$ and $N_{1,60,CS}$, and as a result projects engineered using the original relationship will not need to be re-evaluated.

Updating the updated new predictive relationship either involved, or resulted in, changes to a number of figures and tables. These include Equations 5-2 and 5-6 through 5-8; Figures 4.6 through 4.11, 5.1 through 5.9, 5.11 through 5.15, 5.17, 5.19, 5.21, and 5.23; and Tables 4.2 through 4.5, 4.7, 4.8, 5.1, and 5.2. Although the overall changes are relatively modest, the updated relationship presented here represents the new recommended predictive relationship for engineering practice.

DISCLAIMER

The contents of this report reflect the views of the authors, who are responsible for the accuracy of the information and data presented. The contents do not reflect the official position or policy of the U.S. Nuclear Regulatory Commission.

ABSTRACT

Over the past three decades, engineers working in the area of soil liquefaction engineering have been called upon to develop increasingly well-refined evaluations of expected performance of structures and of critical infrastructure in the event of potential soil liquefaction. A critical element in such evaluations is the engineering assessment of post-liquefaction residual strengths (S_r) of soils; including both natural soils and fills. Prior to the past three decades, it was common practice to ascribe assumed negligible strengths and stiffnesses to liquefied soils for engineering analyses. Today, increasingly higher-order analyses are performed involving either simplified seismic deformation or seismic displacement analysis methods, or fully nonlinear analyses implemented in a finite element or finite difference framework, or using other advanced analytical approaches. In all of these analyses, the evaluation and modeling of post-liquefaction strengths is typically a critical issue.

This has led to a surge of interest, and to a significant amount of research involving laboratory, centrifuge, and analytical studies. The focus for engineering analysis and design efforts for actual projects is often on the use of empirical relationships for engineering evaluation of in situ post-liquefaction strengths. This is due, in large part, to complications and challenges inherent in the use of laboratory-scale physical testing for development of estimates of post-liquefaction strengths at full field scale. These challenges are generally well understood, but some of them (e.g. localized void redistribution under globally "undrained" shearing) continue to confound fully reliable assessment by means of laboratory-scale testing for most projects. As a result, empirical relationships, established based on back-analyses of full-scale field liquefaction failure case histories, are increasingly the common approach for most projects. These current efforts have been focused on this approach.

These current studies began with a technical review of previous efforts. That proved to be a valuable exercise. Evaluation of previous work, and recommendations, with emphasis on strengths and drawbacks of prior efforts, led to some important insights. It turns out that a number of previous efforts had developed important lessons, and in some cases important pieces of the overall puzzle. They also served to provide ideas and to inspire elements of these current studies, and they provided lessons with regard to mistakes to avoid.

A suite of full-scale liquefaction field case histories were then reviewed, vetted and selected for back-analyses. New methods were developed for performing these back-analyses, including methods that more accurately and reliably deal with momentum effects in liquefaction failures that experience large displacements. A suite of additional empirical relationships were developed specifically for cross-comparison of the results of back-analyses of large deformation liquefaction failures. In the end, a suite of geo-forensic back-analysis results of unprecedented reliability were developed, based on (1) improved back-analysis procedures, (2) internal cross-checking within the framework of the empirical relationships developed, and (3) external cross-checking against the results obtained by previous investigations, with an informed and improved understanding of the strengths and drawbacks of the back-analysis methods and assumptions employed in those previous studies.

The resulting back-analysis case history database and results were then used, in the context of probabilistic regressions that incorporated the best obtainable evaluations of uncertainties, to perform probabilistic regressions by the maximum likelihood method in order to develop new predictive relationships for engineering evaluation of post-liquefaction strength as a function of both (1) corrected SPT penetration resistance, and (2) initial in situ effective vertical stress.

These new relationships were then compared with previous relationships and recommendations. Here, again, with understanding of the strengths and drawbacks of the procedures by which the previous relationships were developed, and of the details of the back-analyses that often provided the parameters for the earlier efforts, a coherent overall pattern emerged and the relative juxtaposition of values of post-liquefaction strengths provided by different predictive relationships can now be better understood.

The new predictive relationships developed in these current studies agree surprisingly well at relatively low initial (pre-earthquake) effective stresses with the recommendations of Kramer and Wang (2015) who executed a similar overall effort, but with significant differences in approaches, and judgments, at essentially every step of the way. This level of agreement occurs when adjustments are made for apparent errors or biases in development of a number of their field case history back-analyses and resulting predictive model input parameters, and so the work to develop better understandings of strengths and weaknesses of various case history back-analysis approaches was particularly important here. And the level of agreement between these current studies and those of Kramer and Wang falls away at higher values of initial in situ effective vertical effective stress, and at higher ranges of corrected SPT penetration resistance ($N_{1,60,CS}$) values. This divergence at higher initial (pre-earthquake) in situ vertical effective stresses was investigated as part of these current studies, and is now better understood.

Similarly, the results and recommendations from these current studies can also be shown to provide fairly good agreement with earlier recommendations of (1) Seed and Harder (1990), (2) Olson and Stark (2002) and (3) Idriss and Boulanger (2008), but again only over specific ranges of (1) initial in situ effective vertical stress, and (2) corrected SPT penetration resistance for each of the different previous sets of predictive relationships. In other ranges, these previous relationships can now be shown to be either conservative, or unconservative, and the reasons for this can now be understood.

The new predictive relationships for engineering evaluation of post-liquefaction strength are presented in a fully probabilistic form, and can be used for probabilistic risk studies and for analysis, design, or engineering mitigation of high-level projects. They can also be readily recast in a simplified deterministic relationship likely to be more widely applicable to more routine projects.

These new relationships offer potentially significant advantages over previously available recommendations and relationships. They are based on back-analyses, and regressions, which provide insight into the underlying forms of the relationships between post-liquefaction strengths and both (1) penetration resistance and (2) initial effective vertical stress, over the ranges of conditions well-represented in the 30 full-scale field liquefaction case histories back-analyzed. Because they provide insight as to the underlying forms of these relationships, they provide a better

basis for extrapolation to higher ranges of penetration resistance, and to higher ranges of effective stress, than do previous recommendations. The back-analyzed field case history database provides fair to good coverage for values of $N_{1,60,CS}$ up to approximately 14 blows/ft, and for representative effective overburden stresses of up to approximately 4 atmospheres. The range of principal engineering interest is often up to $N_{1,60,CS} \approx$ 10 to 22 blows/ft or higher, however, as it is over that range that field behavior, and project performance, often transitions from unacceptable to acceptable. Similarly, for major projects (e.g. earth and rockfill dams, deep foundations, etc.), ranges of effective overburden stress considerably larger than 4 atmospheres are often of critical importance. The forms of the predictive relationships developed are designed to facilitate extrapolation to higher stresses and higher values of $N_{1,60,CS}$ to provide a means of dealing with these challenges as well.

In addition to the development of improved relationships for engineering evaluation of post-liquefaction strengths, the suite of new empirical relationships developed for use in cross-checking of back-analyses of liquefaction failure case histories will likely also have applications with regard to checking of (1) forward engineering analyses of expected performance for analyses of actual engineering projects for evaluation of existing risk exposure, and (2) for engineering analysis and design to mitigate those risks, including both simplified analyses and higher-level analyses involving fully nonlinear finite element or finite difference analyses, etc. for more critical and/or high risk projects.

TABLE OF CONTENTS

Chapter One

Introduction and Overview

1.1 Introduction

Soil liquefaction came prominently to the attention of the geotechnical engineering profession in the mid-1960's, largely due to the widespread and severe liquefaction-induced damages wrought by the 1964 Great Alaskan Earthquake (M_W = 9.2) and by the 1964 Niigata Earthquake (M_W = 7.7). The phenomenon of soil liquefaction was, of course, already known but prior to these two events there were no well-established engineering methods for dealing with seismically induced soil liquefaction and its consequences.

In the wake of these two events, the first engineering investigation and analysis methods were developed for evaluation of the risk of triggering, or initiation, of soil liquefaction due to seismic loading (e.g.: Kawasumi, 1968; Seed and Idriss, 1971; etc.). Methods for evaluation of seismic soil liquefaction potential, or likelihood of triggering, under both static and cyclic loading have continued to evolve, and today there are a wide variety of well-established methods that range from simplified empirical methods based on in situ testing through laboratory-based methods and also increasingly advanced, fully nonlinear constitutive analysis models and methods implemented in either finite element or finite difference computer analysis frameworks.

The liquefaction-induced failure of the upstream side of the earthen embankment of the Lower San Fernando Dam during the 1971 San Fernando Earthquake (M_W = 6.6) nearly resulted in uncontrolled release of the Van Norman Reservoir, which would have had catastrophic consequences for the large urban population immediately downstream. This embankment failure was followed a year later (1972) by the non-seismically induced liquefaction failure of the Buffalo Creek mine tailings dam in West Virginia. The Buffalo Creek Dam failure resulted in uncontrolled release of the reservoir impoundment, and devastated the community immediately downstream. One hundred and twenty five lives were lost. These two events led to a surge of interest in liquefaction-related risks associated with dams, and helped to lead to the eventual creation of the U.S. National Dam Safety Program in 1986. This program has contributed considerably to the further development of improved methods for engineering treatment of soil liquefaction issues.

Additional impetus for advancement of liquefaction-related engineering analysis methods, and for corollary liquefaction risk mitigation measures, has come from interest and research associated with other critical infrastructure and facilities, and more recently the focus has continued to broaden to include more routine projects and structures.

Both in the U.S. and abroad, much of the focus of the rapidly evolving field of soil liquefaction engineering practice in the 1970's and 1980's was initially on dams and other critical facilities and infrastructure. Over the five decades that have now passed since the mid-1960's, attention has progressively extended to also consider and deal with liquefaction risk for an increasingly broad range of facilities and structures, including ports and harbors, transportation

facilities (bridges, roads, embankments, tunnels, airports, etc.), in-ground lifelines (power, gas water, telecommunications, etc,.), critical structures (power plants, industrial facilities, waste impoundments, etc.), more routine structures (e.g. homes and businesses), and more.

As the breadth of applications has increased, so has the development of increasingly accurate and reliable methods for evaluation not only of the risk of triggering or initiation of soil liquefaction, but also for evaluation of the expected resulting performance or consequences for a given site or facility. Increasingly, engineers are being called upon to assess the expected consequences of potential liquefaction in terms of deformations, displacements, and damages to the structures or systems of concern.

Over the first 10 to 15 years after the two 1964 earthquakes in Alaska and Niigata, most liquefaction-related engineering was focused primarily on evaluation of the risk, or likelihood, of "triggering" or initiation of liquefaction. If liquefaction was considered likely to be triggered, either statically or cyclically, then negligible post-liquefaction strengths and stiffnesses were commonly assigned to the materials judged likely to liquefy for the next (subsequent) steps involved in evaluation of expected consequences.

That was a very conservative approach, and it was clear early on that post-liquefaction strengths were not necessarily equal to zero; certainly not in all cases. The evolving understanding of the mechanics of soil liquefaction, and of critical state soil mechanics (e.g. Casagrande, 1940; Schofield and Wroth, 1968; etc.), and progressively advancing laboratory testing capabilities and also analytical capabilities, led to the continuing development of improved analytical tools for dealing not just with triggering of soil liquefaction, but also with the engineering assessment of resulting deformations and displacements of both the ground and the structures and systems affected.

This, in turn, has led to a need for better assessments of post-liquefaction strengths so that more accurate (and less over-conservative) engineering assessments of expected performance and consequences can be made.

It is here that these current studies are focused.

1.2 Overview of These Current Studies

Chapter 2 presents a brief history of the development of approaches for evaluation of post-liquefaction soil strengths, and a review of important methods, including an assessment of the advantages and drawbacks of the main approaches available for engineering evaluation of in situ post-liquefaction strengths. In most research investigations, this type of review is presented as a bit of a formality. For this current study, however, this close review and re-evaluation of previous efforts was a key element in the development of the findings eventually produced here. Armed with the advantage of hindsight, it turns out that multiple previous investigation efforts, and researchers, had developed important insights and/or elements of work that end up contributing to the overall solutions and findings of these current studies. In some interesting cases, the previous

investigators did not (at the time) recognize the eventual importance of some of those pieces of the puzzle.

Chapter 2 discusses methods for evaluation of post-liquefaction strengths based on laboratory testing, as well as methods for assessment of post-liquefaction strengths using empirical relationships developed based on back-analyses of full-scale field failures. The main emphasis in Chapter 2 is on empirical methods, because a number of difficulties can arise with regard to the direct use of laboratory-based methods for project-specific applications, as is also discussed in this chapter. The development of improved empirical methods is the principal focus of these current studies. Advantages and disadvantages, as well as strengths and weaknesses, in previous approaches are examined. A number of errors by previous investigators and/or studies are also examined and explained. Some of these issues will be addressed again in Chapters 5 and 6, as the results of these current studies are compared against the results of previous efforts.

Chapter 3 presents an explanation of the review and selection of liquefaction field performance case histories for back-analyses in these current studies. A significant number of previous investigators have now worked on this problem, and a large number of potential case histories have been collected and analyzed by various investigators. The quality of case histories available spans a considerable range, both with regard to the quality of data available for each case, and also the caliber of the documentation available regarding those data. In addition, some of the cases represent situations in which the nature of the field performance observed permits reasonably well-defined or well-constrained back-analyses for evaluation of post-liquefaction strengths. In other cases, the nature of the failure mechanism involved simply does not permit such an accurate assessment of post-liquefaction strengths. Selection of cases to be considered, and of cases to be back-analyzed and included in the development of the resulting probabilistic and deterministic relationships for evaluation of post-liquefaction strength, is thus an important issue.

Chapter 4 then presents an explanation of the back-analyses of field failure case histories performed for these current studies. The chapter begins with an overview of significant back-analysis approaches taken in these current studies, as well as approaches taken in previous studies, with an assessment of strengths and drawbacks of each. This is important because the eventual predictive relationships developed will be cross-compared with previously existing relationships in Chapter 5, and it is thus important to understand the relative advantages and drawbacks of some of the back-analysis approaches taken in previous studies.

Chapter 4 then goes on to present and describe the development of a number of new back-analysis methods, and new empirical tools, and their application to the back-analyses of the case histories selected in Chapter 3. Many previous studies have not fully documented, or provided sufficient details, of back-analyses performed for purposes of assessing post-liquefaction strengths, and that has made it difficult to check and verify the general validity and reliability of the resulting recommended approaches for assessment of in situ post-liquefaction strengths for application to engineering analysis and design of real projects. One of the objectives of this current investigation is to break this trend, and to suitably document both the methods employed, and also the details of the analyses as these methods are applied to each individual case history. Methods and assumptions, cross-sections, modeling details and parameters, etc. involved in performing these back-analyses are presented and discussed. Detailed summaries of the back-analyses

performed for each of the individual cases selected and analyzed are presented in Appendices A and B.

Chapter 4 also presents a series of cross-checks of the values and parameters back-calculated from the liquefaction failure case histories. A series of empirical relationships developed in these current studies are used to check the internal consistency of the results of the 30 case histories back-analyzed in these current studies, based on a number of criteria. These cases are then further cross-checked against the values back-calculated by previous investigators, with an understanding of the likely errors, limitations, and systematic biases involved in some of those previous analyses and previous studies.

Chapter 5 then presents and describes the use of the results of the back-analyses performed in Chapter 4 to develop recommended probabilistic and deterministic relationships for engineering evaluation of post-liquefaction strengths. The initial emphasis is on development of fully probabilistic empirical relationships for assessment of in situ post-liquefaction strengths based on engineering evaluations of (1) in situ SPT penetration resistance and (2) initial (pre-liquefaction) in situ vertical effective stresses. These methods are expected to be employed mainly for important projects that warrant a probabilistic or risk-based approach. The probabilistic methods are then used to develop recommended deterministic methods, with likely applications to more routine engineering analysis and design.

Comparisons are then made between the probabilistic and deterministic tools and methods developed in these current studies, and a suite of other empirical approaches and relationships previously developed by other investigators. In the end, a coherent picture emerges and it now appears that the efforts of a number of previous investigations can be fit together, much like assembling a puzzle, and that a relatively coherent overall understanding of methods suitable for engineering evaluation of post-liquefaction strengths is achieved.

Chapter 6 presents an overall summary of the findings and recommendations from these studies.

Chapter Two

Previous Studies

2.1 Introduction

This chapter presents a review of existing methods for engineering evaluation of post-liquefaction strengths. This includes an overview of the historical progression of such methods, and an assessment of the strengths and shortcomings of each of these methods, and of the investigations performed to develop them.

2.1.1 Key Principles and Definitions

The term "soil liquefaction" has had many meanings ascribed to it by a large number of engineers and researchers. In these current studies, soil liquefaction will be taken as being: a significant reduction in strength and stiffness of a soil, primarily as a result of reduction in effective normal stresses due to pore pressure increase. This does not mean that pore pressure increase is the only cause of reduction in effective stress, or of reduction in strength and stiffness.

The term "flow failure" has also had multiple meanings. In these current studies, flow failure will refer to very large ground deformations and displacements that occur primarily because the static (gravity induced, non-seismic) "driving" shear stresses exceed the available shear strengths during some significant portion of the period over which displacements occur.

"Statically-induced liquefaction" will be taken as soil liquefaction that occurs in the absence of cyclic loading, either as a result of (1) monotonic increase in driving shear stresses, (2) decrease in effective stress due to non-cyclically induced increases in pore pressure, or (3) contractive behavior of the liquefying soil in the face of imposed deformations from moving boundary conditions (see the Fort Peck Dam failure).

"Seismically-induced liquefaction" will be taken as liquefaction triggered in some part by cyclic stresses, which may occur in combination with gravity-induced static driving shear stresses already in place. Seismically-induced liquefaction will generally include liquefaction resulting from seismic loading, and also vibrations from explosions, vibro-densification, passing trains, etc. In these current studies it will also include vibrations from large vibro-seis trucks used to generate controlled vibrations for deep geophysical studies (see the Lake Ackerman embankment failure).

"Post-liquefaction strength" has a very broad range of meanings and definitions to various engineers and researchers. In these current studies, the definition of this term will be a matter of context. When referring to post-liquefaction strength as deliberatively determined by others, their definition will generally be employed. When referring to post-liquefaction strength assessed in these current studies, the symbol used will be S_r and it will refer to the post-liquefaction shear strength that can be mobilized at non-insignificant strains to resist deformations and displacements.

Two additional terms warrant definition here as well. The first of these is "post-liquefaction initial yield stress" ($S_{r,yield}$). This is not an actual "strength", but rather the value of shear stress calculated to be needed within liquefied soils to provide an overall (theoretical) static Factor of Safety equal to 1.0 for conditions after (assumed) triggering of liquefaction and before significant resulting displacements begin to occur. This would, of course, over-estimate the actual value of available post-liquefaction strength (S_r) for cases in which significant displacements then do occur. If the value of S_r had actually been equal to $S_{r,yield}$, then large displacements would not have resulted.

An additional term is "post-liquefaction residual strength based on residual geometry" ($S_{r,resid/geom}$), which is also not an actual "strength". Instead, it is the value of S_r back-calculated to provide a static Factor of Safety equal to 1.0 based on post-failure residual geometry. This is an over-conservative basis for estimation of actual post-liquefaction strength, as it neglects momentum effects as the moving slide mass has to be decelerated back to a stable and stationary residual condition. $S_{r,resid/geom}$ will therefore significantly underestimate the actual value of S_r during failure for most cases.

2.2 Laboratory Based Methods

2.2.1 Poulos, Castro, and France (1985)

Poulos et al. (1985) proposed a laboratory based method for engineering assessment of in situ post-liquefaction strengths. This method was generally based upon principles of critical state soil mechanics (Casagrande, 1940; Schofield and Wroth, 1968; etc.), and it involved very carefully performed field sampling efforts as well as high quality laboratory testing.

The basic underlying principal of critical state soil mechanics is illustrated schematically in Figure 2.1. This principle asserts that soils, when sheared, will seek to either dilate or contract depending on whether their current "state" (their current combination of void ratio and effective confining stress) is located above or below a locus of points known as the Critical State Line (CSL) in void ratio (e) vs. effective confining stress (σ_3') space. Soils above the CSL are "loose" and will exhibit contractive behavior when sheared, and soils below the CSL are "dense" and will exhibit dilatant behavior when sheared. Soils will dilate or contract until they reach a new state on the CSL, at which point further changes in void ratio and effective confining stress will cease to occur, and the soil will continue to shear at constant void ratio, constant effective confining stress, and constant shear strength. Soils that have reached the CSL, and that exhibit constant shear strength, void ratio, and effective stress are defined as having reached "critical state". Under drained shearing conditions, soils will change volume (and thus void ratio), moving vertically upwards or downwards in Figure 2.1, in order to proceed towards the CSL. Under undrained shearing conditions, soils instead exhibit either increases in pore pressure (contractive behavior) or decreases in pore pressure (dilatant behavior), resulting in equal and opposite changes in effective confining stress, and thus approach the CSL laterally as shown in Figure 2.1. Eventually all soils, if sheared sufficiently, will theoretically reach a (critical state) condition of constant shearing resistance at some point located on the CSL. The location and shape of the CSL is, of course, different for each individual soil.

Castro and Poulos (1977) and Poulos (1981) define a "steady state" wherein a soil sheared to large enough strains reaches a state of constant shearing resistance, constant effective stress, constant volume and constant strain rate. The main difference between this steady state and the previously defined critical state is the addition of the condition of constant strain rate, and it should be noted that the strain rate part of this definition is often ignored. Accordingly, the steady state and the critical state line are often analogous.

Figure 2.2 then illustrates the laboratory-based steady state method proposed by Poulos et al. (1985) for evaluation of post-liquefaction shear strengths of in situ soils based on sampling and laboratory testing. This illustrative figure shows the application of this approach to a high quality (nearly undisturbed) sample of silty sand hydraulic fill from the downstream shell of the Lower San Fernando Dam.

The first step is to obtain fully disturbed bulk samples of the in situ soils. Samples are then reconstituted in the laboratory, at different void ratios, and these are subjected to isotropically consolidated undrained (IC-U) triaxial compression tests to determine a steady state line (or critical state line) for these reconstituted samples. The resulting steady state line for the Lower San Fernando Dam hydraulic fill is shown by the solid line in Figure 2.2. Critical state lines, and steady state lines, are commonly plotted as void ratio vs. the logarithm of effective confining stress, and in this semi-log space steady state lines are generally approximately log-linear (or nearly so) over the range of principal engineering interest for liquefiable soils, and then they inflect downwards at higher effective stresses. The steady state line developed for these reconstituted samples is not taken directly as a basis for evaluation of in situ steady state strengths. Instead it is then used to "correct" the results of additional IC-U triaxial tests performed on a limited number of higher quality (more nearly undisturbed) samples. This "correction" addresses effects of sampling disturbance, and additional disturbance (and volume changes) that occur during sample transport, extrusion, mounting and reconsolidation prior to undrained shearing in the laboratory.

Higher quality samples are then also obtained, either by advancing sharp-edged and relatively thin-walled samplers, or by excavating a large diameter shaft and then lowering an engineer or technician into the base of the shaft to carefully hand carve a sample while slowly advancing a cylindrical sampling tube (mounted on a tripod) about the sample as it is carved. Advancing sharp-edged samplers is the more common method, and these must be pushed (not driven with hammers) to avoid vibratory densification of the soils being sampled. In either case, as samplers are advanced, the precise depth of penetration or sampler advance is closely measured. Sample recovery is carefully logged. Knowing the length of sampler advance, the radius of the cutting edge, the radius of the inside of the sampler tube, and the length of recovered sample within the tube, a calculation is then made to estimate volume (and thus void ratio) changes during sampling. When the sample is then returned to the laboratory, length is again measured, and any further volume (and void ratio) changes are calculated. When the sample is extruded and trimmed to length, and a confining membrane and top and base caps are applied, the new initial "mounted" sample height and diameter are measured and any further volume (and void ratio) changes are again recorded. Finally, additional volume (and void ratio) changes during reconsolidation are also measured. In this manner, the void ratio of the final, consolidated sample as actually subjected to undrained shearing is "known", and so is the original in situ void ratio prior to sampling.

The undrained shearing portion of the IC-U triaxial test is then performed to measure the undrained steady state strength ($S_{u,s}$) at the sample's final, laboratory consolidated void ratio. This is plotted in the lower right-hand corner of Figure 2.2 (the large, solid "square"), and it is plotted at the laboratory void ratio as tested. This laboratory value of $S_{u,s}$ is then "corrected" back to the initial in situ void ratio by assuming a correction path parallel to the steady state line developed based on testing of reconstituted samples, as shown in Figure 2.2, producing the solid "dot" in the upper left-hand corner of the figure. This assumed parallelism of the correction with the slope of the steady state line previously developed for reconstituted samples represents a major assumption, and there is no good explanation as to (1) why the steady state line for the reconstituted samples is not the same as the steady state line for the higher quality samples, and (2) why the reconstituted and more nearly undisturbed steady state lines would be exactly parallel, justifying this assumption. Corrections in terms of $S_{u,s}$ tend to be very large, and any small change in the slope of the line followed in making this correction can significantly affect the final results.

The upstream slope of the Lower San Fernando Dam failed due to liquefaction that occurred during the 1971 San Fernando Earthquake, and this has been a much-studied case history. A multi-agency effort was formed in the mid-1980's to re-study this case history as one part of a two-part effort to investigate the viability and reliability of the laboratory-based steady state methodology proposed by Poulos et al. for evaluation of in situ post-liquefaction steady state strengths ($S_{u,s}$). The San Fernando Dam studies were overseen primarily by the U.S. Army Corps of Engineers. The other part of this effort was overseen primarily by the U.S. Bureau of Reclamation (USBR), and involved retaining Poulos et al. (GEI Consultants) to employ the steady state method to assess in situ $S_{u,s}$ for a number of soil zones and soil strata for five USBR dams and some of their foundation soils. This second part of the effort will be discussed further at the end of this current Section 2.1.1.

Four teams performed testing on reconstituted samples of the silty sand hydraulic fill materials from the lower portion of the downstream shell of the Lower San Fernando Dam, and one of the questions to be answered was the reliability with which different laboratories could develop similar steady state lines by this approach. Figure 2.3 shows the "consensus" steady state line developed for these studies. The four laboratories were all selected for good reputations with regard to high level testing, and these were (1) GEI Consultants, (2) the U.S. Army Corps of Engineers Waterways Experiment Station (WES), (3) Rensselaer Polytechnic Institute and State University (RPI), and (4) Stanford University working jointly with U.C. Berkeley. As shown in this figure, this was difficult testing and two of the laboratories did not quite develop data that would have usefully defined in good detail the steady state line that was developed by consensus. But this element of the procedure was judged to be at least feasible (Seed et al., 1989).

A series of IC-U triaxial tests were then performed by both the GEI and Stanford laboratories on higher quality (more nearly undisturbed) samples, and these were then corrected using the steady state procedure (assuming parallelism with the steady state line from Figure 2.3). Figure 2.4 shows the resulting corrected estimates of in situ $S_{u,s}$, and the laboratory $S_{u,s}$ values upon which they are based. This is the interpretation by Seed et al. (1989), and a slightly different interpretation was developed by Castro et al. (1989), with one of the main differences being the amount of earthquake-induced void ratio change estimated to have occurred due to cyclic pore pressure generation and then subsequent reconsolidation after the 1971 San Fernando earthquake.

Figure 2.4 illustrates several of the challenges involved in this method. The first is the very large correction from laboratory $S_{u,s}$ to the estimated field (in situ) $S_{u,s}$. Correction factors range from approximately 2.5 to more than 20, with 4 out of the 11 samples having corrections factors of greater that one full log-cycle (factors of 10 or greater). These are very large correction factors to be applying to shear strengths, especially given the unconfirmed assumption of parallelism between the steady state lines of (a) reconstituted samples, and (b) the higher quality (more nearly undisturbed) samples tested for Figure 2.4. A second problem is the wide scatter in the resulting corrected values of estimated in situ $S_{u,s}$ (the large dots in Figure 2.4), which range over more than a full log-cycle.

Back-calculated strengths for the upstream liquefaction-induced slope failure that actually occurred in the Lower San Fernando Dam due to the earthquake fall within the range of "corrected" values of in situ $S_{u,s}$ shown in Figure 2.4, but this is a large range.

A further evaluation of the potential usefulness and reliability of the steady state methodology was provided by the second part of these studies. Figure 2.5 shows the values of estimated in situ $S_{u,s}$ developed based on the steady state laboratory testing method for 35 soil layers and strata at five U.S. Bureau of Reclamation dams (Von Thun, 1986). These values of $S_{u,s}$ are plotted on the vertical axis, and the horizontal axis is the representative $N_{1,60}$ value ascribed to each of those sandy and silty soil units as a result of SPT investigations. Also shown in this figure is a shaded range proposed by Seed (1987) of $S_{u,s}$ values based on back-analyses of a number of full-scale field liquefaction failure case histories. As shown in Figure 2.5, a strong majority of the estimates of in situ $S_{u,s}$ developed by GEI using this procedure are higher than would be suggested by the empirical range suggested by Seed (1987) based on back-analyses of actual full scale field failure case histories.

Further laboratory investigations, and scale model tests, quickly followed and these would shed further light on some of the key issues affecting not only the original steady state methodology as proposed by Poulos et al. (1985), and also on the use of laboratory testing in broader and more general terms for evaluation of in situ post-liquefaction strength $S_{u,s}$ (or S_r).

2.2.2 Additional Laboratory Investigations and Approaches

The steady state methodology proposed by Poulos et al. (1985) led to significant further laboratory investigations, and some of these helped to clarify the likely causes of the apparently variable and often unconservative $S_{u,s}$ values developed based on the original steady state methodology. They also led to improved understanding of a number of mechanisms and factors affecting post-liquefaction strengths.

A number of investigators (e.g.: Vaid et al., 1990;, Riemer and Seed, 1992,1997; Yoshimini et al., 1999) found that stress path (or method of shearing) affected measured $S_{u,s}$, or S_r, with undrained triaxial compression (TXC) tests developing significantly higher $S_{u,s}$ values than either undrained direct simple shear (DSS) tests or undrained triaxial extension (TXE) tests. Triaxial compression is often a largely suitable mode of shearing for representing conditions at the back heel of a landslide, or the back heel of a bearing capacity failure surface. Triaxial extension

generally better represents conditions at the toes of these types of failure surfaces. And conditions across the base, or belly, of a failure surface are generally better represented by DSS. The use of TXC-based $S_{u,s}$ values (as had been employed in the method of Poulos et al., 1985) can significantly overestimate strengths and introduce systematic unconservatism. This could, at least theoretically, be fixed, and the TXC tests of the original steady state procedure can be replaced with more representative tests providing a DSS-type of shearing, as is now often done.

Castro (1969) performed monotonic IC-U TXC tests on soils formed to a range of densities and found three different types of resulting behavior based on initial density or relative density. Yoshimine and Ishihara (1998) further investigated this, and formalized a set of useful principles and nomenclature. Figure 2.6 (from Kramer, 2008) provides a simplified illustration of these findings. Sands and low plasticity silts with very low relative densities tend to follow "contractive" type undrained stress paths (and exhibit stress-strain behaviors) that lead to very low undrained residual strengths ($S_{u,s}$) at large strains. Dense soils, at the other extreme, follow "dilatant" type stress paths (and exhibit stress strain behaviors) that lead to high undrained strengths ($S_{u,s}$) at large strains. Soils of "intermediate" relative density can initially exhibit "contractive" type undrained stress paths and stress strain behaviors that consist of initial post-peak strength reduction (strain softening), but then they can experience a phase transformation to dilatant-type behavior and resulting strength increase at larger strains to a final (very large strain) undrained strength higher than the "low point" reached along the way.

The condition at which a locally minimum value of strength is observed at moderate strains (marked with a small "x" in Figure 2.6) in samples of intermediate density is increasingly referred to a "quasi-steady state" (after Alarcon-Guzman et al., 1988), and the values subsequently reached at very large strains can be referred to as ultimate steady state. Yoshimine and Ishihara (1998) investigated this, based on more extensive laboratory test data for a number of clean sands, and proposed four ranges of behavior based on initial relative densities from very low to high. Their resulting recommendations fit well within the behaviors shown in the simplified illustration of Figure 2.6. As shown in Figure 2.6, quasi-steady state strength can be lower than ultimate steady state strength for soils of intermediate relative density. Multiple additional investigators have now produced similar results (e.g. Yamamuro and Convert, 2001, etc.), and these behaviors are now well established. There is no full consensus as to whether ultimate steady state strength, or quasi-steady state strength, is the better engineering basis for post-liquefaction strength and modeling/analyses. Ishihara (1993) recommends in favor of quasi-steady state strength, and the authors here generally concur.

Another factor investigated by a number of researchers is the effect of the initial level of effective confining stress on post-liquefaction strengths observed. This issue is clouded to some extent by the question as to whether ultimate steady state strength or quasi-steady state strength should be taken as the basis. Based on the quasi-steady state basis, Riemer and Seed (1997) found that samples formed and consolidated to exactly the same post-consolidation void ratios, but at different initial effective confining stresses, and then subjected to undrained triaxial compression shearing produced higher $S_{u,s}$ values if the initial effective confining stresses were higher. This increase in $S_{u,s}$ is not linear with increase in initial confining stress, however, and the ratio of eventual steady state strength vs. initial vertical effective confining stress ($S_{u,s}$ /P) decreases with increasing initial effective confining stress.

Numerous additional laboratory investigations, and scale model experiments (both on shaking tables and on centrifuges), have now been performed and these continue to usefully illuminate many of the basic mechanics and fundamental mechanisms involved in the transition to post-liquefaction residual strengths from initial liquefaction-induced shear failures initiated either by monotonic or cyclic loading conditions.

This has not yet, however, resulted in the development of universally accepted laboratory-based approaches for evaluation of post-liquefaction strengths for in situ soils. There are three sets of additional challenges or issues that arise which continue to complicate this issue, and render the use of laboratory test data potentially unconservative with regard to determination of in situ post-liquefaction strengths for full-scale field applications. These are the phenomena of (1) "void redistribution", and the sometimes related issues of (2) "partial drainage", and (3) potential inter-layer particle mixing effects.

2.2.3 Void Redistribution and Partial Drainage

Void redistribution is the movement of both solid particles and also pore fluids within a soil zone of constant overall volume ("globally undrained") so that localized void ratio (and relative density) changes occur in some portions of the overall volume of saturated material. This can produce localized changes in void ratio under monotonic and/or cyclic loading conditions thought to represent "globally" undrained shearing.

A good early discussion of this was presented by the National Research Council (1985), and Figure 2.7 shows a simplified illustration of this phenomenon from that report. In this figure, a layer of more pervious cohesionless soil is confined between less pervious overlying and underlying layers. As a result, this pervious stratum will initially behave in an "undrained" manner, with constant overall volume maintained, if loaded rapidly (e.g. by cyclic loading from an earthquake). Although this stratum is "globally" undrained, internally it will experience some rearrangements of both solids and pore fluids as cyclically generated pore pressures cause fluids to seek to escape towards the ground surface, increasing the void ratio near the top of the layer, while solids settle and void ratio decreases in the lower portions of the layer. This results in development of a looser top region up against the interface with the overlying less pervious stratum, and a slightly denser overall condition deeper within the liquefying stratum.

Minor changes in void ratio can produce significant changes in post-liquefaction steady state strength (e.g.: Figures 2.2 through 2.6). The result can therefore be a significant reduction in strength at the top of the confined stratum as void ratio redistribution occurs. In extreme cases, a "blister" of water, or a water film, can develop at the top of a confined stratum, providing a potential shearing zone of essentially negligible post-liquefaction strength.

These phenomena have been observed and demonstrated in numerous laboratory model tests on both centrifuges and on shaking tables (e.g. Liu and Qiao, 1984; Arulanandan et al., 1993; Fiegel and Kutter, 1994; Kokusho, 1999; etc.). The basic mechanics are generally well understood, and the observed effects in some of these model tests have been shown to be very significant. Failure surfaces have the opportunity to seek out the path of least resistance, and when void

redistribution results in a zone or sub-layer of weaker conditions the failure surface will attempt to exploit this zone of weakness.

This is very challenging with regard to the use of laboratory testing, and classical critical state theory (and steady state theory), to predict post-liquefaction behavior in the field. Post-liquefaction behavior will be controlled by the void ratio after void redistribution has occurred, not by the pre-event void ratio in situ. The mechanics of this void redistribution process are understood, and analytical modeling can be performed (e.g. Malvick et al., 2006), but it is not yet possible to reliably predict the actual amounts and rates of void redistribution likely to occur in the field, and it is not yet feasible to reliably predict by analytical methods the resulting effects on post-liquefaction strengths at field scales.

It is difficult to accurately pre-determine for most field situations the localized scale at which void redistribution will occur. This phenomenon occurs primarily within layered soils where some layers are less pervious and thus impede flow to dissipate excess pore pressures. Most liquefaction failures occur within alluvial sediments, hydraulic fills, poorly compacted fills placed in layers, or loess. All of these deposits are commonly layered (or sub-stratified) in a manner that lends itself to potentially adverse void redistribution effects. And these soils often have layering, and sub-layering, at variable scales in a given stratum or deposit. Figure 2.8 shows a photograph of the side of one of the two investigation trenches excavated through the hydraulic fill near the base of the Lower San Fernando Dam after the dam experienced a liquefaction-induced slope failure in 1971. As shown in this photograph, the material is strongly striated (layered) with lighter colored sub-layers of sandier material and darker sub-layers of siltier soil with higher fines content. Closer inspection of any of the lighter sub-strata would reveal even smaller scale sub-layering within these sub-strata, with coarser and finer (lighter and darker) sublayers occurring within the apparent lighter colored larger strata that are not visible at the scale of this photograph.

As explained by Seed (1987), the problem is not that laboratory testing, or critical state (and steady state) theory, do not serve to explain and characterize soil behavior. The problem is that void redistribution occurs in a manner that cannot yet be reliably well predicted, and that it produces changed conditions (that still conform to critical state and steady state theory); and it is these changed conditions that can control the overall behavior in the field. The inability to pre-determine the scale at which these void ratio distribution effects will occur, and the inability to predict the rate and severity with which these effects will occur, continues (so far) to routinely defeat laboratory-based efforts to reliably deal with them for field design and performance assessments.

Void redistribution effects are naturally included in field performance case histories. These likely vary with the relative contrast in permeabilities between layers and strata, and with the scales and geometry at which this redistribution occurs, so no one individual case history can be expected to provide conclusive data regarding likely post-liquefaction strengths that can be mobilized for other sites. Accordingly, it is important to analyze observed full-scale field performance, and to back-analyze field failure case histories, for multiple field cases in order to inform efforts to evaluate likely post-liquefaction strengths for engineering analysis and design.

A second phenomenon that can be closely related is partial drainage. When pore pressure increases occur, either due to cyclic loading or due to contractive behavior under undrained monotonic loading, the resulting pore pressures begin to dissipate by means of flow away from the area of elevated pore pressure. Intuitively, this dissipation of pore pressures would seem to be a positive thing as it serves to re-establish higher effective stresses and thus higher shear strengths. But as the fluids travel, they can be temporarily impeded at less pervious boundaries, and this can result in a localized build-up in pore pressure, resulting in a second type of void redistribution that can occur over a larger time scale than the more localized type of void redistribution illustrated in Figure 2.7. Partial dissipation of pore pressures, or ongoing dissipation in progress, can thus also potentially serve to locally exacerbate void redistribution effects.

2.2.4 Inter-Layer Particle Mixing

An additional, and related, phenomenon that cannot yet be suitably dealt with either (1) analytically, or (2) by means of direct laboratory testing, is inter-layer particle mixing. When shearing occurs along the interface between two different materials, then the chaotic interactions (rubbing, grinding, etc.) can cause finer particles from one soil to insert themselves between coarser particles of the other soil. This can allow the finer particles and the coarser soil to locally achieve a more efficient "packing" of particles, and it can create a material that occupies less volume than either of the two parent soils per unit weight of solids. In a "globally undrained" shearing situation, this is essentially another form of void (or particle) redistribution, and it can also lead to further reductions in shear strengths along interfaces or boundaries.

Failure mechanisms will tend to seek out and exploit these weaknesses if they are geometrically able to do so. This is thus another mechanism, also favoring failures at and near interface boundaries, that cannot yet be reliably handled either analytically or by means of direct laboratory based testing because it is not generally possible to determine a priori (1) how much mixing may occur, and (2) the extent to which such mixing might degrade "undrained" post-liquefaction strengths.

2.3 Empirical and Semi-Empirical Methods

Because of the currently intractable challenges posed by (1) void redistribution, (2) partial drainage, and (3) inter-layer mixing, it has been necessary to examine full-scale field failures to garner further insight as to likely post-liquefaction strengths that can be mobilized for different sets conditions. This leads to empirical methods for estimation or evaluation of post-liquefaction strength (S_r) based on full-scale field case histories. These case histories, and empirical relationships for evaluation of S_r based upon them, naturally include the effects of all three of these issues or challenges (void redistribution, partial drainage, and interlayer mixing), albeit to varying degrees in any specific case history.

2.3.1 Seed (1987) and Seed and Harder (1990)

The late Prof. H. Bolton Seed developed a suite several successive (evolving) proposed correlations between S_r values back-calculated from liquefaction failure case histories and SPT penetration resistance during the mid-1980's, and these culminated in the relationship proposed in Seed (1987). This relationship is presented in Figure 2.9.

This 1987 paper presented an excellent overview of many of the challenges in evaluating post-liquefaction strength S_r, and it also presented this proposed empirical relationship which Prof. Seed describes as a "tentative" relationship. Immediately after the paper had been published, it was pointed out that one of the twelve case histories back-analyzed had been plotted with S_r values based on pre-failure geometry, which would have provided an unconservative assessment of the likely actual S_r value. Based on an assumption that momentum effects were relatively minor, the Lower San Fernando Dam case is plotted too high in Figure 2.9; with $S_r \approx 750$ lbs/ft^2 and $N_{1,60,CS} = 15$ blows/ft. Prof. Seed subsequently determined this to be an error, but was too ill with the cancer that would shortly take his life to repair it. So his son, and a recent former doctoral student, jointly undertook to posthumously correct this error. The resulting modified relationship was published by Seed and Harder (1990), and it was published in an unusual venue; appearing in the Proceedings of the late Prof. Seed's Memorial Symposium rather than in the ASCE geotechnical journal. Both Seed and Harder had previously been involved in earlier stages of development of some of the case histories involved. They re-evaluated the 12 cases originally presented in Seed (1987), and they added five additional cases to bring the total number of cases to seventeen.

Figure 2.10 shows the resulting revised correlation between post-liquefaction strength S_r and corrected $N_{1,60,CS}$ values of Seed and Harder (1990), with a reduced value of S_r for the Lower San Fernando Dam failure case history, and with additional case histories added.

Back-analysis methods were not yet well-established at this time, so a variety of approaches and assumptions were applied to various cases within this limited suite of available case histories. Many of the "smaller" cases involving embankments and slopes of modest height, and with low values of $N_{1,60,CS}$, were analyzed with relatively approximate methods. The Upper San Fernando Dam case history was a "non-failure" case history, and assessment of the likely value of S_r for this case was based on the value having been higher than that for which a major flow-type failure would have occurred, with some additional judgment as to likely cyclic inertial effects.

Three of the largest failures were the Calaveras Dam, the Lower San Fernando Dam and the Fort Peck Dam case histories, and Seed and Harder approximately incorporated "inertial" effects (momentum effects) in the back-analyses of these three cases by selecting S_r values between the values that would have been calculated as $S_{r,yield}$ for pre-failure geometry, and $S_{r,resid/geom}$ for post-failure residual geometry. The "apparent" pre-failure yield stress ($S_{r,yield}$) which is defined as the theoretical strength along liquefied portions of the eventual slide surfaces that would be required to provide a calculated static Factor of Safety equal to 1.0 for pre-failure geometry, and (2) the "apparent" residual stress based on final residual geometry ($S_{r,resid/geom}$) defined as the strength along liquefied portions of the failure surface that would be required to provide a post-

failure calculated static Factor of Safety equal to 1.0 for the final, residual post-failure geometry. The actual post-liquefaction strength (S_r) would be less that $S_{r,yield}$; otherwise the post-liquefaction failure mass would be statically stable and would experience only small displacements due to cyclic lurching. Similarly, $S_{r,resid/geom}$ would over-estimate the actual post-liquefaction strength (S_r); as the moving failure mass would accumulate momentum, and would have to be decelerated and brought back to rest at its final resting position. Neglect of the shear strength needed to decelerate the moving failure mass (to overcome momentum effects) would cause $S_{r,resid/geom}$ to underestimate the actual value of S_r (see Sections 4.3.2 and 4.4.1, and Chapters 5 and 6). Davis et al. (1988) were also performing back-analyses during this same period, and their method for more explicitly incorporating inertial effects also produced values between $S_{r,yield}$ and $S_{r,resid/geom}$. Seed and Harder were aware that their estimates would be reasonable approximations of S_r with inertial effects included, and they adopted values of S_r nearer to $S_{r,resid/geom}$ than to $S_{r,yield}$ for cases in which runout distances of the failure mass had been very large.

For several other cases (the La Marquesa Dam and the La Palma Dam case histories), cyclic inertial effects were approximately accounted for by initially adopting values of S_r nearly intermediate between $S_{r,yield}$ and $S_{r,resid/geom}$, and then adding additional strength to approximately account for cyclic inertial effects due to strong shaking for cases in which (1) overall displacements were somewhat limited, and (2) seismic loading intensity was high; conditions in which cyclic inertial effects were considered to be potentially significant.

The S_r values of Seed (1987) and Seed and Harder (1990) were plotted as a function of procedurally corrected, overburden corrected, and fines adjusted $N_{1,60,CS}$ values.

The fines adjustment proposed by Seed (1987) differed slightly from that of contemporary SPT-based liquefaction triggering correlations, and was as follows:

$$(N_1)_{60\text{-}CS} = (N_1)_{60} + \Delta(N_1)_{60} \qquad \text{[Eq. 2-1]}$$

where $\Delta(N_1)_{60}$ was the fines adjustment, which was a function of fines content as

Fines Content (%)	SPT Correction, $\Delta(N1)_{60}$ in blows/ft
0	0
10	1
25	2
50	4
75	5

Seed and Harder (1990) employed the same fines adjustment.

Figure 2.11 repeats the base figure of Figure 2.10, but this time adds the result of a least squares regression performed as part of these current studies. The resulting R-square value of $R^2 = 0.64$ indicates a moderately good overall fit.

Seed and Harder (1990) recommended a "one-third" value for simplified, deterministic analyses; a value approximately one-third of the way "up" between the lower bound and the upper bound lines shown in Figure 2.10.

2.3.2 Idriss (1998)

Idriss (1998) would go on to employ the same suite of 17 failure case histories to develop an additional proposed relationship. He "re-interpreted" the case history database of Seed and Harder (1990), but in fact employed the same S_r values as proposed by Seed and Harder for all 17 cases. He did modify selection of "representative" $(N_1)_{60}$ values to formally employ median values, but the values plotted did not visibly change as Seed and Harder had previously done largely the same. He then presented a single central curve fitting the data, as shown in Figure 2.12, rather than the upper and lower bounds as proposed by Seed and Harder (1990), and extended this curve beyond the upper bound of the available data with a dashed line that presumably indicates extrapolation beyond the range of the available data. This curve fits neatly between the upper and lower bounding curves proposed by Seed and Harder (1990) as presented in Figure 2.10, and is largely parallel to these upper and lower bounding curves but at a location slightly below the mid-point between the bounding curves of Seed and Harder. Seed and Harder (1990) had recommended approximately "one-third" values as a basis for typical engineering analyses, and the curve proposed by Idriss (1998) was very similar to this.

2.3.3 Stark and Mesri (1992)

Stark and Mesri examined the available data, and concluded that post-liquefaction strength S_r was likely linearly dependent upon initial vertical effective stress ($\sigma_{v,i}'$). They took the S_r values back-calculated for 17 cases by Seed and Harder (1990), and added three additional case histories. They calculated average initial effective vertical stress along the eventual failure surface for each case, and developed ratios of S_r/P where P = initial vertical effective stress within liquefiable materials on the failure plane. Their resulting relationship was the first to express post-liquefaction strength in terms of liquefied "strength ratio" (S_r/P). This relationship is shown in Figure 2.13.

This relationship proposed by Stark and Mesri (1992) established a second "school of thought", and set up a contrast between empirical relationships based (1) on classical critical state theory wherein post-liquefaction strength (S_r) would be expected to be constant for any given relative density, as suggested by the form of the Seed and Harder (1990) relationship, and (2) relationships based on assumed constant strength ratio (S_r/P) in a manner somewhat analogous to the framework of SHANSEP for clays.

This led to some debate within the profession, but it was never a serious issue. It was clear early on that the best answer likely lay between these two points of view. In the end, in these current studies, that turns out to be the case.

A series of nonlinear least squares regressions were performed on the data from Stark and Mesri (1992). A second order polynomial curve was fit to the data, but the inflection was a slight

downward curvature with increasing penetration resistance. The resulting R^2 value was $R^2 \approx 0.22$. Because the curvature of the initial regression was slightly downwards, and the associated regressed quadratic coefficient was very close to zero, a linear fit was next investigated. This also resulting in a value of $R^2 \approx 0.22$, as shown in Figure 2.14. Second order polynomial curves with a positive quadratic coefficient (which would produce an upwards inflection) were then also imposed on the data, but resulting R^2 values were very low. A curve that approximately represented the median line recommended by Stark and Mesri was then imposed, and manual calculations showed that this resulted in a value of $R^2 = 0.12$. These results suggest that the data is poorly behaved (randomly scattered) and that the regression is not well able to provide a good predictive "fit", especially when compared to the correlation bounds proposed in Stark and Mesri (1992).

This does not mean, however, that there is no merit to their suggestion of a relationship between S_r and initial effective stress, and the results of these current studies will in fact result in findings that suggest that initial in situ vertical effective stresses do indeed potentially significantly affect S_r (see Chapter 5). It simply suggests that the data as plotted in Figures 2.13 and 2.14 do not support a well-defined relationship between penetration resistance and post-liquefaction strength as plotted.

2.3.4 Ishihara (1993)

Prof. Ishihara developed a multi-step procedure based on extensive laboratory test data for estimation of post-liquefaction strength (S_r) as a function of SPT penetration resistance. The data were developed for a number of Japanese sands, and were of high quality. As discussed previously in Section 2.2.2, Prof. Ishihara preferred to use quasi-steady state strength rather than ultimate steady state strength, and so targeted this approach accordingly. Prof. Ishihara noted a clear dependence of $S_{u,s}$ on initial effective confining stress. He suggested that while there is a clear dependence here, it is a different relationship for different sands. His approach was based on an assumed log-linear relationship between void ratio (e) and logarithm of effective vertical stress (σ_v') for steady state lines, and he characterized the slopes of the quasi-steady state lines in e vs. log σ_v' space based on indices derived from the laboratory data for each of several well-characterized clean sands. SPT $(N_1)_{60}$ values were also inferred for each sand as a function of density (void ratio) and effective overburden stress.

He then compared the resulting relationships between quasi-steady state strength against the values of strength ratio calculated by Stark and Mesri (1992), with an adjustment of $(N_1)_{60}$ values to conform with Japanese standards of practice with regard to SPT equipment and procedures. Figure 2.15 shows the proposed relationships for several test sands, and a comparison with the values of strength ratio calculated by Stark and Mesri. As shown in this figure, the relationships developed appear to provide unreasonably steep curves of strength ratio vs. $(N_1)_{60}$, when compared to the relationships developed based on back-analyses of field case histories by most other investigators, including Seed and Harder (1990), Stark and Mesri (1992), Idriss (1998), Olson and Stark (2002), Kramer (2008) and these current studies.

The reasons for this are not fully clear, but it is noted that this procedure assumes a log-linear relationship for the slope of the quasi-steady state line, which may not be valid at the low densities (high void ratios) of principal interest here, and that the high quality laboratory data sets employed did not include potential full scale "field" effects such as void redistribution, partial drainage, and inter-layer mixing as shearing occurs along interfaces between soil layers. It is also interesting to note, however, that Wride et al. (1999) subsequently developed a proposed relationship between $(N_1)_{60\text{-}CS}$ and S_r based on back-analyses of a selected suite of liquefaction failure case histories, but employing "reasonable lower bound" values of $(N_1)_{60}$ as being "representative" based on the assumption that the weakest strata would control the failures. Their resulting relationship between post-liquefaction strength ratio (S_r/P) and $(N_1)_{60}$ also has a form much like that of Ishihara, with steeply rising values of S_r/P at relatively low $(N_1)_{60}$ values (see Section 2.3.6).

2.3.5 Konrad and Watts (1995)

Konrad and Watts proposed a method for estimation of post-liquefaction strength S_r as a function of SPT penetration resistance that was based on a theoretical framework based on critical state soil mechanics. This framework was then calibrated based on a limited number of back-analyzed failure case histories. As with Ishihara (1993), this methodology assumed a series of log-linear relationships, including a log-linear slope of the steady state line, but an additional calibration factor χ was then developed based on back-analyses of five large displacement liquefaction failure case histories. Figure 2.16 shows the estimated relationship between this calibration factor χ and the slope of the steady state line (λ) based on the five field case histories. Three of the five case histories are represented with two points each in this figure, reflecting the ranges of values employed.

This was a "hybrid" method, involving both an empirically-based calibration factor based on S_r values back-calculated from a limited number of previous field failure case histories, and also laboratory tests for the specific soil of interest for a given project. A four step procedure was employed. Step 1 was site characterization by means of SPT. The fines adjustment of Seed (1987) was employed here. Step 2 was the performance of laboratory tests to ascertain the maximum void ratio (e_{max}) and the slope (λ) of the steady state line. Step 3 was the estimation of χ based on the relationship shown in Figure 2.12. Step 4 was then the estimation of mobilized shear strength (S_r) based on (1) the laboratory determined value of shear strength at e_{max}, (2) the slope (λ) of the laboratory determined steady state line, and (3) the calibration factor χ.

Konrad and Watts reportedly employed this procedure to successfully predict cases of failure and non-failure of artificial sand fills (islands) constructed in the Beaufort Sea for offshore petroleum exploration. This procedure was apparently effective in estimating values of S_r for newly created loose sand fills, but there are a number of important assumptions involved (e.g. a log-linear slope of the steady state line). Additional potential drawbacks of this procedure include the need to accurately determine the slope of the steady state line, the assumption that laboratory-based tests will correctly determine the steady state line for field placement conditions, the assumption that the steady state line is log-linear over the full range of interest, and the neglect of potential void redistribution effects, etc. in the field.

2.3.6 Wride, McRoberts and Robertson (1999)

Wride et al. (1999) performed a thoughtful review of 20 liquefaction failure case histories that were available and being back-analyzed and used at that time for development of one or more empirical relationships between penetration resistance and either post-liquefaction strength or post-liquefaction strength ratio. This was a paper that warranted more attention than it received.

Wride et al. studied all 20 cases, and eliminated the Lake Merced bank case from their data set. The remaining 19 cases were then examined in a number of ways and were characterized as to mode of failure, method of initiation of failure, and failure mass runout characteristics (various measures of eventual displacement or runout distances, some of them normalized vs. slope height). A number of useful insights were developed as a result of this exercise. Having learned some important lessons from this, indices regarding failure and displacement modes, and runout characteristics, are also developed and employed in these current studies.

Wride et al. then re-evaluated the "representative" $(N_1)_{60}$ values being used to characterize the 19 failure case histories of interest. They took an approach that had been discussed, but not employed, before. It was their view (widely shared) that failure surfaces would tend to seek out and follow weak spots and weak sub-strata, and that it might be more reasonable to use a much lower than mean or median value of penetration resistance to characterize the failure zones controlling displacements and deformations. This was analogous to the "weakest-link-in-the chain" argument of Fear and Robertson (1995) with regard to triggering or initiation of liquefaction for these types of failures. Based on the work of Popescu et al. (1997) regarding effects of spatial variability on soil liquefaction, Yoshimine et al. (1999) had recommended the use of a 20^{th} percentile value (20% of the measured penetration resistances are lower) for CPT tip resistance data for liquefaction studies. Wride et al. took a similar view, and targeted a "reasonable lower bound" which, in practice, was either the lowest value measured for cases where penetration data were sparse, or the near lower bound when more data were available.

There is less explanation and discussion presented regarding selection of representative post-liquefaction strengths for each of the 19 case histories considered. Values of S_r developed by previous investigators were collected and tabulated, and the values then selected as best estimates for each case history are tabulated and presented as well. The most useful comment in the text of the paper regarding the basis for selection of representative S_r values for each case is to note that "When possible, the value of S_u was selected as one which incorporated energy effects (Poulos, 1988; Davis et al. 1988) as this was felt to be closer to the "true" value of S_u". On balance, the values of S_u (or S_r) selected appear generally reasonable.

Figures 2.17 and 2.18 present the resulting data points for the 19 case histories re-evaluated, and also a number of relationships developed by previous investigators for comparison. It should be noted that most previous investigators did not take a near lower bound approach to estimation of $(N_1)_{60\text{-}CS}$.

Figure 2.17 shows data points plotted as post-liquefaction strength (S_u) vs. "reasonable minimum" $(N_1)_{60\text{-}CS}$ as developed by Wride et al. (1999). The range proposed by Seed and Harder (1990) is shown, and so is the additional (more steeply rising) range proposed by Konrad

and Watts (1995) for Kogyuk and Erksak sands. Also shown are (1) the lower bound relationship proposed by Ishihara (1993), (2) the relationship proposed by Yoshimine et al. (1999) for triggering of flow slides, and (3) an additional material-specific relationship developed by Fear and Robertson (1995) for Ottawa sand based on laboratory testing and CPT data.

Figure 2.18 shows data points plotted as post-liquefaction strength ratio (S_u/P) vs. minimum $(N_1)_{60\text{-}CS}$ as developed by Wride et al. The range proposed by Stark and Mesri (1992) is shown, and so is the additional (more steeply rising) range proposed by Konrad and Watts (1995) for Kogyuk and Erksak sands. Also shown are (1) the lower bound relationship proposed by Ishihara (1993), (2) the relationship proposed by Yoshimine et al. (1999) for triggering of flow slides, and (3) an additional material-specific relationship developed by Fear and Robertson (1995) for Ottawa sand based on laboratory testing and CPT data.

In both of these figures, data points for cases where there is especially high uncertainty (or variance) with regard to SPT N-values are highlighted by open symbols around the solid symbols.

In examining these figures, it appears that the available data, as interpreted by Wride et al. (1999), could be construed as supporting, or at least partially supporting, any of the previous relationships shown, especially given that some of the relationships did not employ near lower bound assessments of penetration resistance. This served to illustrate the importance of being clear on the basis for development of empirical relationships for estimation of in situ S_r, and it also suggests the potential validity of near lower bound strengths (and associated penetration resistances) asserting some measure of control over field failure outcomes.

2.3.7 Olson (2001) and Olson and Stark (2002)

Olson and Stark performed studies to develop their own evaluations of post-liquefaction strengths for an expanded suite of 33 field failure case histories. Olson (2001) employed two types of approaches to the back-analyses of the 33 case histories studied. Olson employed an adapted version of the methodology of Davis et al. (1988) to account for the "kinetics" of flow failures (i.e. momentum effects), and applied this to 10 of the field failure case histories for which it was judged that sufficient information and data were available, in order to develop new estimates of S_r that explicitly included consideration of momentum effects. For the remaining 23 cases that they studied, it was judged that the available information and data were insufficient for a full "kinetics" analysis, and these cases were back-analyzed either by directly calculating the theoretical value of $S_{r,resid/geom}$ that would provide a static Factor of Safety equal to 1.0 for the residual geometry, or with a "simplified" back-analysis that was essentially a simplified infinite slope analysis that also targeted an approximate value of $S_{r,resid/geom}$. As discussed previously in Section 2.3.1, and as discussed at more length on Sections 4.3.2 and 4.3.3 and Chapters 5 and 6, these simplified analyses would have been systematically over-conservative due to their failure to include momentum effects. Ordinarily, some measure of conservatism might be appropriate for simplified analyses. Unfortunately, as described in Section 2.3.7.2, and in Chapters 4 through 6, the degree of over-conservatism was significantly larger than Olson and Stark had anticipated, and the use of $S_{r,resid/geom}$ instead of S_r for these 23 of the 33 overall case histories back-analyzed significantly damaged the resulting predictive relationship for post-liquefaction strength (S_r).

2.3.7.1 Kinetics Analyses

The analytical approach employed to incorporate "kinetic" effects (momentum and inertia) in analyses of 10 of the best-documented case histories was adapted, with some modifications, from the approach proposed by Davis et al. (1988) as illustrated schematically in Figure 2.19.

Davis et al, proposed that a displacing failure mass would initially accelerate downslope, accumulating increasing velocity and momentum, and then it would decelerate, with reducing velocity and momentum until it finally came to rest. With simplifying assumptions, it is then possible to track the progressive development and dissipation of acceleration, velocity, displacement, and momentum of the center of gravity.

Davis et al. (1988) also postulated that at some point between start and finish there would be a transition from acceleration to deceleration, and that there would be no net shear force transfer of inertial force to the base of the moving slide mass (which would be at peak displacement velocity) at that moment. That, in turn, means that at this intermediate displacement condition (at the moment of transition from acceleration to deceleration) when there is zero inertial force transfer, that a static stability analysis can be performed to calculate S_r directly, and the resulting value would correctly incorporate inertial (momentum) effects. There is, however, significant difficulty and subjective judgment involved in ascertaining the likely geometry of the failing slope at this moment of transition. As a result, Seed and Harder (1990) preferred to calculate the "apparent" $S_{r,yield}$ for the pre-failure geometry, and the "apparent" $S_{r,resid/geom}$ for the final, residual (post-failure) geometry, and then adopt a value of S_r between these two as the best estimate of S_r with consideration of inertial forces (momentum) being a function of apparent runout of the failure mass. Wang (2003) and Kramer (2008) chose, instead, to attempt to infer the geometry (displaced cross-section) of this intermediate transitional condition with zero inertial force (ZIF), giving rise to their "ZIF method" for back-analyses incorporating inertial effects as will be discussed in Section 2.3.8. In these current studies, a new method is presented that incrementally tracks the evolving displaced geometry and uses this as the basis for a progressive analysis that incorporates inertial effects (momentum) in back-calculation of S_r from failure case histories.

Olson elected to perform a full progressive inertial analysis tracking the evolution of acceleration, velocity and displacement of the center of gravity of the failure mass. Olson's analysis procedure is illustrated schematically (for the Wachusett Dam case history) in Figure 2.20.

The first step, as described by Olson (2001), was to determine the initial and final locations of the center of gravity for the full failure mass, as shown at the top of Figure 2.20.

A third order polynomial function was then fitted to approximate the progressive locus of points through which the center of gravity would then be assumed to travel from inception of failure to post-failure residual geometry. It was stated that it was important that this polynomial function produced a "curve" parallel to the average curvature of the overall sliding surface, or at least with a localized slope parallel to the average slope of the overall sliding surface associated with each successive position of the overall (field) sliding surface, as best this could be estimated.

The preceding conforms to the explanation of this approach as presented by Olson (2001), but it does not appear to quite correctly capture the physics of this approach, and it also appears likely that Olson may have actually performed better analyses than the preceding text would suggest.

Driving forces in the downslope direction (tangent to the polynomial curve) at any laterally displaced location (x) of the center of gravity were taken as being equal to the weight of the overall failure mass (W) multiplied by $\sin\Theta$, where Θ is the slope at any point on the polynomial curve.

As a result, it was important that this slope of the polynomial curve results in a good approximation of the total downslope driving shear stresses in the field at any laterally displaced location of the center of gravity. It was not important that the polynomial curve approximated the actual loci of points through which the center of mass of the overall failure surface passed; instead it was important that the local slope of the polynomial function defining the "sliding surface" on which the centroid "slid" had a value of Θ such that, at each lateral location (x) that the displaced center of mass passes by provides a calculated total driving downslope shear force ($W \bullet \sin\Theta$) approximately equal to the actual total downslope driving shear forces of the overall displaced failure mass at that stage of lateral centroid displacement.

Based on the good matches achieved between the values of S_r calculated by Olson (2001) for nine of the 10 cases that Olson analyzed by this "kinetics" approach, and values calculated in these current studies using a more rigorous "incremental momentum analysis" approach for these same cases, it appears likely that he realized this and accommodated it with careful selections of at least the initial (zero displacement) and final (ultimate displacement) slopes of the polynomial sliding surface. But this is not documented either in his thesis (Olson, 2001) or in the subsequent paper (Olson and Stark, 2002) and so this must be considered to be a "surmise" here.

The current investigation team have performed a number of these analyses for selected cases to assess this approach. It is a relatively simple matter to determine the initial downslope driving shear forces along the base of the full failure mass, and thus to determine the initial (steepest) "equivalent" slope $\Theta_{initial}$ at null displacement. It is similarly easy to determine the final "equivalent" slope Θ_{final} at full runout that would produce final downslope static driving shear forces equal to those calculated by simple two-dimensional limit equilibrium analyses for the final (residual) displaced geometry.

It is then considerably more difficult to determine "correct" values of Θ at intermediate levels of lateral displacement at all stages from the initial slope (and null displacement) to the final slope (and final, residual displacement). To do that accurately would require the careful inference and drawing of multiple stages of partially-displaced geometries between the initial (pre-failure) and the final (residual) geometry. Olson did not do that. On the other hand, this investigation team has determined that reasonably good calculated values of S_r can be developed so long as (1) the initial slope $\Theta_{initial}$ suitably matches initial driving forces, (2) the final slope Θ_{final} suitably matches residual driving forces, and (3) the instantaneous (local) slope angle Θ transitions smoothly between initial to final slope; ideally with a smooth tapering off of slope severity as progressively larger movements (displacements) develop.

A single strength S_r was reportedly assigned by Olson (2001) along the failure surface in the full-scale cross-section, and the shear strength along the failure plane multiplied by the length of the failure plane was then calculated and used as the resisting (upslope) force acting on the center of gravity in a direction tangent to the sliding surface of the polynomial curve. Comparing upslope vs. downslope forces at each point in time, any force imbalance was then applied to create acceleration [a] based on Newton's second law [F = M • a]. The system was then solved incrementally using a time-step algorithm to calculate progressive changes in accruing and dissipating acceleration, velocity and displacement of the center of gravity.

The value of S_r employed was iteratively adjusted until the calculated final displacement of the center of gravity of the failure mass equaled the observed displacement of this center of gravity in the field failure. At that point, the post-liquefaction strength along the actual lengths of the failure surface controlled by liquefiable materials was reportedly adjusted to account for strengths of non-liquefied materials based on Equation 2-2 as

$$S_u(LIQ)=\frac{S_u-\left(\frac{L_d}{100}\cdot S_d\right)}{\left(1-\frac{L_d}{100}\right)} \qquad \text{[Eq. 2-2]}$$

in which the overall average shear strength along the failure plane is sub-partitioned into (a) S_r for the lengths of the failure plane controlled by post-liquefaction strengths, and (b) drained strength, S_d, for the portions of the failure plane controlled by non-liquefied materials, L_d.

This conforms to the description and explanation presented in Olson (2001), but it appears that Olson actually did a better and more clever job than this with these analyses. Failure plane lengths and geometries, and the sub-sections of the failure plane controlled by liquefied and non-liquefied materials, change progressively as failure displacements accrue. Olson also modeled reduced shear strength at the base of portions of the toe of the failure mass that entered into water to account for potential hydroplaning effects. And Olson also accounted for progressive buoyancy increase as failure masses entered into bodies of water. Each of these effects would likely have been progressively adjusted as failure movements progressed, and that would have involved a far more detailed, tedious, and time consuming analytical effort than is suggested by Equation 2-2. Alternatively, Olson may have exercised judgment in approximately accounting for these progressively changing factors in his more simplified analyses.

Examining a number of the calculated plots of shear strength mobilized along the failure plane (e.g. the one near the top of Figure 2.16) in Olson's dissertation, it is clear that overall shear strength along the failure plane progressively changes as the failure displacements proceed. This suggests that an even more correct analysis was performed which included progressively implementing some level of changes in conditions and geometry as displacements progressed.

Olson assigned reduced shear strengths (50% reduction) for soils that travelled beyond the initial toe of a slope and entered into a reservoir to account for potential hydroplaning effects and what he termed reservoir mixing, and then allowed this to vary from 0% to 100% for subsequent parameter sensitivity studies. He did not explicitly discuss potential sliding along the top of weak reservoir sediments, or weak offshore slope sediments, beneath the advancing toe of the failure, but his approximation of 50% strength reduction is reasonable for both situations. Wang (2003),

and these current studies, each take different approaches on these issues (hydroplaning and potentially weak reservoir sediments), but it should be noted that Olson's modeling approach was also reasonable here.

Figure 2.20 shows an example calculation for the Wachusett Dam failure case history. The top of the figure shows the shape of the selected polynomial curve along which the center of gravity of the overall failure mass is assumed to slide. The next four figures below show the evolution (vs. time) of: (1) total shear resistance along the field failure surface, (2) acceleration (and then deceleration) of the center of gravity, (3) velocity of the center of gravity (which initially increases and then eventually drops back to zero), and (4) accumulated displacements of the center of gravity.

Figure 2.21 shows another illustration of this analytical procedure, this time for the upstream slope failure of the Lower San Fernando Dam. The top figure shows the pre-failure and post failure geometries, and also the pre-failure and post-failure positions of the center of gravity of the overall failure mass, and the shape of the curved (polynomial) curve "surface" along which the sliding of the center of gravity was calculated. The four figures below show (1) total shear strength vs. time along the failure surface, (2) acceleration vs. time of the center of gravity of the overall failure mass, (3) velocity vs. time of the center of gravity, and (4) displacement vs. time of the center of gravity.

There are a number of challenges and drawbacks to this analytical approach by Olson's kinetics method.

One of these is potential sensitivity of the calculations to the selected shape of the polynomial curve along which the center of gravity slides, and the concurrent difficulty of suitably modelling a slope that approximates the overall "driving" shear stresses along the actual (full scale) field failure plane at each successive stage of calculated displacement of the center of gravity. As discussed previously, simply aiming at being largely "parallel" to the overall failure surface is not sufficient here; it is the sum total of driving shear stresses in the field (associated with field conditions and geometry) that should match well with the driving shear stresses resulting from the modeling of the slope of the curved path along which the center of gravity slides, and at each successive step of development of displacements.

Another challenge is the fact that non-liquefied soils routinely had to be modeled with fully drained frictional shear strengths, so that S_d was also a function of effective normal stresses on those portions of the field failure plane. This is difficult to implement in the framework as described by Olson (2001) because effective normal stresses (and geometry) would have been changing as movements occurred. Olson does not explain how this was treated.

A similar challenge would have been the modeling of shear strengths along portions of the field failure surface where two different soil materials progressively come into contact as the failure movements progress. Ideally, the weaker of the two materials should control shear strength over portions of the failure surface where two different materials progressively come into contact. Olson does not explain how this was treated.

Another (similar) challenge would have been the modeling of undrained shear strength in cohesive soils, where the large displacements involved in the case histories back-analyzed would have been expected to result in a transition from peak to residual undrained shear strengths as failure movements progressed. Olson does not explain how this was treated.

Finally, it appears that several of the failure case histories may have been incrementally progressive (retrogressive) failures, with initial failures (or failure "slices") initially occurring close to the front of the eventual overall failure mass, followed by retrogressive development of additional slices farther from the front face, with each successive slice sequentially beginning to initiate its own displacements as it becomes partially unbraced due to movements of the preceding slice(s), until the failure surface eventually reaches the back heel of the final, overall failure. This would be tremendously difficult to model with the simplified kinetics approach that tracks only a monolithic single failure mass or "block".

In the face of all of these challenges, it should also be noted that the overall value of S_r calculated is well "bounded" for these analyses. As observed by Davis et al. (1988), and Seed and Harder (1990), assessment of the initial yield stress ($S_{r,yield}$) required within liquefiable materials to provide a calculated Factor of Safety equal to 1.0 will necessarily overestimate the actual value of S_r, because otherwise large displacements would not have occurred. Similarly, assessment of the "apparent" value of $S_{r,resid/geom}$ required within liquefied soils to provide a calculated Factor of Safety equal to 1.0 for the eventual post-failure residual geometry will significantly underestimate the actual value of S_r as it fails to account for momentum effects as the moving slide mass must be brought to rest. So a finite range of possible values of S_r would be between $S_{r,yield}$ and $S_{r,resid/geom}$. If the initial slope of the polynomial curve along which the center of gravity of the failure mass will slide is "set" so as to provide the correct initial (pre-failure) overall driving shear stresses, and the final slope of the polynomial curve is "set" so as to provide the correct final (post-failure, residual) overall driving shear stresses, then values of S_r calculated by this type of kinetics approach would tend to naturally fall within this finite range. With better modeling, and judgment, significantly better answers could be expected.

And Olson appears to have executed excellent kinetics analyses, and with good judgment. His calculated values of S_r for nine of the ten case histories to which this kinetics analysis method was applied produced values of S_r are in generally good agreement with the values subsequently back-calculated employing other methods by (1) Wang and Kramer (2003, 2008) and (2) these current studies. For the other case (Shibecha-Cho Embankment) Olson's back-calculated value of S_r was significantly lower than those subsequently calculated by Wang and Kramer, and by these current studies. Based on the cross-sections and explanations of Olson's analysis for this case, the Shibecha-Cho failure was modeled as a progressively incremental (retrogressive) failure, proceeding in a "slice by slice" fashion from the initial toe failure until the final slice reached the eventual overall back-heel of the failure. But Olson's kinetics analysis method could not handle a progressive (retrogressive) incremental failure. Recognizing this, Olson made an effort at simplification and analyzed only the movements of the first failure slice (the initial slice nearest the front face of the eventual overall failure); for which acceleration, velocity and displacement were tracked by the kinetics analysis performed. Because only the first (initial) slice was modeled and analyzed, the overall scale of the failure (and failure mass) was underestimated; so that overall driving forces, and momentum, and post-liquefaction strength (S_r), were underestimated. This

highlights the difficulty of applying the simplified "kinetics" analysis approach to analyses of these types of incrementally progressive failures. This Shibecha-Cho case history, and the challenges of back-analyses of progressively incremental (retrogressive) liquefaction-induced failures in general, will be discussed further in Chapters 4 through 6.

Overall, Olson's back-calculated values of S_r for nine of the ten cases that he analyzed using the kinetics method to account for momentum effects appear to have produced generally good answers. The tenth case history (Shibecha-Cho Embankment) produced a conservative (low) estimate of S_r.

2.3.7.2 Back-Analyses of the 23 Less Well Documented Case Histories

There were then 23 additional (less well documented) case histories for which Olson judged that there were insufficient information and data available as to justify the full incrementally progressive kinetics analysis approach. For 11 of these cases "simplified" analyses, or estimates, were employed to assess values of S_r. These were approximate approaches, and so they were (appropriately) conservatively implemented and tended to produce conservative estimates of S_r. For the most part, these simplified analyses amounted to essentially back-calculating the values of $S_{r,resid/geom}$ that would be required to produce a "theoretical" static factor of Safety equal to 1.0 for the residual geometry with zero inertial forces (no momentum effects) using an infinite slope analysis to approximate the actual field geometry. For the other 12 cases, the apparent post liquefaction strength ($S_{r,resid/geom}$) required to provide a calculated static Factor of Safety equal to 1.0 for residual post-failure geometry and conditions was directly calculated, using full post-failure geometry (rather than an approximated infinite slope analysis), and this value of $S_{r,resid/geom}$ was then taken as the value of S_r. Accordingly, for all 23 of the less well documented case histories, Olson calculated and employed $S_{r,resid/geom}$ instead of the actual post-liquefaction strength S_r.

As discussed previously, and as demonstrated later in Chapter 4, this use of $S_{r,resid/geom}$ was very conservative and would have significantly underestimated the actual values of S_r because it neglected to account for the effects of momentum as the moving failure masses had to be decelerated back to zero velocity at the end of slide movements. This underestimation would likely have produced values of S_r that would have been low by factors of between approximately 1.2 to 3.4 (see Chapter 4, Section 4.4.1, and Fig. 4.9).

As a result of these over-conservative approaches taken to the back-analyses of these 23 less-well defined and less-well characterized case histories, there was then a disparity between the S_r values calculated for the 23 lesser cases and the remaining 10 cases to which the higher order kinetics analysis approach had been applied. The 23 lesser cases had overly conservative (low) values of S_r, and 9 of the 10 kinetics cases had what tended to be more accurate (higher) values. One kinetics-analyzed case (Shibecha-Cho Embankment) had a low S_r value as discussed in the previous Section 2.3.7.1 because Olson's kinetics method was not able to correctly handle this strongly incrementally progressive (retrogressive) failure. The two sets of cases (the 10 high quality cases, and the 23 lesser quality cases) were essentially analyzed on very different bases, and the disparity in bias (or level of conservatism) of estimated S_r values served to obscure trends

when the data were subsequently plotted jointly as a function of representative penetration resistance.

2.3.7.3 Predictive Relationship

Olson then calculated average values of initial vertical effective stress along portions of the eventual plane occupied by liquefiable materials, and the S_r values determined for the full 33 case histories were divided by the effective vertical stresses to produce back-calculated values of post-liquefaction strength ratio (S_r/P) for each case.

Representative values of $(N_1)_{60}$ were also developed for each case. It was the position of Olson (2001), and of Olson and Stark (2002), that the fines adjustment proposed by Seed (1987) was not well founded, and they elected to apply no fines adjustment at all, and so the values employed were $(N_1)_{60}$ values rather than $(N_1)_{60,CS}$ values. That was unfortunate, because a significant number of the 33 case histories that they analyzed had liquefiable soils that were comprised mainly of silty sands and sandy silts, and those materials likely warranted significant fines adjustments. So the lack of a fines adjustment may have biased the representations of some of the penetration resistances for this particular data set. That may have also contributed to the lack of a well-defined relationship between S_r and $N_{1,60}$ that was eventually developed.

Figure 2.22 shows the overall relationship recommended by Olson and Stark (2002) for estimation of post-liquefaction strength ratio as a function of $(N_1)_{60}$, along with the data points from the 33 back-analyzed case histories. The two solid lines show the recommended range, and the heavy dashed line between these is the center of this range.

The recommended range and best estimate relationship proposed represents some degree of engineering judgment, because it does not adequately match the slope of the overall trend of the data presented. A least squares regression was performed as part of these current studies, and the results are presented with a red line in Figure 2.23. As shown in this figure, the actual slope of the regressed relationship is somewhat flatter than the recommended relationship, and the calculated R-squared value ($R^2 = 0.23$) indicates that the data is poorly behaved (randomly scattered) and that the regression is not well able to provide a good predictive "fit".

The recommended relationship is likely strongly conservatively biased overall, due in large part to the conservative underestimation of S_r for the 23 (out of 33) back-analyzed case histories that were evaluated on an overly conservative basis (as $S_{r,resid/geom}$ instead of S_r), as discussed in the previous Section 2.3.7.2, and the conservatively low value of S_r calculated for one of the 10 high quality cases (Shibecha-Cho Embankment), as discussed in the previous Section 2.3.7.1.

The lack of a clearly discernable strong trend between S_r and $(N_1)_{60}$ in Figures 2.22 and 2.23 appears to have three main causes. The first of these is the disparity in the average level of conservatism between the S_r values calculated for 10 case histories based on the kinetics back-analysis approach, and the far more conservatively biased S_r values calculated for the remaining 23 cases, as discussed previously. A second contributing cause may have been the lack of an

applied fines adjustment for the SPT penetration resistances. A third cause was the assumption that ratios of S_r/P would not vary as a function of effective overburden stress (see Chapter 5).

It is interesting to note that Olson had also directly calculated the initial post-liquefaction yield stress ($S_{r,yield}$) for each of his 33 case histories, although he did not employ these back-analysis results in the subsequent development of a predictive relationship for post-liquefaction strength (S_r). Instead, these $S_{r,yield}$ calculations were targeted at development of an un-related liquefaction triggering analysis method.

As a result, Olson had back-calculated both the initial yield strength ($S_{r,yield}$) and also the "apparent" post-liquefaction residual strength based on residual post-failure geometry ($S_{r,resid/geom}$) for all but one of the 33 cases. As demonstrated in Chapters 4 and 5, averaging these two values (simply adding then together and then dividing by two) might have been expected to produce significantly better estimates of the actual S_r values for the 23 case histories that Olson did not back-analyze by the higher-order kinetics method. Even better estimates of S_r for those 23 cases could have been obtained by adding together $S_{r,yield}$ and $S_{r,resid/geom}$, then dividing by two, and then multiplying that result by a number slightly less than 1 (e.g. multiplying by ~ 0.8 or so), as demonstrated later in Chapters 4 and 5.

Finally, it should be noted that Olson's work was a significant milestone achievement in its day. Those were turbulent times, rife with discussion and debate. Olson made two important contributions that were likely not fully appreciated at the time. The first of these was the level of detail and transparency with which he documented his analyses (the assumptions, procedures, cross-sections, properties, failure surfaces analyzed, etc.). This had no similar precedent, and no subsequent study has (yet) been as well documented either. One of the objectives of these current studies is to set a similarly high standard for documentation and transparency as well.

A second important contribution was that he calculated $S_{r,yield}$ and also $S_{r,resid/geom}$ for all but one of his 33 case histories. Because the analyses were reasonably well documented, the details of these calculations are generally well understood. Now, 21 years later, these values turn out to be an important piece of the overall puzzle, and good use is now made of them in these current studies as they are a very useful basis for comparison with values back-calculated for the same case histories when they are back-analyzed in these current studies.

2.3.8 Wang (2003), Kramer (2008), and Kramer and Wang (2015)

Wang (2003) working on his doctoral research with Kramer examined the case histories that had been used by previous investigators, and developed his own estimates of the key indices (S_r, $N_{1,60,CS}$ and $\sigma'_{v,i}$) that would eventually be employed to develop new probabilistic relationships for SPT-based assessment of in situ post-liquefaction strengths (Kramer, 2008). The regressed relationships developed by Kramer (2008) would subsequently be re-published in an archival journal (Kramer and Wang, 2015).

Wang's initial work had developed values of fines-corrected $N_{1,60,CS}$, but the relationships subsequently developed by Kramer (2008) and published by Kramer and Wang (2015), were based

on non-fines-corrected values of $N_{1,60}$. There is some confusion here, because the report by Kramer (2008) inadvertently presents a table of "input" values to the regressions performed, and this table (Table G.4, which is re-produced here as Table 2.4) lists $N_{1,60,CS}$ values. That was essentially a typographical error (Kramer, 2015). The wrong table was inserted in the report; the regressions, and the predictive relationships that resulted, were actually based on non-fines-corrected $N_{1,60}$ values. Kramer and Wang (2015) present a new (and correct) table of input values for their regressions showing the penetration resistances correctly presented in terms of $N_{1,60}$. These corrected values are shown in Table 4.5.

Because these current studies employ $N_{1,60,CS}$ as the penetration resistance measure, values of $N_{1,60,CS}$ developed for each individual case history will be cross-compared with Wang's values of $N_{1,60,CS}$ (rather than the subsequent $N_{1,60}$ values) for cases analyzed by both investigation teams for purposes of cross-checking the results of back-analyses of individual case histories. It will later be necessary, however, to make a modest approximate modification of the predictive relationship developed by Kramer (2008) in order to compare that relationship with the relationship developed in these current studies; both will be compared on an approximated $N_{1,60,CS}$ basis (see Section 5.4.1).

2.3.8.1 Wang (2003)

Both the 2008 and the 2015 relationships are based on the initial case history evaluations developed by Wang (2003). As a first step, Wang examined and vetted case histories of small to moderate displacement (e.g. most of the lateral spreading case histories) and compared observed displacements against the values that would be predicted by the empirical relationship for lateral spreads developed by Youd et al. (2002). Cases where the observed displacements were not significantly greater than predicted by the relationship of Youd et al. were deleted from further study, because it was assumed that cyclic inertial forces were a significant contributor to observed displacements, and current analytical methods do not yet permit very accurate assessment of S_r based on back-analyses of such cases.

The remaining 31 cases were then examined more closely, and 9 of them were judged to have sufficient data and information as to warrant independent re-analyses. These 9 cases were designated as the Primary case histories, and each was back-analyzed to develop estimates of the three indices (S_r, $N_{1,60,CS}$ and $\sigma'_{v,i}$), and also assessments of uncertainty or variance associated with these estimates. The remaining 22 cases were judged to not have sufficient data and information as to warrant full re-analyses. These were designated as Secondary cases, and the 22 Secondary cases were not back-analyzed; instead values of S_r back-calculated by previous investigators were collected, and then generally averaged together, to develop values of S_r and $\sigma'_{v,i}$ for these remaining 22 case histories. Interestingly, independent values of representative $N_{1,60,CS}$ values appear to have been developed for each of these 22 secondary cases, though documentation of details is poor on this issue.

The details of the implementation of each of these two approaches (for Primary and for Secondary cases) are important, and these will be discussed in Sections 2.3.8.1 (a) and (b) that follow.

The assessments performed for the 9 Primary case histories appear to have been reasonable, and to have produced values in good general agreement with the values produced for these same case histories in these current studies. There were a number of apparent errors and/or shortcomings in the assessments of key parameters for a number of the 22 Secondary case histories, however, and these appear to be the issues principally responsible for the apparent shortcomings in the predictive (regressed) relationship of Kramer (2008) and Kramer and Wang (2015).

2.3.8.1(a) Zero Inertial Factor Back-Analyses of the Nine Primary Case Histories

The 9 highest quality case histories were considered to be "Primary" cases by Wang (2003), and these were back-analyzed using a new methodology that Wang developed that he referred to as the zero inertial factor (or ZIF) method. These were 9 of the same 10 highest quality case histories which Olson (2001) had back-analyzed using his "kinetics" analysis method.

This ZIF method was based on the observation by Davis et al. (1988), as described previously and illustrated in Figure 2.19, that a slide mass moving downslope initially accelerates, and then decelerates and comes to rest. Davis et al. further postulated that at some point between start and finish there would be a transition from acceleration to deceleration, and that there would be no net shear transfer of inertial force to the base of the moving slide mass (which would be at peak displacement velocity) at that moment. That, in turn, means that at this intermediate displacement condition (at the moment of transition from acceleration to deceleration) when there is zero overall net inertial force transfer, a simple static stability analysis can be performed to calculate S_r directly, and the resulting value would correctly incorporate inertial effects.

Wang elected to attempt to estimate or infer the displaced position and geometry (displaced cross-section) corresponding to this transitional moment of zero inertial force. The fraction of eventual overall (final) displacement required to reach this transitional displaced cross-section geometry was termed the zero inertial factor (or ZIF). Once this fractional ZIF displacement had been estimated, the pre-failure geometry was then judgmentally transitioned part-way towards the final displaced (post-failure) geometry in proportion to this ZIF. Static limit equilibrium stability analyses were then performed using this ZIF cross-section to back-solve for the post-liquefaction strength needed to provide a static Factor of Safety equal to 1.0 at this ZIF displacement geometry.

The estimation or inference of the likely displaced (and deformed) cross-section geometry at this ZIF moment for any given geometry is very challenging. And it relies heavily on engineering judgement. One cannot simply assume a displaced condition exactly mid-way between the initial geometry and location and the final residual geometry and location, in part because the ZIF transition from overall acceleration to overall deceleration appears to usually occur before half of the overall displacements have accrued; due to progressive diminishment of driving static shear stresses as the failure progresses and as the slope "flattens". This is clearly illustrated in the "kinetics" analyses performed by Olson (2001), and also in the incremental inertial analyses performed for these current studies as described in Chapters 3 and 4, and as presented in Appendix A.

The difficulties involved in estimating this displaced geometry at the transitional moment of zero inertial force transfer were recognized by Wang (and Kramer) who explained that the approach taken was to begin by examining the pre-failure and post-failure geometries (cross-sections) for selected, well-characterized case histories. Then the kinetics displacement analyses performed by Olson (2001) for these nine cases were next examined to determine what fraction of overall (final) displacement, or ZIF, appeared to correspond to the point of transition from acceleration to deceleration of the overall failure mass. A number of "points" on the pre-failure cross-section were then selected, and these were partially displaced towards the final (post-failure cross-section) geometry in approximately the estimated proportion required. This was used to create an approximate cross-section, and this was then iteratively refined to develop a cross-section that was reasonable based on considerations of soil mechanics, the materials and geometries involved, conservation of mass, the inferred failure mechanism and mechanics, and the observed pre-failure and post-failure cross-sections. This was an iterative process, requiring both art and judgment.

Wang (2003) provided only a single illustration of this process; for the Wachusett Dam failure case history. There was no documentation presented for the other eight case to which the ZIF method was applied. Figure 2.24(a) shows points selected on the pre-failure cross-section (solid line) and connected locations of the same points on the post-failure cross-section (dashed cross-section). For this case, Olson estimated that the ZIF was 43.3%, so 43.3% of the displacements from initial to final locations of each of the points selected was targeted, and the resulting initial estimates of the locations of these points on the zero inertial geometry in Figure 2.24(a) were then projected as the initial best estimates of the locations of those points for the ZIF cross-section. This was then artfully modified, allowing for curved paths between initial and ZIF locations of selected points, in a manner judged to be consistent with soil mechanics and the inferred failure mechanism. The resulting eventual ZIF displaced cross-section for the Wachusett Dam that was analyzed by means of static limit equilibrium methods is then shown in Figure 2.24(b).

As Kramer (2008) notes: "The procedure was laborious and is recognized as being approximate, a fact that was accounted for in the Monte Carlo analyses described subsequently."

There are a number of challenges and potential drawbacks to this approach. One is the question as to whether the ZIF calculated by Olson (2001) was fully accurate, so that the correct fractional displacement was modeled for the ZIF cross-section in Wang's subsequent studies. Wang's "ZIF" was dependent upon both the accuracy of Olson's calculations for each case history, and the judgments made with regard to modeling of progressively changing shear strengths as failure masses displaced. Another question is the reliability with which the actual ZIF cross-section details (geometry and stratigraphy, etc.) can be inferred by this approach. Another is the question as to whether the projected ZIF cross-section developed for any specific case history could then be suitably further advanced to eventually produce the post-failure cross-section actually observed. [In the incremental inertial analyses performed for these current studies, incremental displaced/deformed cross-sections are developed progressively from initial to final observed field cross-section geometries; much like an "animation" or progressive simulation of the progressing failure. This turned out to be very useful, providing insights as to progression paths of successive incremental geometries that could successfully finish with the actual observed

post-failure cross-section. In some cases this helped to shed light on likely failure mechanics details. See Chapter 4 and Appendix A.]

Despite these challenges, it is the opinion of the current investigation team that for well-characterized failure case histories, with well-defined pre-failure and post-failure cross-section geometries, this ZIF approach can (if wielded with suitable engineering judgment) be expected to provide useful back-calculated values of S_r with levels of accuracy and reliability at least compatible with those developed by the kinetics method employed by Olson (2001); but not fully compatible with the results of back-analyses by the "incremental inertia" method used in these current studies (see Chapter 4 and Appendices A and C). Cross-comparisons between S_r values back-calculated (1) by this ZIF method, (2) by the kinetics method of Olson (2001), and (3) by the incremental inertial analysis method employed in these current studies (see Chapters 4 and 5) bear this out.

Wang (2003) developed a simplified approach to estimate the amount of hydroplaning that would occur as the toes of failure masses entered into bodies of water, based on a review of available research. The likelihood and lateral extent of hydroplaning at the toe was taken as a function of displacement velocity of the displacing mass, and the extent over which hydroplaning would occur was limited to a distance beneath the toe of the slide mass extending inboard not more than 10 times the thickness of the toe mass entering the reservoir. This was a rational approach, but the procedure should be considered somewhat speculative, however, as it was constructed based on research that was far from definitive. Wang recognized this, and he took a probabilistic approach to implementation of modeling of hydroplaning effects.

Wang systematically varied a number of parameters and variables for each of the 9 case histories back-analyzed by this ZIF approach. Cross-section details, failure surface locations, phreatic surface locations, unit weights, and soil material strength parameters for soils that did not liquefy were then all systematically varied within estimated reasonable ranges, and 50,000 Monte Carlo simulations representing randomized combination within these ranges were analyzed for each individual case. This was done to provide an assessment of variability in S_r values back-calculated, and also to provide a basis for more formal assessment of both means and variability of means expressed in terms of standard deviation of the means for the three key indices (S_r, $N_{1,60,CS}$ and $\sigma'_{v,i}$). The established ranges of variations of parameters and geometry actually pre-established the variances that would be produced by the Monte Carlo analyses, but this was not a bad overall procedure for development of estimates of standard deviations of mean values of S_r for each case.

Unfortunately, the actual ZIF cross-sections used and other key analysis details (including failure surfaces considered, phreatic surfaces, and soil properties, etc.) were not presented for 8 of the 9 cases histories back-analyzed, so it is not possible to check these analyses, nor to know exactly what was done for each individual case history. The example illustrative ZIF cross-section for the Wachusett Dam case history shown in Figure 2.24 was the only ZIF cross-section presented, and other key details for even this case are not presented.

This lack of documentation and transparency is unfortunate.

It should be noted that these nine ZIF analyses were performed before the incremental momentum analyses that were developed and performed for these current studies, and that Wang and Kramer thus did not know what the answers developed by these current studies would be. There is generally reasonably good agreement between the results from seven of these nine ZIF back-analyses, and the corresponding results of the incremental inertial back-analyses from these current studies for these same nine cases (see Chapter 4). And so it must be assumed/concluded that the judgments required for implementation of the ZIF approach were generally well executed.

One of the nine common cases was the Shibecha-Cho Embankment, which was discussed previously in Section 2.3.7. This was an incrementally progressive (retrogressive) failure that Olson's kinetics method could not correctly analyze. Olson settled for analyzing only the first (toe) slice, and so significantly underestimated overall momentum, overall scale, and S_r for this case history. Wang (2003) employed Olson's back-calculated displacement time history to select his "ZIF", and then applied it to the overall cross-section as a monolithically triggered failure. This was clearly an incompatible set of assumptions and analyses. Fortunately, the overall value of S_r back-calculated by Wang (2003) for this case history (S_r = 208.8 lbs/ft^2) agrees very well with the value of S_r back-calculated in these current studies (S_r = 224 lbs/ft^2) using the incremental inertial method.

In the end, Wang's (2003) values of S_r back-calculated by the ZIF method for these 9 cases agreed within a factor of +/- 1.31 or better with the values back-calculated for these same 9 cases in these current studies using the more complex and more flexibly adaptable incremental momentum analysis method. This provides good support for Wang's values, at least for these nine cases, and it also provides good support for the incremental momentum analysis method that will be the primary tool of choice in these current studies.

Wang's values of mean $N_{1,60,CS}$ for these nine Primary case histories generally agree reasonably well, but not perfectly, with the values developed for these same case nine histories in these current studies.

In addition to difficulties in estimating the intermediate ZIF cross-section geometries, an additional source of differences between Wang's studies and these current studies is differences in the fines adjustments made. The text of Wang (2003) appears to indicate that a fines adjustment approximately compatible with the fines adjustments proposed for post-liquefaction strength by Seed (1987) and by Stark and Mesri (1992) was employed. These two fines adjustments are fairly closely similar, and they both add potentially very large blowcount increases at even very low $N_{1,60}$ values when fines contents are high. Differences between the resulting $N_{1,60,CS}$ values based on variations between these approaches would have been relatively small for most of the cases, and the values developed by Wang (2003) appear to be generally reasonable given these fines corrections. This will be discussed further in Chapters 4 and 5.

Wang's values of standard deviation in mean $N_{1,60,CS}$ were developed by a rigidly formulaic approach, and some of these appear (for some of the case histories) to be excessively large, and this will also be discussed further in Chapters 4 and 5. This does not appear to have had a very significant adverse impact on the predictive correlations and relationships eventually developed.

The approach taken by Wang (2003) to evaluate $\sigma'_{v,i}$ for his nine "primary" case histories was a bit convoluted, but it appears to have resulted in generally good agreement with values of $\sigma'_{v,i}$ back-calculated by (1) Olson (2001) and (2) these current studies for at least seven of the nine ZIF-analyzed cases, and at least fair agreement for the other two cases (see Table 2.3).

2.3.8.1(b) The Less Well Documented (Secondary) Case Histories

The 22 remaining case histories employed by Wang (2003) and Kramer (2008) were judged to not have sufficient data and information as to warrant or support ZIF-type analyses, and Wang referred to these as the "secondary" cases. Wang was then in the same position as Olson (2001) of having to decide how to develop suitable estimates of his three key sets of indices (S_r, $N_{1,60,CS}$ and $\sigma'_{v,i}$) for these lesser cases.

The approach taken was not to perform independent back-analyses of these cases, but instead to select values of S_r and S_r/P developed by other (previous) investigators, and then use these to develop or infer overall estimates of S_r and $\sigma'_{v,i}$ for each of the secondary cases. A mixed approach was taken in the development of $N_{1,60,CS}$ values, as some of these values were developed largely independently by Wang and some were largely developed based on values from previous investigations.

Discussions of Wang's assessments of each of these three indices follow.

(i) Representative Values of $N_{1,60,CS}$

Wang (2003) collected estimates of either $N_{1,60}$ or $N_{1,60,CS}$ from multiple previous investigators, and then selected his own best overall estimates for these 22 cases. Values of $N_{1,60,CS}$ appear to have been judgmentally modified to be compatible with the values from the 9 primary case histories of Section 2.3.8.1(a), but full details are not presented. With only one exception, the values of $N_{1,60,CS}$ selected by Wang (2003) for these 22 cases agree reasonably well with the values developed in these current studies for these same cases. That singular exception was the El Cobre Tailings Dam case history. Wang's value of best-estimated median $N_{1,60,CS}$ was $N_{1,60,CS}$ = 6.8 blows/ft., while the value from these current studies was $N_{1,60,CS}$ = 2 blows/ft. The difference here appears to be due in large part to a very large fines correction made by Wang for these silt-dominated tailings materials; while in these current studies the fines adjustment is applied as a function in part of the un-corrected $N_{1,60}$ value resulting in a smaller fines adjustment for this case. There are several other case histories in which Wang's selected value of mean $N_{1,60,CS}$ differs by as much as 3 to 4 blows/ft from the value used in these current studies; but this is a relatively small level of difference in a large suite of complex case histories requiring significant engineering judgment for development of estimates of equivalent $N_{1,60,CS}$. Overall, the values of $N_{1,60,CS}$ developed or selected by Wang (2003) for most of these case histories agree well with those developed in these current studies.

Wang (2003) assigned standard deviations in $N_{1,60,CS}$ based on the number, and variability, of SPT N-values available in the liquefiable material of interest. For 13 of the 22 Secondary case

histories, there were no N-values available (and so "representative" N-values had to be estimated or inferred from other data or information). These cases with no N-values available were all assigned a maximum coefficient of variation (COV) equal to 1.5. Lesser values of COV, and corresponding values of standard deviation, were assigned to the remaining case histories for which at least some N-values were available. Values of COV for these remaining 9 cases ranged from 0.15 to 0.75.

Some of the values of COV assigned appear to be unreasonably high; those values are significantly higher than were employed in these current studies for those same case histories. It does not appear, however, that this was a major issue, and the overall predictive correlation developed does not appear to have been much adversely affected by choices of COV, or standard deviation, in $N_{1,60,CS}$ for the 22 Secondary case histories.

(ii) Representative Values of S_r

The mean value of S_r for each of these 22 cases was taken as the average of values selected from among available values back-calculated by previous teams of investigators. Only values considered to be applicable were employed here, and the basis for judgment as to "applicability" was that a preference was made for values that appear to incorporate momentum effects. This was, statistically, likely a better approach than the conservatively biased approach used by Olson (2001) to estimate S_r for his 23 "lesser" cases (see Section 2.3.6) in which he used $S_{r,resid/geom}$ instead of S_r. But it was not an ideal approach, and there appear to have been at least two outright errors, and a number of additional problems or issues.

Table 2.1 presents (1) the selected values collected from previous investigators for each of the 22 Secondary case histories, and (2) the final values selected by Wang (2003). These values are from Table 6-8 from Wang (2003).

There appear to be two significant straightforward errors in this table.

For the El Cobre Tailings Dam case history, Wang lists only a single value of S_r = 195 lbs/ft^2 and cites it as coming from from Olson (2001), and then selects this value of $\underline{S_r = 195 \text{ lbs/ft}^2}$ as his representative mean value for this case history. But Olson's actual reported value for this case was $\underline{S_r = 40 \text{ lbs/ft}^2}$.

For the Hokkaido Tailings Dam case history, Wang lists two values of S_r from two previous investigations as

S_r = 408 lbs/ft^2 (Ishihara, et al., 1990)

and

S_r = 172 lbs/ft^2 (Olson, 2001)

The average of these two values would be 290 lbs/ft^2. But Wang's selected representative value is S_r = 251 lbs/ft^2; making this one of only a few case histories for which Wang's selected value is not a straightforward average of the available S_r values listed. More importantly, the value of S_r = 408 lbs/ft^2 attributed to Ishihara et al. (1990) is in error. The actual value developed by Ishihara et al. (1990) for this case history is only S_r = 137 lbs/ft^2. With this correct value of 137 lbs/ft^2, there would be relatively good agreement between the two values and the average of the two values listed for this case would then be a representative overall value of S_r = 154.5 lbs/ft^2, rather than the value of S_r = 251 lbs/ft^2 that Wang (2003) and Kramer (2008) employ in their regressions for development of predictive correlations.

Finally, unbeknownst to Wang at the time, the value of S_r independently developed in these current studies for the Hokkaido Tailings Dam case history is S_r = 131 lbs/ft2 (see Appendix B.8). So the three values available now are: S_r = 137 lbs/ft^2 (Ishihara et al., 1990), S_r = 172 lbs/ft^2 (Olson, 2001) and S_r = 131 lbs/ft^2 (these current studies). The average of these values would then be S_r = 146 lbs/ft^2. Given the excellent agreement between these three independent assessments, this would appear to be a well-supported number.

In addition to these two apparently straightforward errors, there are additional values of representative S_r values that appear to be questionable; often due to failure to fully back-track into the histories of the development of the values listed in Table 2.1 and to understand their origins.

It is interesting to note that Wang's Table 6-8 (presented here as Table 2.1) lists values of S_r from Olson (2001) for all 22 of the cases. The values listed are not Olson's selected values (of $S_{r,resid/geom}$) upon which Olson and Stark (2002) based their eventual predictive relationship for S_r. Instead, Wang noticed that Olson had calculated both $S_{r,yield}$ and $S_{r,resid/geom}$ for each of these case histories (as discussed previously in Section 2.3.7.2), and so Wang (2003) instead adopted a value of S_r that he "attributed" to Olson (2001) that was the average of these two values as

$$S_r = (S_{r,yield} + S_{r,resid/geom}) \times 0.5 \qquad \text{[Eq. 2-3]}$$

As demonstrated later in Chapter 4, this was a generally good idea, but it would have produced slightly biased (high) estimates of S_r. They would have been much better estimates than the $S_{r,resid/geom}$ values that Olson and Stark (2002) used in their development of predictive relationships for S_r, but even better estimates would have been achieved using an equation

$$S_r = (S_{r,yield} + S_{r,resid/geom}) \times 0.5 \times \xi \qquad \text{[Eq. 2-3a]}$$

where ξ is a function of runout distance of the slide mass normalized by initial failure slope height. The parameter ξ has values that range between $\xi \approx 0.4$ to 0.99 for the case histories in these two sets of studies, with an average of approximately 0.8 for the current suite of case histories (see Chapter 4). On average, a simplistic first-order estimate of S_r based on Olson's values of $S_{r,yield}$ and $S_{r,resid/geom}$ can be taken as

$$S_r = (S_{r,yield} + S_{r,resid/geom}) \times 0.5 \times 0.8 \qquad \text{[Eq. 2-3b]}$$

This implies that Wang's values of S_r inferred from Olson's values of $S_{r,yield}$ and $S_{r,resid/geom}$ are, on average, high by approximately 25%. The impact of this is variable from case history to case history, depending on how many other values of S_r from other previous investigations are averaged in with the value of S_r inferred from Olson. As shown in Table 2.1, there are between zero (four cases) to as many as six (one case) other values of S_r to average in with the inferred values from Olson (2001).

Another issue is the apparent failure of Wang (2003) to investigate the origins and backgrounds of many of the individual values of S_r that he collected and compiled from previous investigations. This also had a potentially significant deleterious effect on some of the results.

A good example of the importance of tracking back to understand the history of development of values from previous investigations is the Nerlerk Berm 1 case history. Wang (2003) lists four values for this case history from four sets of previous teams of investigators as:

$S_r = 42$ lbs/ft^2 (Sladen et al., 1985)

$S_r = 308$ lbs/ft^2 (Jeffries et al., 1990)

$S_r = 300$ lbs/ft^2 (Stark and Mesri, 1992)

$S_r = 54$ lbs/ft^2 (Olson, 2001)

and he then averages these for his selected representative value of $S_r = 179$ lbs/ft^2. (The actual average of these would be $S_r = 176$ lbs/ft^2; the slight difference here may be due to units conversions from the original publications cited.)

But a review of the history of development of the four apparently independent values cited for this case history changes the picture significantly. Sladen et al. (1985) were the original investigators, and their value of $S_r = 42$ lbs/ft^2 thus has good credence. Jeffries presented a value of $S_r = 308$ lbs/ft^2, but did not present the details (or cross-sections, etc.) of the analyses that produced this value; and so they cannot be properly checked. Stark and Mesri (1992) simply adopted the value of $S_r = 308$ lbs/ft^2 from Jeffries et al. without independent analyses of their own, and rounded it to $S_r = 300$ lbs/ft^2. So this is <u>not</u> an additional independent value. Olson (2001) did then, subsequently, perform his own independent analyses to develop the value of $S_r = 54$ lbs/ft^2. Because he published this as Olson and Stark (2002) it may be concluded that this replaces the judgment of Stark and Mesri that the value of Jeffries (1990) was appropriate. Finally, unbeknownst to Wang at the time (2003), the back-analyses performed for these current studies developed a value of $S_r = 68$ lbs/ft^2 for this case history. So a better summary would appear to be:

$S_r = 42$ lbs/ft^2 (Sladen et al., 1985)

$S_r = 308$ lbs/ft^2 (Jeffries et al., 1990)

$S_r = 300$ lbs/ft^2 (Stark and Mesri, 1992) [redundant, from Jeffries et al.]

S_r = 54 lbs/ft^2 (Olson, 2001)

and [S_r = 68 lbs/ft^2] [These current studies.]

The value of Jeffries et al. (1990) is not suitably documented, and it appears to be in error, with three other independent teams of investigators developing values of S_r = 42, 54 and 68 lbs/ft^2 for this case history (in good agreement with each other). Straightforward averaging of these three values would produce a representative value of $\underline{S_r = 55 \text{ lbs/ft}^2}$, a significantly lower value than the $\underline{S_r = 176 \text{ lbs/ft}^2}$ adopted by Wang (2003).

Another good pair of examples are the two La Marquesa Dam case histories (Upstream Face and Downstream Face). Considering only the downstream side case history here; Wang's Table 6-8 lists values from four previous investigation teams. These are

S_r = 423 lbs/ft^2 (De Alba et al., 1987)

S_r = 400 lbs/ft^2 (Seed and Harder, 1990)

S_r = 400 lbs/ft^2 (Stark and Mesri, 1992)

S_r = 190 lbs/ft^2 (Olson, 2001)

The first three of these values are redundant; they do not represent three independent evaluations or back-analyses. De Alba et al. (1987) included both Seed and Harder as members of their investigation team. Seed and Harder (1990) simply rounded the value of S_r = 423 lbs/ft^2 to S_r = 400 lbs/ft^2. Stark and Mesri (1992) did not perform any independent back-analyses; instead they simply adopted the value of S_r = 400 lbs/ft^2 from Seed and Harder (1990). The value of S_r = 190 lbs/ft^2 attributed to Olson (2001) is then the second independent value. This is again, of course, not the (lower) value of $S_{r,yield}$ that Olson (2001) and Olson and Stark (2002) employed in development of their predictive relationship. They employed a value of $S_{r,resid/geom}$ = 111 lbs/ft^2; and Wang (2003) modified this to a value representing instead the average of Olson's values of $S_{r,yield}$ and $S_{r,resid/geom}$ as discussed above to produce the value of S_r = 190 lbs/ft^2. The value of S_r developed by De Alba et al. (1987) probably took excessive account of potential cyclic inertial effects for this case, and it may be somewhat unconservative. Averaging this value three times with only one times the approximate actual S_r value derived (by Wang, 2003) from Olson's analyses of $S_{r,yield}$ and $S_{r,resid/geom}$ would then likely produce an unconservatively biased overall average. Wang's value selected for this case was then S_r = 344 lbs/ft^2.

The value back-calculated in these current studies for this same case is S_r = 214 lbs/ft^2. If only one of the values of approximately $S_r \approx$ 400 lbs/ft^2 was averaged with the other independent value of S_r = 190 lbs/ft^2, then the resulting average would have been S_r = 295 lbs/ft^2, in better agreement with the value back-calculated in these current studies.

The best cross-comparison (now), however, would likely be to use (1) the value of 0.5 times the average of Olson's values of $S_{r,yield}$ and $S_{r,resid/geom}$ multiplied by $\xi \approx 0.8$ (as discussed in Chapter 4) to produce the value of S_r = 152 lbs/ft^2, and (2) the value of S_r = 214 lbs/ft^2

independently back-calculated in these current studies. These two values are in fairly close agreement, and the average of these two independent values would be S_r = 183 lbs/ft^2; a value that is lower than Wang's value of S_r = 344 lbs/ft^2 by a factor of 344/183 = 1.88.

Similar re-evaluation suggests that the value of S_r selected and employed by Wang (2003) for the La Marquesa Dam upstream side case history also significantly over-estimates S_r, and for largely similar reasons.

These same types of issues occur for a number of the other "secondary" case histories as well. Close examination of the values and citations listed in Table 2.1 shows a number of similar issues, though generally of lesser impact on an individual case by case basis. The most common of these issues is that many of the case histories have two sets of S_r values listed as being attributed to Seed and Harder (1990) and to Stark and Mesri (1992). As described previously in Section 2.3.3, Stark and Mesri (1992) simply adopted the values of S_r back-calculated by Seed and Harder (1990), so these are the same numbers (they are redundant) and are not two independent sets of values, and they should not be listed (and used) as two separate sets of independent estimates.

Overall, there are a number of apparent (1) errors and (2) judgments and/or choices made by Wang that appear to produce unconservatively biased (high estimates) of S_r for a significant number of the 22 "secondary" case histories. These appear to be high, on average, by about 10% to 20% (though for some individual cases the degree of bias is greater), and this unconservatism will be more than offset by over-conservatism in many of the values of "representative" values of initial effective vertical stress ($\sigma_{v,i}'$) developed by Wang (2003) and employed by Kramer (2008), as will be discussed in Section 2.3.8.1(b)-(iii) that follows.

Coefficients of variation (COV) for each of the 22 secondary cases were estimated based on (1) the COV's calculated for the nine cases previously back-analyzed using the ZIF-based approach, (2) the perceived quality of data and information available for each case (which was "indexed" to a factor affecting overall COV), and (3) variance or dispersion in available values of S_r from previous studies. The equational relationship inter-relating these factors was designed to increase overall COV somewhat to account for the increased effects of modeling uncertainty in these less well defined case histories. This was an interesting approach, and it was not without merit. It is interesting to contrast the resulting estimates of variance (expressed as standard deviation in mean value of S_r for each case) against the values of standard deviation of S_r for each of these same cases as developed by very different approaches employed in these current studies.

(iii) Representative Values of $\sigma_{v,i}'$

The eventual regressed predictive relationship developed by Kramer (2008) predicted S_r based on both (1) $N_{1,60,CS}$ and (2) initial effective vertical stress ($\sigma_{v,i}'$). Surprisingly, values of mean $\sigma_{v,i}'$, and of the standard deviations of these means, for the 31 cases analyzed were never explicitly stated; neither in the thesis work of Wang (2003) nor in the subsequent WashDOT report of Kramer (2008) which presented the regressions performed and the resulting development of probabilistic and deterministic correlations for evaluation of S_r. Table 2.2 is from Kramer (2008), and it presents the mean values, and standard deviations in mean values, of both S_r and $N_{1,60,CS}$ for

each of the 31 cases, along with weighting factors developed by Kramer for use in performing the regressions which followed. Not listed are the mean values, and standard deviations in mean values, of initial effective vertical stress; despite the fact that initial effective vertical stress turns out to be of essentially co-equal importance along with $N_{1,60,CS}$ for prediction of S_r in the predictive correlations subsequently developed. This was another significant lapse in terms of transparency of documentation.

The eventual journal paper by Kramer and Wang (2015) finally explicitly presented the values of representative initial effective stress ($\sigma_{v,i}'$) used for each case history. These are presented in the column of Table 2.3 labeled "[3]". These values of $\sigma_{v,i}'$ can now be back-tracked and checked in detail. There are some significant problems here.

The process employed by Wang (2003) to develop his estimates of representative values of $\sigma_{v,i}'$ was a very poor one, and it led to a number of significant errors. These errors carried forward into the predictive relationships subsequently developed by Kramer (2008) and published by Kramer and Wang (2015).

In addition to collecting values of S_r from previous investigators for each case history (as presented in Table 2.1), Wang (2003) also collected values of S_r/P from previous investigators, and these are presented in Table 2.2. These values were then averaged to develop estimates of the overall representative values of S_r/P for each case history, as also listed in Table 2.2.

These resulting averaged values of S_r/P were not used to estimate overall values of S_r for any of the cases, but they were used to infer representative values of "P" (or $\sigma_{v,i}'$) for each of the 22 Secondary case histories. Values of S_r (from Table 2.1) were combined with values of S_r/P (from Table 2.2) to derive "representative" values of $\sigma_{v,i}'$ for each of the 22 Secondary case histories. The problem was that the "averaged" evaluations of S_r (Table 2.1) and of S_r/P (Table 2.2) were not developed in a manner intended to be compatible with each other. They were developed by different teams of investigators, and often represented different assumed and/or back-analyzed failure mechanisms or failure surfaces, as well as other differences in technical opinions and modeling or analysis details.

This led to some clearly unreasonable values of "representative" $\sigma_{v,i}'$, which serve to at least partially undermine the validity of the (regressed) probabilistic predictive relationships subsequently developed.

Table 2.3 lists, and cross-compares, the values of $\sigma_{v,i}'$ developed and used by [1] Olson & Stark (2002), [2] these current studies (see Chapter 4), and [3] Kramer (2008) and Kramer & Wang (2015).

The first two columns of numbers in Table 2.3 present the values of $\sigma_{v,i}'$ employed by [1] Olson & Stark (2002) and [2] these current studies. The third column then presents the ratio of values of $\sigma_{v,i}'$ calculated/selected by each team for each of the case histories. Agreement between these two sets of independently developed values of representative $\sigma_{v,i}'$ is very good for most of the 30 case histories (and sub-case histories) analyzed by both investigation teams. For 14 of the common cases agreement is within +/- 10% or better, and for all but 7 cases and sub-

cases agreement is within +/- 25% or better. For two cases (Helsinki Harbor and Lake Merced Bank) the ratios of values between the two studies are 1.62 and 0.61. These differences are the result of different choices of failure planes for these cases by the two different investigation teams. Similarly, for the two sub-cases of the Nerlerk Embankment Slides 1 and 2 (of three Nerlerk Embankment slides analyzed by both teams) the ratios are 1.93 and 1.87, again representing differences in failure planes selected by the two investigation teams. This would appear to indicate that the values are largely "correct", as they are mutually well-supported by the two independent research teams of [1] Olson and Stark (2001, 2002) and [2] these current studies.

Overall, the average of the ratios of $\sigma_{v,i}'$ for the 30 cases and sub-cases analyzed by both teams is 1.11, as shown in Table 2.3, representing an excellent level of agreement for such a complex and judgmental exercise. Most of this difference is associated with differences in the failure planes employed for the four cases discussed in the preceding paragraph, but a bit of this difference is associated with the tendency of Olson (2001) to select slightly shallower "most critical" failure planes for a number of cases while these current studies tended to select most critical potential failure surfaces that plunged a bit more deeply. With the four cases and sub-cases highlighted in yellow deleted (as the failure surfaces used by the two studies differ deliberatively for these four cases), the average of the ratios of $\sigma_{v,i}'$ for the remaining 25 cases is 1.04. That appears to represent a strong level of overall agreement.

The fourth column of values in Table 2.3 (marked with a [3]) presents the values of $\sigma_{v,i}'$ selected and employed by Wang (2003). The final column then compares these with the averages of the two studies of [1] Olson & Stark (2002) and [2] these current studies. Agreement is very poor for many of the 28 cases histories in common among all three investigation teams. Values highlighted in yellow (and shown in rounded parentheses) are values where agreement is not within +/- a factor of 1.5 (ratios of less than 0.67 or greater than 1.5), and values highlighted in green are values where agreement is not within +/- a factor of 2 (ratios of less than 0.5 or greater than 2.0).

The most erroneous value of $\sigma_{v,i}'$ is the value of $\sigma_{v,i}'$ = 9,760 lbs/ft^2 for the El Cobre Tailings Dam failure case history. Olson independently back-calculated a representative (average) value of $\sigma_{v,i}'$ = 1,946 lbs/ft^2 for this case history, and the value independently back-calculated in these current studies if $\sigma_{v,i}'$ = 2,075 lbs/ft^2. It appears that there is good agreement that the appropriate value would be on the order of approximately 2,000 lbs/ft^2, or so. The value developed by Wang by combining his estimated S_r from Table 2.1 with his estimated S_r/P from Table 2.2 is 9,760 lb/ft^2, which is too high by a factor of approximately 4.85. There is some small level of uncertainty in assessment of the unit weight of the tailings in this case history, and also in estimation of the phreatic surface at the time of the failure. And there is also some minor level of uncertainty as to the elevation of the largely horizontal failure surface for this case history. But these are relatively minor issues. The overall height of the tailings impoundment would have to be increased at least four-fold (or more) to generate values of $\sigma_{v,i}'$ in the range of Wang's value. This is clearly a physically impossible value; and it serves as one of the three principal variables representing this case history in the subsequent regressions performed by Kramer (2008) and by Kramer and Wang (2015) to develop predictive correlations for S_r as a function of $N_{1,60,CS}$ and $\sigma_{v,i}'$ or $N_{1,60}$ and $\sigma_{v,i}'$.

There are five additional case histories (highlighted in green) in Table 2.3 for which the values of $\sigma_{v,i}'$ selected by Wang (2003) differ from those of [1] Stark & Olson (2002) and [2] these current studies by factors of more than 2, and there are three additional cases where the factors of difference are greater than 1.8. All of these are associated with cases for which better values appear to be well established by good agreement between the values independently back-calculated by [1] Stark & Olson (2002) and [2] these current studies. Accordingly, these appear to be physically unreasonable values. Nine of the values of $\sigma_{v,i}'$ selected by Wang (2003) appear to be physically unreasonable, and at least six additional values appear to be in at least relatively poor agreement with the values of [1] Stark & Olson (2002) and [2] these current studies.

These errors appear to be mainly the result of the poor procedure of employing incompatible "averaged" values of S_r from Table 2.1 with "averaged" values of S_r/P from Table 2.2 to calculate "P" ($\sigma_{v,i}'$), but two of the cases (highlighted in yellow in Table 2.3) with poor agreement are two of Wang's nine "primary" cases [Uetsu Railway Embankment, and Hachiro-Gata Road Embankment], and it is less clear why these two cases match poorly.

In all but two of the 15 cases for which Wang (2003) appears to have selected either poor or physically unreasonable values of $\sigma_{v,i}'$, the values selected by Wang are far too high. These errors were carried forward into the regressions and resulting predictive correlations subsequently developed by Kramer (2008) and published by Kramer and Wang (2015). As shown in Table 2.3, the overall average ratio of Wang's selected values of $\sigma_{v,i}'$ relative to the values selected by [1] Olson and Stark (2002) and [2] these current studies is approximately 1.57. The effect of these erroneous (high) values of $\sigma_{v,i}'$ would be to "stretch" the $\sigma_{v,i}'$ values to the high side in the regressions performed; resulting in somewhat conservative under-predictions of S_r for any given actual (real) value of $\sigma_{v,i}'$. This conservative bias appears to outweigh the somewhat unconservative bias introduced in some of the evaluations of S_r for some of the Secondary cases, as discussed in the previous Section 2.3.8.1(b)-(ii). This will be discussed further in Chapters 5 and 6.

2.3.8.2 Regressions and Predictive Relationships of Kramer (2008)

Table 2.4 shows the values of two of the three principle indices, and their modeled variances, as listed in Table G.4 of Kramer (2008). These are the values from Wang's (2003) studies, and they are directly comparable to the values developed in these current studies. Unfortunately, Table G.4 made an error in listing values of $N_{1,60,CS}$, as Kramer (2008) actually elected instead to base his regressions on non-fines-corrected $N_{1,60}$ values instead. He found that variance was little different when using either $N_{1,60}$ or $N_{1,60,CS}$, and he elected to switch to $N_{1,60}$ (Kramer, 2015). The other values in Table 2.4 (penetration resistances and initial effective stresses) are correct, and match those used in the regressions of Kramer (2008). A second error in Table G.4 was the omission of the values of $\sigma_{v,i}'$ and of variance in $\sigma_{v,i}'$ for each case history.

Because of these two errors in Table G.4, the actual values used in the regressions of Kramer (2008) were only eventually published in Kramer and Wang (2015). Table 2.5 shows the values of the three principle indices, as employed in the regressions performed by Kramer (2008) and published by Kramer and Wang (2015).

This table does not show values of variance for the three indices, so there are still no published values available documenting the variances of $N_{1,60}$ and $\sigma_{v,i}'$ for each of the case histories. As a result, in these current studies cross-comparisons will be made using the published values of variances in $N_{1,60,CS}$ from Wang (2003) which should be closely similar to variances in $N_{1,60}$, based on the procedures used to develop them. No published values of variance in $\sigma_{v,i}'$ are available, and so no cross-comparisons or checks can be made for those.

The resulting $N_{1,60}$-based equation is not fully compatible for direct cross-comparison with the relationship developed by these current studies due to the differences between $N_{1,60,CS}$ and $N_{1,60}$. Neglecting fines corrections would intrinsically tend to introduce a potentially conservative bias if the regressed relationship was then subsequently applied to sands with lesser fines contents. The overall relationship was already significantly conservatively biased due to errors in derivation of a number of the representative $\sigma_{v,i}'$ values used to represent 13 of the case histories (as discussed previously in Section 2.8.3.1, Part 3). This bias due to erroneous $\sigma_{v,i}'$ values would significantly outweigh any additional (and much lesser) conservative bias introduced by the use of $N_{1,60}$ instead of $N_{1,60,CS}$. This will be discussed further in Chapter 5.

The weighting factors shown in Tables 2.4 and 2.5 are potentially important. These weighting factors were developed by Kramer (2008) in order to account for the variable quality of information and documentation of data available for the individual case histories. Poorer documentation would be expected to lead to higher levels of uncertainty. Unfortunately, full details involved in development of these weighting factors are not presented. They appear to have been a matter of engineering judgment. That said, they do appear to be generally reasonable in the view of the current investigation team, although any two different investigation teams would likely have differences of opinion as to the details or the relative weighting factor assigned for any specific case history. (In these current studies, it was preferred to incorporate uncertainties associated with poor documentation of information and data, as well as with the variable quality of data, directly in the variances ascribed to the key regression parameters; so no additional weighting factors were applied in these current studies.) Weighting factors in Table 2.4 range from w = 1.0 for well documented cases, to very low values for poorly documented cases. The two cases with the lowest assigned weighting factors are Asele Road (w = 0.20) and the Soviet Tajik - May 1 Slide (w = 0.22). With these very low weighting factors, these two cases are virtually eliminated.

Kramer (2008) performed a large number of nonlinear least squares regressions to ascertain the forms of useful predictive relationships (general equation forms) that would be well suited to the data set and provide generally good model fit across the domain of the data set. He then performed fully probabilistic Bayesian regressions using the maximum likelihood method to develop a better probabilistically based relationship incorporating all uncertainties. This relationship was what Kramer described as a "hybrid" model, with predicted values of S_r being dependent upon both SPT penetration resistance and initial effective vertical stress.

In examining the resulting predictive correlation, Kramer observed that values of S_r predicted at very low initial effective stresses appeared to be unreasonably low. He reasoned that if such values actually occurred, then larger numbers of very shallow flow slides would be observed. He examined the suite of available field case history data for lateral spreading cases

(not flow slides) developed by Youd et al. (2002), and reasoned that the value of S_r within the liquefied materials for each of these lateral spreading cases must have been at least as large as the static driving shear stress; otherwise these would have been flow failure case histories rather than lateral spreads. He made simplified estimates of the static driving stresses at shallow depth for these cases, based on an infinite slope assumption, and in this manner estimated the minimum (lower bound) potential value of S_r for each lateral spreading case at initial vertical effective stresses of less than 0.6 atmospheres. These were plotted vs. effective vertical effective, and the resulting plot is shown in Figure 2.25. Based on this, but without explanation of details, Kramer concluded that one of his model fitting parameters (Θ_4) would be modified to slightly increase the values of S_r predicted at very low confining stresses. This was a "judgmental" manipulation, and it served to correct what appear to have been overly conservative predictions of S_r at low initial effective stresses.

His regressed model, with the parameters developed by the maximum likelihood method, but with variance or uncertainty developed based on First Order Second Moment analyses, and with Θ_4 thus slightly constrained, was then reformulated into a more tractable form for use by engineers. The final proposed relationship was then

$$\overline{\ln S_r} = -8.444+0.109N+5.379S^{0.1} \qquad \text{[Eq. 2-4]}$$

where

$$\sigma_{\ln S_r} = \sqrt{\sigma_m^2+0.00073\bar{N}^2\ COV_N^2+4.935S^{-0.2}\ COV_S^2} \qquad \text{[Eq. 2-4a]}$$

and

$$\sigma_m^2 = 1.627+0.00073N^2+0.0194N-0.27NS^{0.1}-3.099S^{0.1}+1.621S^{0.2} \qquad \text{[Eq. 2-4b]}$$

where $N=(N_1)_{60}$, $S=\sigma'_{vo}$(in atm), $\bar{N}$ is the mean value of $(N_1)_{60}$, COV_N is the coefficient of variation of SPT resistance, $\bar{S}$ is the mean initial vertical effective stress (in atm), and COV_S is the coefficient of variation of initial vertical effective stress.

Figure 2.26 shows the median (50th percentile) values of S_r based on this relationship. A series of curves are shown relating S_r to $\overline{N_{1,60,CS}}$, with each curve labeled with the value of $\overline{\sigma'_{vo}}$ for which that curve would apply. The overall relationship is fully probabilistically based, and similar curves can be developed and plotted for other percentiles or likelihoods of exceedance.

Kramer then went on to further consider appropriate levels of conservatism for "deterministic" values of S_r for engineering applications, and determined that 40th percentile values would be appropriate here. These values, recommended for routine geotechnical design, are shown in Figure 2.27.

2.3.8.3 Predictive Relationship of Kramer & Wang (2015)

The predictive relationship developed by Kramer (2008) was subsequently published by Kramer and Wang (2015). This publication presented the actual values of $N_{1,60}$ and of $\sigma_{N1,60}$ that had been employed in the regressions to develop their predictive relationship.

The form of the equation expressing the regressed relationship as published in Kramer and Wang (2015) is

$$\overline{\ln S_r} = -8.444+0.109N+5.379S^{0.1} \qquad \text{[Eq. 2-5]}$$

where

$$\sigma^2_{\ln S_r} = 1.627 +0.00073N^2+0.0194N-0.027NS^{0.1} -3.099S^{0.1}+1.621S^{0.2}+0.00073\sigma^2_N+4.935S^{-1.8}\sigma^2_S \qquad \text{[Eq. 2-5a]}$$

The best-fit mean value surface (Equation 2-5) is exactly identical to the best-fit mean value surface equation of Equation 2-3 from the previous $N_{1,60,CS}$-based formulation. It is only the error term (Equation 2-5a) that has been reformatted slightly from the original publication by combining Equations 2-4a and 2-4b.

2.3.9 Idriss and Boulanger (2008)

Idriss and Boulanger (2008) considered a subset of 18 of the 33 large-displacement liquefaction failure case histories in the data set complied by Olson and Stark (2002). The basis for selection of each of these was not explicitly explained, but it is understood that they selected the cases that they felt were best characterized and best documented, and deleted the rest. They then categorized each of these 18 case histories into one of three groups; Groups 1, 2, and 3. Group 1 were the cases considered to be those that were best characterized and documented, and Group 3 those that were least well characterized.

They did not perform any of their own independent back-analyses of these 18 case histories. Instead, they next adopted the values developed from back-analyses by (1) Seed (1987), (2) Seed and Harder (1990), and (3) Olson and Stark (2002) for those cases which each of these previous teams had analyzed. Ten of the cases had been back-analyzed by Seed (1987), 13 by Seed and Harder (1990) and all 18 by Olson and Stark (2002). Values of S_r back-calculated by Seed (1987) and by Seed and Harder (1990) were normalized by dividing by estimated representative values of effective vertical stress to develop post-liquefaction strength ratios for each case.

The resulting values of strength ratio (S_r/P) were then plotted vs. $N_{1,60,CS}$ values developed by each of the three previous investigation teams. Values of $N_{1,60}$ developed by Olson were modified to approximate $N_{1,60,CS}$ values here. The results are shown in Figure 2.28. In this figure, the shapes of the symbols identify the investigation team responsible for the values of S_r and

$N_{1,60,CS}$ plotted, and the sizes of the symbols indicate whether the case was considered by Idriss and Boulanger to be a Group 1 (high quality) or Group 2 and 3 (lower quality) case.

A line was drawn through these plotted data (the solid line in the lower left-hand portion of the figure), based on judgment, and this line was then extended as a dashed line to express additional judgment as to the likely extrapolation to higher $N_{1,60,CS}$ values. An equation was then fitted to this proposed relationship for ease of implementation in spreadsheet calculations and similar.

A second dashed line was then added, inflecting steeply upwards, to represent recommended values of S_r as a function of $N_{1,60,CS}$ for situations in which void redistribution effects are expected to be negligible. This upper line is not well explained, but it is independent of the back-analyzed field case history data plotted, and it is reportedly based primarily on laboratory test data.

There are a number of problems and drawbacks in this proposed relationship, and with the figure presented. The first of these is the fact that the large, solid "dot" plotted at $N_{1,60,CS}$ = 15 blows/ft and $S_r/P \approx 0.21$ (Point "A" in Figure 2.29) represents the S_r value initially proposed by Seed (1987) for the Lower San Fernando Dam case history. As discussed previously in Section 2.3.1, Prof. H. B. Seed later reconsidered this and concluded that this was an error and that the strength that he had originally proposed was too high. Seed and Harder (1990) and Olson (2001) both back-analyzed this case, and both had developed lower S_r values. The values of Seed and Harder (1990) and Olson and Stark (2002) are in such close agreement that they plot largely over each other in Figure 2.29 (Points B & C in this figure). For clarity, Figure 2.29 repeats Figure 2.28, but this time the erroneous data point for Lower San Fernando Dam is circled with a dashed line (and partly dimmed), and the locations of the (arguably more correct) plots of the data points developed by Seed and Harder, and by Stark and Olson, for the Lower San Fernando Dam are clearly indicated.

This changes the figure significantly, especially on a visceral (graphical) basis. It removes the large "dot" that otherwise appears to "anchor" the upper dashed curve. This dot was never actually part of the upper curve, because all of the back-analyzed field case histories were actually ascribed to situations wherein void redistribution was assumed to have potentially occurred (and so all field cases back-analyzed are associated with the lower curve, not the upper curve). But many engineers do not read text, and simply view the figure and assume that the upper curve is somehow associated with this (very prominent) erroneous data point.

With the erroneous data point thus relocated, Figure 2.29 then shows clearly the very large degree of engineering judgment involved in recommending the upwards bending curve to extrapolate the lower solid line's recommended relationship to values of $N_{1,60,CS}$ greater than about 15 blows/ft. There is nothing obvious in the data, as presented, that supports this interpretation. Neither the slope of the lower portion of the curve, nor the upwards inflection of the upper part of the curve, can be reliably ascribed to the data as plotted.

It should also be noted that six data points plot high in the upper left-hand corners of Figures 2.28 and 2.29. These six high "floating" points are unexplained by this relationship, as

presented and described by Idriss and Boulanger, but it turns out that they are actually well-explained by the predictive relationships developed by Wang and Kramer (see Section 2.3.8) and by these current studies (see Chapter 5).

Finally, it should be noted that the "upper" dashed line is intended to be applied only to field cases in which void redistribution will not be significant. It has proven difficult to define such cases in the field. Many engineers are well used to having an upper bound and lower bound relationship proposed (as with Seed and Harder, 1990, Stark and Mesri, 1992, and Olson and Stark, 2002) and so they are used to interpolating between the upper and lower bounds as presented to select values of post-liquefaction strength for actual projects. This is not the apparent intent of Idriss and Boulanger who intend the lower line to represent not a "lower bound" but rather the "recommended" values for field cases wherein void redistribution effects can occur (most field situations), and who intend the upper dashed line (which was based on laboratory test data rather than back-analyzed field case histories) to represent not an "upper bound" but rather a second relationship for situations in which void redistribution effects will not be significant.

Idriss and Boulanger also present their selected data points, and recommended relationships, in the form of S_r (not S_r/P), and these are shown in Figure 2.30. The same issues discussed above apply here as well. This includes the large solid "dot" representing the values initially proposed by Seed (1987) for the Lower San Fernando case history. Relocation of this data point (to the positions determined by Seed and Harder, 1990, and by Olson and Stark, 2002) is illustrated in Figure 2.31.

2.3.10 Olson and Johnson (2008)

Olson and Johnson (2008) recognized the paucity of liquefaction-induced failure case histories for back-analyses of post liquefaction strengths at full field scale. To address this, they collected a large number of available liquefaction-induced lateral spreading case histories (39 cases). Lateral spreading case histories differ from liquefaction flow failure case histories in that they experience more limited displacements, and a large fraction of their displacements are often driven primarily by cyclic inertial lurching during strong earthquake shaking. Lateral spreads tend to be of finite thickness and/or slope (though they can sometimes be very large), and thus the initial (pre-earthquake) gravity-induced static shear stresses tend in most cases to be equaled or overshadowed by the cyclic "lurching" induced stresses during strong shaking.

Accordingly, Olson and Johnson applied various Newmark-type analyses (Newmark, 1965) to back-analyze the displacements observed in the field for these cases in order to estimate the post-liquefaction strengths involved. Newmark-type analyses are not a very precise analysis methodology (e.g. Bray and Rathje, 1998) and this was further exacerbated by the sensitivity of calculated displacements to the intensity and details of actual earthquake shaking at each site, and the lack of site-specific ground motion records for each case. As a result, there was significant scatter (or variance/uncertainty) in the resulting estimates of S_r for each case.

A tentative recommended relationship between strength ratio (S_r/P) and penetration resistance was developed, but the large variance or uncertainty made this of little apparent value

relative to relationships already available. In the end, the most important lessons from this study were: (1) the difficulty of assessing S_r based on performing back-analyses of cases with only limited displacements wherein cyclic lurching generates a significant fraction of the overall displacements that accrue, and (2) the difficulty of extracting back-analyzed values of S_r by means of simplified Newmark-type analyses.

2.3.11 Gillette (2010)

Faced with the apparently conflicting views that post-liquefaction strengths might best be evaluated [1] based on a "classical" critical state basis using post-liquefaction strength S_r assumed to be independent of effective overburden stress, or [2] on the basis of post-liquefaction strength ratio (S_r/P) with an assumed linear dependence between S_r and initial effective vertical stress, a number of engineers have recommended a middle position.

Baziar and Dobry (1995) had used back-analysis results from liquefaction case histories developed by previous investigators, and had proposed a predictive relationship for S_r that was a function of both $N_{1,60,CS}$ and also effective vertical stress. Unfortunately, that relationship was posed in the form of a figure that was not intuitively transparent, and their relationship did not receive the attention that it may have warranted.

Seed et al. (2003) had suggested that the best answer likely lay somewhere in between these two extreme views, and that there was likely a significant influence of initial effective stress on S_r, but that it was not likely that S_r was fully linearly correlated with initial effective vertical stress. They recommended evaluating S_r based on each approach (S_r and S_r/P), and then averaging the two results (with weighting factors varying a bit as a function of fines content) to produce values of S_r with some partial dependence on initial effective vertical stress until this could be better resolved. This was an interim suggestion, until better "hybrid" approaches could be developed.

As described in Section 2.3.7, Kramer (and Wang) developed "hybrid" predictive correlations for post-liquefaction strength based on both SPT penetration resistance and effective vertical effective stress, with the influence of vertical effective stress modeled as not being linearly related to S_r.

Gillette (2010) used a selected subset of the back-analyzed data bases of Seed and Harder (1990) and Olson and Stark (2002), and performed least squares regressions implementing a number of relatively simple potential equational forms that allowed for varying levels of partial (or nonlinear) dependence of S_r on initial effective vertical overburden stress. His resulting best fit relationship employing back-analysis results for S_r from Seed and Harder (1990) with effective vertical stresses estimated by Olson and Stark (2002) was

$$S_{ur}=0.64\ (N_1)_{60\text{-}cs}^{1.35}+0.1\ \sigma'^{0.80}_{vo}-2.3\pm6\ \text{kPa} \quad \text{with} \quad R^2 \approx 0.78 \qquad \text{[Eq. 2-6]}$$

This R^2 value of 0.78 is significantly higher than the R^2 values previously calculated for the relationships proposed by Seed and Harder (1990), by Stark and Mesri (1992) and by Olson and Stark (2002) in Sections 2.3.1, 2.3.2 and 2.3.6 respectively, further supporting the merit of a middle position wherein S_r would be taken as being nonlinearly dependent upon both penetration resistance and also initial vertical effective stress. But it does not improve on the level of predictive "fit" achieved in the eventual Bayesian regressions presented in later sections of this current report. This is likely due in part to the improved back-analysis methods applied to the field performance case histories, and to the careful wielding of the Bayesian regression methodology in these current studies.

Table 2.1: Compilation of selected values of post-liquefaction strength (S_r) from previous investigations for the 22 Secondary Case Histories and the representative mean values adopted by Wang (2003) as reported in Table 6.8 from Wang (2003).

Case	References	S_r Values (psf)	Mean S_r (psf)
Asele Road	Konrad and Watts (1995) Olson (2001)	11 241	164
Chonan Middle School	Ishihara et al (1990) Ishihara (1993) Olson (2001)	167 194 178	179
El Cobre	Olson (2001)	195	195
Helsinki Harbor	Olson (2001)	53	53
Hokkaido Tailings	Ishihara et al. (1990a) Olson (2001)	408 172	251
Kawagishi-cho	Seed (1987) Seed and Harder (1990) Stark and Mesri (1992)	120 120 120	120
Koda Numa	Lucia (1981); Lucia et al. (1982) Seed (1987) Seed (1987) Olson (2001)	25 50 50 66	48
La Marquesa Downstream	De Alba et al. (1987) Seed and Harder (1990) Stark and Mesri (1992) Olson (2001)	423 400 400 190	344
La Marquesa Upstream	De Alba et al. (1987) Seed and Harder (1990) Stark and Mesri (1992) Olson (2001)	208 200 200 129	181
Lake Merced	Seed (1987) Seed and Harder (1990) Stark and Mesri (1992) Olson (2001)	100 100 100 257	139
La Palma Dam	De Alba et al. (1987) Seed and Harder (1990) Stark and Mesri (1992) Olson (2001)	210 200 200 156	189

Table 2.1 (Cont'd): Compilation of selected values of post-liquefaction strength (S_r) from previous investigations for the 22 Secondary Case Histories and the representative mean values adopted by Wang (2003) as reported in Table 6.8 from Wang (2003).

Case	References	S_r Values (psf)	Mean S_r (psf)
Metoki Road	Olson (2001)	113	133
Mochi Koshi Dike 1	Poulos (1988)	60	159
	Davis et al. (1988)	60	
	Olson (2001)	258	
Mochi Kosho Dike 2	Lucia (1981); Lucia et al. (1982)	210	234
	Seed (1987)	210	
	Seed (1987)	210	
	Poulos (1988)	250	
	Seed and Harder (1990)	250	
	Stark and Mesri (1992)	250	
	Olson (2001)	223	
Nalband	Yegian et al.(1994)	117	140
	Olson (2001)	152	
Nerlerk Berm 1	Sladen et al (1985a)	42	179
	Jeffries et al. (1990)	308	
	Stark and Mesri (1992)	300	
	Olson (2001)	54	
Sheffield Dam	Seed (1987)	50	100
	Seed and Harder (1990)	75	
	Stark and Mesri (1992)	75	
	Olson (2001)	198	
Snow River	Seed (1987)	50	50
	Seed and Harder (1990)	50	
	Stark and Mesri (1992)	50	
Solfatara Canal	Seed (1987)	130	77
	Seed and Harder (1990)	50	
	Stark and Mesri (1992)	50	
	Olson (2001)	88	
Soviet Tajik - May 1 Slide	Ishihara et al (1990b)	167	334
	Olson (2001)	418	
Tar Island Dike	Plewes et al. (1989)	305	346
	Konrad and Watts (1995)	80	
	Olson (2001)	500	
Zeeland	Olson (2001)	226	226

Table 2.2: Compilation of selected values of post-liquefaction strength ratio (S_r/P) from previous investigations for the 22 Secondary Case Histories and the representative mean values adopted by Wang (2003) as reported in Table 6.8 from Wang (2003)

Case	References	S_r/σ'_{vo} Values	Mean S_r/σ'_{vo}
Asele Road	Olson and Stark (2002)	0.104	0.104
Chonan Middle School	Olson and Stark (2002)	0.091	0.091
El Cobre	Olson and Stark (2002)	0.020	0.020
Helsinki Harbor	Olson and Stark (2002)	0.060	0.060
Hokkaido Tailings	Olson and Stark (2002)	0.074	0.074
Kawagishi-cho	Stark and Mesri (1992)	0.098	0.087
	Olson and Stark (2002)	0.075	
Koda Numa	Stark and Mesri (1992)	0.032	0.045
	Wride et al. (1999)	0.032	
	Olson and Stark (2002)	0.040	
La Marquesa Downstream	Stark and Mesri (1992)	0.224	0.186
	Wride et al. (1999)	0.223	
	Olson and Stark (2002)	0.110	
La Marquesa Upstream	Stark and Mesri (1992)	0.125	0.107
	Wride et al. (1999)	0.125	
	Olson and Stark (2002)	0.070	
Lake Merced	Stark and Mesri (1992)	0.105	0.106
	Wride et al. (1999)	0.105	
	Olson and Stark (2002)	0.108	
La Palma Dam	Stark and Mesri (1992)	0.120	0.120
	Olson and Stark (2002)	0.120	
Metoki Road	Olson and Stark (2002)	0.043	0.043
Mochi Koshi Dike 1	Stark and Mesri (1992)	0.092	0.091
	Wride et al. (1999)	0.015	
	Olson and Stark (2002)	0.060	
Mochi Kosho Dike 2	Stark and Mesri (1992)	0.092	0.081
	Wride et al. (1999)	0.048	
	Olson and Stark (2002)	0.104	
Nalband	Olson and Stark (2002)	0.109	0.109
Nerlerk Berm	Jeffries et al (1990)	0.150	0.124
	Stark and Mesri (1992)	0.148	
	Olson and Stark (2002)	0.086	
Sheffield Dam	Stark and Mesri (1992)	0.038	0.043
	Wride et al. (1999)	0.038	
	Olson and Stark (2002)	0.053	
Snow River	Stark and Mesri (1992)	0.024	0.024
Solfatara Canal	Stark and Mesri (1992)	0.052	0.063
	Wride et al. (1999)	0.052	
	Olson and Stark (2002)	0.080	
Soviet Tajik - May 1 Slide	Olson and Stark (2002)	0.082	0.082
Tar Island Dike	Olson and Stark (2002)	0.058	0.058
Zeeland	Olson and Stark (2002)	0.048	0.048

Table 2.3: Cross-comparison of values of initial effective vertical stress employed by [1] Olson & Stark (2002), [2] These Current Studies, and [3] Kramer and Wang (2015)

Class	Case	[1] Olson & Stark (2002) σ'_{vo} (psf)	[2] Current Studdies σ'_{vo} (psf)	Ratio of [2]/[1]	[3] Kramer and Wang (2015) σ'_{vo} (psf)	Ratio of [3]/(0.5 x ([1]+[2]))
A	Wachusett Dam - North Dike	3158	3142	0.99	2558	0.81
	Fort Peck Dam	7341	7258	0.99	7466	1.02
	Uetsu Railway Embankment	1280	1448	1.13	916	(0.67)
	Lower San Fernando Dam - U/S Slope	3482	3174	0.91	3538	1.06
	Hachiro-Gata Road Embankment	670	673	1.00	398	(0.59)
	La Marquesa Dam - U/S Slope	911	981	1.08	1682	(1.78)
	La Marquesa Dam - D/S Slope	1000	1215	1.22	1850	(1.67)
	La Palma Dam	789	767	0.97	1577	[2.03]
	Lake Ackerman Highway Embankment	1076	909	0.84	838	0.84
	Chonan Middle School	1119	1032	0.92	1968	(1.83)
	Soviet Tajik - May 1 Slide	2170	1907	0.88	4122	[2.02]
	Shibecha-Cho Embankement	1351	1416	1.05	1048	0.76
	Route 272 at Higashiarekinai	1030	1285	1.25	1043	0.90
B	Zeeland - Vlietepolder	2396	2488	1.04	4708	(1.93)
	Sheffield Dam	1429	1308	0.92	1389	1.01
	Helsinki Harbor	522	846	(1.62)	887	1.30
	Solfatara Canal Dike	624	669	1.07	1224	(1.89)
	Lake Merced Bank	1372	834	(0.61)	1316	1.19
	El Cobre Tailings Dam	1946	2075	(1.07)	9760	[4.85]
	Metoki Road Embankment	875	871	1.00	2655	[3.04]
	Hokkaido Tailings Dam	1376	1203	0.87	3386	[2.63]
	Upper San Fernando Dam - D/S Slope		3138	N/A		
	Tar Island Dyke	4300	4197	0.98	6279	1.48
	Mochi-Koshi Tailings Dam, Dikes 1 and 2	1251	1564	1.25	1746	1.24
		1090	1447	1.33	2884	[2.27]
	Nerlerk Embankment, Slides 1, 2, and 3	616	1186	(1.93)	1440	(1.60)
		650	1215	(1.87)		
		925	1277	1.38		
	Asele Road Embankment	1251	1037	0.83	1573	1.38
	Nalband Railway Embankment	1101	1209	1.10	1283	1.11
	Sullivan Tailings		2422	N/A		
	Jamuna Bridge		1404	N/A		
C	Calaveras Dam	6422	7097	1.11	6850	1.01
				Avg. = 1.11		Avg. = 1.57

Notes : (Round parentheses) = Ratio <0.67 or >1.5
[Square parentheses] = Ratio <0.5 or >2.0

Table 2.4: Component values and final weighting factors for all case histories as presented in Table G.4 (from Kramer, 2008)

Case History	$\overline{N}$	σ_N	$\overline{S_r}$	σ_{S_r}	w_{total}
Asele Road	11.0	10.7	163.6	54.6	0.20
Calaveras Dam	10.5	9.7	636.9	223.1	0.55
Chonan Middle School	6.4	6.9	178.7	32.0	0.74
El Cobre Tailings Dam	6.8	0.9	195.2	64.8	0.60
Fort Peck Dam	15.8	0.9	671.6	130.2	0.85
Hachiro-Gata Roadway	5.7	2.8	65.0	24.7	0.55
Helsinki Harbor	5.9	8.0	53.2	19.0	0.39
Hokkaido Tailings	5.1	1.4	250.6	71.9	0.31
Kawagishi-cho Building	4.3	1.2	123.5	56.7	0.50
Koda Numa Embankment	3.6	4.1	48.0	15.9	0.44
Lake Ackerman Roadway	4.8	1.2	98.0	20.4	1.00
La Marquesa Downstream	9.9	3.0	343.5	113.8	0.72
La Marquesa Upstream	6.5	2.8	185.1	82.1	0.76
La Palma Dam	4.2	1.8	193.3	86.3	0.80
Lake Merced Bank	5.9	8.0	139.5	41.4	0.39
Lower San Fernando Dam	14.5	1.1	484.7	111.0	1.00
Metoki Road	2.0	1.5	116.8	53.7	0.39
Mochi Koshi Tailings Dam 1	8.9	0.6	158.9	47.7	0.34
Mochi Koshi Tainilgs Dam 2	10.0	1.3	233.6	78.0	0.67
Nalband Railway	6.3	5.6	139.9	40.2	0.51
Nerlerk Berm	11.4	7.7	179.1	32.1	0.41
Route 272 Roadway	8.5	2.6	130.5	33.5	0.70
Sheffield Dam	8.2	6.8	100.0	29.8	0.37
Shibecha-Cho Embankment	5.6	2.2	208.9	38.6	0.70
Snow River Bridge Fill	8.5	9.0	50.1	16.6	0.50
Solfatara Canal Dike	4.9	6.9	77.1	25.6	0.42
Soviet Tajik – May 1 Slide	8.9	5.7	334.3	110.9	0.22
Tar Island Dike	8.9	9.7	364.2	115.6	0.32
Uetsu-Line Railway	2.9	4.2	43.7	24.8	0.55
Wachusett Dam	7.3	1.9	348.0	74.8	1.00
Zeeland	8.5	5.5	226.0	75.0	0.39

Table 2.5: Component values and final weighting factors for all case histories as employed in the regressions performed (from Kramer & Wang, 2015)

Case history type	Case history	Weighting factor	SPT resistance	Fines content (%)	Initial vertical effective stress (atm)	Residual strength (atm)
Primary	Calaveras Dam	0.55	7.9	34	3.237	0.311
	Fort Peck Dam	0.85	11.7	54	3.528	0.322
	Hashiro-Gata	0.55	4.4	15	0.188	0.030
	Lake Ackerman	1.00	4.8	0	0.396	0.045
	Lower San Fernando Dam	1.00	12.6	25	1.672	0.240
	Route 272	0.70	6.6	33	0.493	0.061
	Shibeca-Cho	0.70	3.7	20	0.495	0.099
	Uetsu	0.55	3.0	0	0.433	0.021
	Wachusett Dam	1.00	7.3	8	1.209	0.164
Secondary	Asele road	0.20	8.9	32	0.310	0.060
	Chonan	0.74	5.1	18	0.930	0.085
	El Cobre Tailings Dam	0.60	1.2	95	4.608	0.092
	Helsinki Harbor	0.39	6.1	0	0.417	0.025
	Hokkaido	0.31	1.1	50	1.603	0.119
	Kawagishi-cho	0.50	4.3	2	0.646	0.058
	Koda Numa	0.44	3.05	40	0.504	0.023
	La Marquesa D/S	0.72	8.2	20	0.874	0.163
	La Marquesa U/S	0.76	4.1	30	0.795	0.087
	La Palma Dam	0.80	2.9	15	0.745	0.092
	Lake Merced	0.39	6.1	0	0.620	0.066
	Metoki road	0.39	2.1	0	1.246	0.055
	Mochi-Koshi 1	0.34	4	73	0.826	0.075
	Mochi-Koshi 2	0.67	5.2	73	1.365	0.111
	Nalbland	0.51	4	30	0.607	0.066
	Nerlerk Berm	0.41	10.6	10	0.682	0.085
	Sheffield Dam	0.37	5	40	1.099	0.047
	Snow River	0.50	7	20	0.984	0.024
	Solfatara	0.42	5.1	0	0.578	0.036
	Soviet Tajik	0.22	7.6	15	1.948	0.158
	Tar Island	0.32	8.2	13	2.966	0.172
	Zeeland	0.39	7.7	11	2.225	0.107

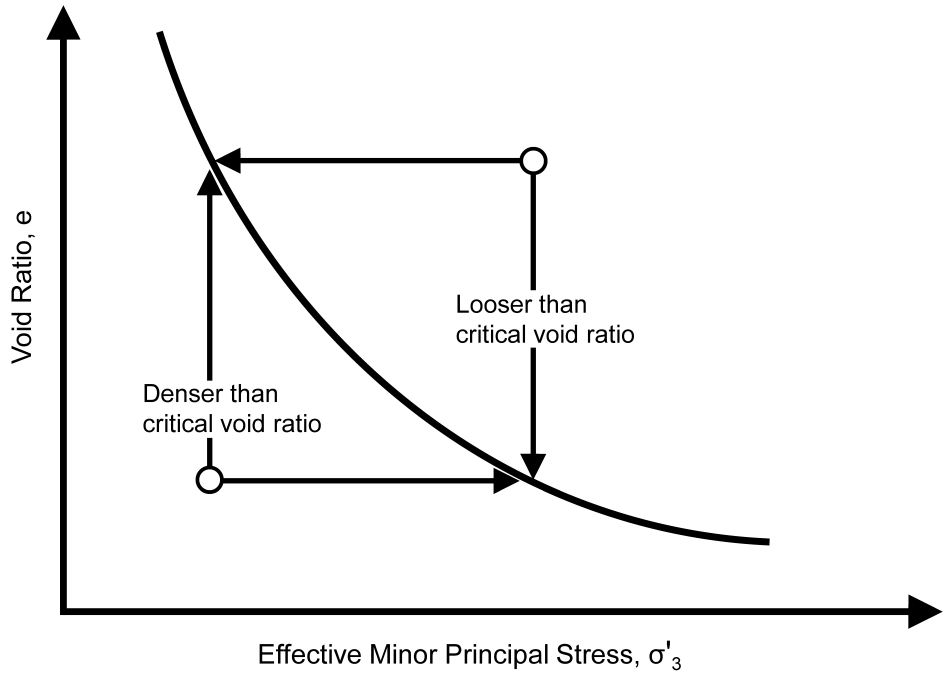

Figure 2.1: Simplified representation of the critical state line.

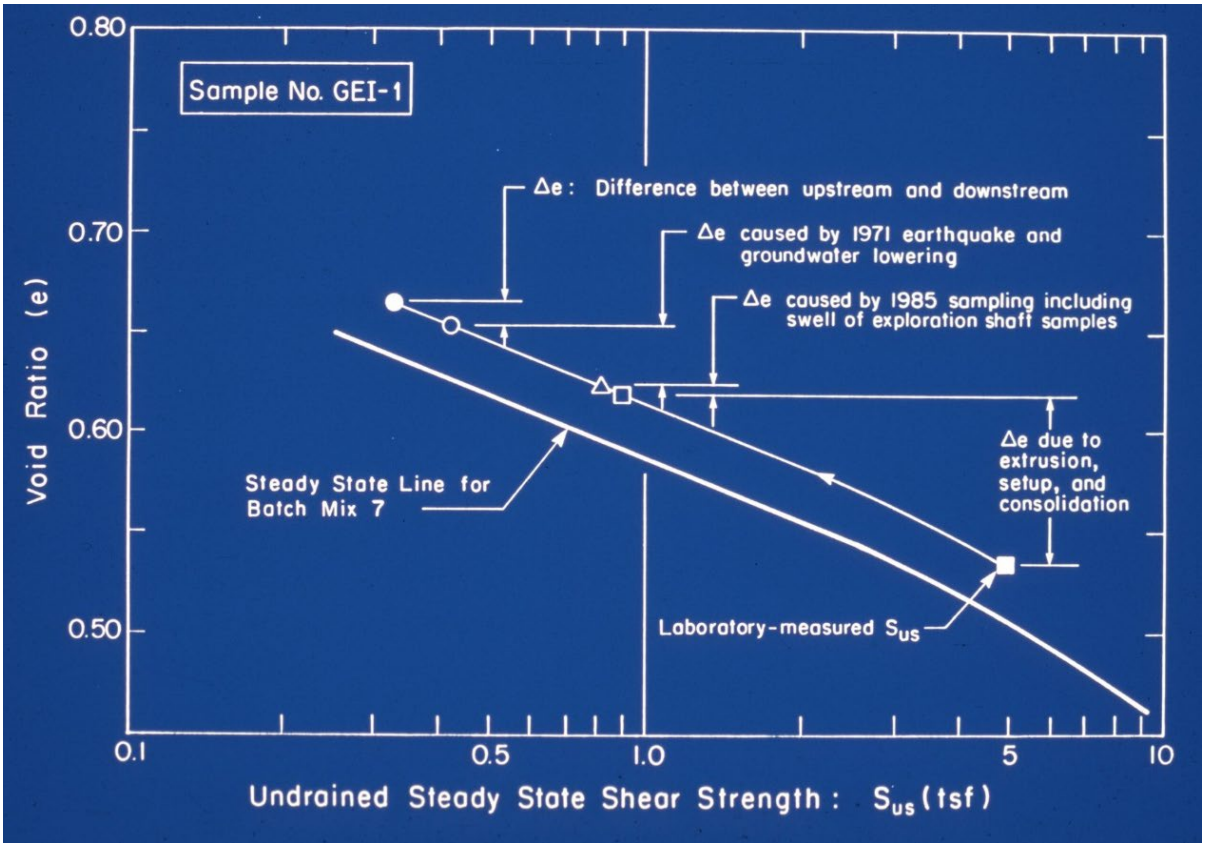

Figure 2.2: Illustration of the Steady State method of Poulos, et al. (1985) for assessing post-liquefaction strength for a sample of silty sand hydraulic fill from the Lower San Fernando Dam (Castro et al., 1992)

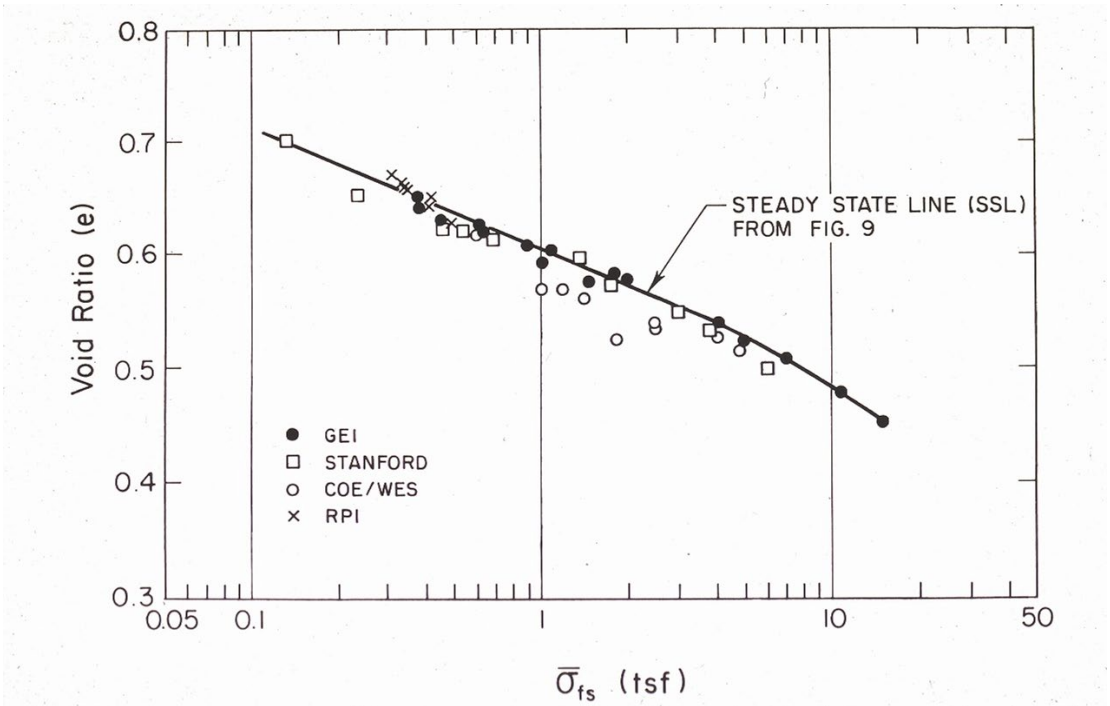

Figure 2.3: Steady state line based on IC-U triaxial tests performed by four laboratories on re-constituted samples of silty sand hydraulic fill from the lower portions of the down-stream shell of the Lower San Fernando Dam. (Figure from Castro, et al., 1992)

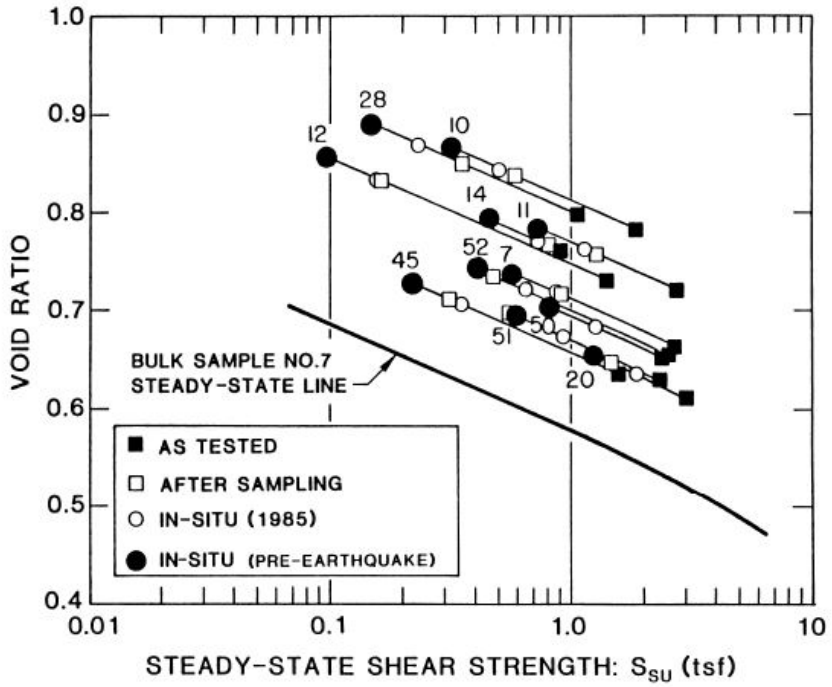

Figure 2.4: Corrections of IC-U triaxial tests of silty sand hydraulic fill from the Lower San Fernando Dam by the steady state method in order to develop estimates of in situ undrained steady state strengths. (Figure from Seed et al., 1988)

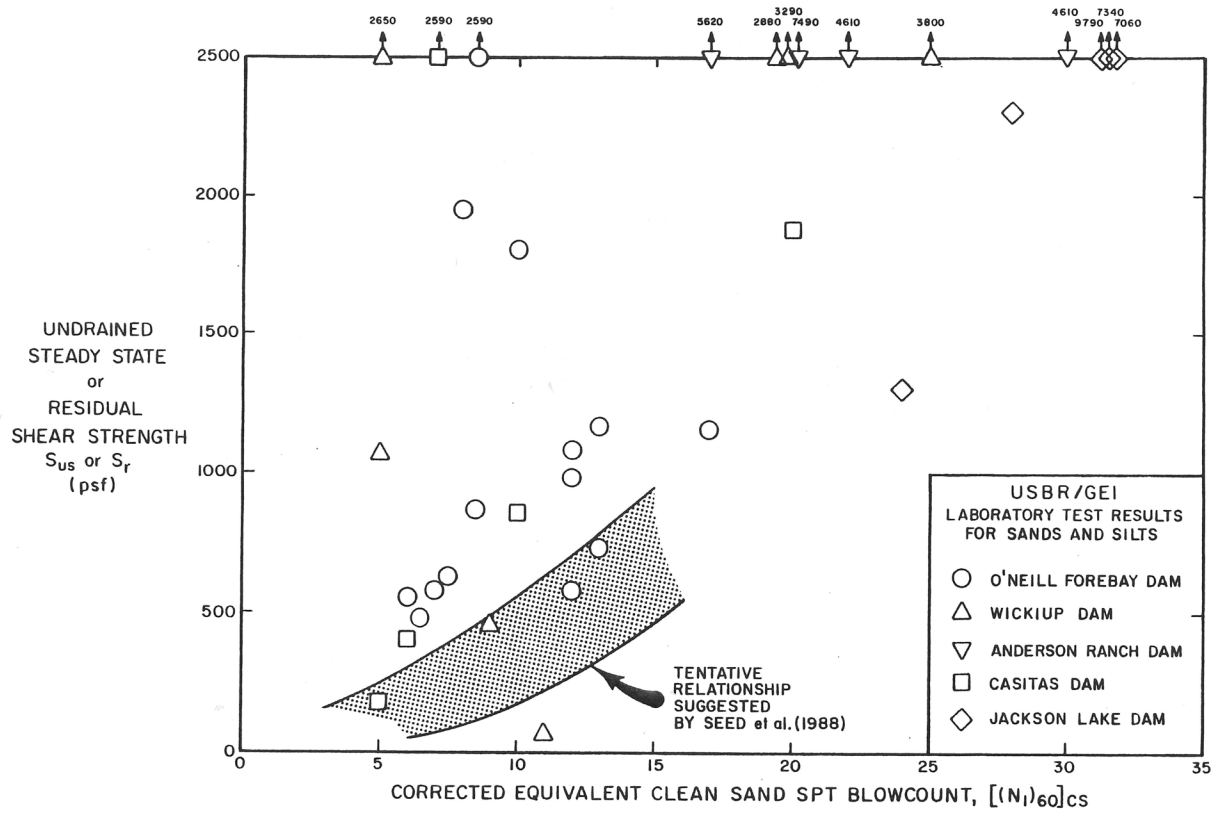

FIGURE 3.17: COMPARISON OF RESIDUAL SHEAR STRENGTHS DETERMINED BY SPT CORRELATION AND BY STEADY STATE STRENGTH TESTS (modified from Von Thun, 1986)

Figure 2.5: Values of estimated in situ steady state strength (S_r) developed by GEI, Inc. based on the laboratory-based steady state method of Poulos et al. (1985) for five U.S. Bureau of Reclamation dams. (Figure from Harder, 1988; modified after Von Thun, 1986)

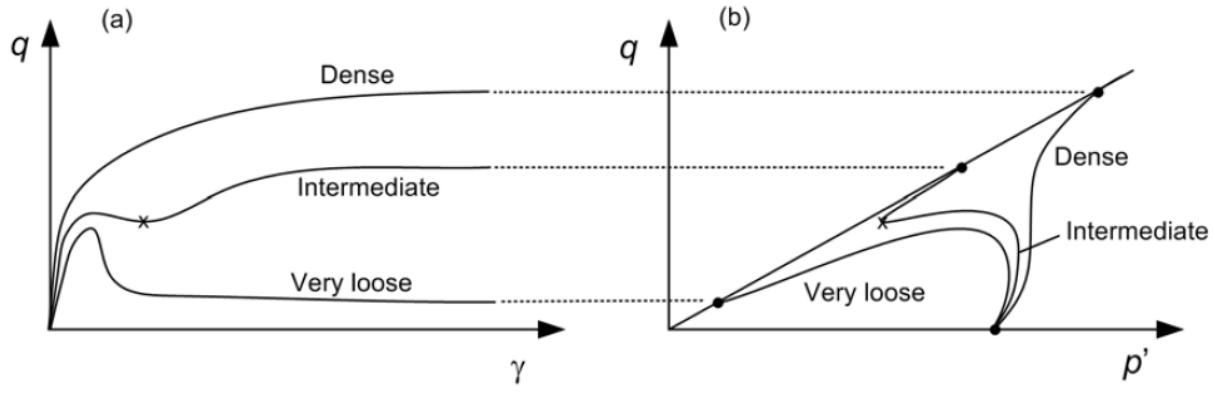

Figure 2.6: Simplified schematic illustration of stress-strain and stress path behaviors of sands of different relative densities under monotonic loading. (Figure from Kramer, 2008)

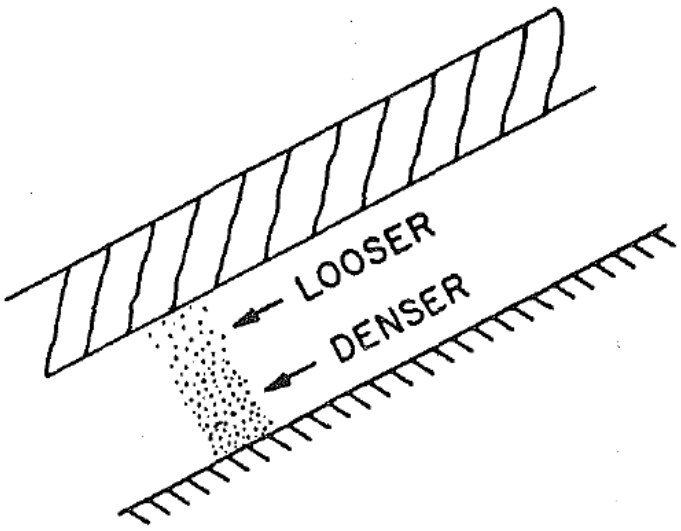

Figure 2.7: Simplified illustration of void redistribution within a confined soil stratum (National Research Council, 1985).

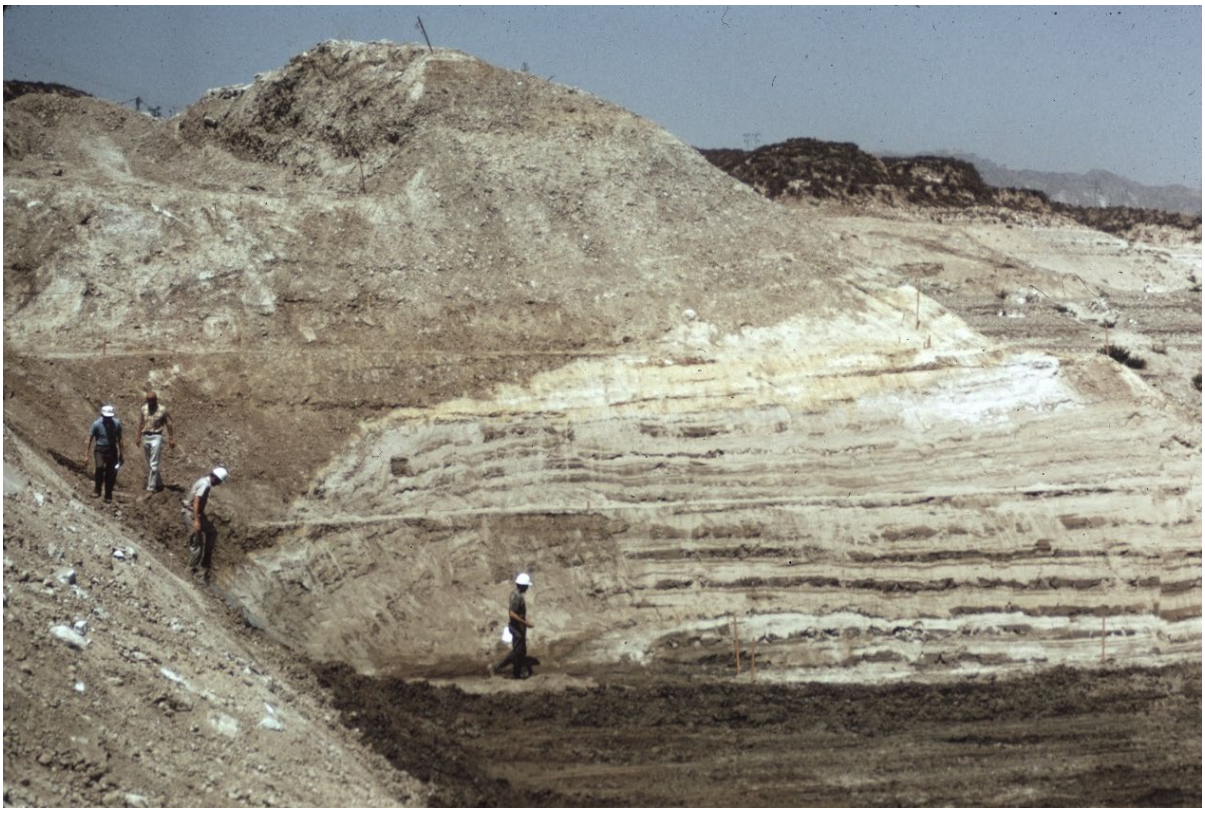

Figure 2.8: Photograph showing layering in the hydraulic fill of the Lower San Fernando Dam (photo by the California Department of Water Resources).

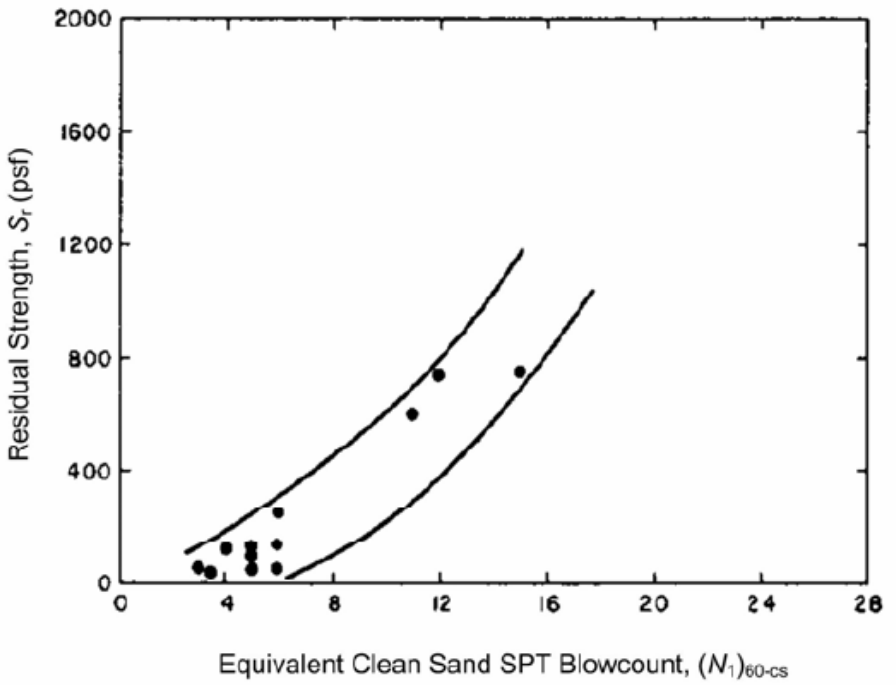

Figure 2.9: Variation of post-liquefaction residual strength Sr as a function of fines adjusted SPT penetration resistance $(N_1)_{60\text{-}CS}$ (Seed, 1987).

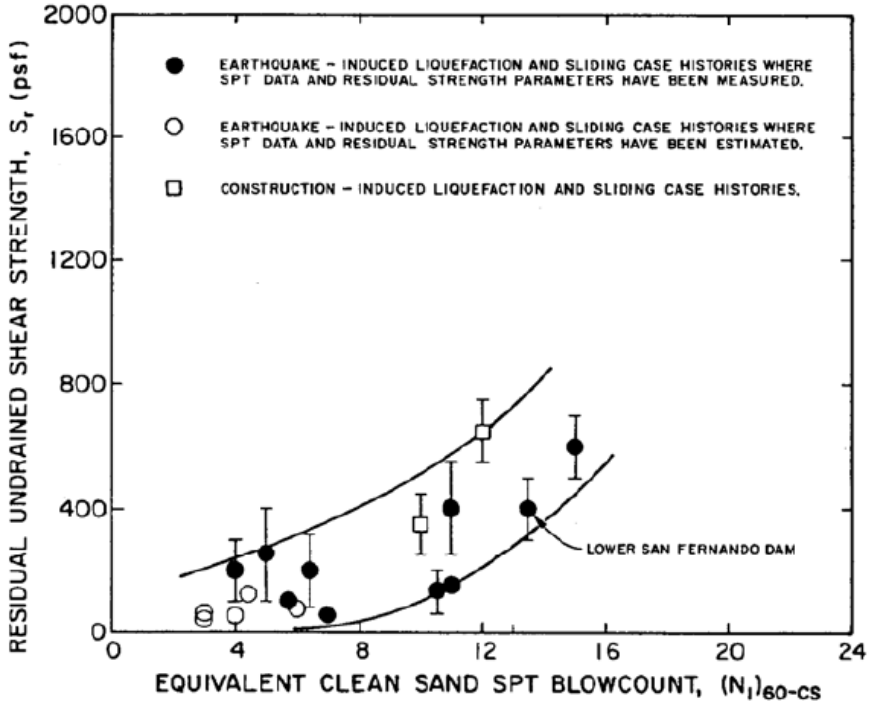

Figure 2.10: Variation of post-liquefaction residual strength S_r as a function of Fines adjusted SPT penetration resistance $(N_1)_{60\text{-}CS}$ (Seed and Harder, 1990).

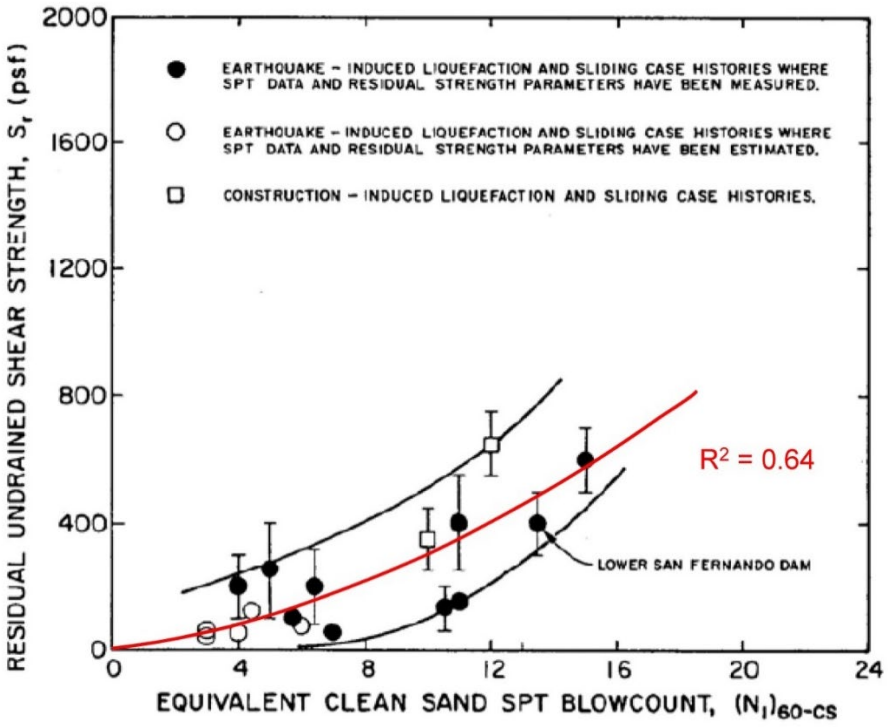

Figure 2.11: Figure 2.10 repeated, this time showing a least squares regression of the data.

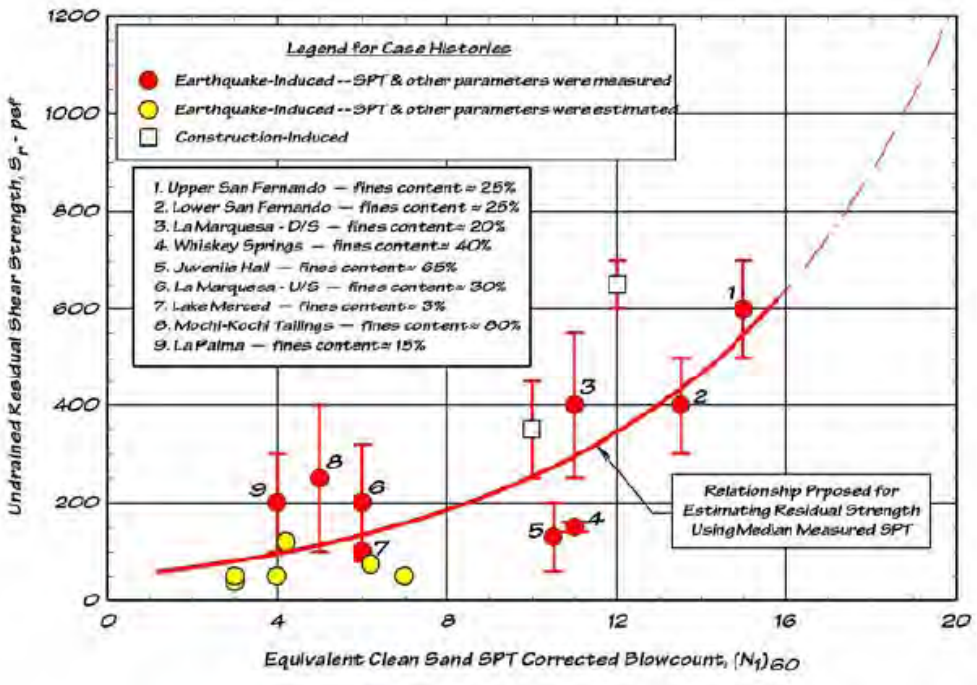

Figure 2.12: Variation of post-liquefaction residual strength S_r as a function of fines adjusted SPT penetration resistance $(N_1)_{60\text{-}CS}$. (Idriss, 1998)

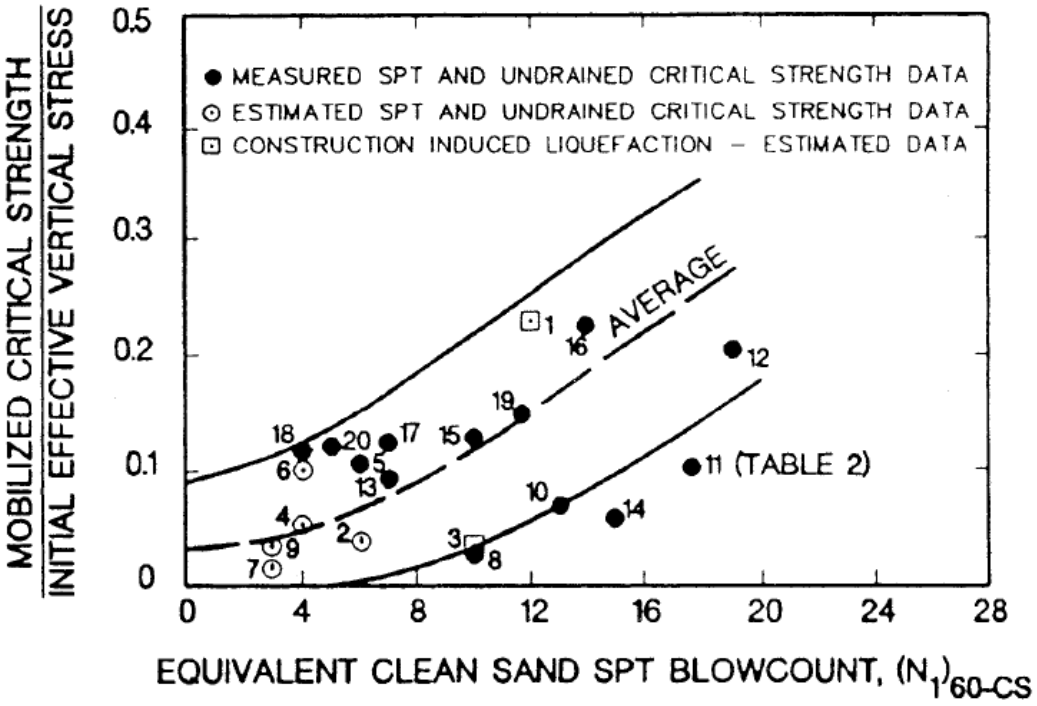

Figure 2.13: Variation of post-liquefaction residual strength ratio (S_r/P) as a function of fines adjusted SPT penetration resistance $(N_1)_{60\text{-}CS}$ (Stark and Mesri, 1992).

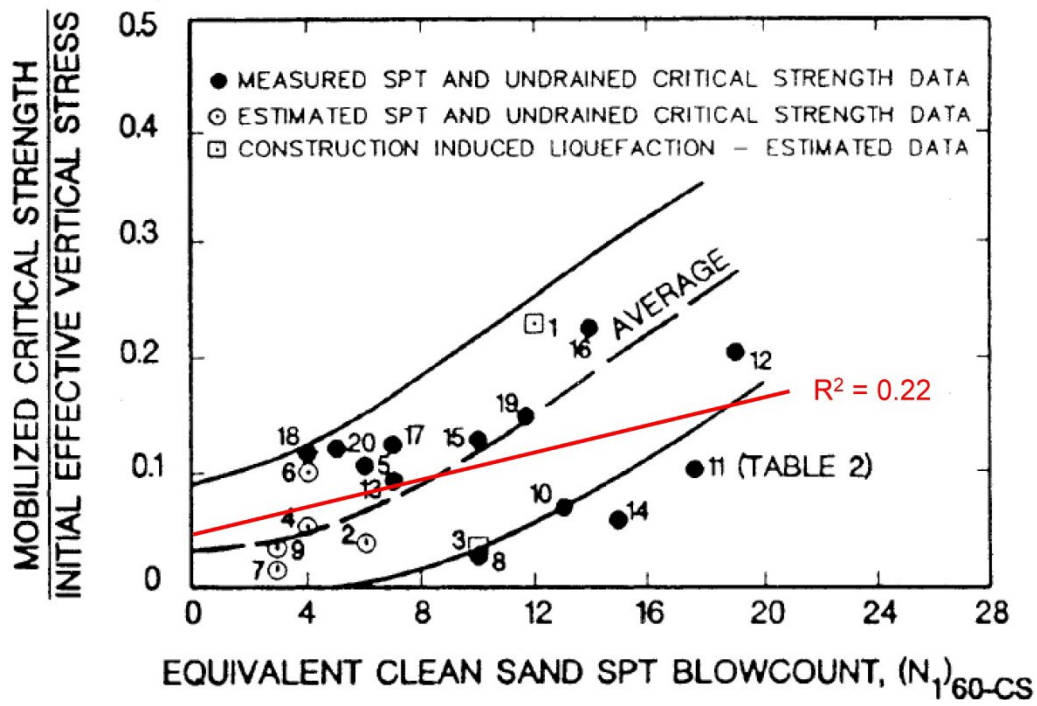

Figure 2.14: Figure 2.13 repeated, this time showing the results of a least squares Regression.

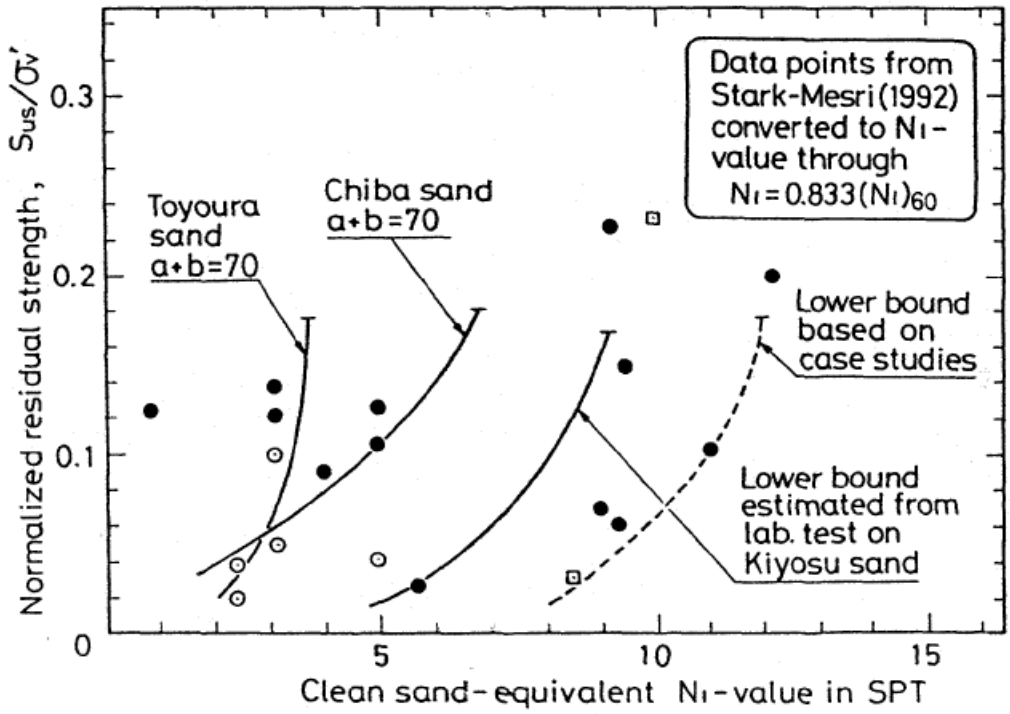

Figure 2.15: Ishihara (1993) relationship between quasi-steady state strength ratio $S_{u,s}/P$ and $(N_1)_{60}$, and comparison with values calculated by Stark and Mesri (1992).

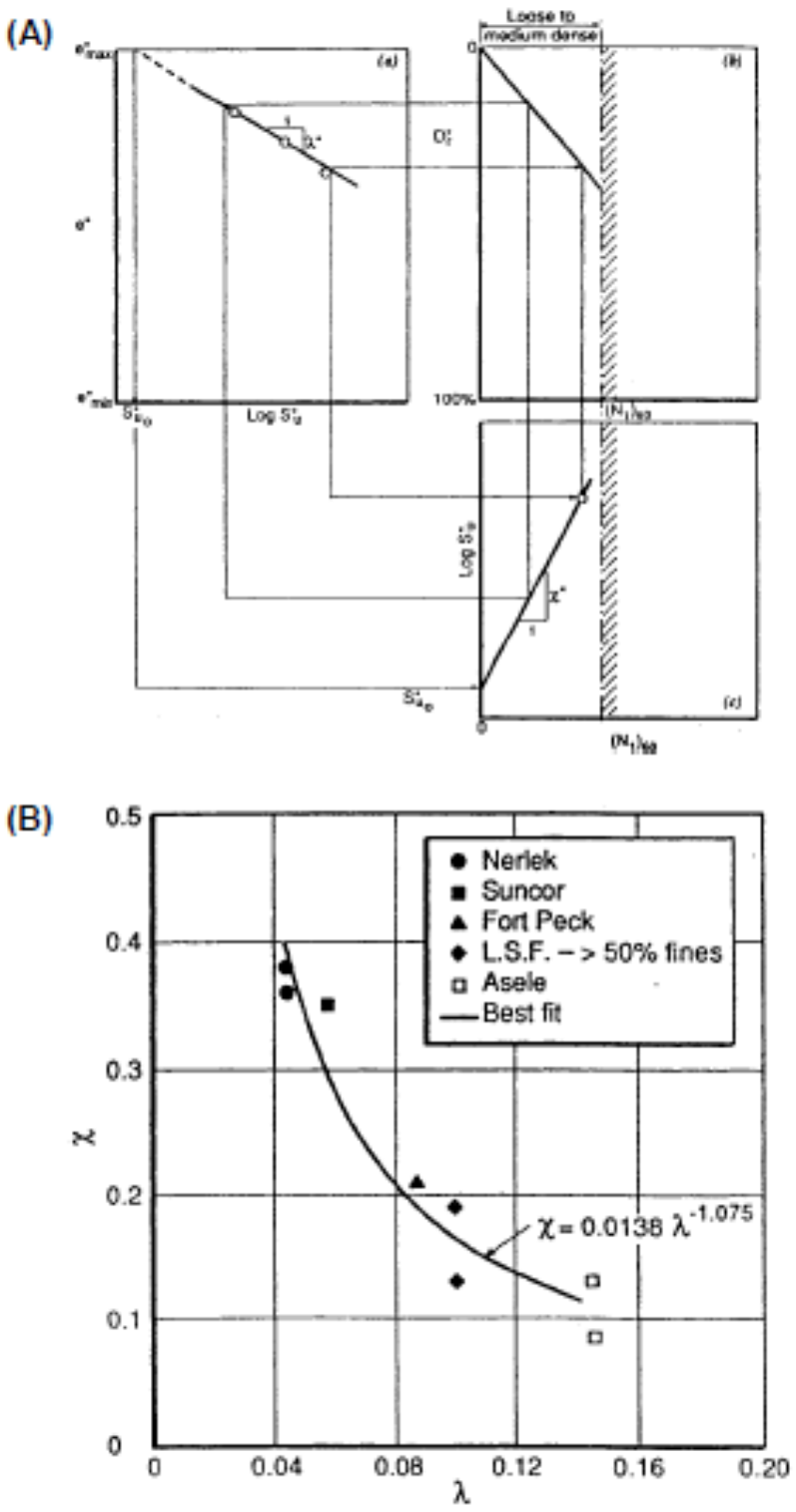

Figure 2.16: Derivation of the calibration factor χ as a function of λ, based on five back-analyzed field failure case histories (Konrad and Watts, 1995).

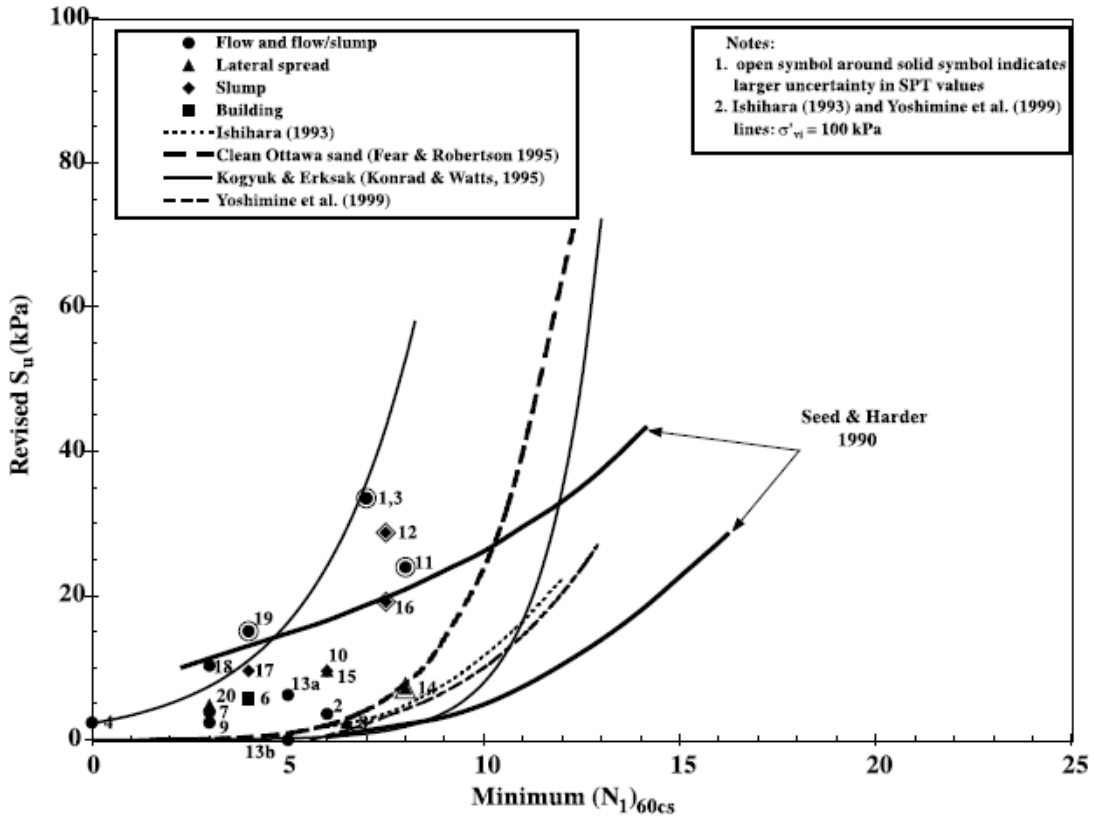

Figure 2.17: Re-evaluated data points (S_u and $N_{1,60,CS}$) for 19 failure case histories, and selected relationships proposed by previous investigators. (Wride et al., 1999)

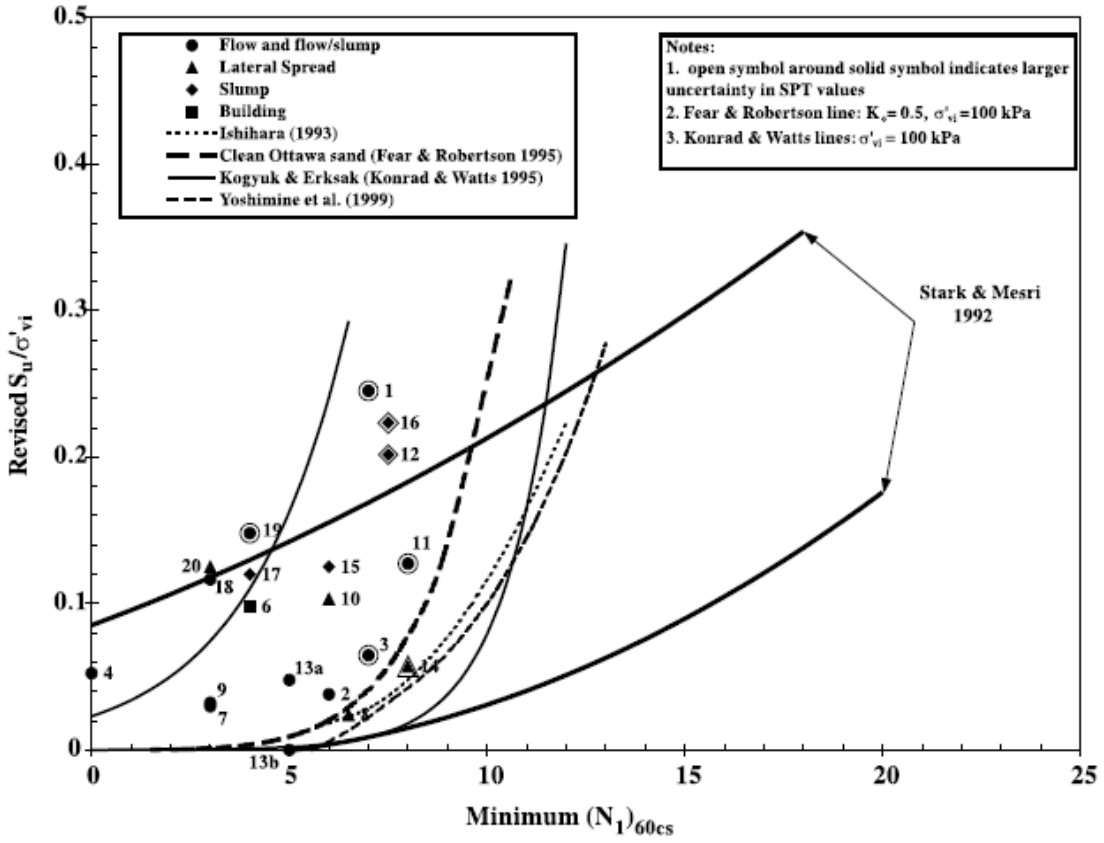

Figure 2.18: Re-evaluated data points (S_u/P and $N_{1,60,CS}$) for 19 failure case histories, and selected relationships proposed by previous investigators (Wride et al., 1999).

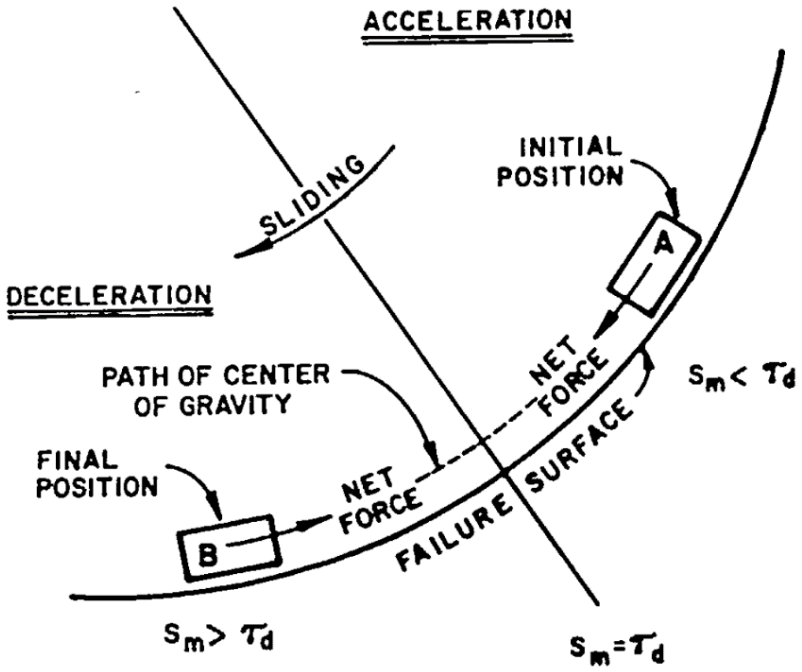

Figure 2.19: Schematic illustration of failure dynamics showing the progression of a mass moving downslope and the net forces on the base shear surface as the mass initially accelerates downslope, and then decelerates and comes to rest (Davis et al. 1988).

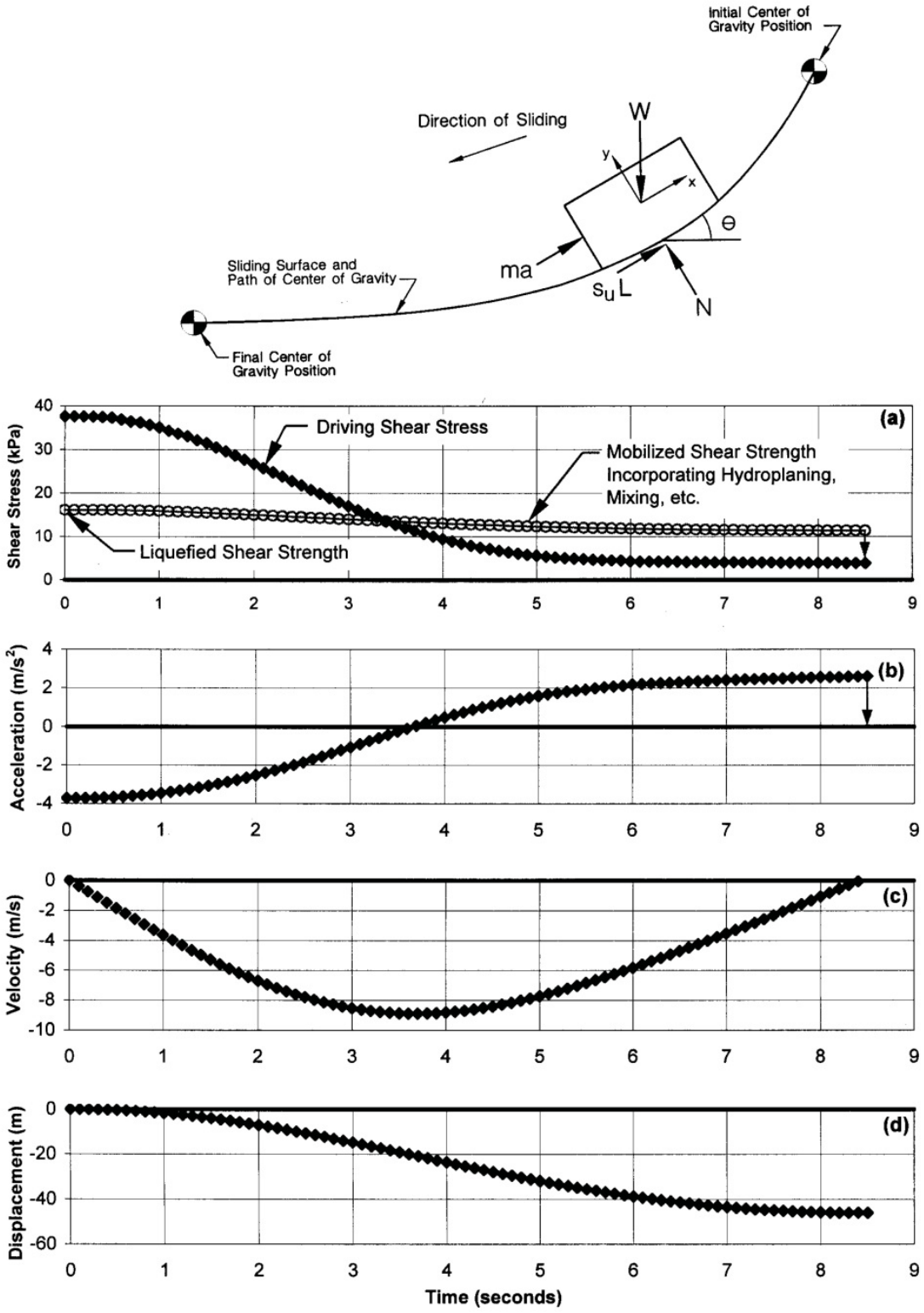

Figure 2.20: Schematic illustration of Olson's "kinetics" analysis of the failure of the upstream slope of Wachusett Dam (Olson, 2001).

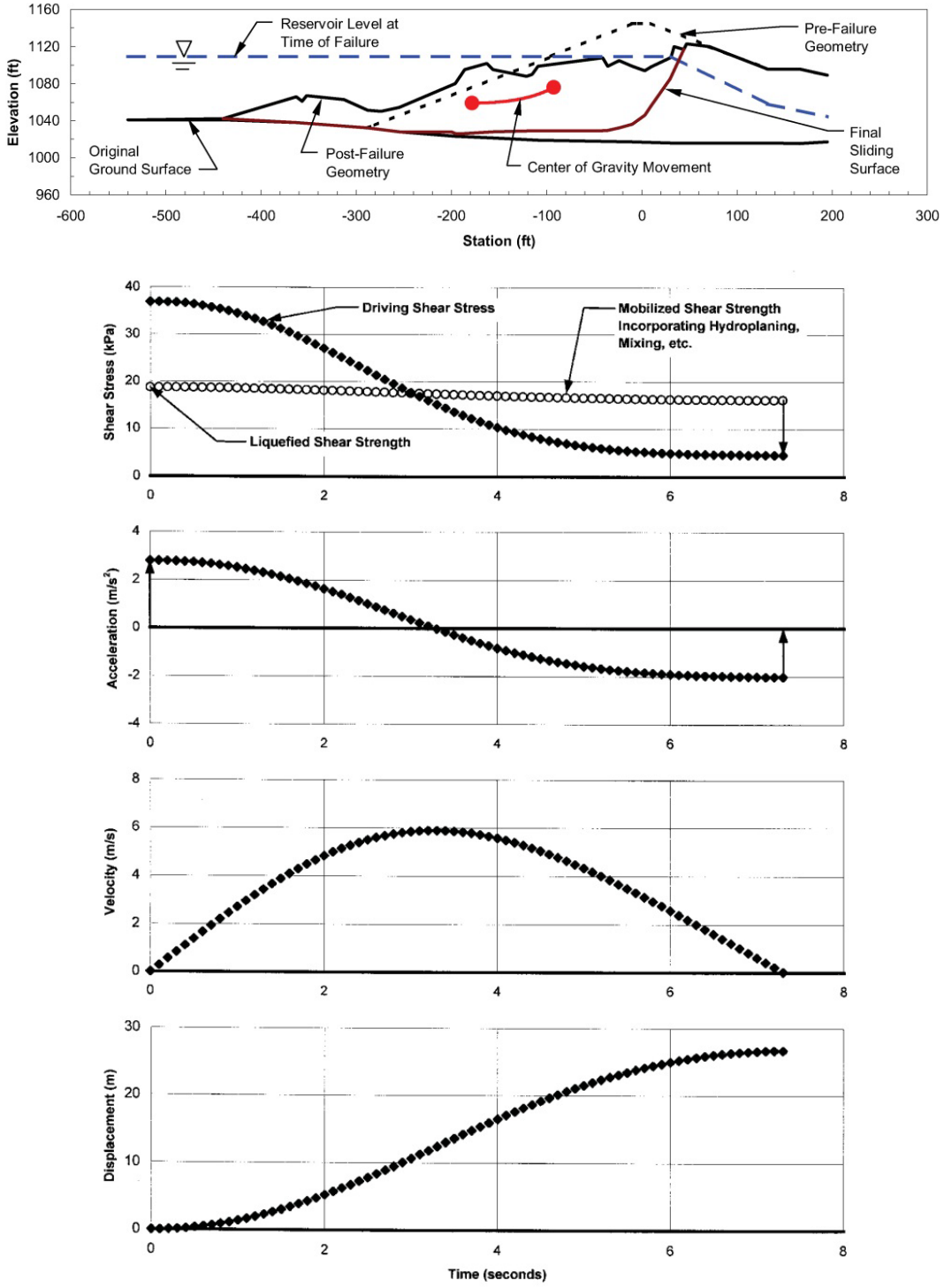

Figure 2.21: Illustration of a "kinetics" analysis of the failure of the upstream slope of the Lower San Fernando Dam (Olson, 2001).

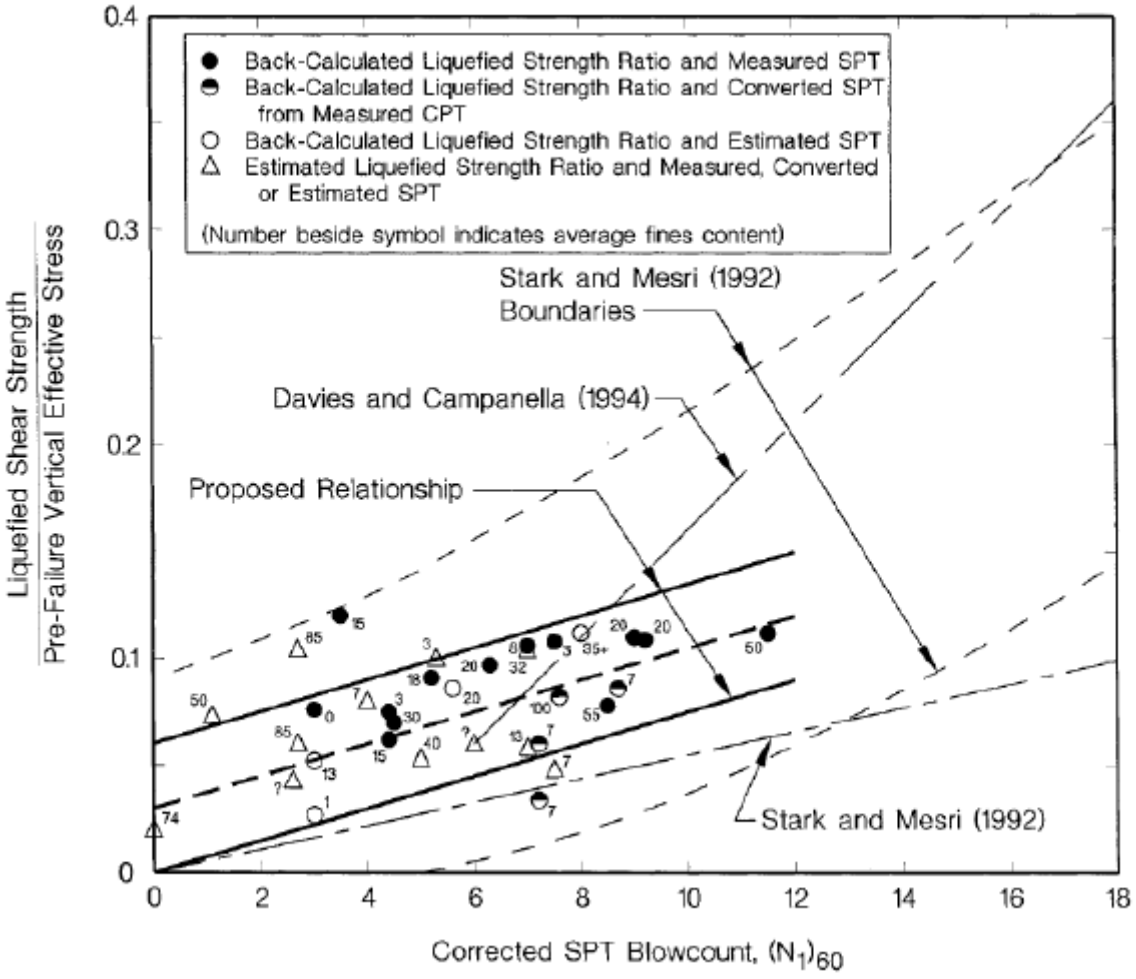

Figure 2.22: Recommended relationship for estimation of normalized residual strength ratio as a function of SPT penetration resistance (Olson and Stark, 2002)

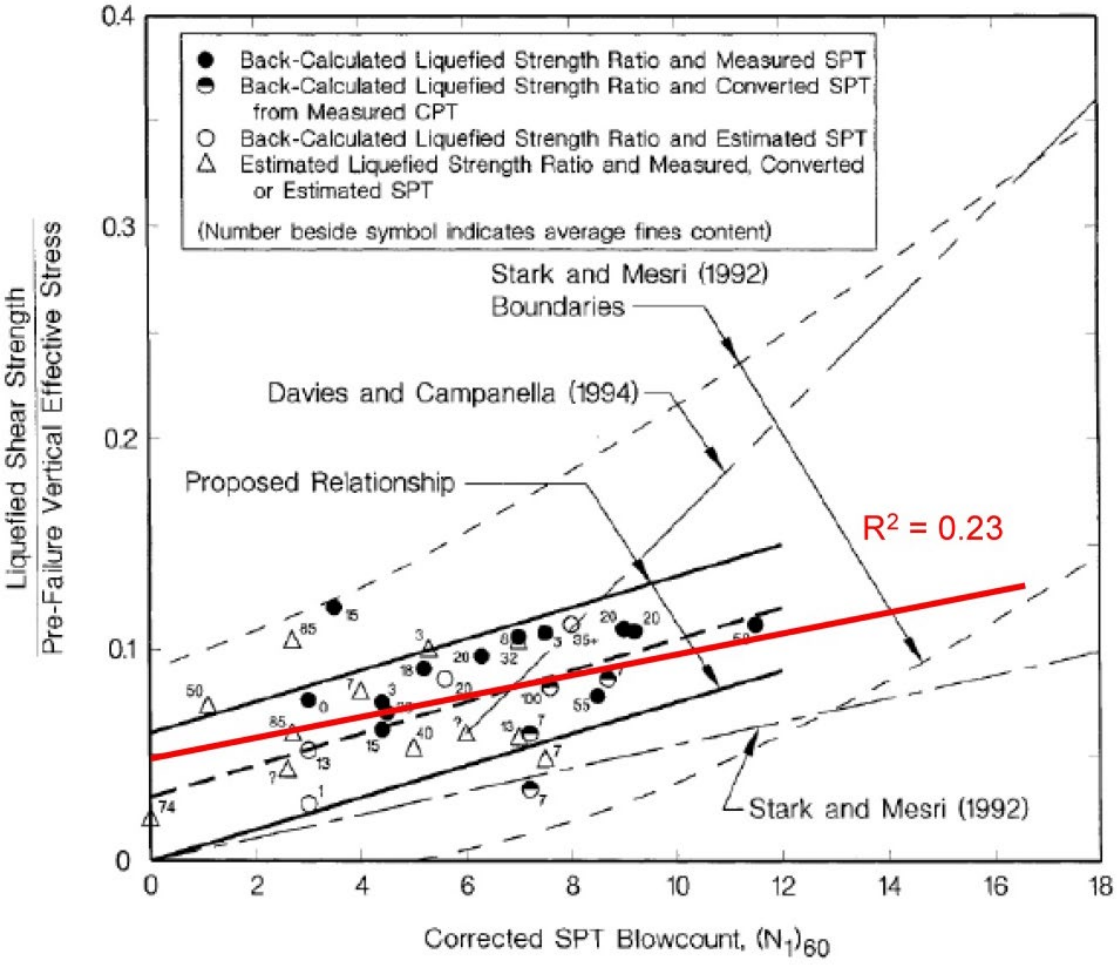

Figure 2.23: Least squares regression of the data set developed by Olson and Stark from Figure 2.22.

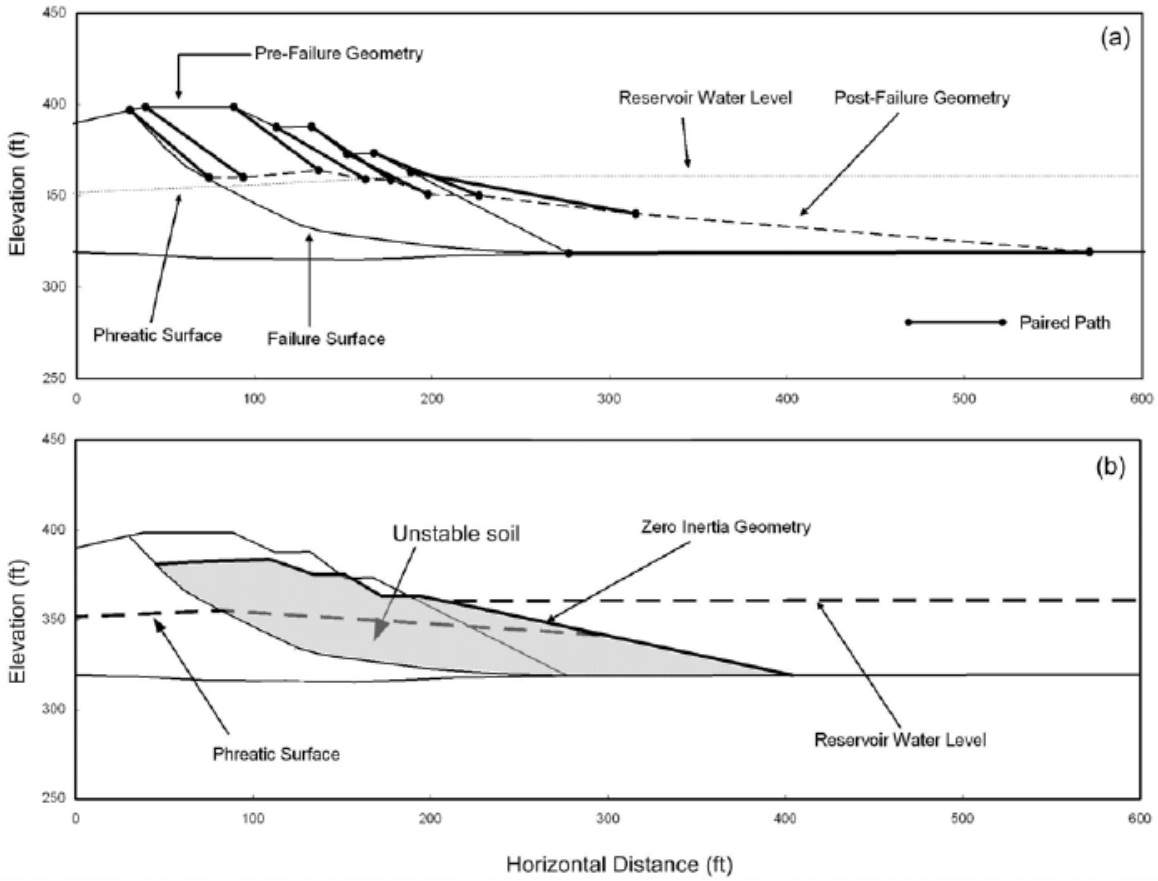

Figure 2.24: Illustration of the procedure employed by Wang (2003) for estimating zero inertial geometry (Figure from Kramer, 2008, after Wang, 2003)

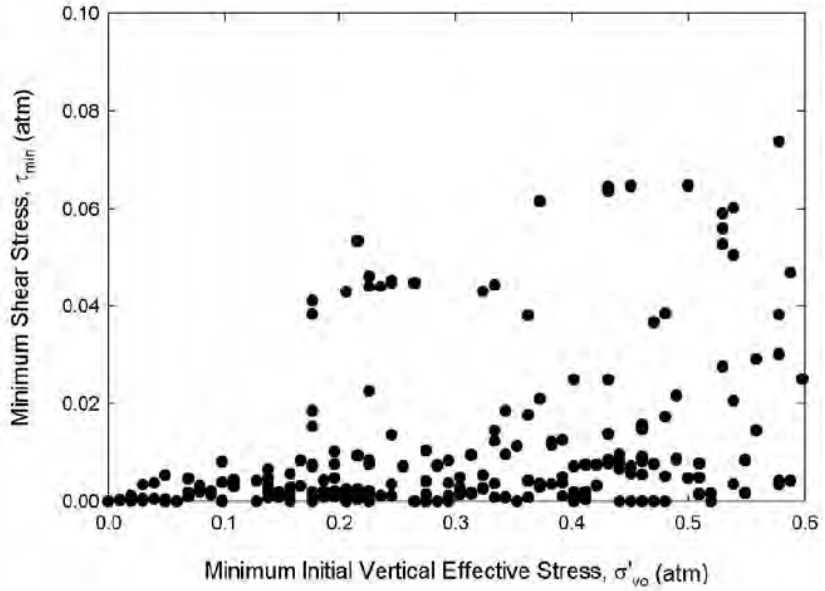

Figure 2.25: Combinations of minimum shear stress and minimum initial vertical effective stress from database of shallow lateral spreading case histories (Kramer, 2008).

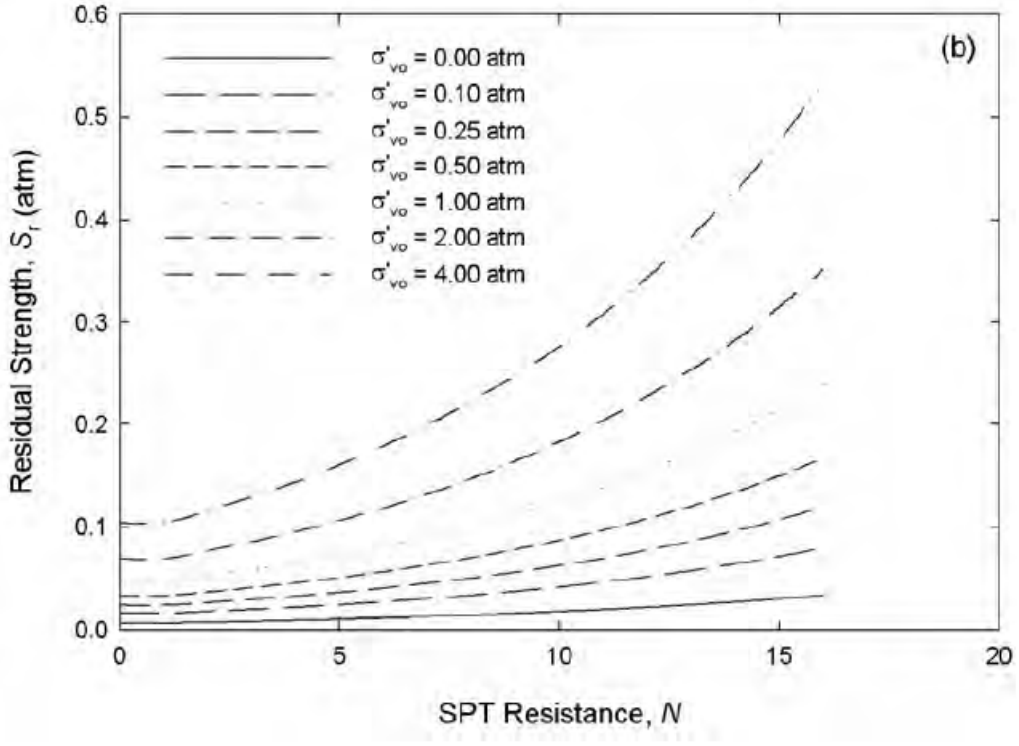

Figure 2.26: Median residual strength curves based on SPT resistance and initial effective vertical stress (Kramer, 2008).

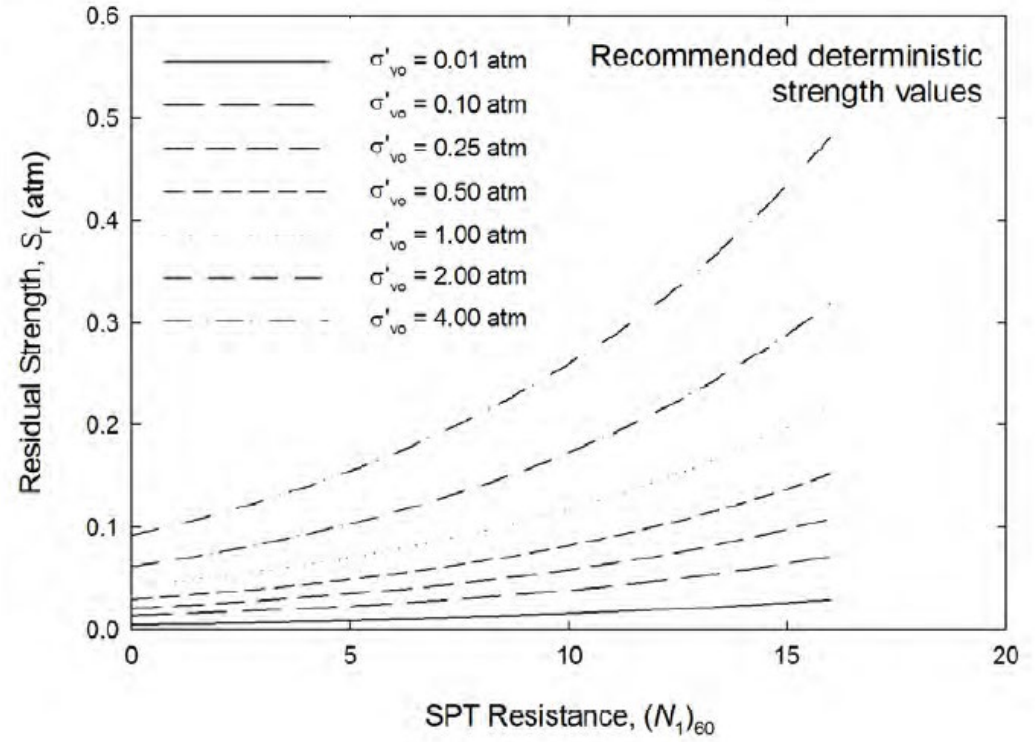

Figure 2.27: Recommended deterministic residual strength curves based on SPT resistance and initial effective vertical stress (Kramer, 2008).

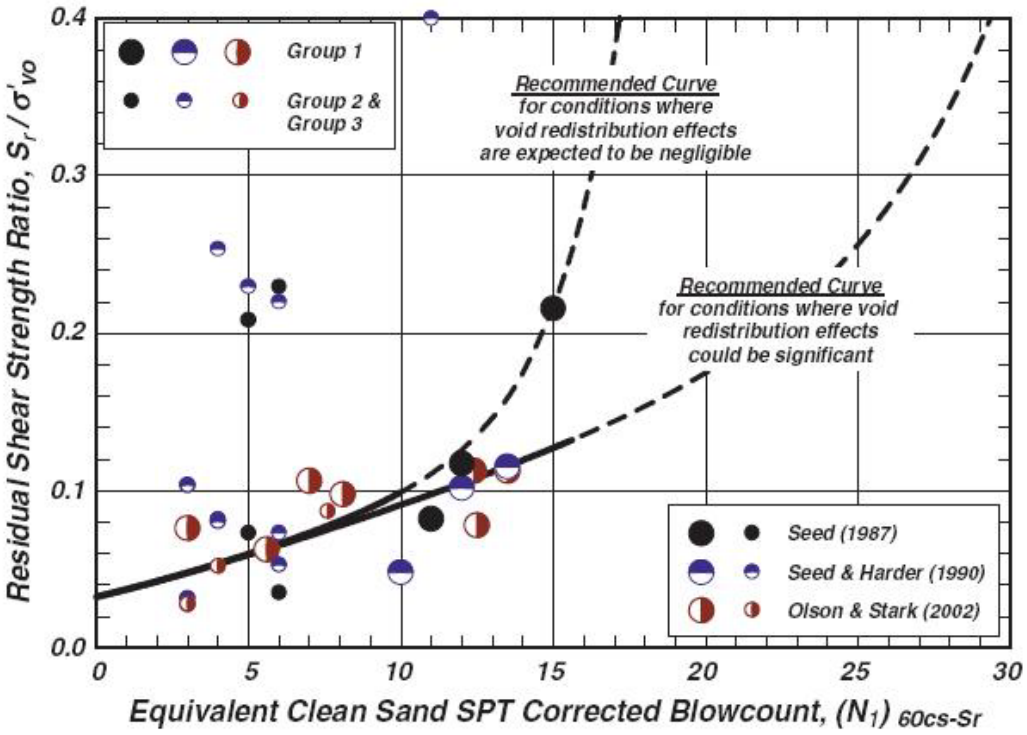

Figure 2.28: Recommended relationship for estimation of normalized residual strength ratio as a function of SPT resistance (Idriss and Boulanger, 2008)

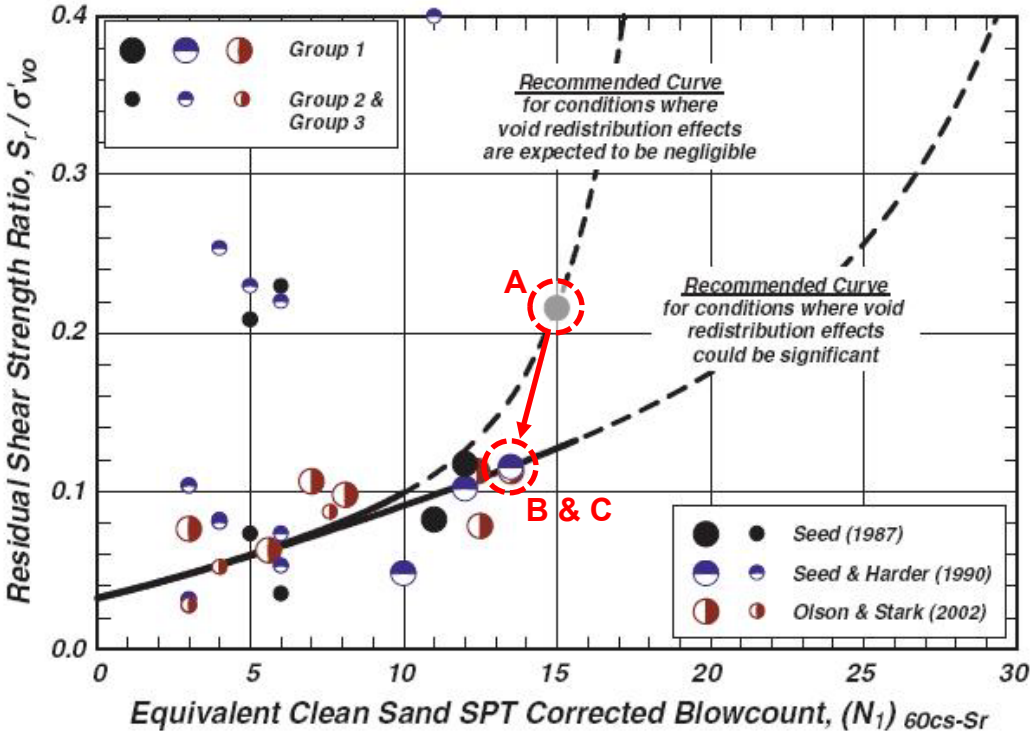

Figure 2.29: Figure 2.28 repeated, showing relocation of the data point for the Lower San Fernando Dam.

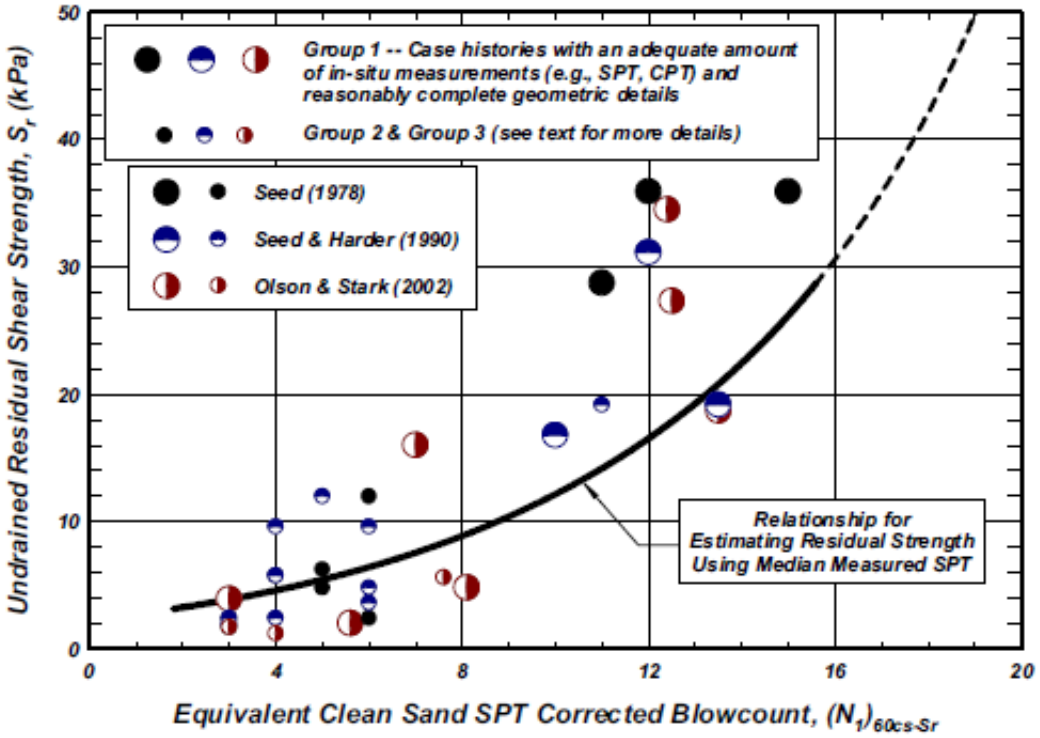

Figure 2.30: Recommended relationship for estimation of residual strength as a function of SPT resistance (Idriss and Boulanger, 2008)

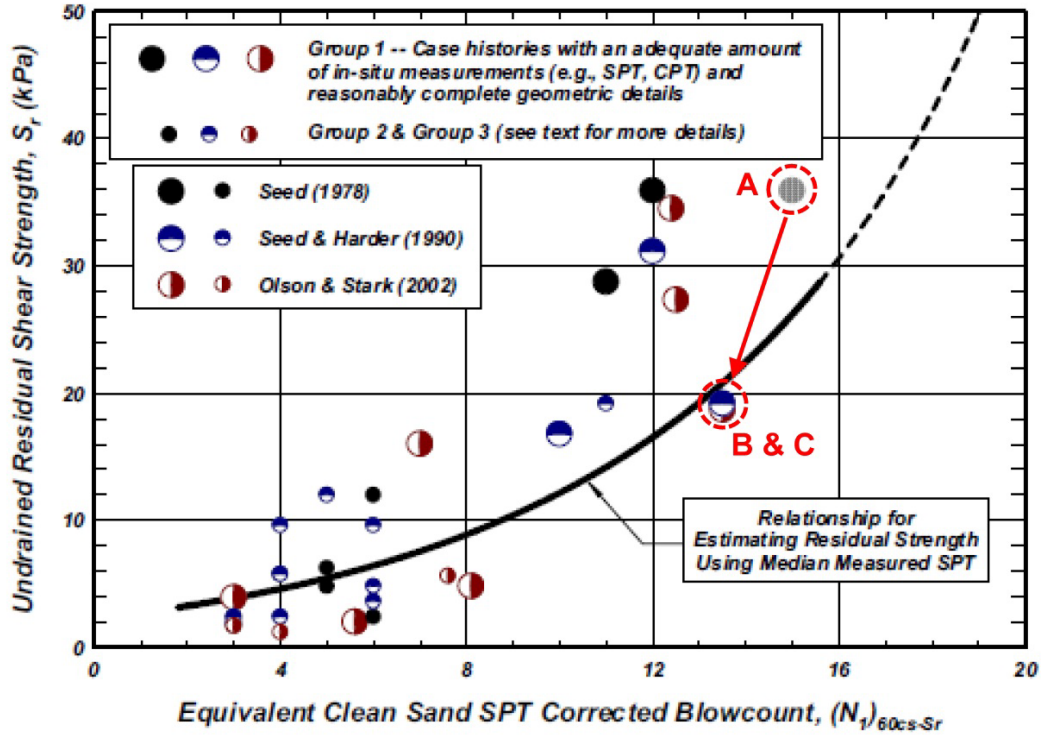

Figure 2.31: Figure 2.30 repeated, showing relocation of the data point for the Lower San Fernando Dam.

Chapter Three

Review and Selection of Liquefaction Case Histories for Back-Analyses

3.1 Introduction

The selection of full-scale liquefaction case histories to be back-analyzed for purposes of development of empirical methods for evaluation of in situ post-liquefaction strengths represents an important set of judgments and decisions.

A large number of previous investigations, and experts, have (a) back-analyzed sub-sets of the available case histories, or (b) employed the results of back-analyses performed by other investigation efforts, in their own development of empirical approaches for evaluation of post-liquefaction strengths. Different decisions, and different selections, were made by various investigators. In some cases (early efforts) there were only a limited number of potential field case histories available, so selections were often made on the basis of attempting to optimize the use of these limited opportunities.

In more recent investigations (after about the mid-1990's), selection or de-selection of cases for back-analyses or for inclusion in development of empirical relationships were more often made on the basis of one or more of the following considerations:

1. Perceived availability, quality and documentation of information regarding pre-failure and post-failure geometry and conditions. In addition to basic geometry and stratigraphy, this also includes information constraining the location of the phreatic surface at the time the failure occurred.
2. Perceived quality and/or availability of information or data available for characterization of the soil units suspected of having liquefied. Highest quality data here were generally considered to be well-documented SPT or CPT data. Lesser quality data were sparse penetration test data, non-standard penetration test data, and cases in which penetration resistance had to be inferred more qualitatively from apparent relative density, soil placement and/or compaction history, etc.
3. Additional data and information, including witness accounts, information and data regarding soil properties (unit weights, strength parameters, etc.) for both liquefied and non-liquefied soils, etc.
4. Tractability of the observed (or suspected) failure mechanism with regard to relatively accurate and reliable back-analysis for the specific purpose of assessment of post-liquefaction strength S_r.
5. Personal preferences. For example, some previous efforts preferred to consider only cases in which CPT data were available.

Not all previous studies presented clear explanations as to the reasons for selection and de-selection of case histories considered and/or back-analyzed.

Some level of general consensus can be inferred by the common choices made by a significant number of previous investigators with regard to a number of the available case histories. But as new information has developed, some of these choices now appear less attractive (e.g. the Calaveras Dam case history).

In these current studies, the full suite of case histories considered to date were fully re-considered, with (1) understanding of the decisions and selections made by previous investigation teams, (2) the benefits of examination and review of previous back-analysis efforts and of previously developed approaches for assessment of in situ post-liquefaction strength (see Chapter 2), and (3) new information that appears to have been developed recently and that was therefore not available to a number of investigation teams (e.g. the Calaveras Dam case history).

Table 3.1 presents a listing of the field liquefaction case histories back-analyzed, or included in empirical correlations, by a select sub-set of six previous investigation efforts. These six previous efforts were selected for presentation in this table because (1) they were notably comprehensive efforts with regard to inclusion of case histories at their time, and (2) between them they comprise a list of essentially all (or at least nearly all) potentially useful cases currently available for purposes of back-analyses to evaluate in situ S_r.

3.2 Lateral Spreading Case Histories

Having noted the relative paucity of available case histories of large-displacement liquefaction failures, Olson and Johnson (2008) back-analyzed a significant number of lateral spreading case histories, many of them from the lateral spreading case history database assembled by Youd et al. (2002), as discussed previously in Section 2.3.9. Youd et al. had compiled this database for purposes of developing empirical methods for prediction of lateral spreading displacements. Olson and Johnson employed simplified Newmark-type methods to attempt to back-analyze the lateral spreading case histories to extract estimates of post-liquefaction strength. One of the principal findings was the difficulty of extracting reliable estimates of back-calculated S_r for cases (lateral spreads) wherein the overall movements included a strong contribution from transient cyclic lurching forces, and generally in situations wherein the cyclic lurching forces interacted with gravitational "downslope" static driving shear stresses or forces.

Lateral spreads are differentiated from the other (and generally larger displacement) cases in these current studies as being cases in which relatively moderate levels of gravity-induced static "driving" shear stresses do not, by themselves, generate a large majority of the observed movements and displacements. Instead, transient cyclic seismic loading, and resulting "cyclic lurching" forces, are also an important contributor. These cyclic forces are difficult to accurately back-analyze for several reasons. One reason is that simplified Newmark-type analysis methods do not provide a high degree of precision here. Another difficulty is the importance of details of the transient seismic loads (e.g. acceleration time histories) that actually occurred at the site in question. A potentially high degree of sensitivity of calculated displacements to these details contributes significantly to the uncertainties involved in back-analyses of these lateral spread case histories for purposes of back-estimation of S_r.

Accordingly, it was determined in these current studies that cases wherein transient cyclic lurching forces appear to be of sufficient importance as to potentially obscure, or prevent reliable assessment of, post-liquefaction strengths would not be included in the data set.

In addition to the lateral spreading cases added by Olson and Johnson (2008), a number of additional lateral spreading cases collected and processed by Faris (2004) specifically for the purpose of developing relationships for prediction of lateral spreading displacements were also examined.

The semi-empirical method for prediction of lateral spreading displacements developed by Faris (2004) was developed specifically for use with cases of limited "lateral spreading-type" displacements in which cyclic lurching forces contributed significantly to overall deformations and displacements. These are cases in which post-liquefaction overall stability has a Factor of Safety greater than 1.0 in the absence of cyclic lurching forces, so that it is primarily cyclic lurching forces (which produce transient periods of time during which the Factor of Safety is temporarily less than 1.0; during which displacements occur) that "drive" observed displacements.

The Faris (2004) semi-analytical method was inverted, and was used as a preliminary screening process to assess the potential usefulness of these lateral spreading cases for purposes of back-evaluation of S_r. If observed field displacements did not significantly exceed those predicted by the Faris (2004) method, then that would represent a situation in which cyclic lurching forces contributed a significant portion of the overall observed displacements. For cases in which observed field displacements were not at least two times greater than those predicted by the Faris (2004) method, the case histories were deleted from the database for these current studies. For cases in which the observed field displacements were more than twice those predicted, but less than about three times greater, the cases were examined on an individual basis to determine whether or not they would be carried forward and included in these current studies.

Figure 3.1 illustrates the use of the Faris (2004) procedure for a typical case; the Shonan-Cho lateral spread which occurred during the 1983 Nihonkai-Chubu earthquake. As shown in the top left figure, a liquefaction triggering evaluation was made for each SPT $N_{1,60,CS}$ value measured within materials considered potentially liquefiable. Those judged likely to liquefy were then re-plotted in the upper right-hand figure on a plot showing shear strain potential as a function of (1) $N_{1,60,CS}$ and (2) equivalent uniform cyclic stress ratio (CSR_{eq}) for a causative event of $M_W = 7.5$. These shear strain potentials are based on laboratory isotropically consolidated and then undrained cyclic triaxial testing, and do not (yet) include effects of initial "driving" shear stresses. The resulting estimates of strain potential are then ascribed to the interval in each boring represented by the individuals $N_{1,60,CS}$ values, and accumulated displacement potential from bottom to top of the boring (up to the ground surface) is then calculated as shown in the plot of the right-hand middle figure. In this figure, depth ranges over which liquefaction strain potential are summed vary due to changes in overall thickness of the potentially liquefiable materials at different borehole locations within the overall lateral spreading feature. This results in an estimated "displacement potential index" (DPI) at the location of each SPT boring.

These estimated DPI values are not direct estimates of expected displacements; they are only indices of stiffness or deformability. Faris compiled these indices for a large number of field case histories, and then performed regressions to develop empirical correlations for prediction of

expected lateral spreading displacements as a function of (1) DPI, (2) initial static driving shear stresses (estimated in a simplified manner based on slope and/or free face height at the toe of a lateral spreading feature), and (3) earthquake magnitude (serving as an approximation of duration or number of cycles). Each value of DPI, for each boring, is then transformed using the regressed relationship, to develop values of predicted actual displacements at each boring location. This is shown in the bottom left-hand corner of the figure. The resulting calculated "predictions" of expected displacement are then averaged together to develop an average calculated displacement (or predicted displacement). The displacements actually observed in the field (ideally at the boring locations) are then also averaged to produce the average observed displacement. These averaged calculated and observed displacements are plotted in the figure in the bottom left-hand corner. The resulting overall average ratio of predicted vs. observed displacements is then calculated.

For this screening level exercise, it was determined that cases in which either (1) observed displacements were less than 3 feet, or (2) the ratio of observed vs. predicted displacements was less than a factor of 2, would be assumed to have had sufficiently significant cyclic lurching effects that it would not be appropriate to attempt to back-analyze them for purposes of trying to accurately discern post-liquefaction strength S_r. Cases only marginally exceeding these two limits would be more closely examined on an individual basis.

This screening level analysis was applied to all of the cases compiled by Olson and Johnson (2008), and to the cases compiled by Faris (2004), for purposes of development of empirical relationships for prediction of lateral spreading displacements. Of the few cases where the ratio of displacements observed vs. those predicted was greater than 2, most had overall (average) displacements of less than 3 feet.

One case that came close to being carried forward for further back-analysis was the Shitayama School lateral spread from the 1964 Niigata earthquake. This case had an observed average displacement of 12.2 feet, and an average calculated (predicted) displacement of 5.4 feet based on Faris' semi-empirical method. The resulting ratio was then 12.7 ft. / 5.4 ft. ≈ 2.4. This case was then examined further, and the engineering team determined that we would not be confident that cyclic inertial effects did not contribute significantly to observed displacements at this site due to (1) the relatively moderate pre-earthquake static driving shear stresses, and (2) the estimated relatively high intensity and duration of strong shaking at this site.

In the end, only two of the "lateral spreading" case histories from either the Youd et al. (2002) database examined by Olson and Johnson (2008) or from the additional cases developed by Faris (2004) were carried forward for further consideration in these current studies of post-liquefaction S_r. These were the San Fernando Valley Juvenile Hall lateral spread case history, and the Whiskey Springs Fan case history, and these will be discussed further in Sections 3.3.3.4 and 3.3.3.5, respectively.

3.3 Remaining Potential Candidate Liquefaction Case Histories

3.3.1 Separation of Case Histories into Classes Based on Assessed Quality and Reliability

With most of the lateral spreading case histories thus eliminated, 36 potential candidate cases remained. These are listed in Table 3.2. When available, the results of back-analyzed values of post-liquefaction strength, or post-liquefaction strength ratio, as well as representative vertical effective stress and SPT penetration resistance are presented, as developed by (1) Seed and Harder (1990), (2) Olson and Stark (2002), and/or (3) Wang and Kramer (2003, 2008, and 2015) are shown.

After studying these cases, they were sub-divided into four classes: Classes A, B, C and D, as shown in Table 3.2.

Class A case histories were judged to be generally of the highest quality with regard to well-documented data and information regarding (1) pre-failure and post-failure geometry, (2) penetration resistance within the critical liquefiable materials, and (3) other details including phreatic surface at the time of failure, shear strengths of non-liquefied soils, etc. These 13 case histories were judged to warrant the application of the incremental momentum back-analysis methods described in Chapter 4, Section 4.2, to develop best possible estimates of post-liquefaction strengths.

The 16 case histories of Class B were judged to have lesser quality data, or less well-documented data, than the Class A cases, leading to greater uncertainties. These cases were judged not to warrant the performance of full incremental momentum analyses, but it was judged that useful estimates of post-liquefaction strength could be made, and useful estimates of representative penetration resistance and of representative vertical effective stress as well. Uncertainties associated with these values would generally be expected to be higher than for Class A cases.

The single Class C case history (Calaveras Dam) was also judged to have high quality data and information regarding geometries, etc., needed for high-level back-analyses to evaluate post-liquefaction strength, and so it was also back-analyzed using the incremental momentum methodology. But this case was <u>not</u> then subsequently used to help to develop empirical relationships for evaluation of in situ post-liquefaction strength, as will be explained further in Section 3.3.2.

The six cases of Class D had all been used in one or more previous studies, but upon detailed review and assessment, these were deleted from further consideration as explained in Section 3.3.3.

3.3.2 The Calaveras Dam Case History

This case had been a prominent case history in the works of multiple previous investigation teams. But information developed in the late 1990's as part of seismic investigations for seismic re-evaluation of the repaired dam showed clearly that many of the embankment's hydraulic fill materials had a significant clay content. The main (pre-failure) dam was being constructed by the

hydraulic fill method, with hydraulic deposition of fill materials simultaneously from the upstream and downstream sides, and was nearing completion when the earthquake-induced failure occurred in 1918. These fill materials were sourced form weathered colluvium on the local hillsides, and from weathered alluvium deposits also derived largely from the weathered colluvium. As shown in Figure 3.3 (and additional Figures in Appendix A, Section A.14), and Table 3.3, the resulting hydraulic fill zones were complex in terms of the nature and distribution of materials (Olivia Chen Consultants, 2003).

The massive failure of 1918 occurred on the downstream side, and so the materials shown in Figure 3.3 on the downstream side of the dam represent the "post-repair" section, and not the original materials that controlled the failure.

In the current cross-section, the materials of Zones V and VI best represent (by approximate symmetry) the materials that would have principally controlled the 1918 failure. Materials in these zones are highly variable, and consist of broadly well-graded mixes of gravels, sands and clayey fines. Gravel contents vary greatly, and are often high enough as to warrant the use of Becker Penetrometer testing (BPT) as well as short-interval SPT (SPT performed with 1-inch blowcounts and then adjusted for apparent gravel effects, as described in Seed et al. (2003)), as part of the 1990's seismic investigations. Gravel contents generally ranged between approximately 20% to 55%, but variability was high enough that some portions of these same hydraulic fill zones were judged to be clearly "cohesive fines dominated". Fines contents also varied greatly, from very low to as high as 70% or more in some zones. The fines were mainly low to moderate plasticity clays (CL), with PI generally between approximately 15% to 25%.

The dam failed in 1918 as initial construction was nearing completion. As a result, these materials, and especially those comprised of sufficient clay as to be subject to significant consolidation, were still consolidating under the rising fill loads. These soils were likely variably under-consolidated, and conditions at the time of failure are not likely to be well-represented by the modern SPT or BPT penetration resistances obtained eight decades later. It is difficult to reliably predict the effects of (1) additional consolidation over the past eight decades for these hydraulic fill materials, some of which were cohesive fines-dominated materials subject to potentially significant consolidation strength gains, and (2) ageing effects over eight decades in these highly variable and challenging mixed soils. As a result, it was the reluctant conclusion of this current investigation team, and with the unanimous concurrence of the informal advisory group of experts that assisted on this overall investigation, that it is not reasonable to attempt to correlate back-calculated strengths from this failure with available penetration resistance data.

This does not mean that this is a poor case for back-analyses. On the contrary, this is an excellent case of liquefaction-induced failure, and it was back-analyzed with the best available methods (including the incremental momentum method) to study the mechanics of this type of failure. The results of these back-analyses were then used, along with the results of back-analyses of the 13 case histories from Class A, to develop empirical correlations for estimation of post-liquefactions strengths as a function of runout characteristics, etc. These, in turn, were then used (1) to internally cross-check the back-analysis results of the case histories in Class A, and (2) to assist in development of assessments of post-liquefaction strengths from the case histories of Class B, and for cross-checking some of the back-analysis results for Class B cases.

But the SPT and BPT penetration resistance values from the "modern" site investigations cannot be directly correlated with the back-analyzed estimates of post-liquefaction strength (S_r) for this otherwise important case history, and so this case history was not employed in the empirical regressions performed to develop new predictive models for assessment of S_r.

It should be noted that most previous efforts to develop relationships for estimation of post-liquefaction strengths did employ the Calaveras Dam case history, and that it was one of a limited number of cases providing high S_r values at relatively high penetration resistances. The information regarding materials character developed by the studies of Olivia Chen Consultants (2003) was not available to most of these previous investigators. Because this case was one of only a few case histories with (1) large effective overburden stresses, and (2) relatively large $N_{1,60,CS}$ values, the deletion of this case history from relationships and correlations based on the new information and data from the recent 1997 - 2002 seismic studies would be expected to result in potentially significant changes in these other/previous relationships.

3.3.3 Class D Cases

The six Class D cases in Table 3.2 were deleted, and were not formally back-analyzed nor used to develop predictive relationships in these current studies.

3.3.3.1 Kawagishi-Cho Building

The Kawagishi-Cho apartment building suffered a liquefaction-induced bearing capacity failure and toppled over during the 1964 Niigata earthquake (M_W = 7.5). This was a well-documented case history, but it is a difficult one to back-analyze. The bearing capacity failure does not appear to have been symmetric and the building toppled as it failed. Cyclic inertial forces are unknown, and difficult to estimate, and the cyclic overturning moments exerted on the structure, and the resulting non-uniform bearing pressures at the base of the structure that contributed to the failure, cannot be reliably estimated. This case was eliminated from further analysis or use in these current studies.

3.3.3.2 Snow River Bridge Fill

The Snow River bridge fill suffered a liquefaction-induced failure during the 1964 Alaskan earthquake (M_W = 9.3). This liquefaction-induced failure has also been employed in multiple previous studies. This case was eliminated from further consideration in these current studies because of (1) uncertainties with regard to pre-failure geometries, (2) uncertainties with regard to actual failure mode (e.g. depth of failure), and (3) uncertainties associated with soil-structure interaction effects associated with the significant numbers of piles supporting the bridge.

3.3.3.3 Koda Numa Railway Embankment

The Koda Numa railway embankment suffered a liquefaction-induced stability failure with large displacements during the 1968 Tokachi-Oki earthquake (M_W = 7.9). This case had also been used in multiple previous studies. This case was eliminated for further back-analyses in these current studies because of lack of confidence in the information and documentation available

regarding the post-failure geometry and runout characteristics. The mass of the post-failure "displaced" material appears to be more than twice the mass that this same material occupied in the pre-failure geometry, and this discrepancy could not be resolved.

3.3.3.4 San Fernando Valley Juvenile Hall

The large hill slope adjacent to the San Fernando Valley Juvenile Hall facility suffered a liquefaction-induced downslope movement during the 1971 San Fernando earthquake (Mw = 6.6). This case had been employed in the previous studies, and relationships, of Seed (1987), Seed and Harder (1990) and Idriss (1998). This was a lateral spreading case history, and it was judged by the current engineering team (1) that the combination of relatively moderate static driving shear stresses and the significant cyclic lurching forces led to a situation in which cyclic lurching forces likely contributed significantly to the observed displacements, and (2) that the difficulties of dealing analytically with these cyclic forces would render accurate assessment of post-liquefaction S_r challenging. This case was therefore deleted from further consideration.

3.3.3.5 Whisky Springs Fan

The Whiskey Springs Fan was essentially another lateral spreading case, and it occurred during the 1983 Borah Peak earthquake (M_W = 7.3). This case had also been employed in the previous studies, and relationships, of Seed (1987), Seed and Harder (1990), and Idriss (1998). It was judged by the current engineering team that cyclic lurching forces likely contributed significantly to the observed displacements, and that the difficulty of having to analytically deal with these cyclic lurching forces would render accurate assessment of post-liquefaction strength challenging at best. This case was also deleted from further consideration.

3.3.3.6 Fraser River Delta

The Fraser River Delta case history involved a static liquefaction flow failure in the Fraser River Delta that occurred in 1985. It was employed in relationships developed by Olson and Stark (2002) and by Robertson (2010). This case was eliminated from further consideration in these current studies (1) because of lack of reliable pre-failure and post-failure geometries, and (2) because the post-liquefaction strength ratio had therefore been estimated only on the basis of laboratory tests performed on reconstituted samples of Fraser River Delta sands; tests that would not have included potential effects of field-scale void redistribution and/or inter-layer mixing.

3.4 Case Histories Selected for Formal Back-Analyses

Table 3.3 lists the 30 full-scale liquefaction field case histories back-analyzed in these current studies. These are divided into three classes (Classes A, B, and C) as described previously. The date of the observed field performance event, and the principal cause or mechanism, is also listed for each case history.

Table 3.1: Candidate Liquefaction Case Histories Considered

Case History	Apparent Cause of Sliding	Seed and Harder (1990)	Stark and Mesri (1992)	Olson and Stark (2002)	Robertson (2010)	Faris (2004)	Olson and Johnson (2008)
Zeeland - Vlietepolder	1889 High Tide	--	--	X	X	--	--
Coyote Creek	1906 San Francisco, California	--	--	--	--	X	--
Salinas River	1906 San Francisco, California	--	--	--	--	X	--
Sullivan Marsh	1906 San Francisco, California	--	--	--	--	X	--
Mission Creek	1906 San Francisco, California	--	--	--	--	X	--
Wachusett Dam - North Dike	1907 Reservior Filling	--	--	X	X	--	--
Calaveras Dam	1918 Construciton	X	X	X	X	--	--
Sheffield Dam	1925 Santa Barbara Eq. (M_L = 6.3)	X	X	X	X	--	--
Helsinki Harbor	1936 Construction	--	--	X	X	--	--
Fort Preck Dam	1938 Construction	X	X	X	X	--	--
Solfatara Canal Dike	1940 El Centro Eq. (M = 7.2)	X	X	X	X	--	--
Lake Merced Bank	1957 San Francisco Eq. (M = 5.7)	X	X	X	X	--	--
Snow River Bridge	1964 Alaska Eq. (M = 8.5)	X	X	--	--	--	--
Kawagishi-Cho Building	1964 Niigata Eq (M = 7.5)	X	X	X	X	X	--
Uetsu Railway Embankment	1964 Niigata Eq (M = 7.5)	X	X	X	X	--	--
North of Bandai Bridge	1964 Niigata, Japan	--	--	--	--	X	--
Echigo Railway	1964 Niigata, Japan	--	--	--	--	X	--
Hokuriku Building	1964 Niigata, Japan	--	--	--	--	X	--
Hotel Niigata	1964 Niigata, Japan	--	--	--	--	X	--
NHK Building	1964 Niigata, Japan	--	--	--	--	X	--
South of Niigata Station	1964 Niigata, Japan	--	--	--	--	X	--
Nerlerk Embankment - Slide 1	1990 Construction	--	--	X	--	--	--
Nerlerk Embankment - Slide 2	1990 Construction	--	--	X	--	--	--
Nerlerk Embankment - Slide 3	1990 Construction	--	--	X	--	--	--
North of Niigata Station	1964 Niigata, Japan	--	--	--	--	X	--
North of Route 345	1964 Niigata, Japan	--	--	--	--	X	--
Shitayama Shool	1964 Niigata, Japan	--	--	--	--	X	--
Showa Bridge	1964 Niigata, Japan	--	--	--	--	X	--
Portage Creek	1964 Prince William Sound, Alaska	--	--	--	--	X	--
Twentymile River	1964 Prince William Sound, Alaska	--	--	--	--	X	--

Table 3.1: Candidate Liquefaction Case Histories Considered (Continued)

Case History	Apparent Cause of Sliding	Seed and Harder (1990)	Stark and Mesri (1992)	Olson and Stark (2002)	Robertson (2010)	Faris (2004)	Olson and Johnson (2008)
El Cobre Tailings Dam	1965 Chilean Eq. (M_L = 7 to 7.25)	--	--	X	X	--	--
Koda Numa Railway Embankment	1968 Tokachi-Oki Eq. (M = 7.9)	X	X	X	X	--	--
Metoki Road Embankment	1968 Tokachi-Oki Eq. (M = 7.9)	--	--	X	X	--	--
Hokkaido Tailings Dam	1968 Tokachi-Oki Eq. (M = 7.9)	--	--	X	X	--	--
San Fernando Valley Juvenile Hall	1971 San Fernando Eq. (M_W = 6.6)	X	X	--	--	X	X
Lower San Fernando Dam U/S	1971 San Fernando Eq. (M_W = 6.6)	X	X	X	X	--	--
Lower San Fernando Dam D/S	1971 San Fernando Eq. (M_W = 6.6)	--	--	--	--	--	--
Upper San Fernando Dam	1971 San Fernando Eq. (M_W = 6.6)	X	X	--	--	--	--
Jensen Filtration Plant	1971 San Fernando, California	--	--	--	--	X	--
Tar Island Dyke	1974 Construction	--	--	X	X	--	--
Mochi-Koshi Tailings Dams	1978 Izu-Oshima Eq. (M = 7.0)	X	X	--	--	--	--
Mochi-Koshi - Dike 1	1978 Izu-Oshima Eq. (M = 7.0)	--	--	X	X	--	--
Mochi-Koshi - Dike 2	1978 Izu-Oshima Eq. (M = 7.0)	--	--	X	X	--	--
Heber Road	1979 Imperial Valley Eq. (M_W = 6.5)	--	X	--	--	X	X
Whiskey Springs Fan	1983 Borah Peak Eq. (M = 7.3)	X	X	--	--	X	X
Pence Ranch	1983 Borah Peak, Idaho	--	--	--	--	X	--
Hachiro-Gata Road Embankment	1983 Nihon-Kai-Chubu Eq. (M = 7.7)	--	--	X	X	--	--
East Slope of Maeyama	1983 Nihonkai-Chubu, Japan	--	--	--	--	X	--
South Slope of Maeyama	1983 Nihonkai-Chubu, Japan	--	--	--	--	X	--
Adjacent to Road No. 7	1983 Nihonkai-Chubu, Japan	--	--	--	--	X	--
Shonan-Cho	1983 Nihonkai-Chubu, Japan	--	--	--	--	X	--
Yoneshiro River	1983 Nihonkai-Chubu, Japan	--	--	--	--	X	--
Asele Raod Embankment	1983 Pavement Repairs	--	--	X	X	--	--
La Marquesa Dam - U/S Slope	1985 Chilean Eq. (M_S = 7.8)	X	X	X	X	--	--
La Marquesa Dam - D/S Slope	1985 Chilean Eq. (M_S = 7.8)	X	X	X	X	--	--
La Palma Dam	1985 Chilean Eq. (M_S = 7.8)	X	X	X	X	--	--
Fraser River Delta	1985 Gas Desaturation and Low Tide	--	--	X	X	--	--
Chonan Middle School	1987 Chiba-Toho-Oki Eq. (M = 6.7)	--	--	X	X	--	--
Landing Road Bridge	1987 Edgecumbe, New Zealand (M_W = 6.5)	--	--	--	--	--	X
James Street Loop	1987 Edgecumbe, New Zealand (M_W = 6.5)	--	--	--	--	--	X

Table 3.1: Candidate Liquefaction Case Histories Considered (Continued)

Case History	Apparent Cause of Sliding	Seed and Harder (1990)	Stark and Mesri (1992)	Olson and Stark (2002)	Robertson (2010)	Faris (2004)	Olson and Johnson (2008)
Whakatane Pony Club	1987 Edgecumbe, New Zealand (M_W = 6.5)	--	--	--	--	--	X
Lake Ackerman	1987 Seismic Survey	--	X	X	X	--	--
Wildlife Site	1987 Superposition Hills (M_W = 6.5)	--	--	--	--	--	X
Nalband Railway Embankment	1988 Armenian Eq. (M_S = 6.8)	--	--	X	X	--	--
Moss Landing MBARI Bldg 4	1989 Loma Prieta (M_W = 7.0)	--	--	--	--	--	X
Moss Landing MBARI Bldg 3	1989 Loma Prieta (M_W = 7.0)	--	--	--	--	--	X
Moss Landing MLML Bldg Eastward Spread	1989 Loma Prieta (M_W = 7.0)	--	--	--	--	--	X
Moss Landing MLML Bldg Westward Spread	1989 Loma Prieta (M_W = 7.0)	--	--	--	--	--	X
Miller Farm	1989 Loma Prieta (M_W = 7.0)	--	--	--	--	X	X
Farris Farm	1989 Loma Prieta (M_W = 7.0)	--	--	--	--	X	X
Leonardini Farm	1989 Loma Prieta (M_W = 7.0)	--	--	--	--	--	X
Sea Mist Farm	1989 Loma Prieta (M_W = 7.0)	--	--	--	--	--	X
Marina District, St. Francis Yacht Club	1989 Loma Prieta (M_W = 7.0)	--	--	--	--	--	X
Treasure Island	1989 Loma Prieta (M_W = 7.0)	--	--	--	--	--	X
MBARI	1989 Loma Prieta, California	--	--	--	--	X	--
MLML	1989 Loma Prieta, California	--	--	--	--	X	--
Leonardini Farm	1989 Loma Prieta, California	--	--	--	--	X	--
Soviet Tajik - May 1 Slide	1989 Tajik, Sovit Union Eq. (M_L = 5.5)	--	--	X	X	--	--
Nerlerk Embankment	1990 Construction	--	X	--	X	--	--
Eastbank	1990 Luzon, Phillippines	--	--	--	--	X	--
Southbank	1990 Luzon, Phillippines	--	--	--	--	X	--
Perez Blvd	1990 Luzon, Phillippines	--	--	--	--	X	--
Magsaysay Bridge, E. bank, d/s	1990 Luzon, Phillippines (M_W = 7.6)	--	--	--	--	--	X
Nable Street West	1990 Luzon, Phillippines (M_W = 7.6)	--	--	--	--	--	X
Nable Street East	1990 Luzon, Phillippines (M_W = 7.6)	--	--	--	--	--	X
Magsaysay Bridge, E. bank, u/s	1990 Luzon, Phillippines (M_W = 7.6)	--	--	--	--	--	X
Magsaysay Bridge, W. bank, u/s	1990 Luzon, Phillippines (M_W = 7.6)	--	--	--	--	--	X
Pogo Chico W. bank	1990 Luzon, Phillippines (M_W = 7.6)	--	--	--	--	--	X
Rudbaneh Town Canal	1990 Manjil, Iran (M_W = 7.4)	--	--	--	--	--	X
Sullivan Tailings	1991 Dyke Rising, British Columbia	--	--	--	X	--	--

Table 3.1: Candidate Liquefaction Case Histories Considered (Continued)

Case History	Apparent Cause of Sliding	Seed and Harder (1990)	Stark and Mesri (1992)	Olson and Stark (2002)	Robertson (2010)	Faris (2004)	Olson and Johnson (2008)
Shibecha-Cho Embankement	1993 Kushiro-Oki Eq.(M_L = 7.8)	--	--	X	X	--	--
Route 272 at Higashiarekinai	1993 Kushiro-Oki Eq.(M_L = 7.8)	--	--	X	X	--	--
Aichi East	1993 Nansei-Oki, Japan	--	--	--	--	X	--
Aichi West	1993 Nansei-Oki, Japan	--	--	--	--	X	--
Jamuna Bridge	1994 Construction, Bangladesh	--	--	--	X	--	--
Balboa Blvd.	1994 Northridge (M_W = 6.7)	--	--	--	--	X	X
Wynne Ave.	1994 Northridge (M_W = 6.7)	--	--	--	--	--	X
Potrero Canyon	1994 Northridge (M_W = 6.7)	--	--	--	--	--	X
Wufeng Site C (A-A')	1999 Chi-Chi, Taiwan (M_W = 7.6)	--	--	--	--	--	X
Wufeng Site C (B-B')	1999 Chi-Chi, Taiwan (M_W = 7.6)	--	--	--	--	--	X
Wufeng Site C1	1999 Chi-Chi, Taiwan (M_W = 7.6)	--	--	--	--	--	X
Wufeng Site B	1999 Chi-Chi, Taiwan (M_W = 7.6)	--	--	--	--	X	X
Wufeng Site M	1999 Chi-Chi, Taiwan (M_W = 7.6)	--	--	--	--	--	X
Nantou Site N	1999 Chi-Chi, Taiwan (M_W = 7.6)	--	--	--	--	--	X
Hotel Sapanca	1999 Kocaeli, Turkey (M_W = 7.4)	--	--	--	--	X	X
Police Station	1999 Kocaeli, Turkey (M_W = 7.4)	--	--	--	--	--	X
Soccer Field	1999 Kocaeli, Turkey (M_W = 7.4)	--	--	--	--	X	X
Yalova Harbor	1999 Kocaeli, Turkey (M_W = 7.4)	--	--	--	--	--	X
Norswing Drive	2003 San Simeon (M_W = 6.5)	--	--	--	--	--	X
Juanita Ave.	2003 San Simeon (M_W = 6.5)	--	--	--	--	--	X
Canadian Mine	(See Robertson (2010))	--	--	--	X	--	--

Table 3.2: Case Histories More Closely Considered for Potential Back-Analyses for Evaluation of Post-Liquefaction Strength (S_r)

Class	Case	Failure Date	Seed and Harder (1990)		Olson and Stark (2002)				Wang (2003) + Kramer (2008)			This Study
			S_r	$N_{1,60,CS}$	S_u(Liq)	S_u(Liq)/σ'_{vo}	σ'_{vo}	$N_{1,60}$ [1]	$\bar{S}_r$ [2]	S_r/σ_{vo}'	$\bar{N}_{1,60,CS}$	
A	Wachusett Dam - North Dike	1907 Reservior Filling			334	0.106	3158	7	348	0.136	7.3[3]	Analyzed
	Fort Peck Dam	1938 Construction	350	10	570	0.078	7341	8.5	671.5	0.091	15.8	Analyzed
	Uetsu Railway Embankment	1964 Niigata Eq (M = 7.5)	40	3	36	0.027	1280	3	43.5	0.048	2.9	Analyzed
	Lower San Fernando Dam - U/S Slope	1971 San Fernando Eq. (M_W = 6.6)	400	13.5	390	0.120	3482	11.5	484.7	0.133	14.5	Analyzed
	Hachiro-Gata Road Embankment	1983 Nihon-Kai-Chubu Eq. (M = 7.7)			42	0.062	670	4.4	65	0.164	5.7	Analyzed
	La Marquesa Dam - U/S Slope	1985 Chilean Eq. (M_S = 7.8)	200	6	65	0.07	911	4.5	(185.2)	0.110	6.5[3]	Analyzed
	La Marquesa Dam - D/S Slope	1985 Chilean Eq. (M_S = 7.8)	400	11	111	0.11	1000	9	(343.5)	0.186	9.9[3]	Analyzed
	La Palma Dam	1985 Chilean Eq. (M_S = 7.8)	200	4	100	0.12	789	3.5	(193.3)	0.123	4.2	Analyzed
	Lake Ackerman Highway Embankment	1987 Seismic Survey			82	0.076	1076	3	98	0.114	4.8	Analyzed
	Chonan Middle School	1987 Chiba-Toho-Oki Eq. (M = 6.7)			100	0.09	1119	5.2	(178.7)	0.091	6.4[3]	Analyzed
	Soviet Tajik - May 1 Slide	1989 Tajik, Sovit Union Eq. (M_L = 5.5)			175	0.08	2170	7.6	(334)	0.082	8.9[3]	Analyzed
	Shibecha-Cho Embankement	1993 Kushiro-Oki Eq.(M_L = 7.8)			117	0.086	1351	5.6	208.9	0.200	5.6	Analyzed
	Route 272 at Higashiarekinai	1993 Kushiro-Oki Eq.(M_L = 7.8)			100	0.097	1030	6.3	130.5	0.125	8.5	Analyzed
B	Zeeland - Vlietepolder	1889 High Tide			115	0.05	2396	7.5	(226.1)	0.048	8.5[3]	Analyzed
	Sheffield Dam	1925 Santa Barbara Eq. (M_L = 6.3)	75	6	75	0.05	1429	5	(99.8)	0.043	8.2[3]	Analyzed
	Helsinki Harbor	1936 Construction			32	0.06	522	6	(52.4)	0.067	5.9[3]	Analyzed
	Solfatara Canal Dike	1940 El Centro Eq. (M = 7.2)	50	4	50	0.08	624	4	(77.1)	0.063	4.9[3]	Analyzed
	Lake Merced Bank	1957 San Francisco Eq. (M = 5.7)	100	6	144	0.11	1372	7.5	(139.5)	0.106	5.9[3]	Analyzed
	El Cobre Tailings Dam	1965 Chilean Eq. (M_L = 7 to 7.25)			40	0.020	1946	0	(195.2)	0.020	6.8	Analyzed
	Metoki Road Embankment	1968 Tokachi-Oki Eq. (M = 7.9)			38	0.04	875	2.6	(116.8)	0.044	2.0	Analyzed
	Hokkaido Tailings Dam	1968 Tokachi-Oki Eq. (M = 7.9)			100	0.07	1376	1.1	(250.6)	0.074	5.1	Analyzed
	Upper San Fernando Dam - D/S Slope	1971 San Fernando Eq. (M_W = 6.6)	600	15								Analyzed
	Tar Island Dyke	1974 Construction			251	0.06	4300	7	(364.2)	0.058	8.9[3]	Analyzed
	Mochi-Koshi Tailings Dam, Dikes 1 and 2	1978 Izu-Oshima Eq. (M = 7.0)	250	5	75	0.06	1251	2.7	(158.9)	0.091	8.9	Analyzed
					113	0.10	1090	2.7	(233.6)	0.081	10.0	
	Nerlerk Embankment, Slides 1, 2, and 3	1983 Construction			52	0.09	616	8.7	(178.5)	0.124	11.4[3]	Analyzed
					36	0.06	650	7.2				
					31	0.03	925	7.2				
	Asele Road Embankment	1983 Pavement Repairs			132	0.10	1251	7	(163.7)	0.104	11.0[3]	Analyzed
	Nalband Railway Embankment	1988 Armenian Eq. (M_S = 6.8)			119	0.11	1101	9.2	(139.9)	0.109	6.3[3]	Analyzed
	Sullivan Tailings	1991 Dyke Rising, British Columbia										Analyzed
	Jamuna Bridge	1994 Construction, Bangladesh										Analyzed
C	Calaveras Dam	1918 Construction	650	12	721	0.112	6422	8	632.7	0.099	10.5[3]	Analyzed
D	Kawagishi-Cho Building	1964 Niigata, Japan (M = 7.5)	120	4	111	0.08	1474	4.4	(123.5)	0.089	4.3	Not Analyzed
	Snow River Bridge Fill	1964 Alaskan Eq. (M = 8.5)	50	7					(50)	0.025	8.5[3]	Not Analyzed
	Koda Numa Railway Embankment	1968 Tokachi-Oki Eq. (M = 7.9)	50	3	25	0.05	485	3	(48)	0.045	3.6	Not Analyzed
	San Fernando Valley Juvenile Hall	1971 San Fernando Eq. (M_W = 6.6)	130	10.5								Not Analyzed
	Whiskey Springs Fan	1983 Borah Peak Eq. (M = 7.3)	150	11								Not Analyzed
	Frasier River Delta	1985 Low Tide			N/A	0.100	N/A	5.3				Not Analyzed

Notes : (1) No fines content correction utilized in Olson and Stark (2002).

(2) Where noted in parentheses, S_r values shown are for secondary cases in Wang (2003) and were not fully reanalyzed by the ZIF Method.

(3) $N_{1,60,CS}$ values were changed in Kramer (2008) from the values reported in Wang (2003). The updated values are shown.

Table 3.3: Case Histories Back-Analyzed for Evaluation of Post-Liquefaction Strength (S_r)

Class	Case Number	Case	Failure Date
A	1	Wachusett Dam - North Dike	1907 Reservior Filling
	2	Fort Peck Dam	1938 Construction
	3	Uetsu Railway Embankment	1964 Niigata Eq (M = 7.5)
	4	Lower San Fernando Dam - U/S Slope	1971 San Fernando Eq. (M_W = 6.6)
	5	Hachiro-Gata Road Embankment	1983 Nihon-Kai-Chubu Eq. (M = 7.7)
	6	La Marquesa Dam - U/S Slope	1985 Chilean Eq. (M_S = 7.8)
	7	La Marquesa Dam - D/S Slope	1985 Chilean Eq. (M_S = 7.8)
	8	La Palma Dam	1985 Chilean Eq. (M_S = 7.8)
	9	Lake Ackerman Highway Embankment	1987 Seismic Survey
	10	Chonan Middle School	1987 Chiba-Toho-Oki Eq. (M = 6.7)
	11	Soviet Tajik - May 1 Slide	1989 Tajik, Sovit Union Eq. (M_L = 5.5)
	12	Shibecha-Cho Embankement	1993 Kushiro-Oki Eq.(M_L = 7.8)
	13	Route 272 at Higashiarekinai	1993 Kushiro-Oki Eq.(M_L = 7.8)
B	15	Zeeland - Vlietepolder	1889 High Tide
	16	Sheffield Dam	1925 Santa Barbara Eq. (M_L = 6.3)
	17	Helsinki Harbor	1936 Construction
	18	Solfatara Canal Dike	1940 El Centro Eq. (M = 7.2)
	19	Lake Merced Bank	1957 San Francisco Eq. (M = 5.7)
	20	El Cobre Tailings Dam	1965 Chilean Eq. (M_L = 7 to 7.25)
	21	Metoki Road Embankment	1968 Tokachi-Oki Eq. (M = 7.9)
	22	Hokkaido Tailings Dam	1968 Tokachi-Oki Eq. (M = 7.9)
	23	Upper San Fernando Dam - D/S Slope	1971 San Fernando Eq. (M_W = 6.6)
	24	Tar Island Dyke	1974 Construction
	25	Mochi-Koshi Tailings Dam, Dikes 1 and 2	1978 Izu-Oshima Eq. (M = 7.0)
	26	Nerlerk Embankment, Slides 1, 2, and 3	1983 Construction
	27	Asele Road Embankment	1983 Pavement Repairs
	28	Nalband Railway Embankment	1988 Armenian Eq. (M_S = 6.8)
	29	Sullivan Tailings	1991 Dyke Rising, British Columbia
	30	Jamuna Bridge	1994 Construction, Bangladesh
C	14	Calaveras Dam	1918 Construction

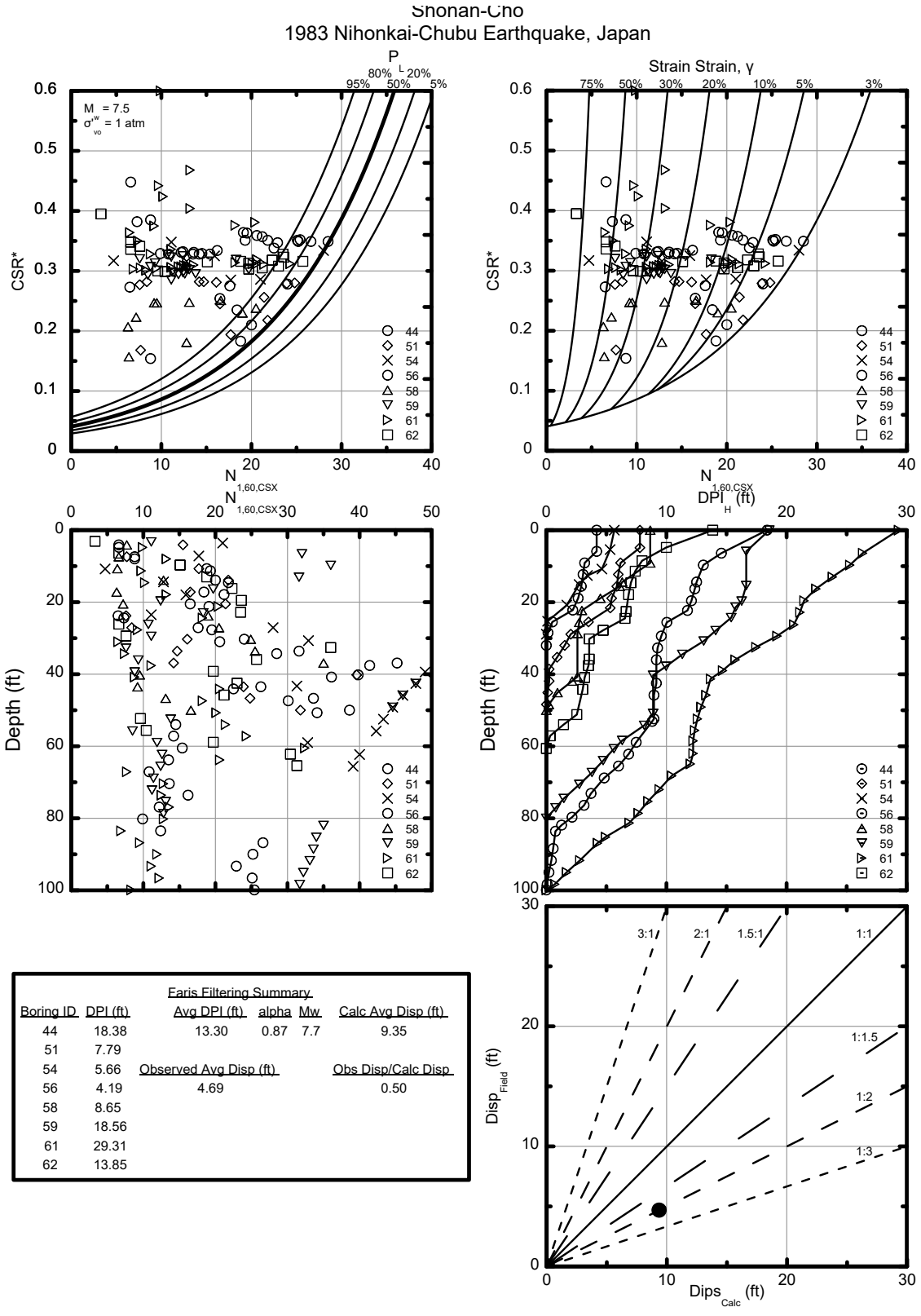

Figure 3.1: Illustration of the methodology developed by Faris (2004) for prediction of lateral spreading displacements; example analysis applied to the Shonan-Cho case history.

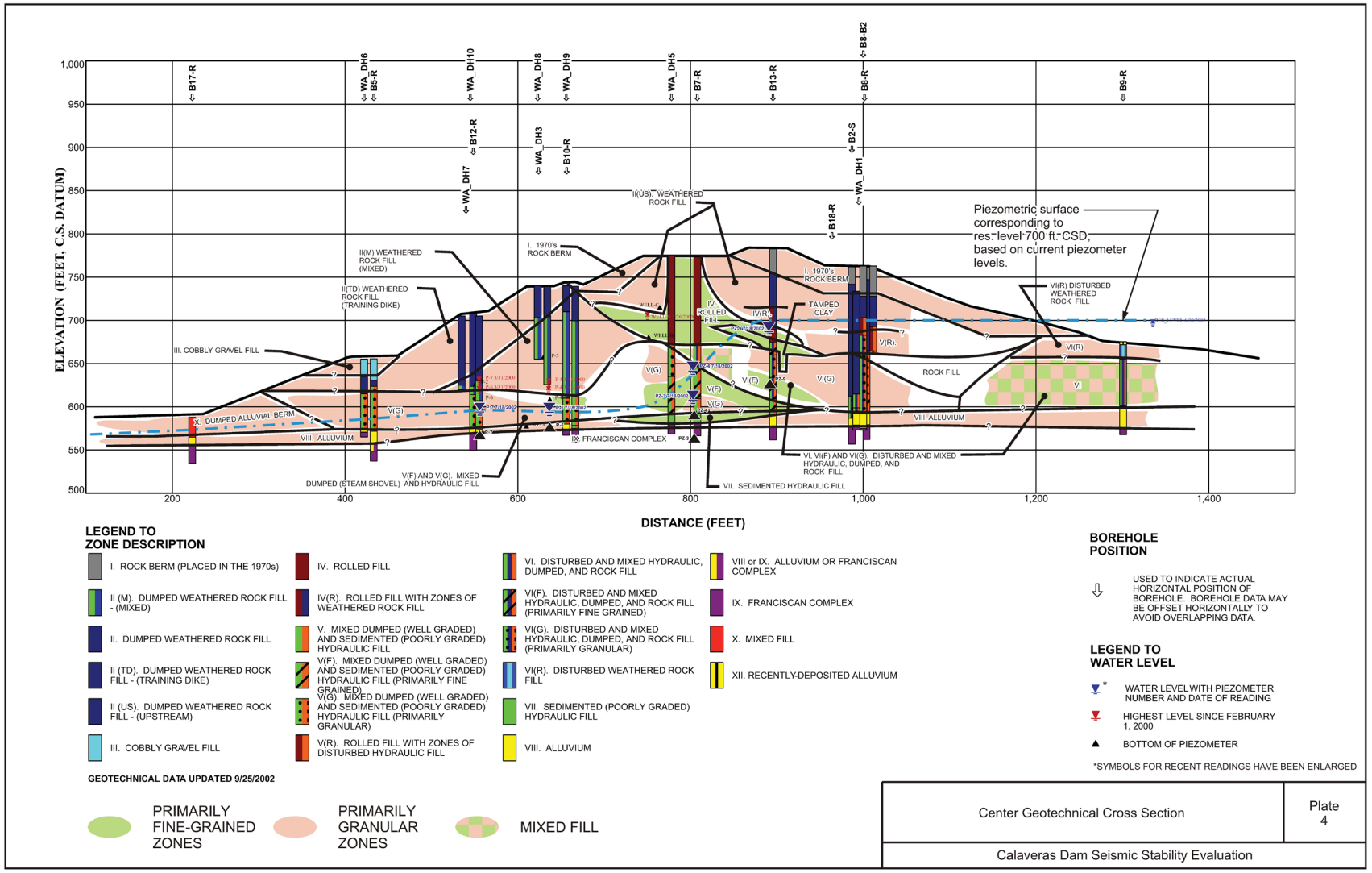

Figure 3.2: Cross-section of the reconstructed Calaveras dam showing general soil material zones as developed based on recent Seismic investigations (Olivia Chen Consultants, 2003).

Chapter Four

Back-Analyses of Liquefaction Failure Case Histories

4.1 Introduction

The 30 liquefaction failure case histories selected for inclusion in these studies (see Table 3.2) were subjected to back-analyses and back-assessments by a variety of methods, depending upon the amounts and quality of data available for each of these cases. Cross-comparisons were made with other case histories back-analyzed in these current studies, and cross-comparisons were also made with the results and findings for many of these case histories from previous investigations.

A number of new methods were developed in these current studies for improved back-analyses and assessments of post-liquefaction strengths, and these will be presented and explained as this chapter proceeds. It is also important to understand the approaches and procedures used by a number of previous investigators for similar back-analyses or back-assessments of post-liquefaction strengths in order to understand the juxtaposition of the results of those previous studies with the new results presented herein. Accordingly, this chapter will also discuss a number of previous back-analysis methods, and their strengths and drawbacks.

Table 4.1 presents a list of the principal methods of interest for these current studies. These include methods employed by previous investigators, and also new methods developed for these current studies. This list provides a useful template for some of the discussions that will follow. Methods listed towards the top of the list tend to provide the highest levels of accuracy and reliability with regard to back-analyzed values of post-liquefaction strengths for cases to which they can be applied. But they also tend to require good quality data and information, and cannot be applied to all case histories. Methods listed lower on the table tend to provide intermediate to lower levels of accuracy and reliability, but can more readily be applied to cases with lesser levels of information and data available.

4.2 The Incremental Momentum Method

4.2.1 General Overview

A new method has been developed to provide a more accurate and reliable means of incorporating momentum effects in back-analyses of large displacement liquefaction failures performed for purposes of assessment of post-liquefaction strength (S_r). This new method will be referred to as the incremental momentum analysis method.

This method is illustrated in Figures 4.1 through 4.3, for the case of the liquefaction-induced slope failure that occurred on the upstream side of the Lower San Fernando Dam as a result of the 1971 San Fernando earthquake. A full explanation of this failure case history, and a

more complete exposition of all back-analyses performed for this case history, are presented in Appendix A, Section A.5.

As shown in Figure 4.1, the upstream slope failure of the Lower San Fernando Dam was the result of liquefaction of the lower portion of the hydraulic fill materials comprising the upstream shell of the dam during the 1971 San Fernando earthquake. This was an unusually well-investigated failure, and two large trenches were excavated fully through the failed embankment so that a detailed mapping of the displaced locations of recognizable portions of the embankment could be documented. Largely intact portions (or "blocks") of the displaced upstream side of the dam were then mapped back to their initial positions, and it could be seen that the failure involved liquefaction of the lower portion of the hydraulic fill on the upstream side (the "dark" zone in Figures 4.1(a) and (b)), with the overlying embankment sections translating outwards in the upstream direction borne along atop the liquefied materials.

The incremental momentum method involves developing a series of estimated (and feasible) cross-sections incrementally tracking the progression of displaced geometries from inception of movements to the final, residual post-failure geometry. This is more challenging than the approach taken in estimation of the "ZIF" interim cross-section geometry by Wang (2003), as discussed previously in Section 2.3.8, because it requires that all intermediate geometries must provide a reasonable path forward all the way to the observed final residual geometry. It is therefore a very tedious and time-consuming process, involving numerous iterations between analyses and estimation and drawing of cross-sections, and one that requires both engineering judgment and some artistic capability.

Important benefits of this approach, relative to the previous "kinetics" approaches taken by Olson (2001), as discussed in Section 2.3.7, and the previous "ZIF" method of Wang (2003), as discussed in Section 2.3.8, include the following:

1. This process is constrained by the eventual need to converge on the observed final geometry, requiring a more reasonable and reliable path forward at each incremental cross-section.

2. The process lends itself to creating a step-wise "animation" which can be clicked forward and in reverse on a computer screen, much like a step-wise video, and these animations have proven to be useful with regards to enhancing engineering insight and understanding.

3. The series of incremental cross-sections permit updated evaluations of (a) driving shear stresses, (b) failure plane details (e.g. lengths of the failure plane currently controlled by liquefied or non-liquefied materials, overall failure plane lengths, sections of the failure plane where stronger or weaker soils have over-ridden weaker or stronger soils as shearing progressed (weaker soils then control), etc.), and (c) evolving geometries and properties (including strengths) as displacing and deforming embankment toes enter into bodies of water and potentially either hydroplane or ride out atop weaker reservoir or offshore sediments, etc. These are potentially very important benefits, but the ability to "update" the evolving analyses in all of these regards also poses an additional set of analytical judgments and responsibilities, and it also takes further time and effort.

4. The analysis is performed with basic physics (Newton's Second Law) and basic soil mechanics governing the progressive evolution of accelerations, velocities, momentum, and displacements during the slide movements. The analysis proceeds continuously from inception of movements to completion. There is therefore no need to "estimate" the partial displacement stage that corresponds to the "ZIF" displacement stage of Wang (2003).

5. Driving shear stresses are correctly calculated at each increment, so there is no difficulty or uncertainty with regard to the level of accuracy with which the curvilinear polynomial surface of the "kinetics" analysis method of Olson (2001) suitably approximates the driving shear forces at each stage of partial lateral displacement.

6. The incremental momentum method is the only method among the three that can largely correctly deal with the issues and effects associated with incrementally developing (retrogressive) failures that initiate and fail in a "slice by slice" progression beginning with an initial slice (or wedge) near the front face and then retrogressing (with successive slices) eventually back to the final back heel of the overall failure.

The resulting analysis is thus more accurate, more reliable, more adaptable, and better able to account for evolving details as the failure progresses. The corollary price to be paid is then the additional level of effort, and time, involved in performing these very challenging and tedious analyses.

Figure 4.2 shows the incremental progression of cross-sections judged to represent this current engineering team's "best estimate" of the likely progressive evolution of failure for the case of the Lower San Fernando Dam upstream slope failure. The benefits of this progressive approach, in terms of approximate "animation" and visualization, were of special value here, as it has long been debated whether this failure occurred either (1) as an initially monolithic failure, with subsequent "break-up" and progressive partial separation (or articulation) of individual slices and blocks occurring as the failure progressed, or (2) as an incrementally progressive failure, with the slices nearest the front face of the slide mass moving first, followed by successive slices, in sequence, as each successive slice was partially "unbraced" by the displacement of the slice that preceded it, until the failure eventually retrogressed in "slice by slice" incremental fashion back to the eventual final back heel. By creating multiple potential realizations of the failure sequence, it became clear that this particular failure likely initiated relatively monolithically, and then broke up as it traveled, because it was otherwise not feasible to re-produce the observed final positions of some of the more rear-ward slices. This could not be reliably ascertained a priori, and it should be noted that some of the other case histories back-analyzed in these current studies clearly did proceed in an incrementally progressive (retrogressive) manner, and that some others did not.

An animation of this incremental analysis of the upstream liquefaction induced slide in the Lower San Fernando Dam can be accessed at the following link:

Link: https://www.jweber.sites.lmu.edu/more/lsfd-us/

The animation presents a series of composite incremental steps of the analysis of the Lower San Fernando Dam failure, showing (1) the incremental evolution of displaced geometries, (2) the

evolution of the displaced location of the center of gravity of the overall failure mass, and (3) incremental evolution of acceleration, velocity and displacement of the center of gravity vs. time. The sequential images of the animation can be "clicked" forward and backward to help engineers better visualize the step-wise progression and mechanics of the incremental momentum analysis, giving the viewer a sense of the motions and of the development of forces and displacements, etc. This can be surprisingly useful, and it can enhance understanding and can also serve as a basis for further tuning of the modeled progression of cross-sections.

Figure 4.3 then illustrates the calculated evolution of acceleration, velocity and displacement of the center of gravity of the eventual overall failure mass. At each step in time, the best estimate of (a) driving (downslope) shear forces and (b) resisting (upslope) shear resistance are compared, and any overall force imbalance is then applied to the overall failure mass by Newton's Second Law ($F = m \bullet a$). The resulting acceleration (or deceleration) is then calculated, and so is the corollary resulting increase or decrease in velocity (of the overall center of gravity), and the associated incremental accumulation of displacements as well. As shown in Figure 4.3, velocity initially increases as the mass begins to move downslope, and then decreases as the mass slows down and then eventually comes to rest.

Shear strengths for non-liquefied soils are modeled at each stage based on the best available information and data, and basic principles of soil mechanics. Liquefied zones are assigned a post-liquefaction strength of S_r, and the value of S_r is then iterated until the calculated progression (e.g. Figure 4.3) shows the final displacements to match those observed in the field. This requires another series of iterative adjustments, and analyses, further adding to the effort required. The seven "dots" for small circles on the plots of Figure 4.3 show the situation at time-steps corresponding to the first seven updated (incremental) cross-sections of Figure 4.2. The eighth and final cross-section of Figure 4.2 differs from the seventh only in that the reservoir has eventually seeped through (likely at a low spot) and infilled the "dip" near the top back-heel of the slide mass of the preceding (seventh) incremental cross-section.

Once a best-estimate case had been established and analyzed, parameter (and assumption) sensitivity studies were next performed. Only a few additional fully incremental momentum analyses were usually performed here. Instead, a case-specific relationship between pre-failure and post-failure geometries, strengths, and representative S_r was established for each case (see Section 4.4), and then simpler analyses of pre-failure and post-failure geometries were performed to more efficiently evaluate the effects of changes in conditions and parameters over the ranges considered plausible and/or feasible. In some cases, additional full incremental analyses had to be performed to examine modeling of challenging situations such as (1) ranges of potential conditions with regard to monolithic vs. incrementally retrogressive initiations of failures, and (2) ranges of modeling choices for toes of slide masses entering into bodies of water, etc.

In this manner, the effects of variations in properties, assumptions, and modeling details on back-calculated values of S_r were evaluated to inform estimates of uncertainty or variance. Variations that were commonly modeled and analyzed here often included: (1) shape and location of the failure surface, (2) whether or not the failure was incrementally progressive (retrogressive) or monolithically initiated, (3) location of the phreatic surface at the time of the failure, (4) shear strengths of soils judged not to have liquefied, (5) variations in unit weights, and (6) variations in

assumptions and modeling of conditions at the bases of toes of failures that enter into bodies of water or that travel outward into areas occupied by weak sediments.

4.2.2 Modeling of Strengths at the Toes of Slide Masses Entering Bodies of Water, and Weak Sediment Effects

A number of the failure case histories involved liquefaction flow slides that either entered into reservoirs, or that progressed underwater in either lakes or offshore waters. In these cases, the question arises as to whether hydroplaning occurred, and if so to what extent, and what effect would it have had on shear strengths at the bases of the toes of these masses. Hydroplaning is the entrapment of water beneath the toe of an advancing slide mass, so that the toe section (or some portion of the toe section) rides out atop the entrapped water; with the strength of water rather than of soil (or liquefied soil) then controlling shear strength beneath some portion of the slide toe.

This had been addressed very approximately on a case by case basis by Seed (1987) and by Seed and Harder (1990). Most other previous investigators did not address this issue or did not elaborate it if they did. Olson (2001) discussed this for some specific cases, and appears to have assigned a 50% reduced post-liquefaction strength (0.5 x S_r) at the bases of toes of a number of slides as they entered into bodies of water, and then examined variations of between 0% reduction to 100% reduction in assessing potential parameter sensitivity effects. Wang (2003) [and Kramer, 2008] examined the available literature regarding hydroplaning, and developed a simplified but repeatable, quantitative (and semi-probabilistic) procedure for analysis of the likelihood that hydroplaning would occur, and for the likely resulting effects on strengths at the bases of toes of slide masses entering into water. They allowed a maximum lateral penetration of hydroplaning effects beneath the toes of slide masses of up to 10 times the thickness of the soils entering into water, and the amount of this maximum distance that was specifically assumed (modeled) as being affected by hydroplaning for any given case was then primarily a function of velocity of movements. Higher velocity movements were assumed to over-ride and capture/entrap larger areas of water (hydroplaning).

In these current studies, yet another approach was taken.

Examining the available research, it was our investigation team's conclusion that the available knowledge does not yet support rigorous analytical treatments of potential hydroplaning. Likelihood of hydroplaning is clearly affected by velocities of the traveling soil masses, but this does not yet give rise to fully reliable calculation methods. Wang (2003) addressed this with probabilistic estimates of likelihood and extent of hydroplaning, and with subsequent Monte Carlo simulations of the effects of these variations on back-calculated S_r values. Similarly, available research suggests that hydroplaning would occur only to some limited depth of penetration beneath advancing toes of slopes, but attempting to extrapolate table-top scale experimental physical models to field situations is challenging, and it is further complicated by the tapered shapes of the toes of advancing slide masses making it difficult to select a "representative" thickness of the slope materials entering the water. As a result, the approach taken to hydroplaning was largely judgmental, informed when possible from evidence from each individual case history. For example; if the runout of a slide mass into a body of water results in separation of some portion of

the toe of the slide mass from the remainder, then it is concluded that the toe section likely hydroplaned and continued to move a bit farther than the remainder of the slide mass. In many cases there was no definitive data or evidence as to the occurrence or absence of hydroplaning; in those cases judgments were made by the engineering analysis team, and then averaged and also bounded as sensitivity studies to inform both best estimates as well as variance or uncertainty.

A second issue potentially also affecting a number of the liquefaction failure case histories is the presence of weak reservoir sediments, or the presence of weak offshore slope sediments, or weak soils or sediments in agricultural fields adjacent to roadway or railway embankments. Advancing toes of slide masses traveling out onto such weaker sediments can be partially "lubricated" at their bases if the advancing slide mass rides atop the weaker sediments, in which case the strengths of the weaker sediments can control. But it is also possible for the toes of slide masses to "plough through" weaker sediments, displacing them, in which case lesser reduction in available strengths beneath the toes would occur. Previous investigations have usually not been clear as to whether, or how, they addressed the effects of potential sliding atop weaker sediments at the advancing toes of failure masses.

In these current studies, it was decided to address these two issues (potential hydroplaning, and potential sliding atop weak sediments) on a case-by-case basis.

In considering hydroplaning, velocities of the advancing toes would be considered but would only provide some guidance. And some limitations on depths of potential penetration of hydroplaning laterally beneath the toes of advancing slide masses would be imposed, but this would vary over a somewhat broader range than just a maximum of 0 to 10 times the thickness of the advancing soils, in part because selection of a representative thickness was not well-defined. When possible, details of the actual observed eventual runout of the failure flow slide mass were examined for clues as to likely hydroplaning. As an example, for the failure of the Fort Peck Dam (see Appendix A, Section A.2) it appears that a portion of the extreme toe of the failure mass separated itself to some extent from the more intact rest of the failure mass, and extended itself more thinly out into the reservoir. This suggests either hydroplaning and/or sliding atop weak reservoir sediments at the toe of this failure. Similarly, the main "toe" section of the failure mass runout of the upstream side of the Lower San Fernando Dam (as shown in the final three cross-sections of Figure 4.2) appears to continue on with its own momentum in late stages of the slide and separates itself a bit from the rest of the slide mass; suggesting either hydroplaning and/or sliding atop soft reservoir sediments. In other cases, failure masses traveled very large distances and did not really "come to rest" in the classical sense; also suggesting hydroplaning. In many cases, however, this was simply a source of uncertainty, and the full range of possible hydroplaning conditions were included within the parameter sensitivity analyses performed. Strengths where hydroplaning was modeled were varied from 20% to 80% of the overlying soil (or liquefied soil) strengths, usually with a "best estimate" value of 50%.

Weak sediments were handled in a similar manner. Strengths at the bases of slide masses traveling outwards onto likely weak sediments were typically assigned strengths equal to values that varied from 25% to 100% of the overlying soil (or liquefied soil) strengths as part of the parameter sensitivity studies performed; again usually with a best estimate value of 50%.

More detailed explanations of modeling and treatment of hydroplaning, and of weak sediments, are presented for each of the individual case histories in Appendices A and B.

4.2.3 Incrementally Progressive (Retrogressive) Failures

A number of the liquefaction failure case histories were suspected of having possibly proceeded in an incrementally progressive manner, initiating with movements of a smaller "slice" or wedge near the front face, and then retrogressing back towards the eventual rear heel of the overall slide in a sequence of subsequent "slice by slice" initiations of movements of additional slices or wedges as each slice becomes partially unbraced by loss of support from the slices that preceded it.

This type of incrementally progressive (retrogressive) failure propagation was not tractable to accurate analyses by previous methods, and so the potential impacts of this (as opposed to assumed monolithic initiation of the entire failure as a single coherent mass right from the start) were initially unknown. It should be noted that failures can be initiated as largely monolithic failures and can then "break up" (or segment and articulate) as they travel, so it can sometimes be difficult to discern whether a given failure was monolithically initiated, or was incrementally progressive (retrogressive) in its initiation mechanics.

The incremental momentum method developed and employed in these current studies can successfully address both monolithic and incrementally progressive (retrogressive) failures.

This is illustrated in Figures 4.4 and 4.5 for the Shibecha-Cho Embankment failure case history. A more complete exposition of this case history is presented in Appendix A, Section A.2.

The Shibecha-Cho Embankment was a very large side-hill fill that supported a populated development, and it failed during the 1983 Kushiro-Oki earthquake. The failure was known to have been an incrementally progressive (retrogressive) failure based on the initial forensic investigation, and so it was analyzed as such in these current studies.

Stability analyses performed for the un-displaced (pre-failure) cross-section, assuming that liquefaction has been "triggered", show that a slice near the front face is the most critical (has the lowest factor of safety). This failure case history was modeled (best estimate case) as beginning with the inception of movements of this first slice, and then progressing with successive inceptions of movements of two additional successive "slices", as shown in Figure 4.4. After the first slice had progressed some distance, a second slice began to move, and then eventually a third.

The analyses tracking the incremental development of acceleration, velocity and displacements for this case were performed for two parallel sets of centers of gravity, and the results are shown in Figure 4.5. The incremental values for the center of gravity of the initial slice (the slice closest to the front face) are initially tracked by the dashed lines in Figure 4.5. Simultaneously, the values for the overall center of gravity of eventual overall failure mass are also calculated (by weighted mass averaging of the moving slice, and of the portions of the eventual failure mass not yet in motion), and these are shown by the solid lines in Figure 4.5. The

initial failure slice is thus the "active" element in the opening stages. When the second slice begins to move, the dashed lines then track the evolving values for the center of gravity of the combined first and second slice masses (by weighted mass averaging), while the solid lines continue to track the evolving movements of the center of gravity of the overall eventual slide mass (also by weighted mass averaging). The same is then done when the third and final slide mass begins to move, at which point the entire failure mass is engaged and the overall slide mass center of gravity is tracked by the remainders of the solid lines.

Modeling initiation of successive slices reduced overall peak velocities, and also reduced corollary overall momentum, and thus produced a lower back-calculated value of S_r than would have been produced by a monolithic inception of failure. The value of S_r back-calculated with modeling of incrementally progressive failure for the Shibecha-Cho Embankment case history (as illustrated in Figures 4.4 and 4.5) was $S_r \approx 224$ lbs/ft^2. When this case was modeled instead as a monolithically initiated failure, the somewhat higher momentum effects produced a higher value of $S_r \approx 263$ lbs/ft^2. The effects of incrementally retrogressive initiation of this failure were thus of moderate magnitude with regard to back-calculated values of S_r for this case; reducing S_r by approximately 15% from the "monolithic inception" failure model for this particular case.

4.2.4 Evaluation of Representative Penetration Resistance

Appendix C presents an expanded discussion of the basis for evaluations of representative SPT $N_{1,60,CS}$ values in these current studies for each of the case histories back-analyzed. An abridged discussion will be presented here.

For cases where modern, and properly well-documented, SPT data were available, correction of SPT N-values to generate equipment and procedurally corrected N_{60}-values were made using largely the corrections proposed by Cetin et al. (2018a,b), except that (1) a slightly reduced adjustment was made for short rod effects at shallow depths as per Deger (2014), and (2) normalization of N_{60}-values for effective overburden stress effects was performed using the relationships recommended by Deger (2014). The slightly reduced short rod correction had essentially negligible effect in these current studies, as few SPT data were used from the very shallow depths at which this might have produced a noticeable difference. The effective overburden stress normalization relationships of Deger (2014) provide normalization curves somewhat intermediate between those of Cetin et al. (2018a,b) and of Idriss and Boulanger (2008). These relationships are presented in Appendix C. For all practical purposes, the SPT correction procedures of Cetin et al. (2018a,b) were employed, and they are the recommended basis for forward analyses of additional cases and/or applications to engineering project evaluations.

The procedural and equipment corrections made herein were largely similar to those of Seed et al. (1984), and of Idriss and Boulanger (2008), and would produce largely compatible results for most of the field liquefaction failure case histories.

Fines corrections for this study were made using the fines corrections recommended by Cetin et al. (2018a,b). This is an area where some minor differences occur between various investigation teams working on studies of post-liquefaction S_r. The fines adjustment of Cetin et

al. (2018a,b) is somewhat intermediate between the fines adjustments of Seed et al. (1984) and the fines adjustment that Seed (1987) suggested specifically for S_r purposes. In the end, the fines corrections of these studies, and (1) those employed by Seed (1987) and (2) those recommended by Idriss and Boulanger (2008) do not produce major differences, but they do vary slightly relative to each other. Olson and Stark (2001, 2002) elected not to employ any fines corrections, so that they used $N_{1,60}$-values rather than $N_{1,60,CS}$-values, and that causes a number of their characterizations of SPT penetration resistance to vary somewhat from the other studies for soils with higher fines contents.

Different investigation teams took different approaches to determining what "representative" penetration resistances were. It is widely understood that lower than median values of penetration resistance will likely control actual field failures because nature (and the laws of physics) will choose to exploit zones of weakness within a zone of heterogeneity of strengths. Wride et al. (1999) specifically developed predictive correlations for estimation of post-liquefaction strength (S_r) based on near lower bound values of penetration resistance, as discussed in Section 2.3.6. A drawback of that approach is volatility of the near lower bound value, especially for cases with sparse data.

In these current studies, it was decided instead to use slightly "scalped" (or selectively filtered) mean and median values of penetration resistance to characterize the liquefiable soils of interest.

"Scalped" in these current studies means deletion of potentially (or likely) spurious high penetration resistance values, and also examination of penetration resistance values for SPT performed in mixed soils with the fines representing potentially cohesive clayey soils. High individual SPT N-values ("flyers") that separate themselves from the main body of data for a soil zone or stratum are examined, and if this separation is large then these anomalously high values are deleted as likely spurious, either because they may represent a local anomaly (or larger coarse particle), or because a localized "denser" zone would likely be bypasses by a failure surface/mechanism; only up to a few percent of the overall data may be deleted here, and in most cases there were no deletions. These anomalously high values may be the result of potential gravel effects, or their cause may be unknown. In addition, when sufficient data are available, SPT performed in soils classified as SC are also deleted. Currently available fines adjustments do not consistently well handle these materials, and their corrected SPT N-values often tend to be lower than many of the rest of the SPT performed on less cohesive materials, even after fines adjustments, in mixed soil zones of varying fines content and consistency (plasticity, or plasticity index: PI).

"Representative" $N_{1,60,CS}$ values were selected in these current studies by examining the median and mean values from the scalped or slightly filtered data sets, and then selecting a value equal to the median except in cases with significant numbers of data where the mean and median differed greatly; for those cases the selected "representative" value was sometimes closer to the average between these two (mean and median). In most data sets, median values were generally used. $N_{1,60,CS}$ values were assumed to be normally distributed in performing regressions to develop empirical relationships between penetration resistance and post-liquefaction strength. Median and mean values were thus assumed to be essentially the same, and standard deviations <u>of the mean</u> of $N_{1,60,CS}$ were modeled as a measure of estimated variance. This standard deviation of the mean is

very different than the standard deviation of the $N_{1,60,CS}$ values, and it exhibits smaller variance. These variances were in many cases affected more by uncertainties involved with conversion of non-standard penetration resistance data to estimates of equivalent SPT $N_{1,60,CS}$ values, than by variance among the individual penetration resistance values measured for a given soil stratum.

When either CPT data, or non-standard penetration data, or lesser quality information regarding placement conditions and history, were used to develop estimates of equivalent SPT $N_{1,60,CS}$ values, the details of ascertaining and/or estimating both mean $N_{1,60,CS}$ values and Standard deviation of the overall mean $N_{1,60,CS}$ values are presented on a case by case basis in Appendices A and B.

For two of the case histories (Wachusset Dam and Fort Peck Dam) additional corrections were required for ageing effects, as multiple decades elapsed between the occurrences of these two failures and the eventual performance of modern SPT investigations. The details of the corrections made for ageing effects in these two cases were case specific, and these details are presented in Appendix A, Sections A.1 and A.2, respectively.

4.2.5 Evaluation of Representative Initial Effective Vertical Stress

Values of "representative" initial effective vertical stress in liquefied materials for each case history were evaluated by averaging the pre-failure effective vertical stresses along the portion of the failure plane that would be controlled by liquefied materials. Approximate calculations were made by summing vertical stresses at the bases of slices in liquefied materials in slope stability calculations for the pre-failure geometries, and averaging these along the liquefied slide plane lengths. These provided adequately close approximations of initial vertical effective stresses, and they also appear to provide good agreement with estimates of initial vertical stresses made by Olson and Stark (2001, 2002) for most cases, especially if Olson's values are adjusted slightly (reduced a bit) to account for the fact that he generally assumed slightly shallower failure surfaces for most of his cases, and (2) Wang (2003) and Kramer (2008) for the nine "primary" case histories for which Wang (2003) performed independent assessments of initial effective vertical stresses.

A more comprehensive discussion and cross-comparisons between values of representative values of initial effective vertical stress for each case history developed and/or employed by different investigation teams is presented in Sections 2.3.8.1(b) – (ii) and at the end of this chapter in Section 4.7.

4.3 Back-Analyses of the 14 Case Histories of Classes A and C

4.3.1 Back-Analyses and Results

The 14 "high quality" case histories of Classes A and C were back-analyzed using the new incremental momentum method, and the details of these analyses are presented in Appendix A. The single Class C case history was back-analyzed using the new incremental momentum method,

but the results were used only to help calibrate and cross-check the other case history back-analyses, and not for development of regressed predictive relationships for evaluation of S_r. The main analyses of the Class A and C cases were performed by the incremental momentum method, and additional analyses were also made using simple static limit equilibrium stability analyses to develop back-calculated values of (1) the "apparent" pre-failure yield stress ($S_{r,yield}$) which is defined as the theoretical strength along liquefied portions of the eventual slide surfaces that would be required to provide a calculated static Factor of Safety equal to 1.0 for pre-failure geometry, and (2) the "apparent" residual stress based on final residual geometry ($S_{r,resid/geom}$) defined as the strength along liquefied portions of the failure surface that would be required to provide a post-failure calculated static Factor of Safety equal to 1.0 for the final, residual post-failure geometry. These values of $S_{r,yield}$ and $S_{r,resid/geom}$ would prove useful (1) in evaluating the results of the incremental momentum analyses, (2) in developing empirical methods for checking these types of back-analyses, and (3) for helping to make back-assessments of S_r for some of the case histories in the set of 16 Class B cases, as will be described in Section 4.4.

Table 4.2 shows the results of the back-analyses performed for the 14 Class A and C case histories (in the columns to the far right). Also shown are values developed by the previous investigations of Seed and Harder (1990), Olson and Stark (2001, 2002), and Wang and Kramer (2003, 2008). Values shown are "representative" values developed by each investigation team. For these current studies these are "best estimate mean values". The values for the other three investigation teams appear to be largely compatible with this basis.

The values of effective vertical overburden stress listed for Wang and Kramer (2003, 2008) in Table 4.2 for the nine "primary" cases to which they applied their "ZIF" back-analysis procedure are based on direct evaluations of overall average initial vertical effective stress on the assumed failure surface; and these evaluations are largely compatible with the approach taken in these current studies (except that different failure surfaces were sometimes employed, and unit weights, etc.). The values of effective vertical overburden stress listed for Wang and Kramer (2003, 2008) in Table 4.2 for the 22 "secondary" cases in which their "ZIF" method was not employed are inferred from their collection and averaging of multiple values of (1) S_r and (2) S_r/σ'_{vo} developed by previous teams of other investigators/analysts for each case, and then using these averaged values to infer σ'_{vo}. As discussed previously in Section 2.3.8.1(b), (and shown in Table 2.3) this proved to be a poor process and it resulted in clearly unreasonable values of σ'_{vo} for at least nine of their "secondary" case histories, and poor values for four additional cases. The secondary case histories of Kramer and Wang (2003, 2008) can be identified in this table because their S_r values are enclosed in parentheses.

4.3.2 Comparison with Results from Previous Studies

Table 4.3 shows a modified presentation of the same cases shown in Table 4.2.

Values of S_u(Liq) [S_r in these current studies] for ten of the field failure case histories studied by Olson and Stark (2002) were calculated using their "kinetics" method (see Section 2.3.6), which appears to have largely correctly incorporated momentum effects. These were the ten case histories that Olson and Stark judged to have sufficient quality of data available as to

justify this relatively advanced analysis approach. The resulting values of post-liquefaction strength for these ten "high quality" case histories back-analyzed by the "kinetics" method which incorporates momentum effects are listed in Table 4.2 without parentheses.

The other 23 cases with lesser quality data or information that Olson analyzed were back-analyzed using what they described as "simplified" methods. This amounted largely to evaluation of the "apparent" post-liquefaction strengths based on the value of S_u(Liq) required to provide a calculated static Factor of Safety equal to 1.0 at the end of deformations/displacements, and those values thus represent values of "$S_{r,resid/geom}$" as defined in these current studies. These $S_{r,resid/geom}$ values would significantly underestimate the actual S_r values, as discussed later in Section 4.4, likely by factors of approximately 1.2 to 3.4 (see Figures 4.8 through 4.11), and so they are not directly comparable with the values calculated in these current studies for the Class A and C cases. Fortunately, Olson (2001) had also calculated values of both $S_{r,yield}$ and $S_{r,resid/geom}$ for all but one of the 33 cases which he back-analyzed. The $S_{r,yield}$ values were developed as part of an examination of a potential triggering analysis approach that was not intended to be directly related to back-analyses of S_r, and the $S_{r,resid/geom}$ values were developed as a primary basis for conservative estimation of S_r for the 23 less well-documented case histories. As a result of Olson having developed both of these values, it is possible to use his values of these two indices to develop better estimates of S_r that would then be more directly comparable with the S_r values back-calculated for the Class A and C cases in these current studies. As will be developed in detail in Section 4.4, reasonably good estimates of the actual S_r values for most cases can be estimated as

$$S_r \approx \xi \bullet (S_{r,yield} + S_{r,resid/geom}) / 2 \qquad \text{[Eq. 4-1]}$$

where ξ can be taken as approximately 0.8.

This produces values of S_r that approximately incorporate momentum effects.

Given the availability of values of $S_{r,yield}$ and $S_{r,resid/geom}$ back-calculated by Olson (2001), the values of S_u(Liq) for cases not calculated by the "kinetics" method can be replaced with values estimated by Equation 4-1, employing a value of $\xi = 0.8$. For 22 of the 23 cases that were not back-analyzed by Olson's "kinetics' method, and for which Olson's own values of values of $S_{r,yield}$ and $S_{r,resid/geom}$ are available, values of S_r as estimated based on Equation 4-1 have been substituted in Table 4.3. These are shown in Table 4.3 [within square brackets], to provide values of S_r that also (at least approximately) incorporate momentum effects. Several of Olson's lesser quality cases were not included in these current studies, so no values for those cases are shown in Tables 4.2 and 4.3.

For one case [El Cobre Tailings Dam] Olson (2001) did not employ his "kinetics" analysis method, and he also did not calculate a value of $S_{r,yield}$. The value of S_r for this case is shown within triangular brackets in Table 4.3, and it represents a very conservative (low) $S_{r,resid/geom}$ value.

Values of S_r were back-calculated by Wang (2003) for the nine highest quality field performance case histories using the "ZIF" method (see Section 2.3.7), which approximately correctly incorporated momentum effects, and the resulting values of post-liquefaction strengths are listed in Table and 4.3 with no parentheses. Values of S_r from Wang and Kramer listed with

parentheses in Tables 4.3 are those for most of the 22 additional "secondary" cases with lesser quality data for which Wang did not perform the full ZIF analyses, and instead adopted values based on judgmental averaging of values developed by other previous teams of investigators. These are probably not strongly systematically biased, but they are less likely to be fully accurate and reliable. Several of Wang's "secondary" cases were not included in these current studies, and so values for those are not shown in Tables 4.2 and 4.3.

The modified values shown in Table 4.3 then represent the best available basis for cross-comparison of back-calculated values of S_r that incorporate momentum effects for the cases of Classes A and C.

The value of S_r from Seed and Harder (1990) shown for the Fort Peck dam case history is notably low compared to the other three investigation teams. That is because the runout distance was very large for this case, and Seed and Harder underestimated the multiplier (ξ) in Equation 4-1 that would provide a good estimate of S_r with approximate inclusion of momentum effects for this case. (Better values of ξ as a function of runout indices are developed next in these current studies, as presented and described in Section 4.4 which follows.)

The value of Olson and Stark (2002) for the Shibecha-Cho Embankment case history is notably low compared to the results of the other investigation teams. This is because, as was discussed and illustrated previously in Section 4.2.3, the Shibecha-Cho failure was a strongly incrementally progressive failure, retrogressing backwards in successive slices towards the eventual back heel. (An even more complete explanation of the analyses of this incrementally progressive failure is presented in Appendix A, Section A.12). Olson correctly recognized that this was an incrementally progressive failure, and attempted to account for this retrogressive progression by performing his "kinetics" analysis while tracking only the initial (front-most) failure slice. This was not successful, as he was only able to track and analyze momentum, forces, and post-liquefaction shear strength, for the first (initial) small "slice" nearest to the front face. This neglected most of the overall failure mass, and most of the momentum, and it resulted in significant underestimation of S_r for this case.

Wang and Kramer (2003, 2008) appear to have selected high averaged values of S_r for the two La Marquesa Dam failures (upstream side and downstream side failures). These were developed by averaging of values developed by multiple previous investigators, and they were affected by high values developed by Seed and Harder (1990) as was discussed previously in Section 2.3.8.1(b).

Wang and Kramer calculated a somewhat lower S_r value, based on their ZIF analysis method, for the Calaveras Dam case history than the values back-calculated by Olson and Stark (2002) and by these current studies. Olson and Stark employed their kinetics method, and these current studies employed the incremental momentum approach. All three of these analysis methods explicitly incorporate momentum effects, and it must be suspected that the differences here are the result of differing modeling and parameter details in the three different sets of analyses. The Calaveras case history results are not employed in development of correlations for forward prediction of S_r in these current studies because, as described in Chapter 3, Section 3.3.2, the combination of still-consolidating cohesive-dominated hydraulic fill zones at the time of the failure, and unpredictable ageing effects occurring in variably cohesive/non-cohesive hydraulic

fills over the eight decades that followed, make it impossible to reconcile modern site investigation results (and recent penetration resistance data) with the original field failure performance observed.

For the remainder of the 14 Class A and C cases, values of S_r are judged to be in generally good agreement among the four investigation teams represented in Tables 4.2 and 4.3, especially given the differences between analytical approaches and modeling details employed by the different investigation teams.

There are approximations and judgments required in each of these analyses, and overall agreement among the 14 cases comprising Classes A and C is judged to be good to excellent.

There is, of course, a preference here for the values developed by the more difficult, more detailed and more flexible incremental momentum method which better addresses some of the details of these cases and appears likely to provide higher levels of reliability of back-calculated S_r values as well. The cross-comparisons of Table 4.3 are interpreted herein as reflecting a good level of support for the values back-calculated by this method.

4.4 Development of New Empirical Relationships for Back-Analyses of Case Histories for Assessment of S_r

The values back-calculated and presented in Section 4.3 for the 14 Class A and C field case histories back-analyzed by the incremental momentum method were next used to develop two sets of empirical relationships for (a) cross-checking the results of back-analyses of liquefaction flow failures for consistency, and (b) making back-estimates of S_r from other liquefaction failure case histories where lesser quality data and information are available. In the end, these new relationships also provide a basis for approximate checking of engineering analyses of expected liquefaction-induced displacements and deformations for large displacements cases, with likely useful applications for evaluations of interim reservoir restrictions for dams that require eventual seismic hazard mitigation.

4.4.1 Pre-Failure and Post-Failure Analyses Calibrated Based on Runout Characteristics

As noted in a number of previous sections, simple static limit equilibrium analyses can be performed to evaluate (1) the back-calculated value of the "apparent" pre-failure stress ($S_{r,yield}$) along liquefied portions of the eventual slide surface required to provide a calculated static Factor of Safety equal to 1.0 for pre-failure geometry, and (2) the "apparent" residual stress ($S_{r,resid/geom}$) required to provide a post-failure calculated static Factor of Safety equal to 1.0 for the final, residual post-failure geometry. $S_{r,yield}$ would, of course, over-estimate the actual post-liquefaction strength; otherwise the failure would not have occurred. And $S_{r,resid/geom}$ would underestimate the actual post-liquefaction strength, as it does not account for momentum effects as the travelling failure mass must be brought back to rest. These values of $S_{r,yield}$ and $S_{r,resid/geom}$ would therefore "bracket" the actual value of S_r for any given case history.

Further discussion of this is now warranted.

For cases in which "flow" or slide displacements are very small, there would be relatively little difference between $S_{r,yield}$ and $S_{r,resid/geom}$, and momentum effects would also be small. In such cases, simply adding $S_{r,yield}$ plus $S_{r,resid/geom}$, and then dividing by two would provide a good estimate of S_r. This could be expressed as

$$S_r \approx \xi \bullet (S_{r,yield} + S_{r,resid/geom}) / 2 \qquad \text{[Eq. 4-2]}$$

where ξ can be taken as nearly 1.0.

At the other extreme, for cases in which runout distances were infinitely large, post-liquefaction strength would be essentially equal to zero, in which case S_r could be estimated as

$$S_r \approx \xi \bullet (S_{r,yield} + S_{r,resid/geom}) / 2 \qquad \text{[Eq. 4-3]}$$

where ξ can be taken as nearly equal to zero.

This reasoning then gives rise to the observation that the general form of Equations 4-1 through 4-3 can be improved by making the value of ξ a function of observed runout distance. Also, it is observed that ξ is bounded, and can have values of between 1.0 and zero. And that values of ξ can be expected to decrease with increases in runout distance.

Figure 4.6 shows best estimate values of post-liquefaction strength (S_r) back-calculated by the incremental momentum analyses for the 14 case histories of Classes A and C, plotted on the vertical axis, and on the horizontal axis it shows the averaged "before and after" values of ($S_{r,yield}$ + $S_{r,resid/geom}$) / 2 as calculated by Equation 4-1 with ξ assumed equal to 1.0. This "before and after" average is simply the average of $S_{r,yield}$ and $S_{r,resid/geom}$.

As shown in this figure, generally good fitting of a majority of the back-calculated data is achieved if the value of ξ is set a bit lower than 1.0, with most of the back-analyses being well-represented by values of ξ of between 0.6 to 1.0.

A fully general form of this relationship can then be expressed as

$$S_r \approx \xi \bullet (S_{r,yield} + S_{r,resid/geom}) / 2 \qquad \text{[Eq. 4-4]}$$

where ξ is a function of runout distance and overall failure mechanism characteristics.

Three of the 14 cases plotted in Figure 4.6 are cases in which incrementally progressive (retrogressive) failure initiation is thought to have affected back-calculated values of S_r, and it was necessary to develop a slightly modified version of Equation 4-4 for these types of cases. The initial value of $S_{r,yield}$ for these cases was calculated for (1) the initial (smaller) initial failure mass nearer the front face of the failure, and (2) for the eventual overall (entire) failure mass. These two values were then averaged to develop the "representative" overall value of $S_{r,yield}$ for purposes of the relationships modeled in Equation 4-4. This was then employed, along with $S_{r,resid/geom}$ from

the eventual (final) post-failure residual geometry (for the entire failure mass) in Equation 4-4 to develop the "before and after" averaged value of $(S_{r,yield} + S_{r,resid/geom}) / 2$ for these incrementally regressive cases. Additional analyses were then also performed for each of these three cases, but this time employing only the $S_{r,yield}$ value for the initial (smaller) initial failure slice and then the $S_{r,resid/geom}$ value for the overall residual post-failure condition of the overall failure mass, as with all of the other case histories (which were not significantly incrementally retrogressive).

The three cases to which this slightly modified calculation was applied were Case A.2 (Fort Peck Dam), Case A.3 (Uetsu Railway Embankment), and Case A.12 (Shibecha-Cho Embankment). For each of these cases, the values calculated based on only the $S_{r,yield}$ values calculated for the initial (smaller) initial failure slices are shown with dashed circles, and the values calculated using the averaged $S_{r,yield}$ values for the initial (smaller) initial slices and the larger (overall) failure mass are shown with solid circles. These latter values are judged to be the better and more representative values.

The Fort Peck Dam failure case history was modeled as being only slightly incrementally progressive/retrogressive (see Appendix A, Section A.2) and the differences here between the two approaches are minor, supporting both the interpretations here, and the modeling of the case as only slightly progressively retrogressive. For the Uetsu and Shibecha Cho Embankment failure case histories, the differences were somewhat more significant, as would have been expected (see Appendix A, Sections A.3 and A.12, respectively).

The next step was then to invert Equation 4-4, using the actual values of S_r as calculated using the incremental momentum method, to develop case-specific values of ξ. These values of ξ for each of the 14 back-analyzed Class A and C case histories were then plotted against different measures of runout distance. The best relationship was found to be achieved by cross-correlation of ξ with "scaled runout distance", defined as the total distance travelled by the center of gravity of the overall failure mass divided by the initial slope height as measured from the toe of the failure to the top of the eventual back heel of the overall failure.

This is plotted for each of the 14 Class A and C case histories back-analyzed by the incremental momentum method in Figure 4.7. As shown in this figure, a relatively strong relationship between ξ and scaled runout resistance can be observed. It can also be seen that the value of ξ would approximately approach 1.0 for zero runout distance, as would be expected if cyclic inertial effects were either zero or were neglected. It can also be seen that ξ appears to trend towards zero (as would theoretically be the case) for a runout ratio equal to infinity.

Figure 4.7 serves to demonstrate the good internal consistency between the back-calculated values of S_r for these 14 well-defined field case histories. It also represents a basis for evaluation of ξ as a function of runout distance, which in turn makes Equation 4-4 significantly more useful for empirical estimation of S_r.

A second set of empirical relationships were then developed by plotting "Initial Factor of Safety" vs. "Final Factor of Safety" for these 14 Class A and C cases, as shown in Figure 4.8. Initial factor of safety here is defined as the apparent static Factor of Safety calculated for pre-failure geometry with the strength of the of the liquefiable soils set equal to the best estimate value

of actual S_r back-calculated using the full incremental momentum method. Similarly, the final factor of safety is the static value of FS calculated using this best estimate value of S_r from the incremental momentum back-analyses and assigning it to the liquefied soils in the post-failure (final) residual geometry configuration.

As shown in Figure 4.8, the values back-calculated for the 14 cases all occur within a reasonably well-defined range. Closer inspection of the individual cases (identified by number in the figure, and by name in the "key" in the upper right-hand corner of the figure) shows that cases with larger "scaled runout distance" have lower Initial FS values, and higher Final FS values. Figure 4.9 then repeats Figure 4.8, but this time each case history's "dot" is annotated (in parentheses) with the ratio representing scaled runout ratio (distance traveled by the center of gravity of the overall failure mass divided by the initial slope height from the toe to the top of the back heel of the failure). It be seen that the cases tend to move from the bottom right hand portion of the observed range, towards the top left portion of the figure, with increasing scaled runout distance.

The two relationships of (1) Figures 4.6 and 4.7 and (2) Figures 4.8 and 4.9 provide a systematic basis for understanding some of the interactions between the runout mechanics of liquefaction failures, and the post-liquefaction strengths and various calculated stability measures associated with these failures.

These relationships can then be used for several purposes:

1. They can be used as an internal check for consistency and reasonableness for back-analyses of S_r performed within a study such as this current one. There had not previously been any useful tools for that.

2. They can also be used to cross-check engineering analyses of expected deformations, and resulting displaced geometries, for forward analyses of engineering projects. As an example, it is not uncommon once a major dam has been studied and found likely to pose an unacceptable risk with regard to potential for liquefaction-induced failure, for the reservoir to be "restricted" to a constrained maximum elevation until repairs/mitigation can eventually be implemented. Reservoir restrictions imposed are usually the result of assessments of likely worst-case deformations, in order to ensure that these will not result in uncontrolled release of the reservoir as long as the reservoir level is kept at or below the restricted level. High-order finite element and finite difference analyses are often brought to bear here. These analyses involve a number of choices and decisions with regard to modeling and parameters, and there are potential additional numerical difficulties associated with extreme mesh deformations as calculated deformations and displacements become large. The accuracy, and the acceptable conservatism, of such analyses can be difficult to verify. There are currently no widely accepted ways to reliably "check" the results of such analyses. Both of the relationships developed here (Figures 4.7 and 4.9) can be employed for that purpose.

3. Finally, these two sets of relationships can also be employed to help to extract reasonable back-analyzed or back-estimated values of S_r for liquefaction failure case histories of lesser

overall quality, reliability, or documentation than the 14 cases of Classes A and C. These relationships are thus useful in back-analyses of a number of the 16 additional liquefaction failure case histories of Class B, as described in Appendix B and in Section 4.5 below.

4.5 Back-Analyses of the 16 Case Histories of Class B

4.5.1 Back-Analyses and Results

The 16 lesser quality liquefaction case histories of Class B were next back-analyzed. Details of individual analyses and assessments for each of these case histories are presented in Appendix B. The quality, quantity, reliability and level of documentation of data and information regarding various aspects of these Class B cases varied considerably. As a result, these cases were judged not to warrant the incremental momentum analyses applied to the Class A and C cases.

But it was not sufficient here to simply take the values back-calculated, or estimated, by previous investigators. One of the objectives of these current studies was to make the best achievable assessments of both the "best estimate" values of $\overline{S_r}$, $\overline{N_{1,60,CS}}$ and representative $\overline{\sigma'_{vo}}$ for each case history, and also the best possible estimates of uncertainty or variance for each of these three indices. Considerable effort was therefore also expended on back-analyses and back-assessments of these "lesser" cases.

This served to differentiate these current studies from all previous efforts. A number of previous studies had done a relatively good job, or at least applied a good deal of effort, to back-analyses of many of the Class A and C cases. But none of those studies had then continued on to devote significant and/or comprehensive efforts to independent evaluation (or re-evaluation) of the significantly larger number of Class B cases as well.

It is not possible to simply and concisely describe the ranges of approaches, judgments, etc. that were employed in back-assessments of the 16 additional cases. Engineers who are interested are encouraged to examine the case-by-case explanations and expositions presented in Appendix B, as the details of the judgments made in processing these cases can be important.

The values that resulted from these back-analyses and assessments generally carried larger values of uncertainty (and thus larger standard deviations) than was common for the Class A and C cases. This often reflected significant uncertainties associated with lack of data, poor quality of data, poor documentation of data, etc. The values of standard deviations reported for each parameter are, for each case, the best estimates of this investigation team taking all uncertainties into account.

Table 4.4 presents a summary of the back-analysis results for the Class B cases, in the form of best estimate values of representative $\overline{S_r}$, $\overline{N_{1,60,CS}}$ and $\overline{\sigma'_{vo}}$ for each case. Four sets of values are shown, corresponding to the values recommended by each of four different investigation teams: (1) Seed and Harder (1990), (2) Olson and Stark (2002), (3) Wang and Kramer (2003, 2008) and (4) these current studies.

Table 4.5 then repeats the presentation of the back-analysis results for the Class B back-analyses, but the values shown in square parentheses for Olson and Stark (2002) again are modified values representing values calculated using Equation 4-1, with $\xi = 0.8$, and using the case-specific values of $S_{r,yield}$ and $S_{r,resid/geom}$ reported by Olson (2001). These replace the systematically biased (low) values estimated by Olson (2001) based on $S_{r,resid/geom}$., and they provide better estimates of S_r because they account (approximately) for momentum effects.

Similarly, the values shown in parentheses in Tables 4.4 and 4.5 for Wang and Kramer (2003, 2008) are values that they selected based on their averaging of selected values from other previous investigators, with no further analyses of their own, and so do not represent fully independent assessments of their own.

Generally good to excellent agreements among the several sets of values shown for the 16 Class B cases in Table 4.5 for most cases (after modifying the S_r values of Olson and Stark, 2002, based on their calculated $S_{r,yield}$ and $S_{r,resid/geom}$ values reported and Equation 4-1) appears to provide good support for the values developed in these current studies.

The value of S_r reported by Olson (2001) for the El Cobre Tailings Dam case history could not be modified to the value produced by Equation 4-1, because the necessary initial yield and post-failure residual geometry values of $S_{r,yield}$ and $S_{r,resid/geom}$ were not presented by Olson for that lone case. The value shown is that recommended by Olson and Stark, but as discussed in Appendix B, Section B.20, it appears to be estimated based on a very conservative back-calculation of $S_{r,resid/geom}$ and thus appears to be unreasonably low. The relationship of Figures 4.8 and 4.9 would suggest that this $S_{r,resid/geom}$ value would underestimate S_r for this case by a factor of approximately 2 to 3. Multiplying Olson's value of $S_{r,yield} = 40$ lbs/ft^2 by 2.5 would produce an estimate of $S_r = 100$ lbs/ft^2, in excellent agreement with the value of $S_r = 95$ lbs/ft^2 back-calculated in these current studies.

Wang and Kramer (2003, 2008) appear to have unreasonably high values of S_r for two cases, the Hokkaido Tailings Dam failure and the Nerlerk Embankment Slides. They did not perform independent back-analyses of their own for these two cases; instead they averaged values from multiple previous investigations. As discussed previously in Chapter 2, Section 2.3.8.2(b), the Hokkaido Tailings Dam value employed by Kramer and Wang appears to be the result of an error. They averaged two values of S_r from previous investigations for this case, and one of these was a value of $S_r = 408$ lbs/ft^2 attributed to Ishihara, et al. (1990); but the actual value developed by Ishihara et al. (1990) for this case history is only $S_r = 137$ lbs/ft^2 . Using the (correct) lower value would significantly lower the overall average. A similar, but more complicated set of apparent poor values led to an error in the value employed by Kramer and Wang for the Nerlerk Embankment Slides; readers are referred to the detailed discussion presented previously in Chapter 2, Section 2.3.8.2(b).

In these current studies, values of S_r back-calculated for the two Moshi-Koshi Tailings Dam failures (Dikes 1 and 2) were averaged (see Appendix B, Section B.25), because these were two very similar failures and it was judged that using them as two separate cases would over-emphasize (over-weight) their contribution to the regressions that will follow. Similarly, the three Nerlerk Embankment slides (Appendix B, Section B.26) were also averaged in these current studies, as they were also similar features and including them as three separate cases would over-emphasize (over-weight) their contribution to the regressions that will follow.

Finally, it is noted that no cross-comparisons can be made for the values calculated in these current studies for two cases: the Sullivan Tailings case history and the Jamuna Bridge case history. This is because the other investigation teams listed in Tables 4.4 and 4.5 did not include these two more recent cases, which had not been available for their earlier studies. There have been previous back-analyses of these cases by other investigators, but those were not well documented and provide a relatively poor basis for cross-comparisons. See Appendix B, Sections B.28 and B.29 for details.

A second comparison of the results developed for the Class B cases can be made by plotting the results onto the figures and relationships previously presented in Figures 4.6 and 4.7.

Figure 4.10 repeats Figure 4.6, but this time the results of back-analyses of the 16 Class B cases have been added (with open triangles). For 8 of the Class B cases, no reliable post-failure geometry was available, so in some of the cases it was necessary to assume approximate values of the "After" value of $S_{r,resid/geom}$. These were, for the most part, cases wherein the post-failure displacements had been very large, often causing much of the failure mass to travel down underwater slopes to such extent that they could not reliably be tracked. Low (but not quite zero) values of $S_{r,resid/geom}$ were modeled for most of these cases. These assumptions, and the bases for them, are presented in detail for each case in the corresponding sections of Appendix B. The uncertainties introduced by these assumptions are incorporated in the modeled values of uncertainty (or standard deviation) for each case as listed in Tables 4.6 and 4.7.

Figure 4.11 then repeats Figure 4.7, but this time the results of back-analyses of the 16 Class B cases have been added (with open triangles). For 6 of the 16 Class B cases, it was not possible to make refined evaluations of the relative displacements in terms of runout ratios (center of failure mas travel distance divided by initial slope height defined as height from toe to back heel of the failure mass), so these cases could not be plotted in this framework. These were generally cases in which runout distances were very large, but they often involved (1) failures that travelled onto relatively steep offshore slopes where the slide masses did not quickly come to rest, (2) situations in which much of the failure mass travelled over a "lip" and then continued down a steeper slope, or (3) cases in which very soft surface sediments may have led to the very large continuing downslope displacements observed.

There is generally good consistency between the Class B cases, and the better-defined and better back-analyzed Class A and C cases, in both Figures 4.10 and 4.11, providing a useful additional check of internal consistency among the back-analyses and evaluations performed for the Class B cases.

4.6 Summary of Back-Analysis Results

The results of the back-analyses of all 30 cases (Classes A, B and C) as developed in these current studies (see Appendices A and B) are presented in Table 4.7. This table presents both the best-estimate mean values, and also the best estimate standard deviations, for each of the three indices that will next be used to develop predictive relationships for in situ S_r.

Only one other previous study has been carried forward far enough as to provide useful values for cross-comparison here, and that is the work of Wang (2003) and Kramer (2008).

Table 4.8 presents a comparison between the indices developed in these current studies and those developed by Wang (2003). The values for penetration resistance were subsequently changed to non-fines-corrected $N_{1,60}$ values by Kramer (2008) in his regressions to develop predictive relationships for S_r. The original fines-corrected $N_{1,60,CS}$ values are more appropriate for direct cross-comparisons, and so those will be used here as a cross-check on the two sets of studies.

As discussed previously in Section 2.3.7, the means and basis by which Wang (2003) and Kramer (2008) developed both their mean estimates and their estimates of standard deviation or variance of these means differed greatly from the approaches taken in these current studies. Their approaches did not fully incorporate the influence of uncertainties related to poor documentation of case history data and information, and poor quality of data and information, and so they subsequently applied judgmental weighting factors to down-weight the contributions of the less well-documented cases. That was prudent with regard to development of predictive relationships with good median fit (50% relationships), but it may not have fully characterized overall model uncertainty. The weighting factors (WF) employed by Kramer (2008) in performing regressions to develop predictive relationships are also listed in Table 4.8. These range from 1.0 for cases that are well-characterized and well-documented, to as low as 0.22 for cases with poor data and information quality.

In these current studies, the investigation team has preferred instead to put forth the best estimates of overall uncertainty of each parameter ($\overline{S_r}$, $\overline{N_{1,60,CS}}$ and $\overline{\sigma'_{vo}}$), including <u>all</u> factors contributing to uncertainty (including paucity of data, poor quality data, poor information on pre-failure or post-failure geometries, uncertainty with regard to phreatic surface, poor documentation, etc.). As a result, the standard deviations shown for these current studies in Tables 4.7 and 4.8 incorporate all uncertainties as best that can be accomplished, and this results in natural "self-weighting" of each case in the probabilistic regressions that will follow in Chapter 5 as cases with higher uncertainties naturally exert less "pull" on the regressed relationships. This approach is preferred here, because (1) it does not require the engineering team to impose its judgment in the form of weighting factors, and (2) it permits the subsequent regressions to incorporate the best available characterizations of individual case history uncertainties in developing assessments of overall predictive model uncertainties. Because the cases are "self-weighting" with their total uncertainty estimates, the additional weighting factors applied to all but one of the cases in these current studies are taken as WF = 1.0.

The single exception is the Calaveras Dam case history, which was reluctantly deleted from use in the regressions that will follow due to new information developed in the late 1990's that led the current investigation team to conclude that it was not possible to cross-relate the S_r values from the failure that occurred in 1918 with SPT data from more recent studies, given the variability of fines contents in some of the main hydraulic fill zones affecting the 1918 slope failure, and the variably cohesive nature of those fines, and the fact that portions of the dam's embankment fill were likely underconsolidated at the time of the failure under the still rising fill loads (see Appendix A, Section A.14). Because the Calaveras Dam case history is deleted from use in the regressions that will follow, the weighting factor assigned in Table 4.8 is WF = 0.

Both the approaches taken in these current studies, and those taken by Wang and Kramer, with regard to treatment of uncertainties should be considered valid alternatives. And so this just represents another set of differences in choices between the current engineering team and the efforts of Wang and Kramer (2003, 2008). In the end, the multiple, and potentially significant, differences in approaches taken by these two studies are a positive thing, as they permit two independent looks at a problem that is only moderately well constrained by data and thus subject to significant engineering judgment at multiple steps along the way.

Another difference between the studies of Wang and Kramer (2003, 2008) and these current studies was the vetting and selection of cases to include. As discussed in Chapter 3, Section 3.3.2, Wang and Kramer elected to include the Calaveras Dam failure case history, and the current investigation did not. Three additional cases included by Wang and Kramer, but deliberatively not included in these current studies, are the three cases listed in Table 4.8 as Class D. These are: (1) Snow River Bridge, (2) Kawagishi-cho Building, and (3) Koda Numa Embankment. Reasons for not including these three cases in the current studies were presented in Chapter 3, Section 3.3.3. Wang and Kramer also elected to employ the Moshi-Koshi Tailings Dam failures as two separate cases, while the current studies elected to combine and average them so that these two very similar cases would not exert inappropriately strong influence on the regressions that will follow.

These current studies include three cases that Wang and Kramer (2003, 2008) did not. The first of these is the Upper San Fernando Dam case history (see Appendix B, Section B.9). The other two cases are (1) Sullivan Tailings Dam, and (2) Jamuna Bridge (see Appendix B, Sections B.15 and B.16, respectively). These two newer cases had not been available to Wang and Kramer.

In the end, as shown in Table 4.8, each team elected to back-analyze and employ slightly different sets of case histories in their studies. Of at least equal importance, each of the two teams employed different analytical approaches, and engineering judgments, in the back-analyses of the cases selected. Many of the cases were common to both studies. A significant number of these have largely similar values in Table 4.7, but a number of them do not. It is therefore interesting to see how these values eventually lead to recommendations with regard to relationships for evaluation of in situ S_r, as are developed and discussed next in Chapter 5, and how the recommendations developed by each of the two investigations compare with each other. It is also interesting to see how they compare with other previous, and in some cases widely-used, recommendations by others as well.

Several important features of the values presented in Table 4.7 should be noted. The values developed for these current studies are the only set of values developed by an engineering team that (1) developed their own best estimate values for all of the cases studied and used in developing correlations, (2) employed back-analysis and assessment methods for all cases that accounted for momentum effects, and (3) developed best estimates of overall uncertainty or variance for each case based on their own assessments and back-analyses.

This does not mean that the current investigation team were not fully cognizant of previous studies, and previous recommendations; but the current team then developed their own best estimates armed with this information. Two former investigation teams had performed reasonably

good back-analyses of 9 or 10 “well documented” case histories employing back-analysis methods that were targeted specifically at inclusion of momentum effects, but each of those teams then either (1) used simpler back-analysis methods for the less well documented cases (which outnumbered the well documented cases by factors of approximately 2 to 1), or (2) they developed values for the less well documented cases based on considering multiple values developed by previous investigations, without performing their own independent analyses and assessments. And because those less well documented case histories outnumbered the well documented cases by factors of approximately 2 to 1 in each of those previous studies, those cases were important contributors to the predictive relationships then developed and proposed.

Another important distinction is the level of effort invested in back-analyses of the 13 well documented Class A cases in these current studies, employing new analysis methods that can largely correctly incorporate, and explore, effects of (1) incrementally progressive (retrogressive) failure, (2) changing conditions (e.g. locally changing failure surface conditions, geometry, etc.), and (3) changes in hydroplaning or sliding on soft sediments, etc. as failure progresses.

A third distinction is the effort made to develop overall best estimates of all key parameter uncertainties, including both variance in the data sets available, as well as quality of data, quality of documentation, field information regarding phreatic surfaces at the time of failure, etc.

And finally, the values presented in Table 4.7 are the first comprehensive set of back-analysis results to have benefitted from internal cross-checking based on new empirical relationships developed earlier in this chapter specifically for characterization of the types of behaviors intrinsic in the suites of failure case histories studied and back-analyzed in these types of studies.

Table 4.1: Selected Methods for Back-Analyses of Liquefaction Failure case Histories for Purposes of Assessing Post-Liquefaction Residual Strength

Group A: Methods that explicitly address momentum effects:
A-1. Incremental momentum analysis method (Current studies). A-2. Kinetics analysis method (Olson and Stark; 2001, 2002). A-3. Zero inertial factor (ZIF) method (Wang, 2003; Kramer, 2008, and Kramer and Wang 2015).
Group B: Methods that implicitly or approximately address momentum effects:
B-1. Displacement-calibrated pre-failure/post-failure analyses (Current studies). B-2. Pre-failure/post-failure analyses (Seed & Harder, 1990).
Group C: Methods that may or may not suitably incorporate momentum effects:
C-1. Adoption of the results of back-analyses from previous investigators.
Group D: Methods that do not incorporate momentum effects:
D-1. Back-analyses of pre-failure geometries with an assumed static factor of safety equal to 1.0. D-2. Back-analyses of post-failure geometries with an assumed static factor of safety equal to 1.0.

Table 4.2: Back-analysis results for the well-defined liquefaction case histories of Classes A and C, and cross-comparisons with (1) Seed and Harder (1990), (2) Olson and Stark (2002) and (3) Wang and Kramer (2003, 2008).

Class	Case	Seed and Harder (1990)		Olson and Stark (2002)				Wang (2003) + Kramer (2008)				This Study			
		S_r (psf)	$N_{1,60,CS}$	S_u(Liq) (psf)	S_u(Liq)/σ'_{vo}	σ'_{vo} (psf)	$N_{1,60}$ (1)	$\bar{S}_r$ (psf) (2)	$\bar{S}_r/\bar{\sigma}'_{vo}$	$\bar{\sigma}'_{vo}$ (psf) (3)	$\bar{N}_{1,60,CS}$	$\bar{S}_r$ (psf)	$\bar{S}_r/\bar{\sigma}'_{vo}$	$\bar{\sigma}'_{vo}$ (psf)	$\bar{N}_{1,60,CS}$
A	Wachusett Dam - North Dike			334	0.106	3158	7	348	0.136	2559	7.3	294	0.094	3142	7.5
	Fort Peck Dam	350	10	570	0.078	7341	8.5	671.6	0.091	7380	15.8	762	0.105	7258	12.5
	Uetsu Railway Embankment	40	3	36	0.027	1280	3	43.7	0.048	910	2.9	38	0.026	1448	3
	Lower San Fernando Dam - U/S Slope	400	13.5	390	0.120	3482	11.5	484.7	0.133	3644	14.5	539	0.170	3174	13.5
	Hachiro-Gata Road Embankment			42	0.062	670	4.4	65	0.164	396	5.7	68	0.101	673	7
	La Marquesa Dam - U/S Slope	200	6	65	0.070	911	4.5	(185.1)	0.110	1683	6.5	103	0.105	981	6.5
	La Marquesa Dam - D/S Slope	400	11	111	0.110	1000	9	(343.5)	0.186	1847	9.9	214	0.176	1215	10.5
	La Palma Dam	200	4	100	0.120	789	3.5	(193.3)	0.123	1572	4.2	136	0.177	767	5
	Lake Ackerman Highway Embankment			82	0.076	1076	3	98	0.114	860	4.8	107	0.118	909	3.5
	Chonan Middle School			100	0.091	1119	5.2	(178.7)	0.091	1964	6.4	141	0.137	1032	6.5
	Soviet Tajik - May 1 Slide			175	0.082	2170	7.6	(334.3)	0.082	4077	8.9	341	0.179	1907	10.5
	Shibecha-Cho Embankement			117	0.086	1351	5.6	208.9	0.200	1045	5.6	224	0.158	1416	7.5
	Route 272 at Higashiarekinai			100	0.097	1030	6.3	130.5	0.125	1044	8.5	138	0.107	1285	8
B	Zeeland - Vlietepolder			115	0.048	2396	7.5	(226.0)	0.048	4708	8.5				
	Sheffield Dam	75	6	75	0.053	1429	5	(100.0)	0.072	1389	8.2				
	Helsinki Harbor			32	0.060	522	6	(53.2)	0.060	887	5.9				
	Solfatara Canal Dike	50	4	50	0.080	624	4	(77.1)	0.063	1224	4.9				
	Lake Merced Bank	100	6	144	0.108	1372	7.5	(139.5)	0.106	1316	5.9				
	El Cobre Tailings Dam			40	0.020	1946	0	(195.2)	0.020	9760	6.8				
	Metoki Road Embankment			38	0.043	875	2.6	(116.8)	0.044	2655	2				
	Hokkaido Tailings Dam			100	0.073	1376	1.1	(250.6)	0.074	3386	5.1				
	Upper San Fernando Dam - D/S Slope	600	15												
	Tar Island Dyke			251	0.058	4300	7	(364.2)	0.058	6279	8.9				
	Mochi-Koshi Tailings Dam, Dikes 1 and 2	250	5	75	0.060	1251	2.7	(158.9)	0.091	1746	8.9				
				113	0.104	1090	2.7	(233.6)	0.081	2884	10				
	Nerlerk Embankment, Slides 1, 2, and 3			52	0.086	616	8.7	(178.5)	0.124	1440	11.4				
				36	0.060	650	7.2								
				31	0.034	925	7.2								
	Asele Road Embankment			132	0.104	1251	7	(163.6)	0.104	1573	11				
	Nalband Railway Embankment			119	0.109	1101	9.2	(139.9)	0.109	1283	6.3				
	Sullivan Tailings														
	Jamuna Bridge														
C	Calaveras Dam	650	12	721	0.112	6422	8	636.9	0.099	6433	10.5	749	0.106	7097	15

Notes : (1) No fines content correction utilized in Olson and Stark (2002).
(2) Where noted in parentheses, S_r values are for secondary cases in Wang (2003) and were not fully reanalyzed by the ZIF Method.
(3) σ'_{vo} not explicitly reported in Wang (2003) or Kramer (2008). Values shown were back calculated from reported S_r and S_r/σ'_{vo}.

Table 4.3: Back-analysis results for the well-defined liquefaction case histories of Classes A and C, and cross-comparisons with (1) Seed and Harder (1990), (2) Olson and Stark (2002) [modified], and (3) Wang and Kramer (2003, 2008).

Class	Case	Seed and Harder (1990)		Olson and Stark (2002)				Wang (2003) + Kramer (2008)				This Study			
		S_r (psf)	$N_{1,60,CS}$	S_u(Liq) (psf) [1]	S_u(Liq)/σ'_{vo}	σ'_{vo} (psf)	$N_{1,60}$ [2]	$\bar{S}_r$ (psf) [3]	$\bar{S}_r$/ $\bar{\sigma}'_{vo}$	$\bar{\sigma}'_{vo}$ (psf) [4]	$\bar{N}_{1,60,CS}$	$\bar{S}_r$ (psf)	$\bar{S}_r$/ $\bar{\sigma}'_{vo}$	$\bar{\sigma}'_{vo}$ (psf)	$\bar{N}_{1,60,CS}$
A	Wachusett Dam - North Dike			334	0.106	3158	7	348	0.136	2559	7.3	294	0.094	3142	7.5
	Fort Peck Dam	350	10	570	0.078	7341	8.5	671.6	0.091	7380	15.8	762	0.105	7258	12.5
	Uetsu Railway Embankment	40	3	36	0.027	1280	3	43.7	0.048	910	2.9	38	0.026	1448	3
	Lower San Fernando Dam - U/S Slope	400	13.5	390	0.120	3482	11.5	484.7	0.133	3644	14.5	539	0.170	3174	13.5
	Hachiro-Gata Road Embankment			42	0.062	670	4.4	65	0.164	396	5.7	68	0.101	673	7
	La Marquesa Dam - U/S Slope	200	6	[104]	0.114	911	4.5	(185.1)	0.110	1683	6.5	103	0.105	981	6.5
	La Marquesa Dam - D/S Slope	400	11	[152]	0.152	1000	9	(343.5)	0.186	1847	9.9	214	0.176	1215	10.5
	La Palma Dam	200	4	[125]	0.158	789	3.5	(193.3)	0.123	1572	4.2	136	0.177	767	5
	Lake Ackerman Highway Embankment			82	0.076	1076	3	98	0.114	860	4.8	107	0.118	909	3.5
	Chonan Middle School			[142]	0.127	1119	5.2	(178.7)	0.091	1964	6.4	141	0.137	1032	6.5
	Soviet Tajik - May 1 Slide			[334]	0.154	2170	7.6	(334.3)	0.082	4077	8.9	341	0.179	1907	10.5
	Shibecha-Cho Embankement			117	0.086	1351	5.6	208.9	0.200	1045	5.6	224	0.158	1416	7.5
	Route 272 at Higashiarekinai			100	0.097	1030	6.3	130.5	0.125	1044	8.5	138	0.107	1285	8
B	Zeeland - Vlietepolder			[180]	0.075	2396	7.5	(226.0)	0.048	4708	8.5				
	Sheffield Dam	75	6	[159]	0.111	1429	5	(100.0)	0.072	1389	8.2				
	Helsinki Harbor			[44]	0.084	522	6	(53.2)	0.060	887	5.9				
	Solfatara Canal Dike	50	4	[71]	0.114	624	4	(77.1)	0.063	1224	4.9				
	Lake Merced Bank	100	6	[205]	0.149	1372	7.5	(139.5)	0.106	1316	5.9				
	El Cobre Tailings Dam			<40>	0.020	1946	0	(195.2)	0.020	9760	6.8				
	Metoki Road Embankment			[90]	0.103	875	2.6	(116.8)	0.044	2655	2				
	Hokkaido Tailings Dam			[138]	0.100	1376	1.1	(250.6)	0.074	3386	5.1				
	Upper San Fernando Dam - D/S Slope	600	15												
	Tar Island Dyke			[401]	0.093	4300	7	(364.2)	0.058	6279	8.9				
	Mochi-Koshi Tailings Dam, Dikes 1 and 2	250	5	[207]	0.165	1251	2.7	(158.9)	0.091	1746	8.9				
				[180]	0.165	1090	2.7	(233.6)	0.081	2884	10				
	Nerlerk Embankment, Slides 1, 2, and 3			[44]	0.071	616	8.7	(178.5)	0.124	1440	11.4				
				[50]	0.077	650	7.2								
				[52]	0.056	925	7.2								
	Asele Road Embankment			[192]	0.153	1251	7	(163.6)	0.104	1573	11.0				
	Nalband Railway Embankment			[121]	0.110	1101	9.2	(139.9)	0.109	1283	6.3				
	Sullivan Tailings														
	Jamuna Bridge														
C	Calaveras Dam	650	12	721	0.112	6422	8	636.9	0.0993	6433	10.5	749	0.106	7097	15

Notes : (1) Where noted in brackets, S_u(Liq) and S_u(Liq)/σ'_{vo} for Olson (2001) reinterpreted using reported values of Su Yield and S_u Residual in Olson (2001) and the equation S_u(Liq) = 0.8 (S_u Yield + S_u Residual)/2. Reinterpretation of S_u(Liq) performed for cases not calculated using the Kinetic procedure in Olson (2001). Where noted in triangular brackets, no S_u Yield value reported in Olson (2001).

(2) No fines content correction utilized in Olson and Stark (2002).

(3) Where noted in parentheses, S_r values are for secondary cases in Wang (2003) and were not fully reanalyzed by the ZIF Method.

(4) σ'_{vo} not explicitly reported in Wang (2003) or Kramer (2008). Values shown were back calculated from reported S_r and S_r/σ'_{vo}.

Table 4.4: Back-analysis results for the less well-defined liquefaction case histories of Class B, and cross-comparisons with (1) Seed and Harder (1990), (2) Olson and Stark (2002) and (3) Wang and Kramer (2003, 2008).

Class	Case	Seed and Harder (1990)		Olson and Stark (2002)				Wang (2003) + Kramer (2008)				This Study			
		S_r (psf)	$N_{1,60,CS}$	S_u(Liq) (psf)	S_u(Liq)/σ'_{vo}	σ'_{vo} (psf)	$N_{1,60}$ [1]	$\bar{S}_r$ (psf) [2]	$\bar{S}_r/\bar{\sigma}'_{vo}$	$\bar{\sigma}'$vo (psf) [3]	$\bar{N}_{1,60,CS}$	$\bar{S}_r$ (psf)	$\bar{S}_r/\bar{\sigma}'_{vo}$	$\bar{\sigma}'_{vo}$ (psf)	$\bar{N}_{1,60,CS}$
A	Wachusett Dam - North Dike			334	0.106	3158	7	348	0.136	2559	7.3				
	Fort Peck Dam	350	10	570	0.078	7341	8.5	671.6	0.091	7380	15.8				
	Uetsu Railway Embankment	40	3	36	0.027	1280	3	43.7	0.048	910	2.9				
	Lower San Fernando Dam - U/S Slope	400	13.5	390	0.120	3482	11.5	484.7	0.133	3644	14.5				
	Hachiro-Gata Road Embankment			42	0.062	670	4.4	65	0.164	396	5.7				
	La Marquesa Dam - U/S Slope	200	6	65	0.07	911	4.5	(185.1)	0.110	1683	6.5				
	La Marquesa Dam - D/S Slope	400	11	111	0.11	1000	9	(343.5)	0.186	1847	9.9				
	La Palma Dam	200	4	100	0.12	789	3.5	(193.3)	0.123	1572	4.2				
	Lake Ackerman Highway Embankment			82	0.076	1076	3	98	0.114	860	4.8				
	Chonan Middle School			100	0.09	1119	5.2	(178.7)	0.091	1964	6.4				
	Soviet Tajik - May 1 Slide			175	0.08	2170	7.6	(334.3)	0.082	4077	8.9				
	Shibecha-Cho Embankement			117	0.086	1351	5.6	208.9	0.200	1045	5.6				
	Route 272 at Higashiarekinai			100	0.097	1030	6.3	130.5	0.125	1044	8.5				
B	Zeeland - Vlietepolder			115	0.05	2396	7.5	(226.0)	0.048	4708	8.5	156	0.063	2488	8
	Sheffield Dam	75	6	75	0.05	1429	5	(100.0)	0.072	1389	8.2	138	0.106	1308	7
	Helsinki Harbor			32	0.06	522	6	(53.2)	0.060	887	5.9	48	0.057	846	6
	Solfatara Canal Dike	50	4	50	0.08	624	4	(77.1)	0.063	1224	4.9	64	0.096	669	4.5
	Lake Merced Bank	100	6	144	0.11	1372	7.5	(139.5)	0.106	1316	5.9	136	0.163	834	8.5
	El Cobre Tailings Dam			40	0.020	1946	0	(195.2)	0.020	9760	6.8	95	0.046	2075	2
	Metoki Road Embankment			38	0.04	875	2.6	(116.8)	0.044	2655	2	92	0.106	871	2.5
	Hokkaido Tailings Dam			100	0.07	1376	1.1	(250.6)	0.074	3386	5.1	131	0.109	1203	4
	Upper San Fernando Dam - D/S Slope	600	15									726	0.231	3138	15
	Tar Island Dyke			251	0.06	4300	7	(364.2)	0.058	6279	8.9	516	0.123	4197	11
	Mochi-Koshi Tailings Dam, Dikes 1 and 2	250	5	75	0.06	1251	2.7	(158.9)	0.091	1746	8.9	211	0.138	1532	6
				113	0.10	1090	2.7	(233.6)	0.081	2884	10				
	Nerlerk Embankment, Slides 1, 2, and 3			52	0.09	616	8.7	(178.5)	0.124	1440	11.4	68	0.058	1171	7.5
				36	0.06	650	7.2								
				31	0.03	925	7.2								
	Asele Road Embankment			132	0.10	1251	7	(163.6)	0.104	1573	11.0	137	0.132	1037	9.5
	Nalband Railway Embankment			119	0.11	1101	9.2	(139.9)	0.109	1283	6.3	167	0.138	1209	7.5
	Sullivan Tailings											277	0.114	2422	9.5
	Jamuna Bridge											175	0.125	1404	10.5
C	Calaveras Dam	650	12	721	0.112	6422	8	636.9	0.0993	6433	10.5				

Notes : (1) No fines content correction utilized in Olson and Stark (2002).
(2) Where noted in parentheses, S_r values are for secondary cases in Wang (2003) and were not fully reanalyzed by the ZIF Method.
(3) σ'_{vo} not explicitly reported in Wang (2003) or Kramer (2008). Values shown were back calculated from reported S_r and S_r/σ'_{vo}.

Table 4.5: Back-analysis results for the less well-defined liquefaction case histories of Class B, and cross-comparisons with (1) Seed and Harder (1990), (2) Olson and Stark (2002) [modified], and (3) Wang and Kramer (2003, 2008).

Class	Case	Seed and Harder (1990)		Olson and Stark (2002)				Wang (2003) + Kramer (2008)				This Study			
		S_r (psf)	$N_{1,60,CS}$	S_u(Liq) (psf) [1]	S_u(Liq)/σ'_{vo}	σ'_{vo} (psf)	$N_{1,60}$ [2]	$\bar{S}_r$ (psf) [3]	$\bar{S}_r/\bar{\sigma}'_{vo}$	$\bar{\sigma}'_{vo}$ (psf) [4]	$\bar{N}_{1,60,CS}$	$\bar{S}_r$ (psf)	$\bar{S}_r/\bar{\sigma}'_{vo}$	$\bar{\sigma}'_{vo}$ (psf)	$\bar{N}_{1,60,CS}$
A	Wachusett Dam - North Dike			334	0.106	3158	7	348	0.136	2559	7.3				
	Fort Peck Dam	350	10	570	0.078	7341	8.5	671.6	0.091	7380	15.8				
	Uetsu Railway Embankment	40	3	36	0.027	1280	3	43.7	0.048	910	2.9				
	Lower San Fernando Dam - U/S Slope	400	13.5	390	0.120	3482	11.5	484.7	0.133	3644	14.5				
	Hachiro-Gata Road Embankment			42	0.062	670	4.4	65	0.164	396	5.7				
	La Marquesa Dam - U/S Slope	200	6	[104]	0.114	911	4.5	(185.1)	0.110	1683	6.5				
	La Marquesa Dam - D/S Slope	400	11	[152]	0.152	1000	9	(343.5)	0.186	1847	9.9				
	La Palma Dam	200	4	[125]	0.158	789	3.5	(193.3)	0.123	1572	4.2				
	Lake Ackerman Highway Embankment			82	0.076	1076	3	98	0.114	860	4.8				
	Chonan Middle School			[142]	0.127	1119	5.2	(178.7)	0.091	1964	6.4				
	Soviet Tajik - May 1 Slide			[334]	0.154	2170	7.6	(334.3)	0.082	4077	8.9				
	Shibecha-Cho Embankement			117	0.086	1351	5.6	208.9	0.200	1045	5.6				
	Route 272 at Higashiarekinai			100	0.097	1030	6.3	130.5	0.125	1044	8.5				
B	Zeeland - Vlietepolder			[180]	0.075	2396	7.5	(226.0)	0.048	4708	8.5	156	0.063	2488	8
	Sheffield Dam	75	6	[159]	0.111	1429	5	(100.0)	0.072	1389	8.2	138	0.106	1308	7
	Helsinki Harbor			[44]	0.084	522	6	(53.2)	0.060	887	5.9	48	0.057	846	6
	Solfatara Canal Dike	50	4	[71]	0.114	624	4	(77.1)	0.063	1224	4.9	64	0.096	669	4.5
	Lake Merced Bank	100	6	[205]	0.149	1372	7.5	(139.5)	0.106	1316	5.9	136	0.163	834	8.5
	El Cobre Tailings Dam			<40>	0.020	1946	0	(195.2)	0.020	9760	6.8	95	0.046	2075	2
	Metoki Road Embankment			[90]	0.103	875	2.6	(116.8)	0.044	2655	2	92	0.106	871	2.5
	Hokkaido Tailings Dam			[138]	0.100	1376	1.1	(250.6)	0.074	3386	5.1	131	0.109	1203	4
	Upper San Fernando Dam - D/S Slope	600	15									726	0.231	3138	15
	Tar Island Dyke			[401]	0.093	4300	7	(364.2)	0.058	6279	8.9	516	0.123	4197	11
	Mochi-Koshi Tailings Dam, Dikes 1 and 2	250	5	[207]	0.165	1251	2.7	(158.9)	0.091	1746	8.9	211	0.138	1532	6
				[180]	0.165	1090	2.7	(233.6)	0.081	2884	10				
	Nerlerk Embankment, Slides 1, 2, and 3			[44]	0.071	616	8.7	(178.5)	0.1239	1440	11.4	68	0.058	1171	7.5
				[50]	0.077	650	7.2								
				[52]	0.056	925	7.2								
	Asele Road Embankment			[192]	0.153	1251	7	(163.6)	0.104	1573	11	137	0.132	1037	9.5
	Nalband Railway Embankment			[121]	0.110	1101	9.2	(139.9)	0.109	1283	6.3	167	0.138	1209	7.5
	Sullivan Tailings											277	0.114	2422	9.5
	Jamuna Bridge											175	0.125	1404	10.5
C	Calaveras Dam	650	12	721	0.112	6422	8	636.9	0.099	6433	10.5				

Notes : (1) Where noted in brackets, S_u(Liq) and S_u(Liq)/σ'_{vo} for Olson (2001) reinterpreted using reported values of Su Yield and S_u Residual in Olson (2001) and the equation S_u(Liq) = 0.8 (S_u Yield + S_u Residual)/2. Reinterpretation of S_u(Liq) performed for cases not calculated using the Kinetic procedure in Olson (2001). Where noted in triangular brackets, no S_u Yield value reported in Olson (2001).

(2) No fines content correction utilized in Olson and Stark (2002).

(3) Where noted in parentheses, S_r values are for secondary cases in Wang (2003) and were not fully reanalyzed by the ZIF Method.

(4) σ'_{vo} not explicitly reported in Wang (2003) or Kramer (2008). Values shown were back calculated from reported S_r and S_r/σ'_{vo}.

Table 4.6: Back-analysis results for liquefaction case histories of Class A, Class B, and Class C, and cross-comparisons with (1) Seed and Harder (1990), (2) Olson and Stark (2002) [modified], and (3) Wang and Kramer (2003, 2008).

Class	Case	Seed and Harder (1990)		Olson and Stark (2002)				Wang (2003) + Kramer (2008)				This Study			
		S_r (psf)	$N_{1,60,CS}$	S_u(Liq) (psf) [1]	S_u(Liq)/σ'_{vo}	σ'_{vo} (psf)	$N_{1,60}$ [2]	$\bar{S}_r$ (psf) [3]	$\bar{S}_r/\bar{\sigma}'_{vo}$	$\bar{\sigma}'_{vo}$ (psf) [4]	$\bar{N}_{1,60,CS}$	$\bar{S}_r$ (psf)	$\bar{S}_r/\bar{\sigma}'_{vo}$	$\bar{\sigma}'_{vo}$ (psf)	$\bar{N}_{1,60,CS}$
A	Wachusett Dam - North Dike			334	0.106	3158	7	348	0.136	2559	7.3	294	0.094	3142	7.5
	Fort Peck Dam	350	10	570	0.078	7341	8.5	671.6	0.091	7380	15.8	762	0.105	7258	12.5
	Uetsu Railway Embankment	40	3	36	0.027	1280	3	43.7	0.048	910	2.9	38	0.026	1448	3
	Lower San Fernando Dam - U/S Slope	400	13.5	390	0.120	3482	11.5	484.7	0.133	3644	14.5	539	0.170	3174	13.5
	Hachiro-Gata Road Embankment			42	0.062	670	4.4	65	0.164	396	5.7	68	0.101	673	7
	La Marquesa Dam - U/S Slope	200	6	[104]	0.114	911	4.5	(185.1)	0.110	1683	6.5	103	0.105	981	6.5
	La Marquesa Dam - D/S Slope	400	11	[152]	0.152	1000	9	(343.5)	0.186	1847	9.9	214	0.176	1215	10.5
	La Palma Dam	200	4	[125]	0.158	789	3.5	(193.3)	0.123	1572	4.2	136	0.177	767	5
	Lake Ackerman Highway Embankment			82	0.076	1076	3	98	0.114	860	4.8	107	0.118	909	3.5
	Chonan Middle School			[142]	0.127	1119	5.2	(178.7)	0.091	1964	6.4	141	0.137	1032	6.5
	Soviet Tajik - May 1 Slide			[334]	0.154	2170	7.6	(334.3)	0.082	4077	8.9	341	0.179	1907	10.5
	Shibecha-Cho Embankement			117	0.086	1351	5.6	208.9	0.200	1045	5.6	224	0.158	1416	7.5
	Route 272 at Higashiarekinai			100	0.097	1030	6.3	130.5	0.125	1044	8.5	138	0.107	1285	8
B	Zeeland - Vlietepolder			[180]	0.075	2396	7.5	(226.0)	0.048	4708	8.5	156	0.063	2488	8
	Sheffield Dam	75	6	[159]	0.111	1429	5	(100.0)	0.072	1389	8.2	138	0.106	1308	7
	Helsinki Harbor			[44]	0.084	522	6	(53.2)	0.060	887	5.9	48	0.057	846	6
	Solfatara Canal Dike	50	4	[71]	0.114	624	4	(77.1)	0.063	1224	4.9	64	0.096	669	4.5
	Lake Merced Bank	100	6	[205]	0.149	1372	7.5	(139.5)	0.106	1316	5.9	136	0.163	834	8.5
	El Cobre Tailings Dam			<40>	0.020	1946	0	(195.2)	0.020	9760	6.8	95	0.046	2075	2
	Metoki Road Embankment			[90]	0.103	875	2.6	(116.8)	0.044	2655	2	92	0.106	871	2.5
	Hokkaido Tailings Dam			[138]	0.100	1376	1.1	(250.6)	0.074	3386	5.1	131	0.109	1203	4
	Upper San Fernando Dam - D/S Slope	600	15									726	0.231	3138	15
	Tar Island Dyke			[401]	0.093	4300	7	(364.2)	0.058	6279	8.9	516	0.123	4197	11
	Mochi-Koshi Tailings Dam, Dikes 1 and 2	250	5	[207]	0.165	1251	2.7	(158.9)	0.091	1746	8.9	211	0.138	1532	6
				[180]	0.165	1090	2.7	(233.6)	0.081	2884	10				
	Nerlerk Embankment, Slides 1, 2, and 3			[44]	0.071	616	8.7	(178.5)	0.1239	1440	11.4	68	0.058	1171	7.5
				[50]	0.077	650	7.2								
				[52]	0.056	925	7.2								
	Asele Road Embankment			[192]	0.153	1251	7	(163.6)	0.104	1573	11	137	0.132	1037	9.5
	Nalband Railway Embankment			[121]	0.110	1101	9.2	(139.9)	0.109	1283	6.3	167	0.138	1209	7.5
	Sullivan Tailings											277	0.114	2422	9.5
	Jamuna Bridge											175	0.125	1404	10.5
C	Calaveras Dam	650	12	721	0.112	6422	8	636.9	0.099	6433	10.5	749	0.106	7097	15

Notes : (1) Where noted in brackets, S_u(Liq) and S_u(Liq)/σ'_{vo} for Olson (2001) reinterpreted using reported values of Su Yield and S_u Residual in Olson (2001) and the equation S_u(Liq) = 0.8 (S_u Yield + S_u Residual)/2. Reinterpretation of S_u(Liq) performed for cases not calculated using the Kinetic procedure in Olson (2001). Where noted in triangular brackets, no S_u Yield value reported in Olson (2001).

(2) No fines content correction utilized in Olson and Stark (2002).

(3) Where noted in parentheses, S_r values are for secondary cases in Wang (2003) and were not fully reanalyzed by the ZIF Method.

(4) σ'_{vo} not explicitly reported in Wang (2003) or Kramer (2008). Values shown were back calculated from reported S_r and S_r/σ'_{vo}.

Table 4.7: Summary of the back-calculated values of this study for (1) post-liquefaction strength, (2) representative initial vertical effective stress, and (3) penetration resistance, with inclusion of uncertainties.

Class	Case	This Study					
		$\bar{S}_r$ (psf)	$\sigma_{\bar{S}}$	$\bar{\sigma}'_{vo}$ (psf)	$\sigma_{\bar{\sigma}}$	$\bar{N}_{1,60,CS}$	$\sigma_{\bar{N}}$
A	Wachusett Dam - North Dike	294	31	3142	132	7.5	1.6
	Fort Peck Dam	762	118	7258	687	12.5	2.7
	Uetsu Railway Embankment	38	8	1448	116	3	0.8
	Lower San Fernando Dam - U/S Slope	539	47	3174	281	13.5	1.8
	Hachiro-Gata Road Embankment	68	12	673	41	7	1.2
	La Marquesa Dam - U/S Slope	103	33	981	134	6.5	1.8
	La Marquesa Dam - D/S Slope	214	57	1215	103	10.5	2.2
	La Palma Dam	136	23	767	42	5	1.2
	Lake Ackerman Highway Embankment	107	19	909	61	3.5	0.7
	Chonan Middle School	141	35	1032	82	6.5	2.1
	Soviet Tajik - May 1 Slide	341	57	1907	177	10.5	2.7
	Shibecha-Cho Embankement	224	37	1416	95	7.5	1.7
	Route 272 at Higashiarekinai	138	17	1285	104	8	1.6
B	Zeeland - Vlietepolder	156	37	2488	431	8	2.1
	Sheffield Dam	138	23	1308	71	7	2.3
	Helsinki Harbor	48	14	846	105	6	2.0
	Solfatara Canal Dike	64	22	669	59	4.5	1.5
	Lake Merced Bank	136	21	834	102	8.5	2.2
	El Cobre Tailings Dam	95	31	2075	183	2	1.0
	Metoki Road Embankment	92	20	871	85	2.5	0.9
	Hokkaido Tailings Dam	131	45	1203	191	4	1.1
	Upper San Fernando Dam - D/S Slope	726	138	3138	278	15	1.8
	Tar Island Dyke	516	119	4197	484	11	2.3
	Mochi-Koshi Tailings Dam, Dikes 1 and 2	211	38	1532	165	6	1.7
	Nerlerk Embankment, Slides 1, 2, and 3	68	19	1171	129	7.5	1.8
	Asele Road Embankment	137	27	1037	77	9.5	2.0
	Nalband Railway Embankment	167	15	1209	94	7.5	2.5
	Sullivan Tailings	277	24	2422	142	9.5	2.4
	Jamuna Bridge	175	22	1404	210	10.5	2.5
C	Calaveras	749		7097		15	

Table 4.8: Comparison between the back-calculated values of this study and those developed by Wang (2003) for (1) post-liquefaction strength, (2) representative initial vertical effective stress, and (3) penetration resistance, with inclusion of uncertainties and case history weighting factors.

Class	Case	Wang (2003) + Kramer (2008)							This Study						
		$\bar{S}_r$ (psf) [1]	$\sigma_{\bar{S}}$	$\bar{\sigma}'_{vo}$ (psf) [2]	$\sigma_{\bar{\sigma}}$	$\bar{N}_{1,60,CS}$	$\sigma_{\bar{N}}$	WF	$\bar{S}_r$ (psf)	$\sigma_{\bar{S}}$	$\bar{\sigma}'_{vo}$ (psf)	$\sigma_{\bar{\sigma}}$	$\bar{N}_{1,60,CS}$	$\sigma_{\bar{N}}$	WF
A	Wachusett Dam - North Dike	348	74.8	2559	(-)	7.3	1.9	1.00	294	31	3142	132	7.5	1.6	1.00
	Fort Peck Dam	671.6	130.2	7380	(-)	15.8	0.9	0.85	762	118	7258	687	12.5	2.7	1.00
	Uetsu Railway Embankment	43.7	24.8	910	(-)	2.9	4.2	0.55	38	8	1448	116	3	0.8	1.00
	Lower San Fernando Dam - U/S Slope	484.7	111.0	3644	(-)	14.5	1.1	1.00	539	47	3174	281	13.5	1.8	1.00
	Hachiro-Gata Road Embankment	65	24.7	396	(-)	5.7	2.8	0.55	68	12	673	41	7	1.2	1.00
	La Marquesa Dam - U/S Slope	(185.1)	82.1	1683	(-)	6.5	2.8	0.76	103	33	981	134	6.5	1.8	1.00
	La Marquesa Dam - D/S Slope	(343.5)	113.8	1847	(-)	9.9	3.0	0.72	214	57	1215	103	10.5	2.2	1.00
	La Palma Dam	(193.3)	86.3	1572	(-)	4.2	1.8	0.80	136	23	767	42	5	1.2	1.00
	Lake Ackerman Highway Embankment	98	20.4	860	(-)	4.8	1.2	1.00	107	19	909	61	3.5	0.7	1.00
	Chonan Middle School	(178.7)	32.0	1964	(-)	6.4	6.9	0.74	141	35	1032	82	6.5	2.1	1.00
	Soviet Tajik - May 1 Slide	(334.3)	110.9	4077	(-)	8.9	5.7	0.22	341	57	1907	177	10.5	2.7	1.00
	Shibecha-Cho Embankement	208.9	38.6	1045	(-)	5.6	2.2	0.70	224	37	1416	95	7.5	1.7	1.00
	Route 272 at Higashiarekinai	130.5	33.5	1044	(-)	8.5	2.6	0.70	138	17	1285	104	8	1.6	1.00
B	Zeeland - Vlietepolder	(226.0)	75.0	4708	(-)	8.5	5.5	0.39	156	37	2488	431	8	2.1	1.00
	Sheffield Dam	(100.0)	29.8	1389	(-)	8.2	6.8	0.37	138	23	1308	71	7	2.3	1.00
	Helsinki Harbor	(53.2)	19.0	887	(-)	5.9	8.0	0.39	48	14	846	105	6	2.0	1.00
	Solfatara Canal Dike	(77.1)	25.6	1224	(-)	4.9	6.9	0.42	64	22	669	59	4.5	1.5	1.00
	Lake Merced Bank	(139.5)	41.4	1316	(-)	5.9	8.0	0.39	136	21	834	102	8.5	2.2	1.00
	El Cobre Tailings Dam	(195.2)	64.8	9760	(-)	6.8	0.9	0.60	95	31	2075	183	2	1.0	1.00
	Metoki Road Embankment	(116.8)	53.7	2655	(-)	2.0	1.5	0.39	92	20	871	85	2.5	0.9	1.00
	Hokkaido Tailings Dam	(250.6)	71.9	3386	(-)	5.1	1.4	0.31	131	45	1203	191	4	1.1	1.00
	Upper San Fernando Dam - D/S Slope								726	138	3138	278	15	1.8	1.00
	Tar Island Dyke	(364.2)	115.6	6279	(-)	8.9	9.7	0.32	516	119	4197	484	11	2.3	1.00
	Mochi-Koshi Tailings Dam, Dikes 1 and 2	(158.9)	47.7	1746	(-)	8.9	0.6	0.34	211	38	1532	165	6	1.7	1.00
		(233.6)	78.0	2884	(-)	10.0	1.3	0.67							
	Nerlerk Embankment, Slides 1, 2, and 3	(178.5)	32.1	1440	(-)	11.4	7.7	0.41	68	19	1171	129	7.5	1.8	1.00
	Asele Road Embankment	(163.6)	54.6	1573	(-)	11.0	10.7	0.20	137	27	1037	77	9.5	2.0	1.00
	Nalband Railway Embankment	(139.9)	40.2	1283	(-)	6.3	5.6	0.51	167	15	1209	94	7.5	2.5	1.00
	Sullivan Tailings								277	24	2422	142	9.5	2.4	1.00
	Jamuna Bridge								175	22	1404	210	10.5	2.5	1.00
C	Calaveras Dam	636.9	223.1	6433	(-)	10.5	9.7	0.55	749		7097		15		0.00
D	Snow River Bridge Fill	(50.1)	16.6	2088	(-)	8.5	9.0	0.50							
	Kawagashi-cho Building	(123.5)	56.7	1388	(-)	4.3	1.2	0.50	`						
	Koda Numa Embankment	(48.0)	15.9	1067	(-)	3.6	4.1	0.44							

Notes : (1) Where noted in parentheses, S_r values are for secondary cases in Wang (2003) and were not fully reanalyzed by the ZIF Method.
(2) σ'_{vo} not explicitly reported in Wang (2003) or Kramer (2008). Values shown were back calculated from reported S_r and S_r/σ'_{vo}.

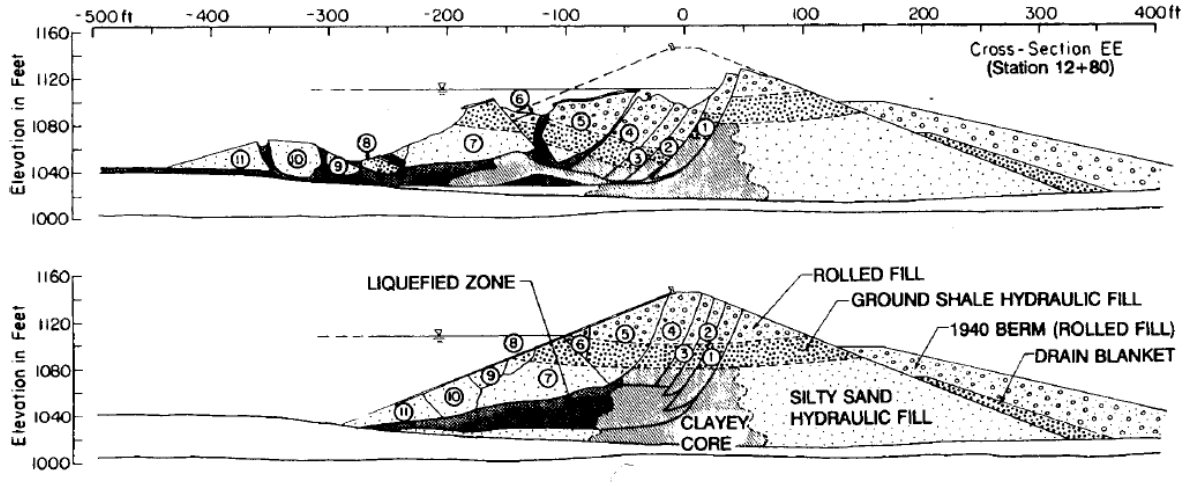

Figure 4.1: Pre-failure and post-failure cross-section of the Lower San Fernando Dam (Castro et al., 1992)

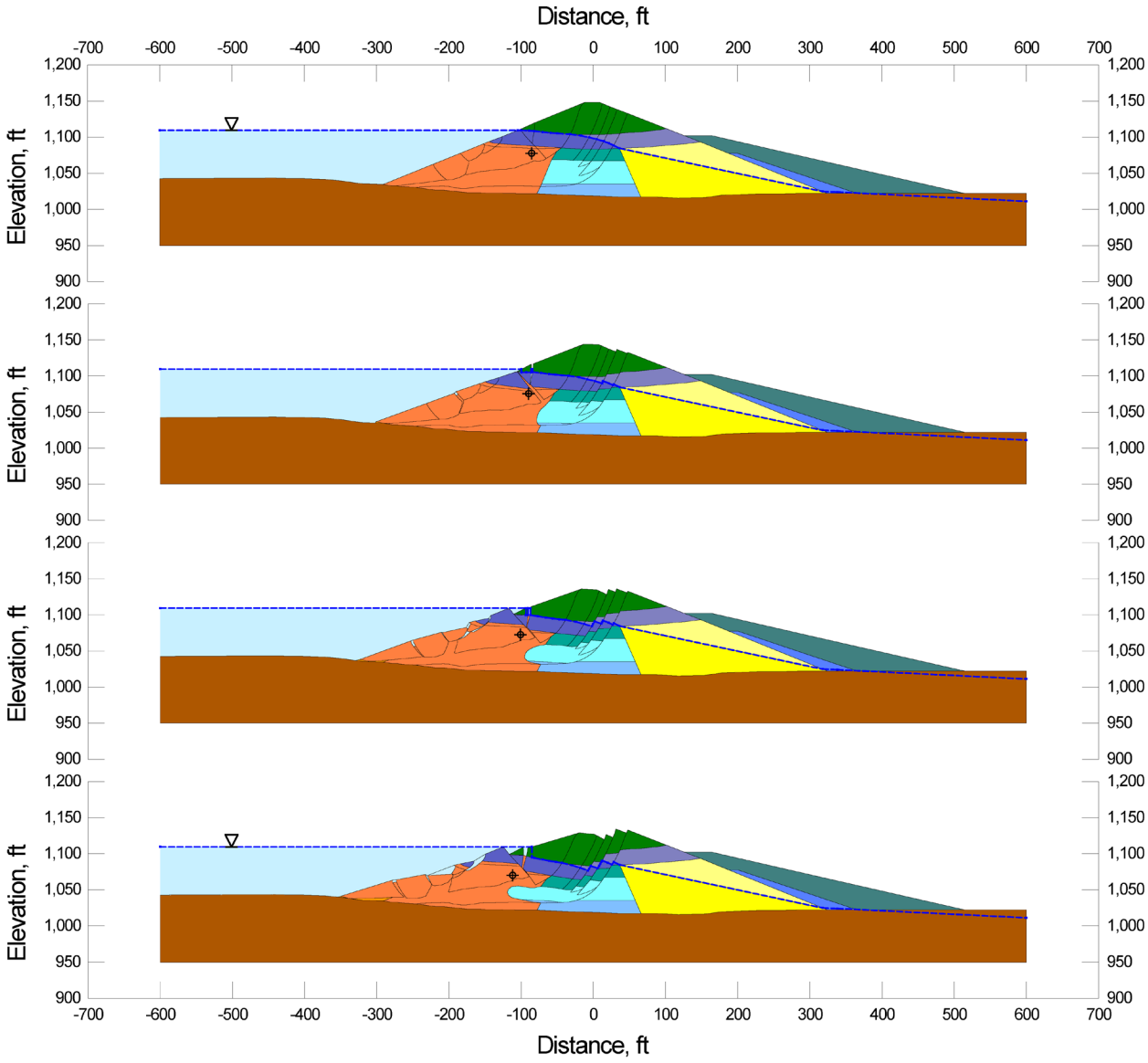

Figure 4.2: Incremental cross-sections used to model and back-analyze the liquefaction-induced upstream slide of the Lower San Fernando Dam (showing the first four cross-sections).

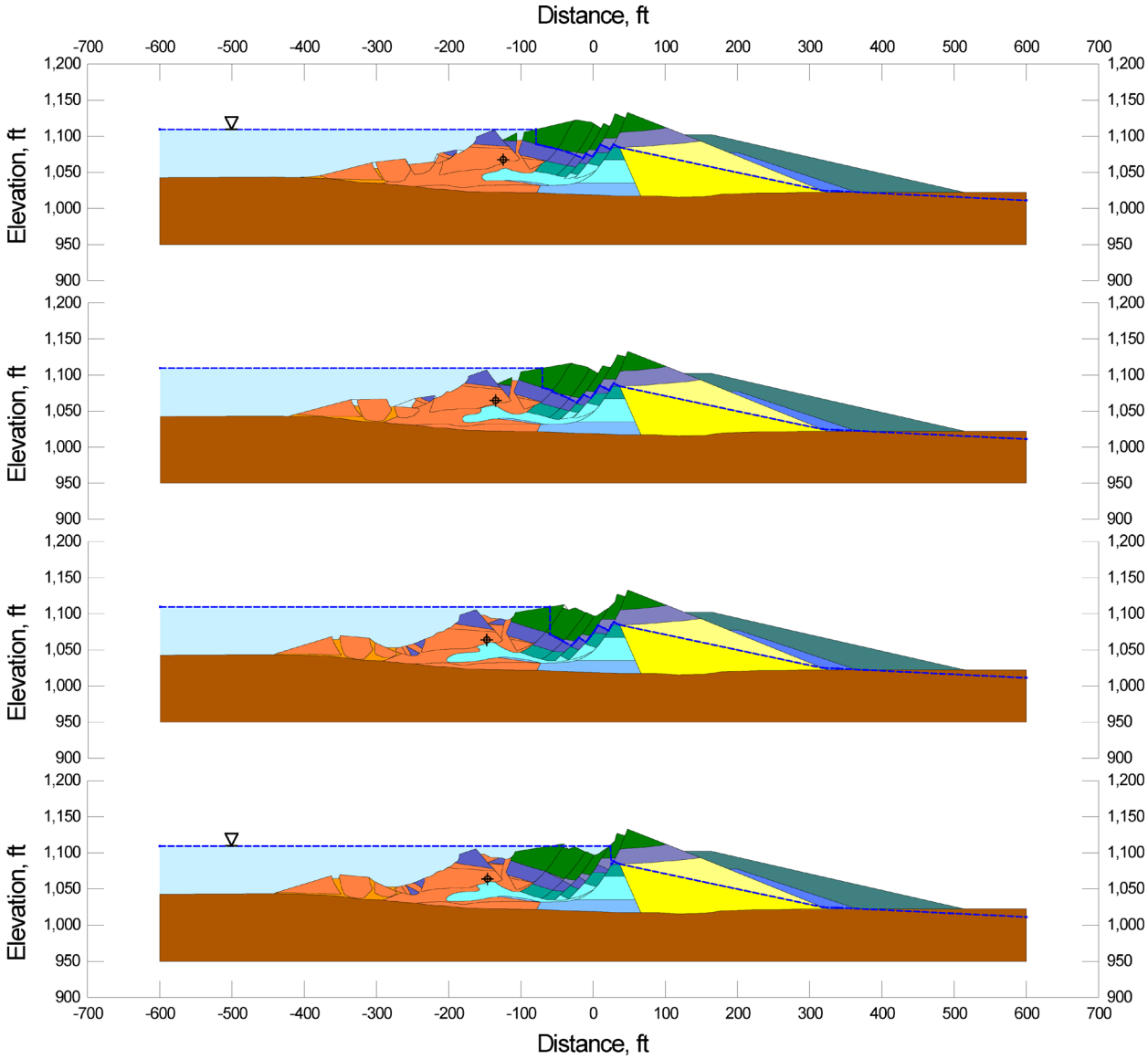

Figure 4.2 (Continued): Incremental cross-sections used to model and back-analyze the liquefaction-induced upstream slide of the Lower San Fernando Dam (showing the final four cross-sections).

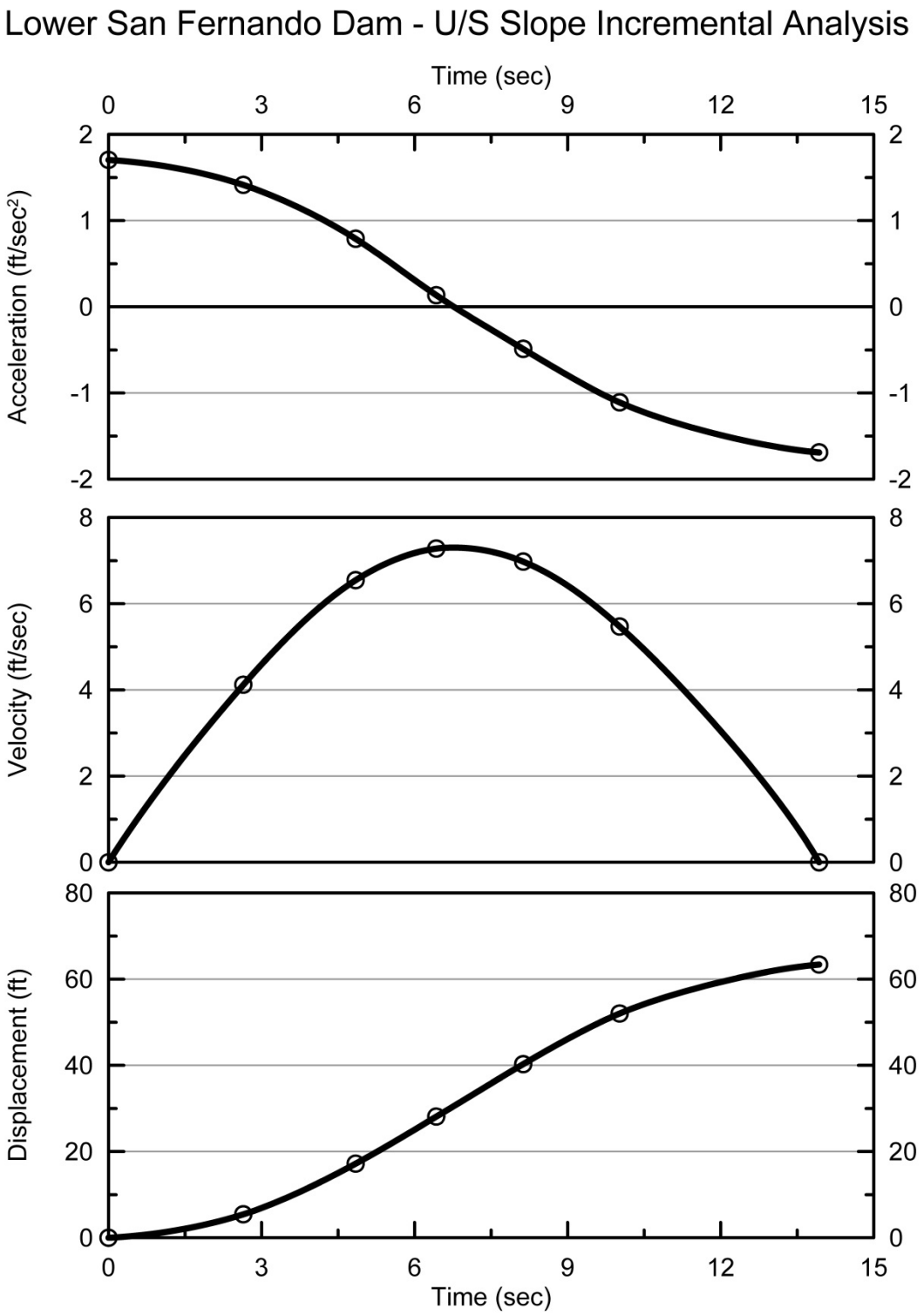

Figure 4.3: Calculated evolution of (1) acceleration vs. time, (2) velocity vs. time, and (3) dis-placement vs. time of the center of gravity of the overall failure mass of the Lower San Fernando Dam based on the progression scenario illustrated in Figure 4.2.

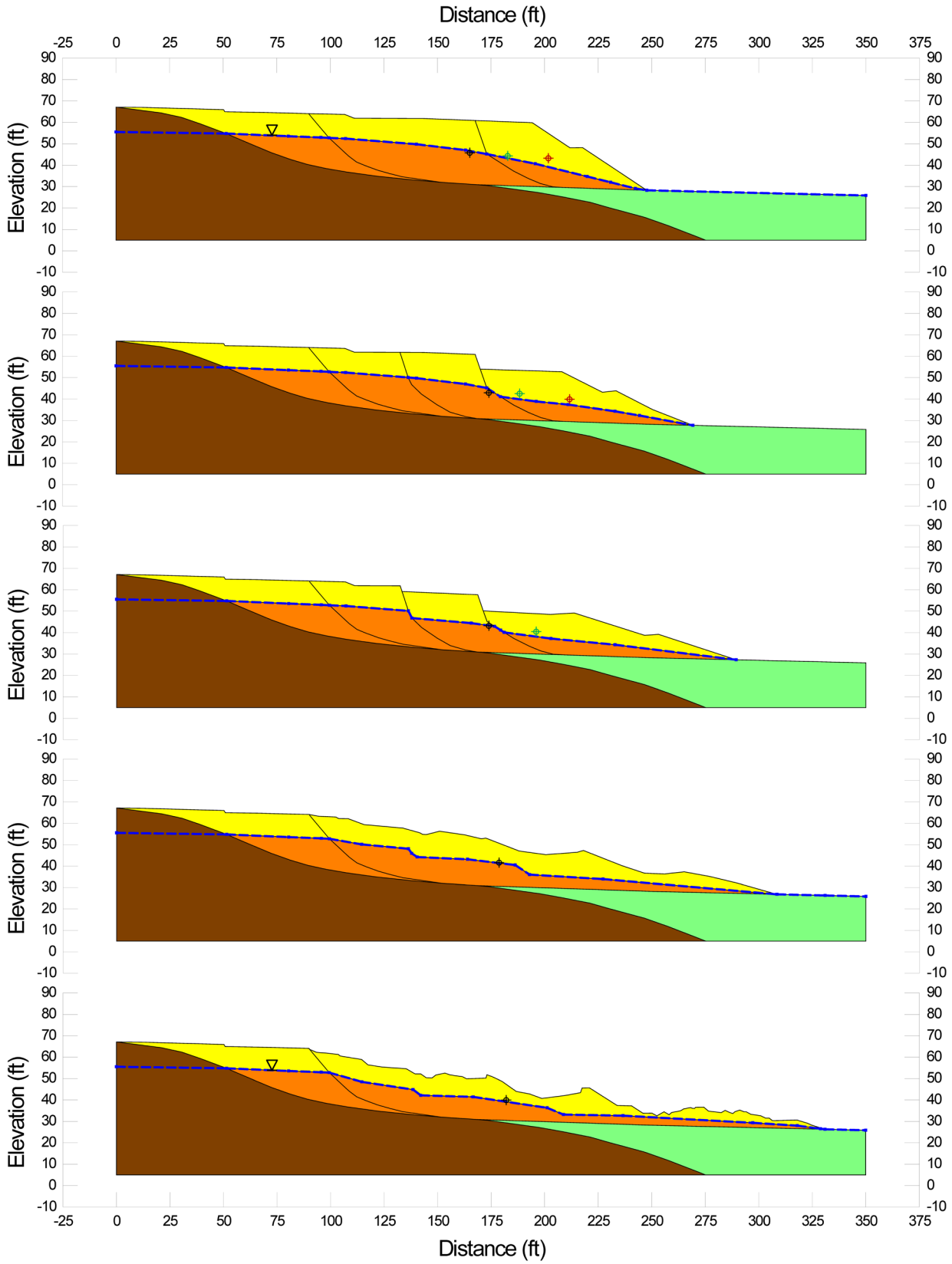

Figure 4.4: Incremental cross-sections used to model and back-analyze the liquefaction-induced failure of the Shibecha-Cho Embankment.

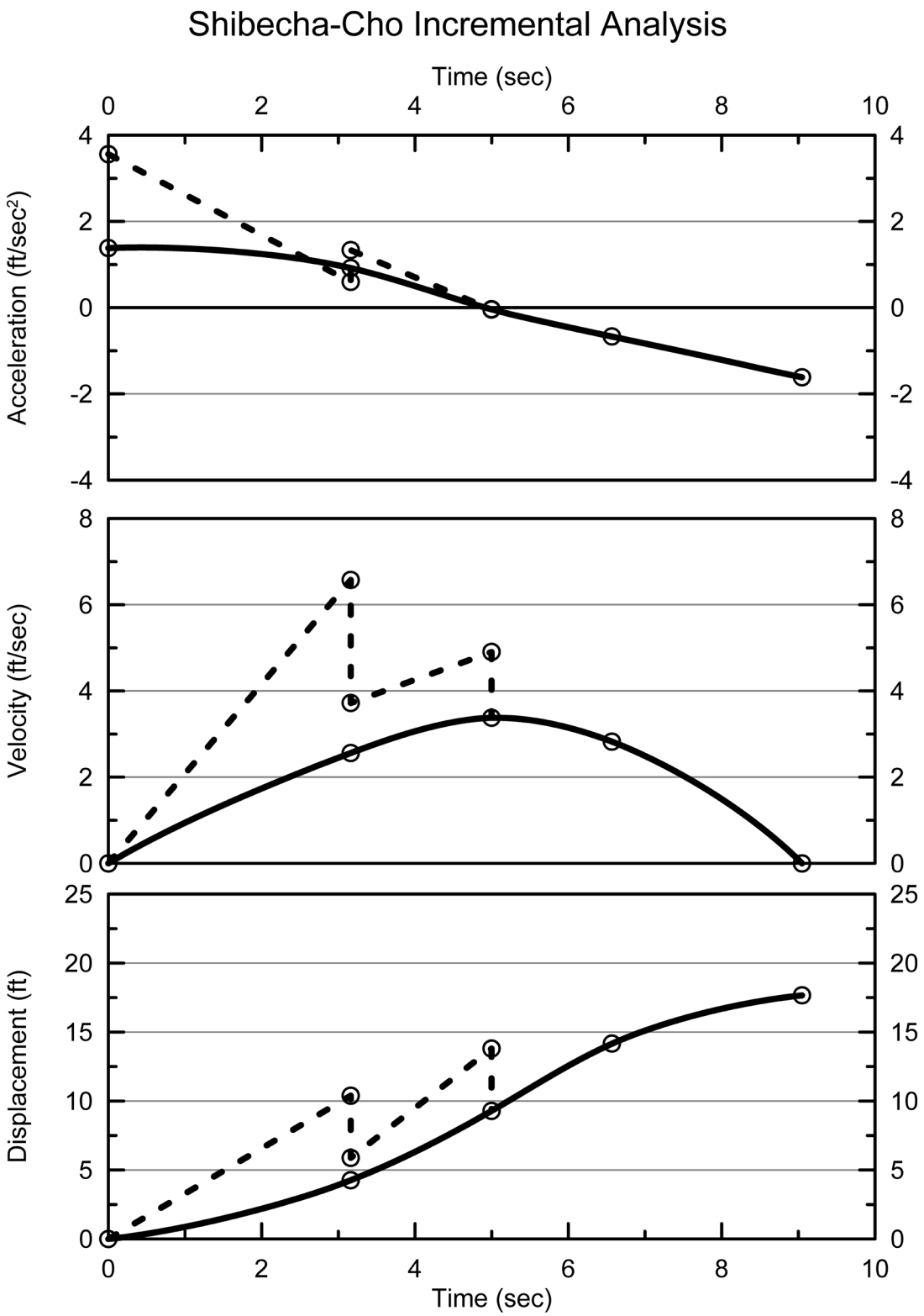

Figure 4.5: Calculated evolution of (1) acceleration vs. time, (2) velocity vs. time, and (3) displacement vs. time of the center of gravity of the overall failure mass of the Shibecha-Cho Embankment fill (solid line), and of incremental partial failure masses (dashed lines), based on the failure progression shown in Figure 4.4.

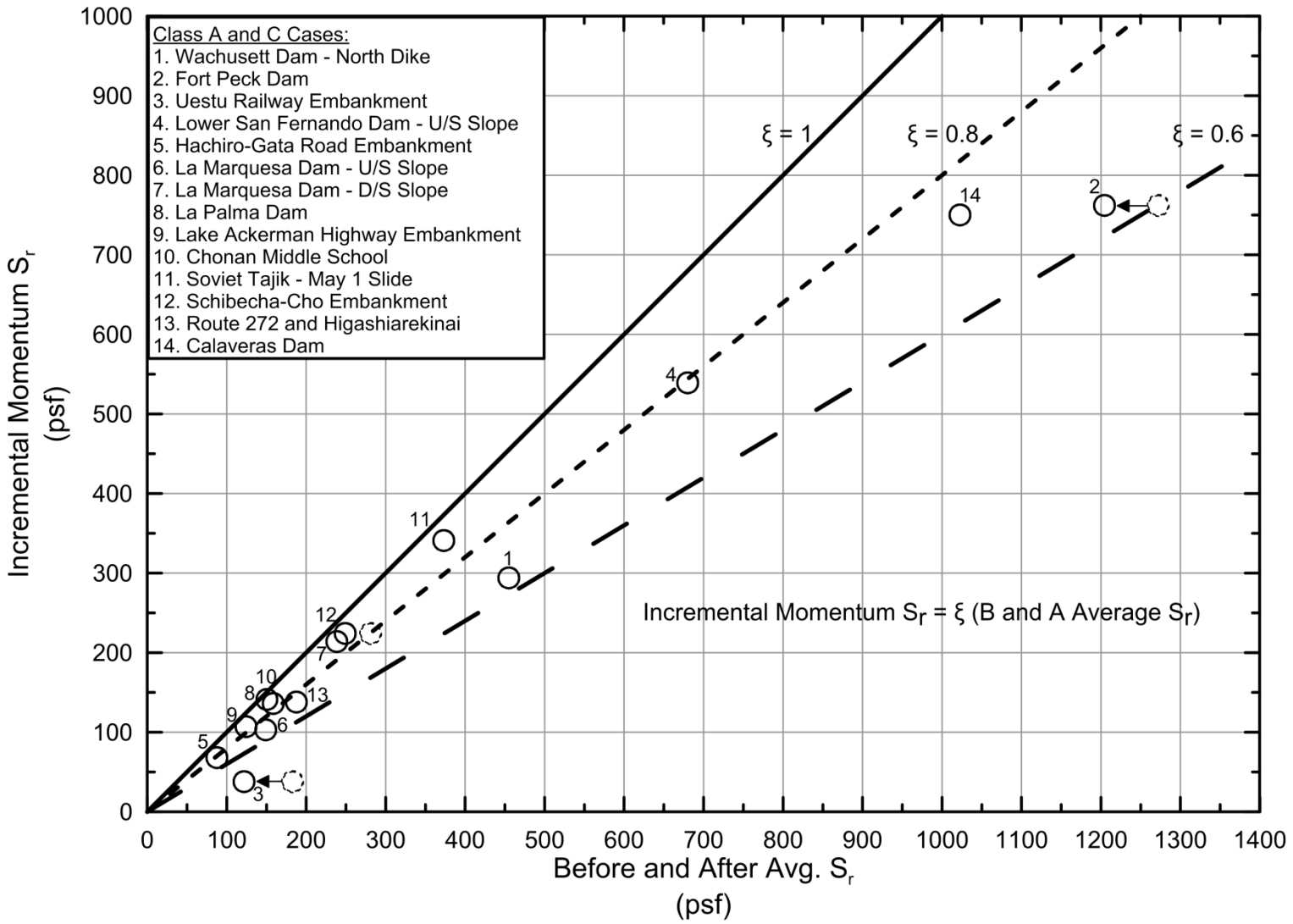

Figure 4.6: Plot of the results of back-analyses of the 14 Class A and C case histories, showing (1) the value of post-liquefaction strength S_r back-calculated by the incremental inertial method vs. (2) "before and after average S_r" which is the average of $S_{r,yield}$ and $S_{r,resid/geom}$ [taken as $(S_{r,yield} + S_{r,resid/geom})/2$].

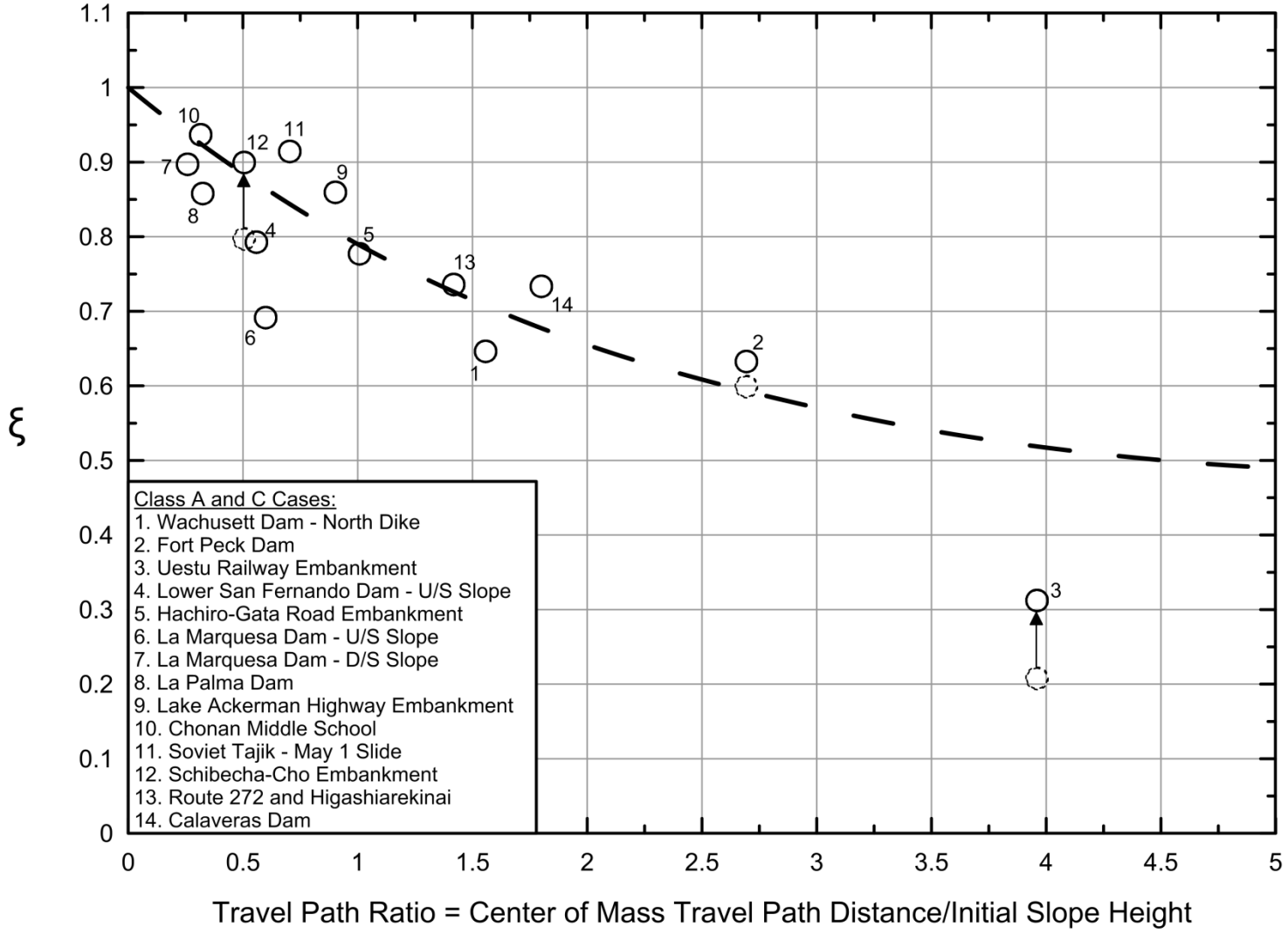

Figure 4.7: The empirical scaling parameter ξ for Equation 4-4, as a function of scaled runout distance.

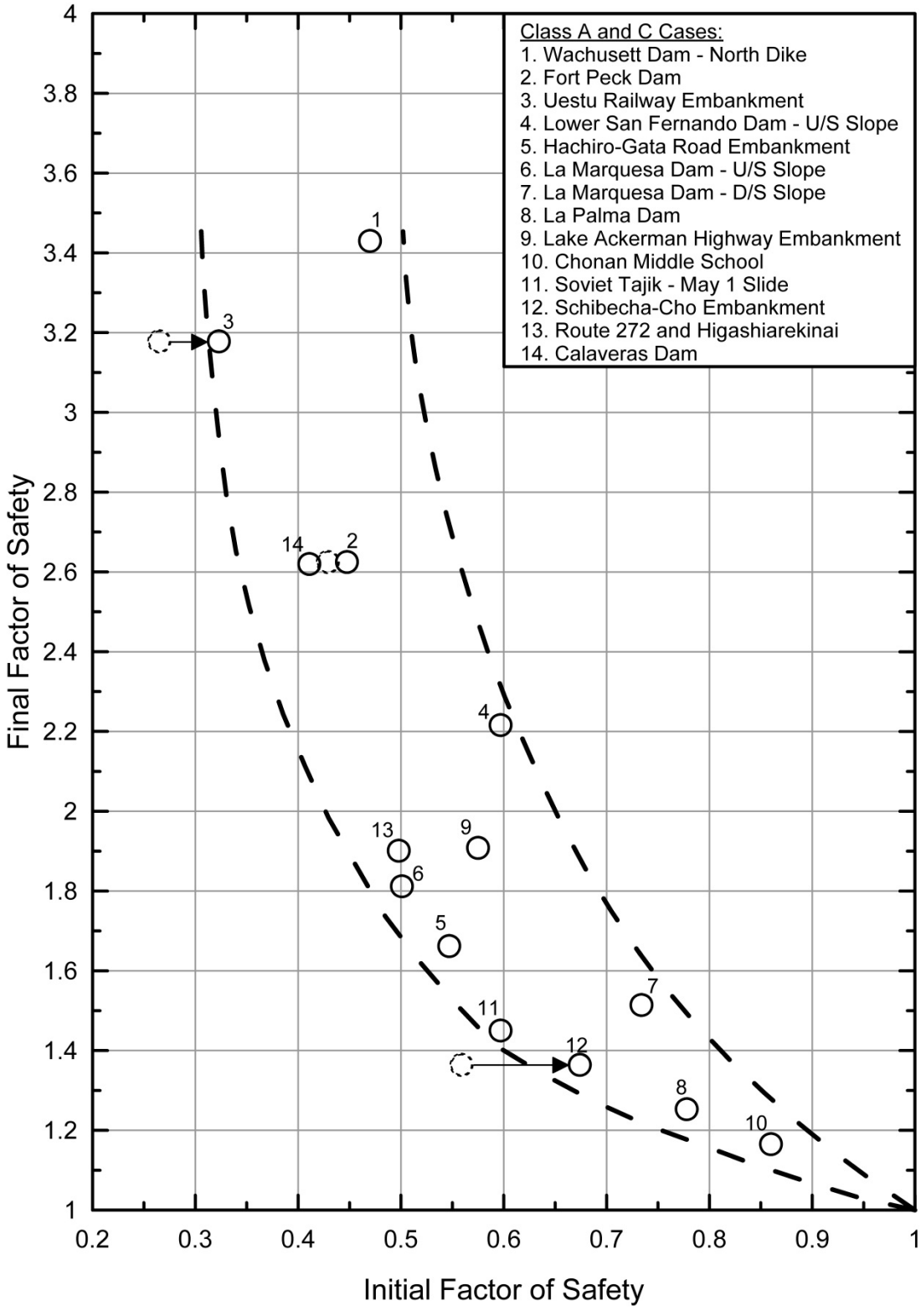

Figure 4.8: Plot of values of pre-failure FS_{liq} vs. post-failure FS_{liq} for the 14 back-analyzed liquefaction failure case histories of Classes A and C.

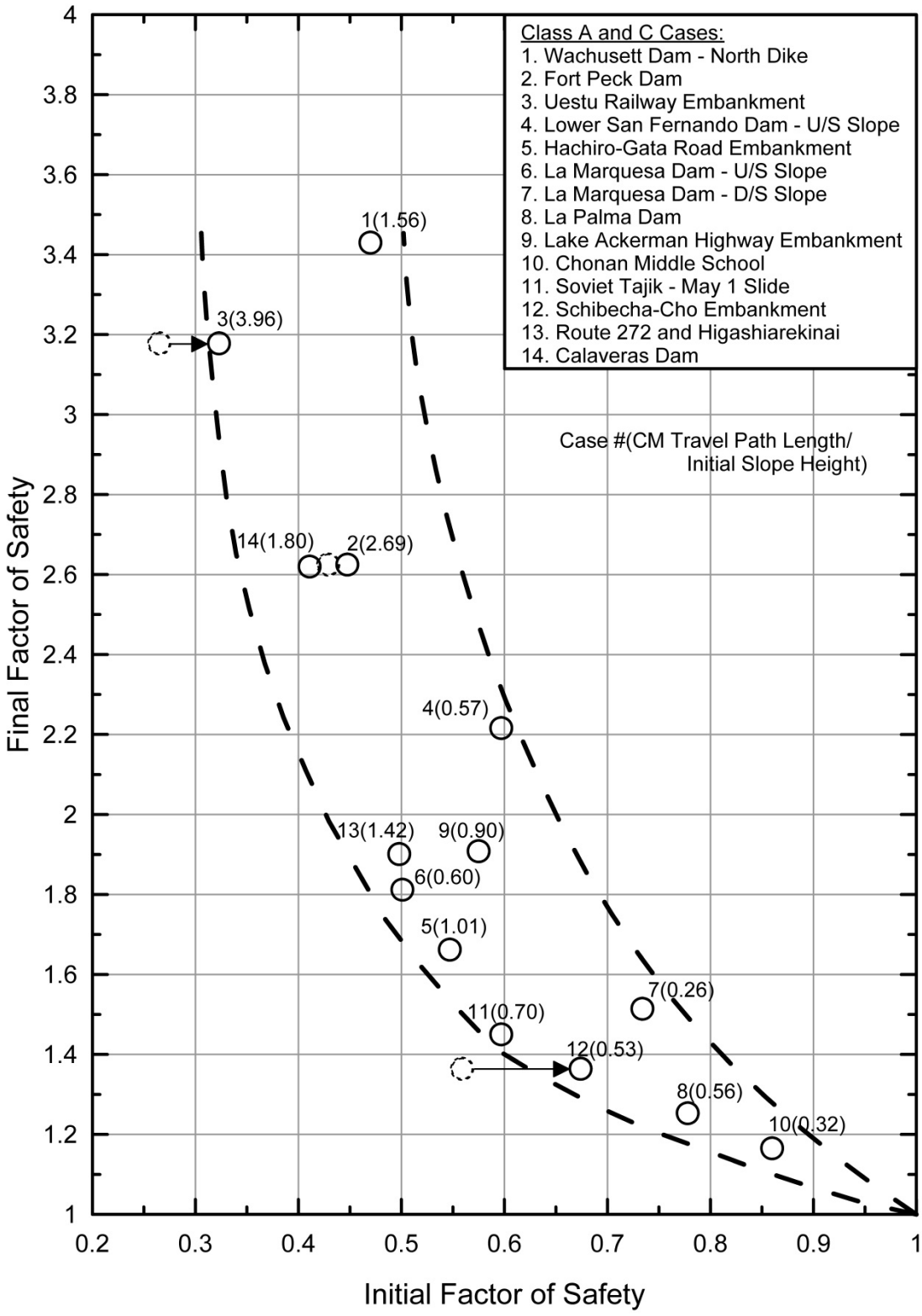

Figure 4.9: Figure 4.8 repeated, this time with the back-analyzed failure case histories annotated (in parentheses) with scaled runout distance ratio (travel distance of the center of gravity of the overall failure mass divided by the initial slope height as measured from the toe to the back heel of the failure)

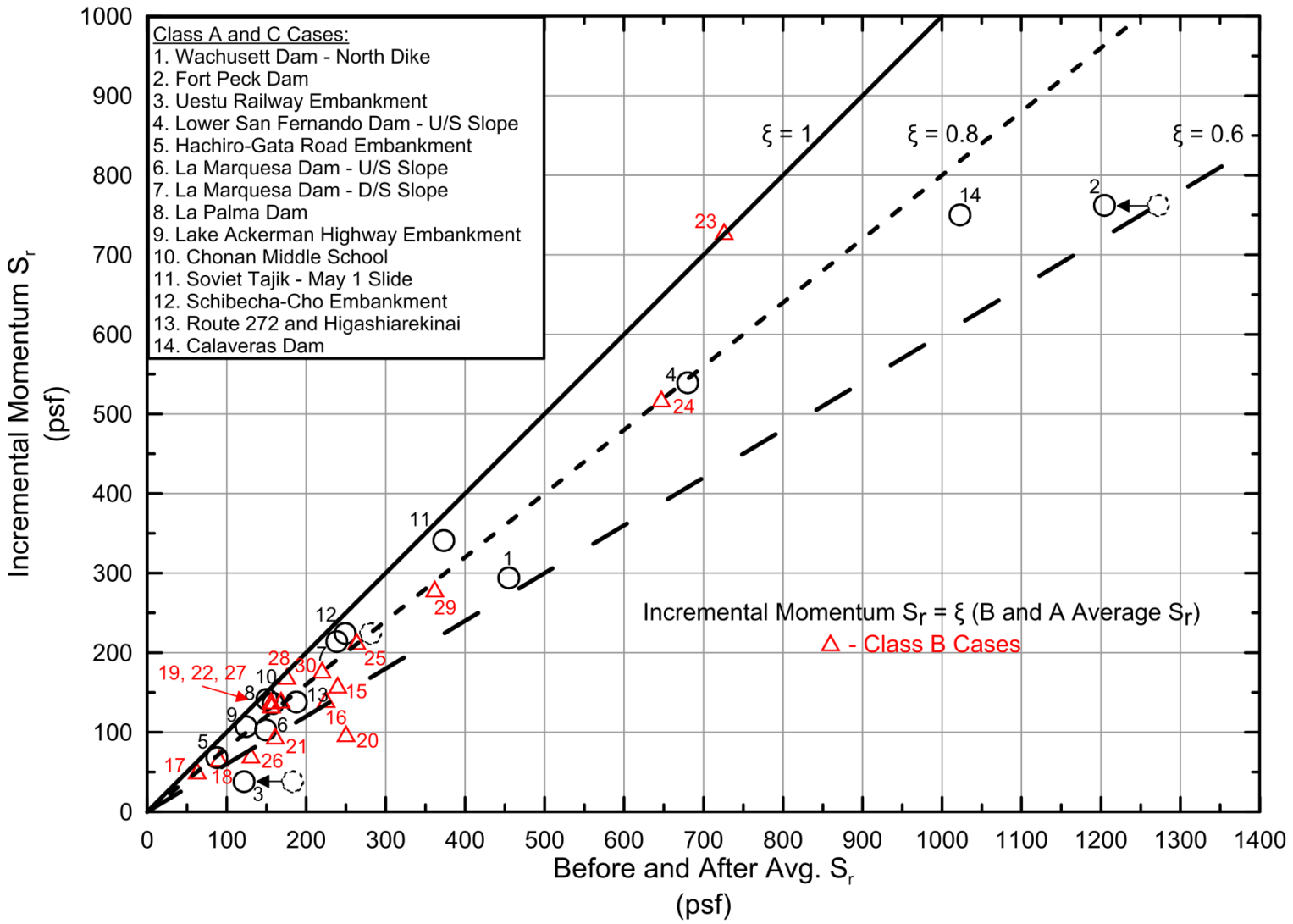

Figure 4.10: Figure 4.6 repeated, this time adding the back-analyzed Class B failure case histories (red triangles).

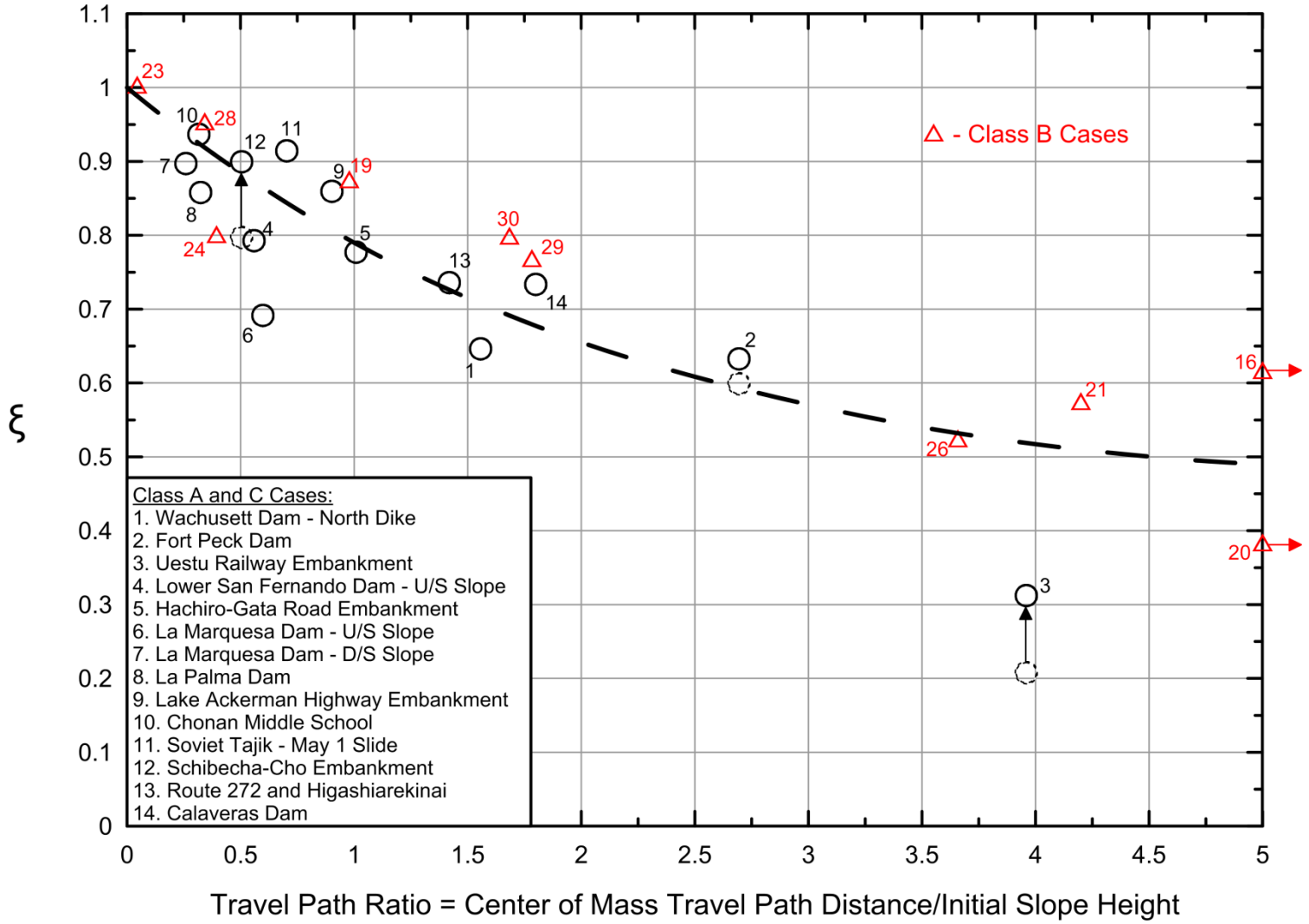

Figure 4.11: Figure 4.7 repeated, showing the empirical scaling parameter ξ for Equation 4-4, as a function of scaled runout distance this time adding the back-analyzed Class B failure case histories (red triangles).

Chapter Five

Development of Relationships for Evaluation of Post-Liquefaction Strength

5.1 Introduction

Chapter 4 presented back-analyses of field liquefaction case histories to develop indices for subsequent use here in the development of empirically-based correlations for engineering assessment of in situ post-liquefaction strengths (S_r) as a function of both (1) penetration resistance and (2) initial effective vertical stress. The indices from the individual case histories were internally cross-checked based on a series of calibrated empirical relationships and guidelines that were dependent upon failure mechanics and runout characteristics, etc. They were also checked against available values from other investigators who employed back-analysis methods that incorporated the effects of momentum and inertia. And they were also cross-checked against additional back-analyses performed by other investigators who employed methods that did not incorporate momentum effects, but for which the apparent resulting biases can now be at least approximately estimated.

The result is an unprecedented data set of reasonably well-constrained values of (1) back-calculated representative post-liquefaction strengths (S_r), (2) representative penetration resistances, and (3) representative initial effective vertical stresses on portions of the failure planes judged to have liquefied. Estimates of variance, or uncertainty, in each of these three indices were also developed for each of the 29 case histories back-analyzed in these current studies.

In Chapter 5, this hard-earned data set will now be used to develop improved relationships for assessment of in situ post-liquefaction strength (S_r).

5.2 Non-Probabilistic Regressions

The first step was to perform non-probabilistic (or deterministic) regressions by the least squares method to investigate functional equational forms, and associated shapes of model fitting surfaces, to determine a promising basic equational form for subsequent fully probabilistic regressions to be performed by Bayesian regression. These subsequent probabilistic regressions will incorporate all key sources of uncertainty, and will also permit modeling of heteroskedacity (variance of uncertainty across the domain of interest).

For this first step, the representative median values of $\overline{S_r}$, $\overline{N_{1,60,CS}}$ and $\overline{\sigma'_{vo}}$ for all 29 cases were assembled, as shown in Table 5.1. These mean values are assumed to also represent median values as all three indices are approximated as having normal distributions.

For these deterministic least squares regressions, the median values of Table 5.1 were taken as deterministic "best estimates", with no associated probabilistic likelihood. No weighting factors were assigned to the different cases, as the purpose of the exercise was only to determine promising potential (or candidate) equational forms for subsequent use in fully probabilistic regressions. This

permitted the performance of large numbers of nonlinear least squares regressions, using a large number of candidate equational forms.

A large number of candidate equational forms were regressed, and the most promising candidate form of equation was judged by the highest R-squared value to be

$$S_r = \exp\left(\theta_1 \cdot N_{1,60,CS} + \theta_2 \cdot \sigma_v'^{\theta_3}\right) \qquad \text{[Eq. 5-1]}$$

The resulting coefficients with this equational form was found to be

$$S_r = \exp\left(0.1625 \cdot N_{1,60,CS} + 4.004 \cdot \sigma_v'^{0.120}\right) \qquad \text{[Eq. 5-2]}$$

with $R^2 = 0.911$

In this equation:

S_r = Post-liquefaction shear strength [lbs/ft^2]

$N_{1,60,CS}$ = Overburden and equipment and procedurally corrected SPT penetration resistance with fines adjustment [blows/ft]

σ_v' = Initial vertical effective stress [atmospheres].

Figure 5.1(a) shows the shape of the resulting fitted surface for this relationship, as a multi-colored surface in three-dimensional space with $\overline{S_r}$ plotted on the vertical axis, and $\overline{N_{1,60,CS}}$ and $\overline{\sigma'_{vo}}$ plotted on the two horizontal axes. Residuals for each field case history are plotted, but in the upper figure's oblique view only the residuals above the multi-colored surface can be seen. Figure 5.1(b) shows the residuals for all 29 field case histories, plotted relative to a "flattened" best-fit surface. The residuals in Figure 5.1(b) are shown at exaggerated vertical scale for clarity; residuals are vertically exaggerated by a factor of 5 in this figure.

The curved surface shown in Figure 5.1(a) reflects the influences of both penetration resistance and initial effective vertical stress on post-liquefaction strength (S_r). The calculated R^2 value of 0.911 indicates an excellent level of "fit" for the data set. Examination of the residuals shows no significant patterning or systematic skew, suggesting that the regression (and the equational form) have successfully characterized most of the available information.

Figure 5.2(a) shows the best-fit Equation 5-2 plotted as $\overline{S_r}$ vs. $\overline{N_{1,60,CS}}$, with the different curves labeled with the initial effective vertical stress $\overline{\sigma'_{vo}}$ (in units of atmospheres). Also plotted in this figure are the values back-calculated for each of the 29 liquefaction failure case histories (from Table 5.1), with case history data points "binned" by ranges of effective vertical stress as indicated in the key in the upper left-hand corner of the figure, and with solid symbols indicating cases of cyclic initiation of liquefaction and open symbols indicating static initiation of

liquefaction, and with larger symbols indicating case histories with larger initial effective vertical stresses.

Figure 5.2(b) also shows the best-fit Equation 5-2, but this time plotted in terms of post-liquefaction strength ratio ($\overline{S_r}/\overline{\sigma'_{vo}}$) vs. $\overline{N_{1,60,CS}}$, with the different curves again labeled with the initial effective vertical stress $\overline{\sigma'_{vo}}$ (in units of atmospheres), and the values back-calculated for the 29 liquefaction case histories again binned and labeled as in Figure 5.2(a). There is more apparent scatter in this figure, but in the end the same data points are presented, and the curved lines shown reflect the same relationship from Equation 5-2 and Figure 5.1.

The relationship of Equation 5-2 (and Figures 5.1 and 5.2) provides an R-square value of 0.911, indicating a better level of "fit" for this data set and this relationship than has been achieved in previous studies by any regression employing 20 or more field case histories. This does not mean that this is the recommended final relationship, however, as this regression does not yet incorporate available information regarding the estimated uncertainties associated with the indices of $\overline{S_r}$, $\overline{N_{1,60,CS}}$ and $\overline{\sigma'_{vo}}$ for each of the 29 liquefaction field case histories. Instead, this is simply the opening step, and it serves mainly to show the promise of the data set and of the equational form selected at this stage.

5.3 Probabilistic Regressions by Bayesian Regression

Having thus ascertained and established an initially promising functional form for regression, the next step was to incorporate the full available information regarding variance and uncertainties, and to develop fully probabilistically based relationships between post-liquefaction strength and both (1) penetration resistance and (2) effective vertical stress.

The approach here was to employ Bayesian regression which can (1) model all key sources of variance or uncertainty, and (2) model heteroskedastic variation of model error or variance over the problem domain of interest. This Bayesian procedure can be employed in a manner that is largely analogous to least squares regression, but with the ability to accommodate and model both parameter uncertainty and overall model uncertainty (Gelman and Hill, 2006; Moss, 2009; Moss, 2011; Schmidt and Moss, 2021).

Table 5.2 shows the input variables for each of the 29 liquefaction field case histories as evaluated in Chapters 3 and 4, and Appendices A and B. Normal distributions were assumed for (1) mean post-liquefaction strength $\overline{S_r}$, (2) mean fines-corrected penetration resistance $\overline{N_{1,60,CS}}$, and (3) mean initial effective vertical stress $\overline{\sigma'_{vo}}$ for the portions of the field failure surfaces along which liquefaction was judged to have occurred in each of the case histories. Variances in these means were also evaluated, and these are also shown in Table 5.2. These variances, expressed as standard deviations of the respective means, were incorporated in these probabilistic regressions. It is important to note that the standard deviations listed are not standard deviations of the values of each of the respective indices for each case (e.g. individual $N_{1,60,CS}$ values); instead they are standard deviations of the <u>means</u> of these indices for each individual case.

Because the values listed in Table 5.2 include the engineering team's assessments of all sources of uncertainty or variance, no additional (judgmental) weighting factors were applied to each case history to further account for apparent data quality, or level of documentation, etc. The relative "weighting" of the information/data for each case history was thus a natural function of the variances in the three principal indices (or means) for each case, with cases that have higher variances or higher standard deviations having a lesser impact on the regressed relationships than cases with lower variances or standard deviations.

The same functional form as in the deterministic regressions of Section 5.2 was implemented in the Bayesian regression. The results are a set of three-dimensional surfaces of different probabilities of exceedance of S_r, where the median values of S_r (50% probability of exceedance) are treated as equivalent to the linear least squares regression trend relationship. The results are in the form of:

$$P \cong \Phi\left(\frac{g - S_r}{\Theta_\varepsilon}\right) \qquad \text{[Eq. 5-3]}$$

where

$P = probability$

$\Phi = cummulative\ standard\ normal\ distribution$

$g = functional\ form = exp\left(\theta_1 \cdot N_{1,60,CS} + \theta_2 \cdot {\sigma_v'}^{\theta_3}\right)$

$S_r = post - liquefaction\ residual\ strength\ [lbs/ft^2]$

$\theta_\varepsilon = error\ term$

Solving for the dependent variable can be accomplished by rearranging the equation:

$$S_r \cong g + \theta_\varepsilon \cdot \Phi^{-1}(P) \qquad \text{[Eq. 5-4]}$$

where $\Phi^{-1} = the\ inverse\ cummulative\ standard\ normal\ distribution$,

and P = probability of exceedance.

The equation that results from this analysis then becomes:

$$S_r = exp\left(\theta_1 \cdot N_{1,60,CS} + \theta_2 \cdot {\sigma_v'}^{\theta_3}\right) + \theta_\epsilon \cdot \Phi^{-1}(P) \qquad \text{[Eq. 5-5]}$$

where θ_ε is the error term.

Setting P = 0.50 produces a median curve that is similar, but not identical, to the deterministic relationship of Equation 5-2. Evaluating for other probabilities of exceedance will provide an estimate of the model uncertainty as captured by the Bayesian regression. The error term is a standard normal variate with zero mean and a standard deviation that equals the median

value found in the Bayesian regression over the range of blow counts and effective stresses in the database.

The overall resulting best-fit relationship was then determined to be

$$S_r = exp\left(0.1407 \cdot N_{1,60,CS} + 4.2399 \cdot \sigma_v'^{0.120}\right) + \Phi(\theta_\epsilon) \qquad \text{[Eq. 5-6(a)]}$$

where

$$\theta_\epsilon = N_{1,60,CS}{}^{1.45} + 0.2 * N_{1,60,CS} \cdot \sigma_v'^{2.48} + 41.13 \qquad \text{[Eq. 5-6(b)]}$$

and

S_r = Post-liquefaction strength [lbs/ft^2]

$N_{1,60,CS}$ = Overburden and equipment and procedurally corrected SPT penetration resistance with fines adjustment [blows/ft]

σ_v' = Initial vertical effective stress [atmospheres].

and these can be combined into spreadsheet format as

$$S_r = exp\left(0.1407 \cdot N_{1,60,CS} + 4.2399 \cdot \sigma_v'^{0.120}\right) + NORMINV(\mathrm{P}, 0, \theta_\epsilon) \qquad \text{[Eq. 5-7]}$$

Figure 5.3(a) illustrates the resulting median (50th percentile) fitted surface for this relationship, as a multi-colored surface in three-dimensional space with $\overline{S_r}$ plotted on the vertical axis, and $\overline{N_{1,60,CS}}$ and $\overline{\sigma'_{vo}}$ plotted on the two horizontal axes. Residuals for each field case history are plotted, but in his upper figure's oblique view only the residuals above the multi-colored surface can be seen. Figure 5.3(b) shows the median residuals for all 29 field case histories, plotted relative to the best-fit median (50th percentile) surface from Figure 5.3(a).

The variance or error term of Equation 5-6(b) varies over the problem domain as a function of both $\overline{N_{1,60,CS}}$ and $\overline{\sigma'_{vo}}$. This variance increases with increases in both $\overline{N_{1,60,CS}}$ and $\overline{\sigma'_{vo}}$ as will be discussed later, and as illustrated in Figure 5.5.

Figure 5.4(a) shows the median (50th percentile) relationship of Equation 5-6, this time plotted as curves of post-liquefaction strength S_r vs. $\overline{\sigma'_{vo}}$, with the different curves again labeled with the initial effective vertical stress $\overline{\sigma'_{vo}}$ (in units of atmospheres), and the values back-calculated for the 29 liquefaction case histories are again binned and labeled as in Figure 5.2(a).

Figure 5.4(b) shows the median (50th percentile) relationship of Equation 5-6, this time plotted as curves of post-liquefaction strength ratio S_r/σ'_{vo} vs. $\overline{\sigma'_{vo}}$, with the different curves again

labeled with the initial effective vertical stress $\overline{\sigma'_{vo}}$ (in units of atmospheres), and the values back-calculated for the 29 liquefaction case histories again binned and labeled as in Figure 5.2(a). A second important attribute of the Bayesian regression is the ability to model all sources of variance or uncertainty, and the resulting modeling of the distribution of variance (the error term) as a function of $N_{1,60,CS}$ and σ'_v that can be achieved.

Figure 5.5 shows the distribution of standard deviation of post-liquefaction strength (σ_{Sr}) as a function of $N_{1,60,CS}$ and σ'_v resulting from the probabilistic Bayesian regression, as quantified in Equation 5-6(b). Standard deviation of S_r increases with both (1) increase in $N_{1,60,CS}$ and (2) increase in σ'_v, but comparison of Figure 5.5 with Figure 5.3(a) shows that these increases are not fully directly proportional to the similar increases in S_r with increases in both $N_{1,60,CS}$ and σ'_v. This reflects (1) the differing variances associated with the parameters developed from each of the case histories, (2) the relative paucity of data (or the availability of data) over different portions of the problem domain, (3) variability in residuals from the mean for each case history, and (4) resulting variability or uncertainty in the best estimate values of S_r for different areas of the domain of Figures 5.5 and 5.3.

A further examination of the means by which the Bayesian regression deals with variance and uncertainty can be achieved by examining the effects of either (1) including the Upper San Fernando Dam case history in these regressions, or (2) deleting this case history and regressing only the other 28 case histories. One of the differences between the relationships developed or proposed by (1) Olson and Stark (2002) and (2) Wang and Kramer (2003, 2008) vs. those of (3) Seed and Harder (1990) and (4) these current studies, was the inclusion of the "non-failure" liquefaction case history for the Upper San Fernando Dam in the 1990 studies and in these current studies. It was the unanimous advice of the informal expert advisory panel that this was a suitable case to include, but the potential sensitivity of the resulting relationship to this decision then warrants examination. Figure 5.6 shows a comparison between the median (50^{th} percentile) values of S_r from the probabilistic regression of Figures 5.3 and 5.5 (and Equation 5-6) as shown with the black lines vs. the 50^{th} percentile probabilistic regressions results performed with the Upper San Fernando Dam case history deleted, as shown by the red lines. As shown in this figure, deletion of this case did not make a very significant difference. This was due in large part to the relatively high levels of uncertainty, or variance, assigned to the Upper San Fernando Dam case history, so that it did not exert strong control over the regressed fitting surfaces in its local neighborhood. It is the judgment of this engineering team that the data and information from the Upper San Fernando Dam case history is both valid and useful, and that the probabilistically regressed relationship with this case included (as expressed in Equation 5-6) is preferred.

The relationship of Equation 5-6 is fully probabilistic, and values for any percentile of non-exceedance can be generated. It is the recommendation of this engineering team that 33^{rd} percentile values (33% of values would be expected to be lower) represent a suitable level of conservatism for typical design applications. This represents a nearly mean-minus-one-half-standard-deviation level (more precisely, a mean minus 0.44 sigma level), and there is strong tradition for the use of this sort of "one third" level of enveloping (or similar) in geotechnical practice. Additionally, engineers are familiar with and tend to and have good experience with this level of conservatism for shear strengths.

For larger projects, or projects of special importance, a fully probabilistic (or risk-based) analysis can be performed using the full range of values of S_r and their associated probabilities as can be developed using the full form of Equation 5-6.

The recommended simplified "deterministic" values of S_r for routine design are then the 33rd percentile values, and these can be calculated by a simplified version of Equation 5-6 as

$$S_r(33rd\ Percentile) = exp\left(0.1407 \cdot N_{1,60,CS} + 4.2399 \cdot {\sigma'_v}^{0.120}\right) - 0.43991\left({N_{1,60,CS}}^{1.45} + 0.2 * N_{1,60,CS} \cdot {\sigma'_v}^{2.48} + 41.13\right)$$

[Eq. 5-8]

Figure 5.7 repeats Figure 5.4(a), showing the median (50th percentile) relationship of Equation 5-6 plotted as curves of post-liquefaction strength S_r vs. $\overline{\sigma'_{vo}}$, with the different curves again labeled with the initial effective vertical stress $\overline{\sigma'_{vo}}$ (in units of atmospheres), and the values back-calculated for the 29 liquefaction case histories again binned and labeled as in Figure 5.4(a). The red lines added to Figure 5.7 then show the 33rd percentile values calculated by Equation 5-8. This serves to illustrate the differences between the 50th percentile and the 33rd percentile values of S_r, and it also shows the relative juxtaposition of the recommended "simplified, deterministic" (33rd percentile) values relative to the "best-estimate" (median, or 50th percentile) values of each of the 29 back-analyzed individual field case histories.

Figures 5.8(a) and 5.8(b) then present the recommended deterministic relationship of Equation 5-8 (which is also the 33rd percentile probabilistic relationship of Equation 5-6) in two formats; showing S_r and $S_r/\sigma_{v,i}'$ as functions of penetration resistance and initial effective vertical stress.

The probabilistic and deterministic relationships of Equations 5-6 and 5-8, respectively, are based on a data set from field case histories that is confined to cases of large-displacement liquefaction failures with values of $N_{1,60,CS}$ of less than or equal to 15 blows/foot, and to cases with maximum values of initial effective stress (σ'_{vo}) of less than approximately 7 atmospheres, and "representative" values of initial effective stress ($\overline{\sigma'_{vo}}$) of less than four atmospheres. It must be anticipated, however, that these relationships are likely to be extrapolated to higher levels of both $N_{1,60,CS}$ and σ'_{vo}, because there are currently no viable alternatives for projects with larger ranges of stresses. This is not, however, an unbounded problem.

Figure 5.9 shows extrapolation of the 33rd percentile values of S_r from Equation 5-6 extended to higher $N_{1,60,CS}$ values and to higher effective stresses. Also shown in this figure are two dashed lines that delineate a shaded region that represents an approximate zone within which "drained friction cut-off" is likely to occur. Dilatant soils bifurcate narrowly, producing narrowly confined shear bands or "failure surfaces". That means that molecules of water have to travel only small distances to enter into the dilating zones in order to satisfy the "demand" created by dilatant reduction in pore pressures (below pre-failure phreatic conditions) during the rapid shearing or "failure". In the field, it is not safe to count on reduced (or even negative) pore pressures being fully maintained for any significant period of time, given these short distances that fluids must

travel to begin to satisfy dilatant demand, especially in the cohesionless sandy and silty soils which are prone to classic liquefaction, and for which the relationships developed here for evaluation of S_r are intended to be applied.

Accordingly, at any given location, the post-liquefaction strength should be taken as the lower of either (a) the "undrained" post-liquefaction strength (S_r) which includes effects of localized void redistribution in otherwise globally undrained soil strata, or (b) the fully drained residual strength. The fully undrained residual shear strength $S_{r,drained}$ can be approximated as

$$S_{r,drained} \approx \sigma'_{n,o} \bullet \tan \varnothing_r' \qquad \text{[Eq. 5-9]}$$

where $\sigma'_{n,o}$ = initial (and current) effective stress normal to the failure plane, and $\varnothing_r'$ is a residual effective friction angle.

For cohesionless soils, and for silty soils of low plasticity, the residual (non-dilatant) effective friction angle can be taken as approximately 28° to 31°. The upper bound of the "drained frictional cut-off" range shown in Figure 5.9 is established by assuming that vertical effective stress is approximately equal to the normal effective stress on failure surfaces that are horizontal (e.g. basal failure surfaces for lateral translational failures, or the "bellies" of rotational failure surfaces). This then leads to an approximate upper bound drained frictional cut-off at

$$S_{r,drained} \approx \sigma'_{n,o} \bullet \tan \varnothing_r' \approx \sigma'_{v,o} \bullet \tan 30° \approx \sigma'_{v,o} \bullet 0.577 \qquad \text{[Eq. 5-10]}$$

And so the approximate upper bound of the drained frictional cut-off range in Figure 5.9 is shown at a ratio of $S_r/P \approx 0.577$.

For the steeply inclined (or even vertical) back heel of a failure surface, the effective normal effective stress can be very roughly approximated as being equal to the coefficient of at-rest lateral earth pressure (K_o) times the effective vertical stress, and for most problems of interest with regard to potential liquefaction failures the soils can be expected not to be very heavily overconsolidated, and K_o can be very roughly approximated as $K_o \approx 0.5$.

For very steeply inclined (or vertical) failure surfaces, the drained frictional cutoff strength can then be approximated as

$$S_{r,drained} \approx \sigma'_{n,o} \bullet K_o \bullet \tan \varnothing_r' \approx \sigma'_{v,o} \bullet 0.5 \bullet \tan 30° \approx \sigma'_{v,o} \bullet 0.5 \bullet 0.577 \approx \sigma'_{v,o} \bullet 0.29$$

[Eq. 5-11]

And so the lower bound of the approximate drained frictional cut-off range shown in Figure 5.9 is shown at $S_r/P \approx 0.29$.

Of course, engineers will need to more closely calculate the actual expected drained frictional cut-off strengths at each location on potential failure surfaces based on project-specific details. Figure 5.9 then shows (approximately) the range of extrapolation of the 33rd percentile S_r relationships developed here. In this figure, it can be seen that (a) the drained frictional cut-off

occurs at higher values of $N_{1,60,CS}$ for soils at higher initial effective stresses; in agreement with basic laws of soil mechanics and critical state principles. For soils with low initial effective vertical stresses (e.g. ~ 0.1 atmospheres), the value of $N_{1,60,CS}$ at which the drained frictional cut-off comes into effect can be as low as $N_{1,60,CS} \approx 10$ or 11 blows/foot on very steeply inclined failure surfaces. Conversely, at very high effective stresses (e.g. ~ 8 atmospheres), the value of $N_{1,60,CS}$ at which the drained frictional cut-off comes into effect can be as high as $N_{1,60,CS} \approx 28$ to 30 blows/foot on essentially horizontal failure surfaces.

The relationships shown in Figure 5.9 are approximate guides, but they are in good general agreement with both basic soil mechanics and with the principles of critical state soil mechanics. They serve to illustrate the limits of the ranges over which values of S_r are likely to be needed by engineers. They also serve to illuminate an additional issue; the lack of large-displacement liquefaction field failure case histories for soils with high $N_{1,60,CS}$ values. For soils with $N_{1,60,CS}$ values of greater than about 15 to 20 blows/foot, the soils would behave sufficiently dilatantly that the behavior would be limited by fully drained frictional "cut-off" strengths except at very high initial effective overburden stresses. There are relatively few large geotechnical structures or systems where very high effective vertical stresses are critical, and it is hoped that there are even fewer that have not been well-engineered. As a result, there have been no opportunities for "triggering" of large-displacement liquefaction-induced failures for soils with higher values of $N_{1,60,CS}$.

Values in this range will continue to be of interest, however, for a limited number of critical applications. The most apparent of these are large structures (e.g. major earth dams), and these are of course usually critical structures with regard to public safety. Another example is bearing capacity, and tip settlements, for piles or piers bearing at depth. And so it must be expected that the relationships of Equation 5-6 will be extrapolated to higher ranges of $N_{1,60,CS}$ and to higher ranges of initial effective vertical stress.

Finally, it should be noted that it is routinely over a range of $N_{1,60,CS} \approx 10$ to 22 blows/foot that engineers are usually most concerned. For lower blowcount materials ($N_{1,60,CS} <$ 10 blows/foot), post-liquefaction strength is usually insufficient, and mitigation of the likely consequences of liquefaction is often required. For higher blowcounts ($N_{1,60,CS} >$ 22 blows/foot) post-liquefaction strengths are often sufficient (for all but the highest vertical effective stress situations). And so it is over this range ($N_{1,60,CS} \approx 10$ to 22 blows/foot) that these relationships are expected to be most important, and to affect most projects.

5.4 Comparisons with Selected Previous Relationships for Evaluation of Post-Liquefaction Strength (S_r)

5.4.1 Wang (2003), Kramer (2008), and Kramer and Wang (2015)

Kramer (2008) and Kramer and Wang (2015) extended the work of Wang (2003), and performed regressions to develop both probabilistic and recommended simplified deterministic relationships for in situ post-liquefaction strength (S_r). The work of Wang and Kramer (2003,

2008, and 2015) is the only fully comprehensive study available for direct comparison with these current studies.

As discussed previously in Section 2.3.7, Kramer and Wang made different choices with regard to selection of approaches at nearly every step of the way than those choices made by this current investigation team. They also made a number of very different judgments in implementing their selected approaches.

Table 4.7 presented a direct comparison between their table of values as employed in the probabilistic regressions of Kramer (2008), and the values employed in these current studies (as repeated in Table 5.1). As shown in Table 4.7, there are some significant differences in the case histories selected for inclusion by each of the two investigation teams, and the values back-calculated from some of the case histories common to both data sets also differ for some of the cases. Wang and Kramer made different choices and judgments that represent differences in engineering opinions, and both studies generally conform to acceptable standards in that regard.

An overview of significant differences between the two studies is as follows:

1. Wang and Kramer employed the Calaveras Dam failure case history, as they were not yet aware of the new investigations (Olivia Chen Consultants, 2003) that showed the hydraulic fill materials to be more variably clayey and cohesive than had previously been suspected. The current engineering team, with concurrence of the advisory panel, judged that it would not be possible to cross-correlate the modern SPT and BPT performed many decades after the slope failure of 1918, given nearly a century of ongoing consolidation and ageing effects in these complicated and challenging soils, and it was also the unanimous consensus of the informal group of expert advisors that this case should not be included in the regressions for S_r. So the current studies did not employ the Calaveras Dam case history in our regressions.

2. The current studies do include the back-analyzed "non-failure" (small displacement) case of the Upper San Fernando Dam, and the regressions of Kramer (2008) do not. This does not have a very significant influence on the relationships developed in these current studies, however, as shown in Figure 5.6.

3. Wang and Kramer included three other case histories that were deliberatively not included in these current studies. These were (1) Snow River Bridge Fill, (2) Kawagishi-Cho Building, and (3) Koda Numa Embankment. Reasons for deleting these cases for the current studies are presented in Chapter 3, Sections 3.3.3.1 through 3.3.3.3.

4. These current studies include two newer case histories that had not been available to Wang (2003). These were (1) Sullivan Tailings and (2) Jamuna Bridge.

5. Wang and Kramer included the Moshi-Koshi Tailings Dam failures as two separate cases, while the current studies "averaged" them together so that these two very similar failures would not overly impact the overall correlations developed.

In the end, Wang (2003) and Kramer (2008) employed 31 case histories, and the current studies employed 29 case histories.

Different approaches were taken to the back-analyses of the field performance case histories.

6. Wang (2003) employed the Zero Inertial Factor (ZIF) method to incorporate momentum effects in back-analyses of the 9 best-documented case histories. These appear to have provided good to excellent results; matching up fairly well with the incremental momentum analyses performed for these same case histories in these current studies. But the details of these analyses were not presented, and so they could not be checked in detail.

7. Wang (2003) then developed estimates of parameters for the remaining 22 less well documented case histories, designated as the "secondary" case histories, based on the back-analyses of multiple previous investigators, without performing any additional analyses of his own. Multiple values were collected from previous investigations, and these were then generally averaged. This left a bit more than two-thirds (22 out of 31) of the cases at least partially dependent upon the judgments and analysis choices of others. Chapter 2, Section 2.3.8, discusses a number of apparent errors and biases that occurred here. Especially notable cases where Wang's values of S_r values differed by more than +/− 50% from the S_r values employed in these current studies are: (1, 2) the two La Marquesa Dam cases (Upstream slope failure, and Downstream slope failure), where Wang's selected values of S_r were significantly higher than those of this current study (probably due to inclusion of significant allowance for cyclic inertial effects in the previous back-analyses by de Alba, et al, 1987), (3) Hokaido Tailings dam where Wang's value of S_r is approximately twice as high as the S_r values back-calculated by either Olson (2001) or in these current studies, and (4) the Nerlerk Embankment offshore slides where Wang's selected values are slightly more than twice as high as the values used by either Olson (2001) or in these current studies. Overall, there was a moderate tendency for Wang's selected values of S_r to be biased slightly to the high side (see Chapter 2, Section 2.3.8). Problems occurred due to the approach used to infer initial effective vertical stress, and the values of $\sigma'_{v,i}$ adopted by Wang for at least nine of the secondary case histories are unreasonably high (see Section 2.3.8.1(b) – (iii)). These excessively high values of $\sigma'_{v,i}$ served to "stretch" the $\sigma'_{v,i}$ axis in the regressions that were performed, and resulted in somewhat conservative under-prediction of S_r by the eventual regressed relationship, especially at high initial effective stresses in the final relationship developed. The two sets of apparent errors in parameters from the "secondary" case histories were thus (a) unconservatively biased (overall) values of S_r, and (b) conservatively biased (overall) values of $\sigma'_{v,i}$. These two sets of biases offset each to some extent, but the errors in $\sigma'_{v,i}$ were the stronger influence and the overall resulting (regressed) relationship appears to have been moderately conservatively biased as a result.

8. These current studies employed the incremental momentum method to incorporate momentum effects in the back-analyses of the 13 best-documented case histories. Results compared reasonably well with those of Wang (2003) for the 9 cases Wang analyzed with the ZIF method.

9. These current studies then made independent (new) assessments in back-analyzing the remaining 16 less well documented case histories, while cognizant of the back-analyses and assessments of previous investigators.

10. Kramer (2008) and thus also Kramer and Wang (2015) elected to employ non-fines-corrected $N_{1,60}$ values rather than $N_{1,60,CS}$ values as the basis for their regressions and relationships. These current studies elected instead to use fines-corrected $N_{1,60,CS\ values}$. The field case history database is comprised largely of cases involving silty sands and sandy silts, and it appears to the current investigation team that fines corrections are potentially important. Kramer based his decision to switch to $N_{1,60}$ (from Wang's initial 2003 assessments of $N_{1,60,CS}$) on the observation that $N_{1,60}$ gave a similar degree of model "fit" as measured in terms of dispersion or variance. The current investigation team did not find that fully compelling, given that so many of the cases had significant fines corrections. Due perhaps in part to different processing and back-analyses of the case histories, including new procedures and both internal cross-checks and external cross-checks, the current investigation team achieved an $N_{1,60,CS}$-based relationship with a significantly smaller overall dispersion (uncertainty) than the relationship of Kramer and Wang (2015).

Very different approaches were also taken with regard to evaluation of uncertainties in all parameters, and in the incorporation of these uncertainties in the probabilistic regressions performed by the two investigation teams.

11. Wang (2003) used Monte Carlo simulations to assess parameter uncertainty for the 9 best-documented case histories, but this primarily served to help to quantify variability of parameters (especially S_r) already established by engineering judgments made with regard to modeling of variability in geometry, failure surfaces, phreatic conditions and properties of non-liquefied soils. The Monte Carlo modeling simply reflected these judgments. These current studies performed back-analyses of the 13 best-documented case histories using the incremental momentum method, and preferred to employ parameter sensitivity studies and engineering judgment directly in the development of characterizations of variability (e.g. standard deviations) of back-calculated indices from the case histories.

12. For his 22 "secondary" case histories, Wang's estimates of variability (e.g. standard deviations) were based on the back-analyses performed by multiple previous investigators, but it is unclear how judgments were made with regard to interpretations of these previous analyses to develop variance estimates for the indices of interest. In these current studies, new back-analyses were performed for all 16 of the less well documented case histories (the 16 Class B case histories), and these results, with sensitivity studies by means of parameter and geometry variations, as well as consideration of previous back-analyses by other investigators, were jointly used to develop estimates of variability (expressed as estimated standard deviations) of the three key indices from each case history.

13. Another significant difference between the two studies was the manner in which variance or uncertainty was evaluated and modeled for all cases. Wang (2003), Kramer (2008), and Kramer and Wang (2015) performed as formal as possible an assessment of variability of the data available (e.g. variability of actual reported penetration resistance values), but they

did not directly incorporate additional uncertainties associated with poor quality of data or information, or poor quality of documentation, into these estimates. Instead, they subsequently applied judgmental "weighting factors" to each of their 31 cases to reflect these additional uncertainties. That was likely effective with regard to development of good estimates of the median relationship for S_r, but it may not have been ideal with regard to evaluation of overall model uncertainties. The current engineering team preferred instead to incorporate uncertainties associated with poor quality data, poor documentation, uncertainties in transforming non-standard penetration resistances to equivalent SPT values, etc., into combined (overall) estimates of variance (standard deviations) for each of the three principal indices. In these current studies, estimated variances in all back-analyzed parameters included all of these sources of uncertainty, so no additional weighting factors were then applied to the individual case histories.

14. Kramer (2008) developed estimates of model uncertainty by two different methods: Maximum Likelihood Estimation (MLE) and First-Order, Second Moment (FOSM). The MLE estimates of variance developed were judged to be excessively large, and were discarded. So the FOSM-based estimates of variance or model uncertainty are the basis for his overall probabilistic model uncertainty. The uncertainties (standard deviations) developed by this approach also appear to be large, as illustrated in Figure 5.13(b), and this will be discussed further a bit later. These current studies employed the Bayesian regression method as a basis for development of estimates of model uncertainties, and the results are somewhat smaller values of variance or standard deviation for S_r across most of the problem domain, as illustrated in Figure 5.13(a). This may be due in part to the different overall treatments of uncertainty in the back-analysis data set, and it also likely due to the level of effort and care expended in performing and cross-checking the individual back-analysis results for <u>all</u> of the case histories studied.

15. Kramer (2008) studied a suite of lateral spreading case histories, and concluded that his regressed relationship warranted revision in order to ensure that post-liquefaction strengths for very low initial effective overburden stresses would not be under-predicted. He intervened, and fixed the value one of his parameters (Θ_4) in performing his final regressions. That appears to have been a valid approach to fixing the problem of excessively low predicted S_r values at low $\sigma'_{v,i}$., but it may have introduced some bias in other parts of the overall problem domain. In these current studies, the shape and position of the regressed surface for S_r was judged to be suitable at low effective initial overburden stresses without this type of additional manipulation.

16. Kramer (2008) and Kramer and Wang (2015) selected the 40^{th} percentile values of post-liquefaction strength (S_r) as the recommended "deterministic" values for routine projects. This was based on his observation that all of the best-documented field case histories produced S_r values that plotted above the probabilistic 40^{th} percentile value. These current studies preferred to assume that the probabilistic regressions performed had largely correctly characterized overall accuracy, and that a more traditional 33^{rd} percentile value would be appropriate for more simplistic "deterministic" values. This, too, will be discussed further.

The two investigation teams of (1) Wang and Kramer (2003, 2008, and 2015) and (2) these current studies, took different approaches at virtually every step or decision point. These were all valid approaches, and reasonable judgments, given the state of knowledge and information available at the time, and so it is interesting now to cross-compare the overall results of these two studies.

Kramer (2008) selected the 40th percentile values of post-liquefaction strength (S_r) as the recommended "deterministic" values for routine projects. Figure 5.10 presents these 40th percentile values, based on the probabilistically regressed relationship that he developed based on the first-order second moment (FOSM) method.

In these current studies, 33rd percentile values are recommended as "deterministic" values for routine design, and Figure 5.11 compares Kramer's recommended 40th percentile values (red lines) vs. the 33rd percentile values (black lines) recommended in these current studies. The level of approximate agreement between these two sets of recommended values is surprisingly good. Especially given the very different steps, procedures, assumptions, and judgments that went into the development of each set of values shown. And the differences can now be explained and understood.

A better comparison is achieved by slightly modifying the curves of Kramer and Wang (2015) by adding an approximate adjustment for fines so that both relationships can (approximately) be compared on an $N_{1,60,CS}$ basis. The average fines correction made for the 30 case histories back-analyzed in these current case histories was $\Delta N_{fines} \approx 1.3$ blows/ft, and the fines correction employed in these current studies progressively increased fines corrections as $N_{1,60}$ values increase, in addition to increasing them with increased fine content. Accordingly, an approximate adjustment was made by adding $\Delta N_{fines} \approx +0.5$ blows/ft to the relationship of Kramer and Wang at $N_{1,60} = 0$, and $\Delta N_{fines} \approx +2.0$ blows/ft at $N_{1,60} = 15$ blows/ft, so that an average correction of approximately +1.2 blows/ft is inferred over the range of the actual case histories. This was applied as a linear correction, so slightly increasing corrections continue to be added at $N_{1,60}$ values higher than 15 blows/ft.

Figure 5.12 repeats Figure 5.11, this time with this modest adjustment of the relationship of Kramer and Wang (2015) to an approximate a clean-sand-corrected basis. This is then the best (nearly direct) comparison of the two relationships.

As discussed in Chapter 2, there are three issues that principally affect the relationship of Kramer and Wang, and these can be seen in this comparative figure. These are as follow.

1. The first of these is the suite of errors made by Wang in estimation of $\sigma'_{v,i}$ for a significant number of his 22 secondary case histories due to the over-simplified procedure that he employed here. As discussed in Section 2.3.8.1(b)-(iii), and illustrated in Table 2.3, many of the values of $\sigma'_{v,i}$ are clearly too high, and some of them are physically impossible. As shown in Figure 2.3, this appears to result in an average overestimation of $\sigma'_{v,i}$ by a factor of approximately 1.57. This has the effect of "stretching" the $\sigma'_{v,i}$ axis, and results in (over-conservative) under-prediction of S_r for real values of $\sigma'_{v,i}$, especially at high values of $\sigma'_{v,i}$.

This causes the resulting predicted S_r values to be over-conservative, and to drop below those of this current study, especially at increasing $\sigma'_{v,i}$.

2. The second issue was problems with Wang's selections of values of S_r for some of the secondary case histories. These were more subtle issues, and they appear to have affected a lesser number of cases, and to lesser degree (see Section 2.3.8.1(b)-(ii). Most of these led to somewhat unconservative over-estimates of S_r for the individual cases affected. This tended to introduce a source of unconservative bias, but because of the lesser degree, and the lesser number of cases, it did not fully offset the over-conservatism due to the overestimation of numerous values of $\sigma'_{v,i}$. So the overall correlation remained overly-conservative.

3. Kramer (2008) noticed that the predicted values of S_r appeared to be too low at very low $\sigma'_{v,i}$, and so he performed a study of lateral spreading case histories, and established a fixed value of Θ_4 to raise up S_r values for low $\sigma'_{v,i}$ based on an estimated lower bound for S_r at low $\sigma'_{v,i}$. He then used this as a basis for modifying his overall regression by fixing the value of one of his parameters (Θ_4) in his regressions. Because the suite of field case histories present in the liquefaction flow failure case history database was internally correlated in terms of lower $\sigma'_{v,i}$ cases also tending to be lower $N_{1,60}$ cases, this had the effect of also increasing S_r values at low $N_{1,60}$.

All three of these effects can be seen in Figure 5.12. The relationship of Kramer and Wang (2015) falls away below the relationship developed in these current studies at progressively higher values of $N_{1,60,CS}$ (and also $\sigma'_{v,i}$) due to the over-conservatism introduced by the errors in $\sigma'_{v,i}$ values out-weighing the errors in S_r values. At low $N_{1,60}$ (and at low $\sigma'_{v,i}$) the "fix" applied by Kramer (2008) suitably raises up the predicted S_r values, and both relationships agree well here. This "fix" also appears to result in higher predicted values of S_r, however, at low $N_{1,60,CS}$ but higher $\sigma'_{v,i}$; a range that was not analytically considered in the lateral spreading case history study that led to this fixing of (Θ_4). Because the case histories data set is internally correlated, with cases having lower N-values being correlated to some extent with cases that have lower $\sigma'_{v,i}$ values, the effect of imposing a fixed value of Θ_4 to slightly raise up predicted values of S_r at low $\sigma'_{v,i}$ also inadvertently slightly "tilted" the overall relationship; further lowering predicted values of S_r at higher N-values.

Overall, however, these two sets of results (and "deterministic" recommendations) would appear to largely represent what passes for the beginnings of "consensus" for these types of challenging geotechnical issues, especially across the ranges of the available field case history data, and at blowcounts of $N_{1,60,CS} \leq 16$ blows/ft, if the over-conservative errors in selection of $\sigma'_{v,i}$ values made by Wang (2003) for at least 13 of the secondary case histories are taken into account. With those errors included, however, the relationship of Kramer and Wang systematically conservatively under-predicts S_r at high values of $\sigma'_{v,i}$.

Figure 5.13 shows the two different surfaces representing the estimated values of variance, expressed as standard deviation of S_r developed based on the probabilistic regressions of (a) these current studies, and (b) Kramer (2008). The standard deviations of Kramer are very similar to those of these current studies in the lower front corner, where both $N_{1,60,CS}$ and initial effective

vertical stress are relatively low, but they increase more rapidly with increasing $N_{1,60,CS}$ and with increasing effective vertical stress. This has some ramifications for (a) the selection of recommended exceedance levels for the simplified "deterministic" relationships developed for the two different relationships, and (b) for the levels of conservatism that will be associated with more comprehensive use of the two fully probabilistic relationships (for all exceedance levels) on more complex and/or higher risk projects to which risk-based methods may be applied.

Kramer recommended setting his simplified "deterministic" relationship for S_r at the 40th percentile, based on the observation that all of the 9 well characterized field case histories exceeded this value. The current studies selected instead the 33rd percentile value, based on the assumption that the field case history data set had been properly characterized in its entirety, and that the use of this more traditional value of level of conservatism would be more familiar and would be better understood and thus better employed by working engineers.

Figure 5.14 shows a comparison between Kramer's 33rd percentile values (red lines) vs. the 33rd percentile values (black lines) recommended in these current studies. These "equal risk" based lines show that the relationship developed by Kramer and Wang drops away from the relationship developed in these current studies at higher $N_{1,60,CS}$ values when equal levels of non-exceedance are targeted. That has ramifications for fully risk-based engineering analyses for major projects involving higher initial effective stresses.

Figure 5.15 then shows the recommended "deterministic" relationship (40th percentile) of Kramer (2008), this time expressed in terms of strength ratio (S_r/P) format, extrapolated to higher $N_{1,60,CS}$ values (red lines) and the recommended "deterministic" relationship (33rd percentile) of these current studies also extrapolated. This figure also shows the range of likely fully drained frictional cut-off as presented previously in Figure 5.9. This shows even more clearly how the relationship developed in these current studies rises more quickly at $N_{1,60,CS}$ values greater than about 10 to 15 blows/ft, and it also shows how the range of interest is limited by the likely range of drained frictional cut-off. (It should be noted that it is often values at and near the top of the drained frictional cut-off range, corresponding to largely horizontal failure surfaces in the field, that are of principal interest for many significant engineering projects).

Overall, agreement between the relationships developed by Wang and Kramer (2003, 2008, and 2015) and by these current studies is judged to be reassuringly good, if allowance is made for the excessively high (and incorrect) representative $\sigma'_{v,i}$ values that Wang (2003) selected for at least 12 of his "secondary" (Class B) case histories; and the consequent degree of excessive conservatism (especially at high penetration resistances and high initial effective overburden stresses) that resulted.

5.4.2 Olson and Stark (2002)

Figure 5.16 shows the recommended relationship between S_r/P and $N_{1,60}$ proposed by Olson and Stark (2002). Figure 5.17 then shows this relationship super-imposed (red lines) on the 33rd percentile relationship developed in these current studies. The relationship of Olson and Stark modeled the post-liquefaction strength ratio (S_r/P) as being independent of initial effective overburden stress, and so it was to be expected that their recommended relationship would be

conservative for very low initial effective overburden stresses, and unconservative for very high initial effective overburden stresses. In addition, because 23 of their 33 liquefaction case histories were back-analyzed in a manner that produced values of $S_{r,resid/geom}$, instead of values of S_r that incorporated momentum effects, 23 of their case histories systematically underestimated S_r, and likely by factors of approximately 1.2 to 3.4, as discussed previously in Section 2.3.6. The other 10 cases were back-analyzed by their kinetics method, which did specifically incorporate momentum effects, and this appears to have produced generally reasonably good back-calculated values of S_r for those cases. Overall, however, it would be expected that their relationship would be significantly conservatively biased by the 23 cases for which S_r was systematically (and significantly) underestimated.

This is what Figure 5.17 shows. Allowing for the fact that their horizontal axis is $N_{1,60}$ rather than fines-adjusted $N_{1,60,CS}$, their recommended range of S_r/P values appears to be generally suitable at initial effective vertical stresses of approximately 1 to 4 atmospheres, and for $N_{1,60}$ values of less than about 10 to 12 blows per foot. At higher values of penetration resistance, their relationship lacks upward curvature, and would provide increasingly over-conservative values. And this over-conservatism would also be greater at lower effective overburden stresses. Their relationship fails to capture the "upwards curvature" inherent in the S_r values for any given level of effective overburden stress, and it also fails to capture the partial dependence of S_r/P on effective vertical stress.

5.4.3 Idriss and Boulanger (2008)

Figures 5.18 and 5.19 show the recommended relationships of Idriss and Boulanger (2008) for evaluation of post-liquefaction strength ratio (S_r/P) as a function of penetration resistance. Figure 5.18 shows the relationship of Idriss and Boulanger for residual strength ratio (S_r/P). Figure 5.19 then shows the relationship of Idriss and Boulanger (red lines) for residual strength ratio (S_r/P) from Figure 5.18 superimposed on the 33rd percentile relationship developed in these current studies (black lines). It is the lower of the two diverging lines in Figure 5.18 and 5.19 that represents Idriss and Boulanger's recommended relationship for field situations (in which void redistribution effects can occur), as the upper line is applicable only to a theoretical situation in which void redistribution does not occur). As shown in these figures, the relationship of Idriss and Boulanger (2008) fails to capture the dependence of S_r/P on effective vertical stress. It provides reasonable values of S_r/P for $N_{1,60,CS}$ values of less than about 12 blows/ft and for effective stresses of between about 0.5 to 2 atmospheres. In this same range of $N_{1,60,CS}$ values of less than about 12 blows/ft, the relationship is unconservative at higher effective stresses. At lower effective stresses the relationship is overly conservative. In this same range of $N_{1,60,CS}$ values of less than about 12 blows/ft, the relationship is unconservative higher effective stresses. But at higher $N_{1,60,CS}$ values and higher effective overburden stresses the relationship of Idriss and Boulanger becomes increasingly conservative, and progressively matches up well with higher effective stress ranges while being increasingly over-conservative for lower effective stresses. The "upper" dashed red line of the two diverging dashed lines in Figure 5.19 is a theoretical relationship, based on laboratory testing (see Section 2.3.10), and it is recommended only for cases in which void redistribution is not expected to occur. This upper dashed line is therefore not applicable to field conditions as considered in these current studies and no comparison is appropriate here.

Figure 5.20 shows the recommended relationship of Idriss and Boulanger (2008) for S_r as a function of penetration resistance ($N_{1,60,CS}$). Figure 5.21 shows this relationship of Idriss and Boulanger (red lines) superimposed on the 33rd percentile relationship developed in these current studies black lines). This relationship also fails to capture the dependence of S_r on initial effective vertical stress. The relationship appears to be suitable for initial effective overburden stresses of approximately 1 atmosphere, and the upward curvature out to blowcounts as high as 16 blows per foot appears to continue to be generally appropriate for this level of effective overburden stress. This relationship would generally be increasingly overconservative for effective overburden stresses significantly greater than 1 atmosphere, and it would be unconservative for effective overburden stresses significantly lower than 1 atmosphere.

5.4.4 Seed and Harder (1990)

Figure 5.22 shows the relationship recommended by Seed and Harder (1990). Figure 5.23 shows this relationship (red lines) superimposed on the 33rd percentile relationship developed in these current studies (black lines). The relationship proposed by Seed and Harder (1990) is the oldest of the previously proposed relationships considered here, and it too fails to capture the partial dependency of S_r on effective vertical stress. This relationship is often employed based on an interpretation of S_r as being one-third of the way up from the bottom boundary curve towards the top boundary curve. The relationship of Seed and Harder (1990), taken at this "one-third" level, is fairly similar to the relationship of Idriss and Boulanger (2008) shown previously in Figures 5.20 and 5.21, and it has similar strengths and weaknesses. It too fails to capture the partial dependence of S_r on effective vertical stress. An approximate one-third interpretation appears to provide reasonable values of S_r for effective overburden stresses of approximately 1 to 2 atmospheres, and for $N_{1,60,CS}$ values of less than about 16 to 18 blows/ft. And it would be over-conservative for higher initial effective vertical stresses, and if extrapolated to values of $N_{1,60,CS}$ greater than about 17 blows/ft it would be unconservative for effective stresses less than about 2 atmospheres.

5.5 Remaining Uncertainty and Overall Conservatism

The new relationships developed herein appear to fit well with the previous relationships developed and presented by others, especially when the underlying bases of those previous relationships are closely examined with regard to (1) the strengths and drawbacks of the back-analyses of case histories performed to develop the data upon which the previous relationships were developed, and (2) the strengths and drawbacks of the basic forms and assumptions upon which the previous relationships were based.

The new relationships are also based upon an internally consistent, and cross-checked, suite of back-analysis results from a large suite of field performance case histories.

But there remain three principal sets of uncertainties, and potential sources of systematic conservatism or unconservatism, in the new relationships. And these warrant further discussion.

5.5.1 Monotonic vs. Cyclically-Induced Values of Post-Liquefaction Strength (S_r)

A question that arises is whether cyclically-induced soil liquefaction will produce a greater amount of void redistribution, or a greater amount of inter-layer mixing, than monotonically-induced (or "static") liquefaction failures, and whether this might lead to systematically lower values of post-liquefaction strength (S_r) for cyclic cases than for monotonic cases.

In examining the database of case histories, there are eight cases that are purely monotonically-induced liquefaction failures, and these are plotted in all figures in this chapter with open symbols, while cyclically-induced failures are plotted with closed (solid) symbols. There are not enough monotonic cases available as to perform a separate regression for these cases, but by inspection it does not appear that there is a strong systematic bias between S_r values for monotonic and cyclic cases. Two of the static cases with higher $N_{1,60,CS}$ values plot towards the upper portion of Figure 5.4(a), potentially giving the impression that monotonically-induced failures might produce higher values of S_r, but closer inspection shows (1) that these cases also have higher values of $\sigma'_{v,o}$ which explain the higher S_r values, and (2) additional monotonically-induced liquefaction cases with lower $N_{1,60,CS}$ values occur lower on the figure, where they mix well with cyclically-induced cases.

Overall, the current field case history database does not appear to support the use of systematically higher values of S_r for monotonically-induced liquefaction failures.

5.5.2 Effects of Cyclic Inertial Forces

The back-analyses performed in these current studies, and in most previous studies, did not directly incorporate the potential effects of cyclic inertial forces on the deformations and displacements observed, and on the values of post-liquefaction strength back-calculated as best explaining these displacements. The question thus arises as to whether the back-calculated values of S_r may be systematically biased conservatively, as the cyclic "driving" shear forces associated with cyclic lurching have not been included.

Table 5.3 lists the case histories back-analyzed in these current studies. In this table, the cases have been sub-divided into four sub-sets based on liquefaction triggering mechanism and on the mechanisms that then produced the observed resulting deformations and displacements.

Group 1 is comprised of ten cases in which liquefaction was monotonically (or "statically") induced, and in which there were no cyclic inertial forces.

Group 2 is comprised of five cases in which liquefaction was "triggered" by cyclic loading, but in which there were again no significant cyclic inertial forces acting to contribute towards the displacements that ensued. The first three of these cases are (1) the Lower San Fernando Dam upstream slope failure, and (2, 3) the two Moshi-Koshi Tailings Dam dike failures. In these three cases, liquefaction was triggered by seismic (earthquake) loading, but there was then a delay before the ensuing large displacement slope failures occurred. These delays have been attributed to time required for pore pressure re-distribution (and for satisfaction of local dilation in the denser starter

dikes of the Lower San Fernando Dam) such that a sufficient amount of liquefied material lost enough strength that the large failures could proceed. Delays of multiple hours were observed by witnesses in the case of the Moshi-Koshi dikes. In the case of the Lower San Fernando dam, the delay was only a matter of several tens of seconds, and it was recorded on an unusual strong motion instrument on the dam's crest which recorded multi-directional seismic movements due to strong shaking on a rounded glass ball, with time marks (tics) for timing during the earthquake, and then, subsequently, produced a largely linear record as the instrument was progressively tipped (tilted) by the subsequent large scale landslide in which it participated. Similar situations occurred with the Lake Ackerman Highway Embankment failure and with the Asele road embankment failure and they were handled similarly. These five cases thus experienced a majority their large displacements in the absence of any significant strong shaking.

Group 3 is comprised of eight case histories which experienced liquefaction, and liquefaction-induced large displacements, during earthquakes. These eight cases all experienced only moderate levels of strong shaking (peak ground accelerations on level ground of less than approximately 0.2 g), and many of them experienced relatively short durations of shaking in small magnitude seismic events. These moderate levels of shaking, and of duration, were sufficient to initiate (or trigger) liquefaction, but would not have contributed significantly to the observed large (gravity-driven) displacements that ensued.

Group 4 is comprised of eight cases in which strong levels of seismic shaking occurred, and often with significant duration. These are thus cases in which cyclic inertial forces may have contributed meaningfully to the observed displacements. Two of these cases; the Shibecha-Cho Embankment Failure and the El Cobre Tailings Dam failure are marked with three asterisks. These two cases experienced catastrophic flow failures with very large displacements; displacements so large that cyclic inertial forces were unlikely to have contributed significantly to the overall (final) displacements.

It is then the remaining six cases of Group 4 in which cyclic inertial forces may have contributed at a potentially significant level to the observed displacements. It was not possible to incorporate cyclic inertial forces in the analyses performed in these current studies, nor in any of the previous studies by others, with good accuracy and reliability. Neglect of cyclic inertial forces may have caused the back-calculated values of S_r to be somewhat conservative (low) for these six cases.

Consideration was given to performing fully nonlinear time-domain finite element or finite difference analyses in order to simultaneously model both gravity-induced driving shear forces and cyclic lurching forces. Challenges here would include: (1) The inherent difficulties and challenges involved in performing fully nonlinear seismic response analyses in at least a two-dimensional context, and with ongoing changes in material strengths and stiffnesses as the events proceed, and (2) numerical issues associated with very large (and strongly localized) displacements. It was judged that this is difficult to accomplish, and that the reliability of these types of calculations is not yet consistently high. It may be hoped that future investigators may pursue this further.

Overall, having back-analyzed all of the case histories, it is the judgment of this investigation team that any potentially conservative bias due to neglect of cyclic inertial forces for this suite of field case histories is likely to have had relatively little or no impact on the relationships developed.

5.5.3 Potential Case History Sampling Bias

A third issue is the question of potential sampling bias with regard to the use of the selected suite of large displacement liquefaction failure case histories. The issue here is not whether the current investigation team, or previous investigators, introduced bias in their selection of case histories to back-analyze or employ in development of relationships. Instead, the issue is whether the cases themselves have "self-selected" themselves in a systematically biased manner by exhibiting large displacements, while other, similar, situations and conditions did not produce observed failures and so did not become available for the database.

There is no good way to fully reliably address this question, nor to accurately quantify the potential bias that might result. And so it must be noted that if this bias exists, then the currently available relationships (including the new relationships developed and presented herein) would be somewhat conservative as a result.

Table 5.1: Values of (1) representative post-liquefaction strength, (2) representative penetration resistance, and (3) initial effective vertical effective stress for each of the 29 back-analyzed liquefaction case histories as employed in the deterministic least squares regressions.

Class	Case	This Study		
		$\bar{S}_r$ (psf)	$\bar{\sigma}'_{vo}$ (psf)	$\bar{N}_{1,60,CS}$
A	Wachusett Dam - North Dike	294	3142	7.5
	Fort Peck Dam	762	7258	12.5
	Uetsu Railway Embankment	38	1448	3
	Lower San Fernando Dam - U/S Slope	539	3174	13.5
	Hachiro-Gata Road Embankment	68	673	7
	La Marquesa Dam - U/S Slope	103	981	6.5
	La Marquesa Dam - D/S Slope	214	1215	10.5
	La Palma Dam	136	767	5
	Lake Ackerman Highway Embankment	107	909	3.5
	Chonan Middle School	141	1032	6.5
	Soviet Tajik - May 1 Slide	341	1907	10.5
	Shibecha-Cho Embankement	224	1416	7.5
	Route 272 at Higashiarekinai	138	1285	8
B	Zeeland - Vlietepolder	156	2488	8
	Sheffield Dam	138	1308	7
	Helsinki Harbor	48	846	6
	Solfatara Canal Dike	64	669	4.5
	Lake Merced Bank	136	834	8.5
	El Cobre Tailings Dam	95	2075	2
	Metoki Road Embankment	92	871	2.5
	Hokkaido Tailings Dam	131	1203	4
	Upper San Fernando Dam - D/S Slope	726	3138	15
	Tar Island Dyke	516	4197	11
	Mochi-Koshi Tailings Dam, Dikes 1 and 2	211	1532	6
	Nerlerk Embankment, Slides 1, 2, and 3	68	1171	7.5
	Asele Road Embankment	137	1037	9.5
	Nalband Railway Embankment	167	1209	7.5
	Sullivan Tailings	277	2422	9.5
	Jamuna Bridge	175	1404	10.5

Table 5.2: Values of (1) median post-liquefaction strength, (2) median penetration resistance, and (3) median effective vertical effective stress for each of the 29 back-analyzed liquefaction case histories, and standard deviations for each of these, as employed in the fully probabilistic regressions.

Class	Case	This Study					
		$\bar{S}_r$ (psf)	$\sigma_{\bar{S}}$	$\bar{\sigma}'_{vo}$ (psf)	$\sigma_{\bar{\sigma}}$	$\bar{N}_{1,60,CS}$	$\sigma_{\bar{N}}$
A	Wachusett Dam - North Dike	294	31	3142	132	7.5	1.6
	Fort Peck Dam	762	118	7258	687	12.5	2.7
	Uetsu Railway Embankment	38	8	1448	116	3	0.8
	Lower San Fernando Dam - U/S Slope	539	47	3174	281	13.5	1.8
	Hachiro-Gata Road Embankment	68	12	673	41	7	1.2
	La Marquesa Dam - U/S Slope	103	33	981	134	6.5	1.8
	La Marquesa Dam - D/S Slope	214	57	1215	103	10.5	2.2
	La Palma Dam	136	23	767	42	5	1.2
	Lake Ackerman Highway Embankment	107	19	909	61	3.5	0.7
	Chonan Middle School	141	35	1032	82	6.5	2.1
	Soviet Tajik - May 1 Slide	341	57	1907	177	10.5	2.7
	Shibecha-Cho Embankement	224	37	1416	95	7.5	1.7
	Route 272 at Higashiarekinai	138	17	1285	104	8	1.6
B	Zeeland - Vlietepolder	156	37	2488	431	8	2.1
	Sheffield Dam	138	23	1308	71	7	2.3
	Helsinki Harbor	48	14	846	105	6	2.0
	Solfatara Canal Dike	64	22	669	59	4.5	1.5
	Lake Merced Bank	136	21	834	102	8.5	2.2
	El Cobre Tailings Dam	95	31	2075	183	2	1.0
	Metoki Road Embankment	92	20	871	85	2.5	0.9
	Hokkaido Tailings Dam	131	45	1203	191	4	1.1
	Upper San Fernando Dam - D/S Slope	726	138	3138	278	15	1.8
	Tar Island Dyke	516	119	4197	484	11	2.3
	Mochi-Koshi Tailings Dam, Dikes 1 and 2	211	38	1532	165	6	1.7
	Nerlerk Embankment, Slides 1, 2, and 3	68	19	1171	129	7.5	1.8
	Asele Road Embankment	137	27	1037	77	9.5	2.0
	Nalband Railway Embankment	167	15	1209	94	7.5	2.5
	Sullivan Tailings	277	24	2422	142	9.5	2.4
	Jamuna Bridge	175	22	1404	210	10.5	2.5

Table 5.3: Classification of Failure Case Histories with Regard to Potential Effects of

Cyclic Inertial Forces on Observed Displacements

Group 1: Static/Monotonic Failures:

- Wachusett Dam U/S Slope Failure
- Fort Peck Dam U/S Slope Failure
- Zeeland-Vietepolder Offshore Slope Failure
- Sheffield Dam Slope Failure
- Helsinki Harbor Slope Failure
- Tar Island Dike Slope Failure
- Nerlerk Embankment Slides No's. 1, 2 and 3
- Sullivan Tailings Impoundment Slope Failure
- Jamuna Bridge
- Calaveras Dam Slope Failure

Group 2: Cyclically-Induced Liquefaction, but "Static" Failures:

- Lower San Fernando Dam U/S Slope Failure*
- Moshi-Koshi Tailings Dam, Dikes 1 and 2*
- Lake Ackerman Highway Embankment Failure**
- Asele Road Embankment**

Group 3: Cyclically-Induced Liquefaction, and Low to Moderate Cyclic Inertial Forces:

- Uetsu Railway Embankment
- Hachiro Gata Roadway Embankment
- Chonan Middle School
- Soviet Tajik, May 1 Slide
- Solfatera Canal Dike
- Lake Merced Bank
- Metoki Roadway Embankment
- Hokaido Tailings Dam

Group 4: Cyclically-Induced Liquefaction and Strong and Sustained Cyclic Inertial Forces:

- La Marquesa Dam Upstream Slope Failure
- La Marquesa Dam Downstream Slope Failure
- La Palma Dam Upstream Slope Failure
- Shibecha-Cho Embankment Failure***
- Route 272 Embankment Failure
- El Cobre Tailings Dam Failure***
- Nalband Railway Embankment Failure
- Upper San Fernando Dam Downstream Slope Displacement****

*Seismically-induced soil liquefaction triggering, but subsequent slope failure after strong shaking had ceased.
**Liquefaction triggered by vibratory vehicles, no strong cyclic inertial forces.
***Very large runout displacements, significantly exceeding cyclic inertial deformations.
****Cyclic inertial forces were considered in these current studies.

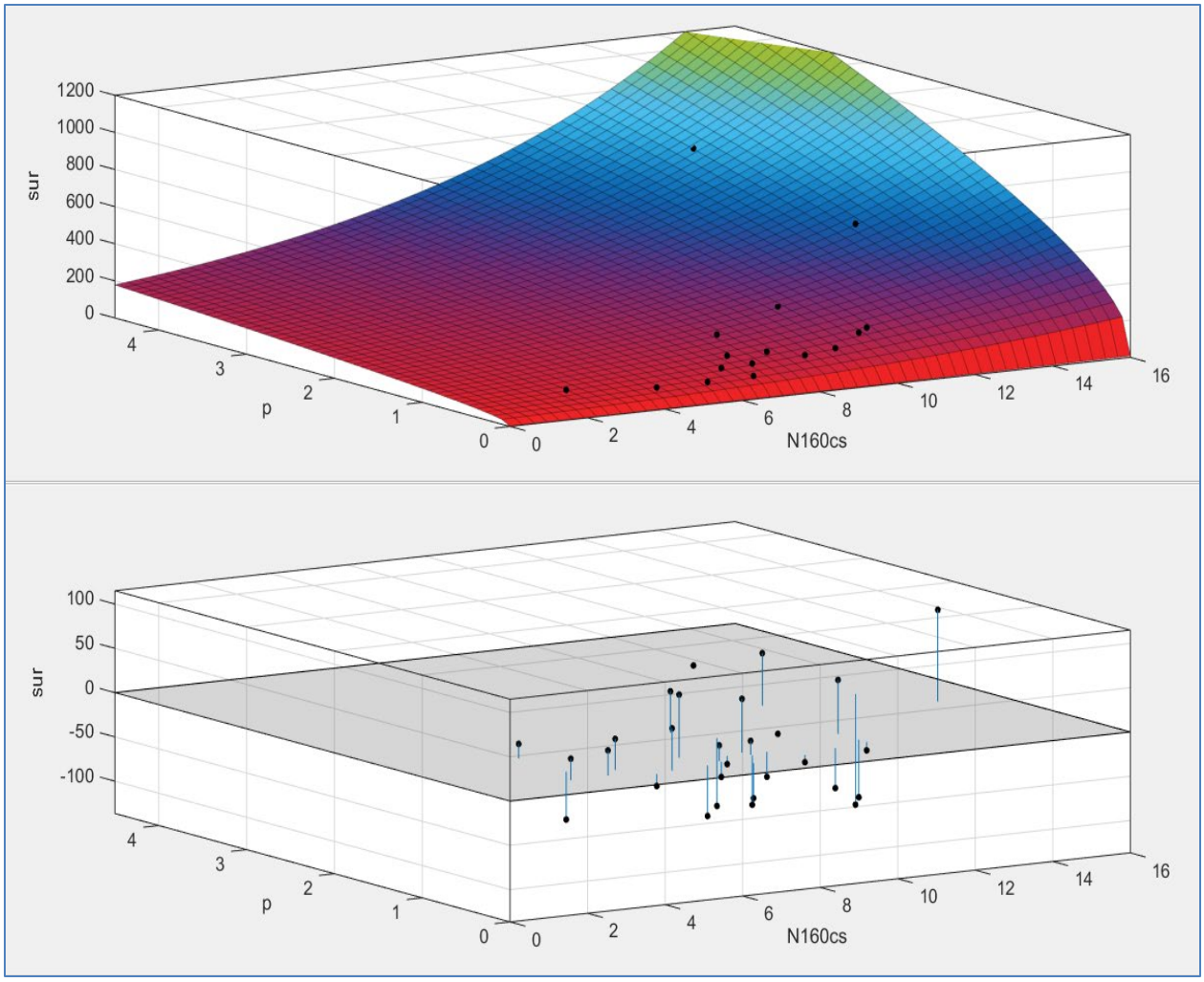

Figure 5.1: Results of deterministic least squares regression showing (a) the relationship for post-liquefaction strength ($\overline{S_r}$) as a function of both $\overline{N_{1,60,CS}}$ and $\overline{\sigma'_{vo}}$, and (b) residuals from the deterministic least squares regression in terms of predicted vs. observed $\overline{S_r}$ for each of the 29 liquefaction field case histories. [Note 1-Residuals in the lower figure are vertically exaggerated by a factor of 5 for clarity. Note 2-$\overline{S_r}$ is denoted by "sur" and $\overline{\sigma'_{vo}}$ is denoted as "p" in the figure above.]

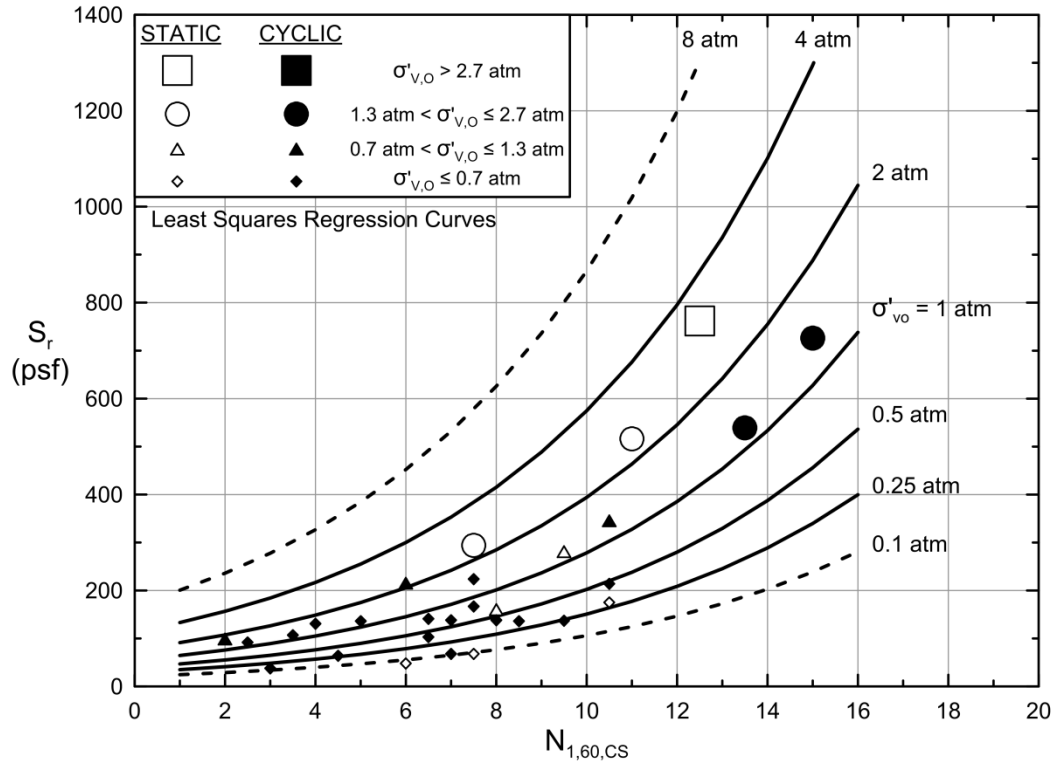

Figure 5.2(a): Results of deterministic regression showing post-liquefaction strength (S_r) as a function of both penetration resistance and initial effective vertical stress.

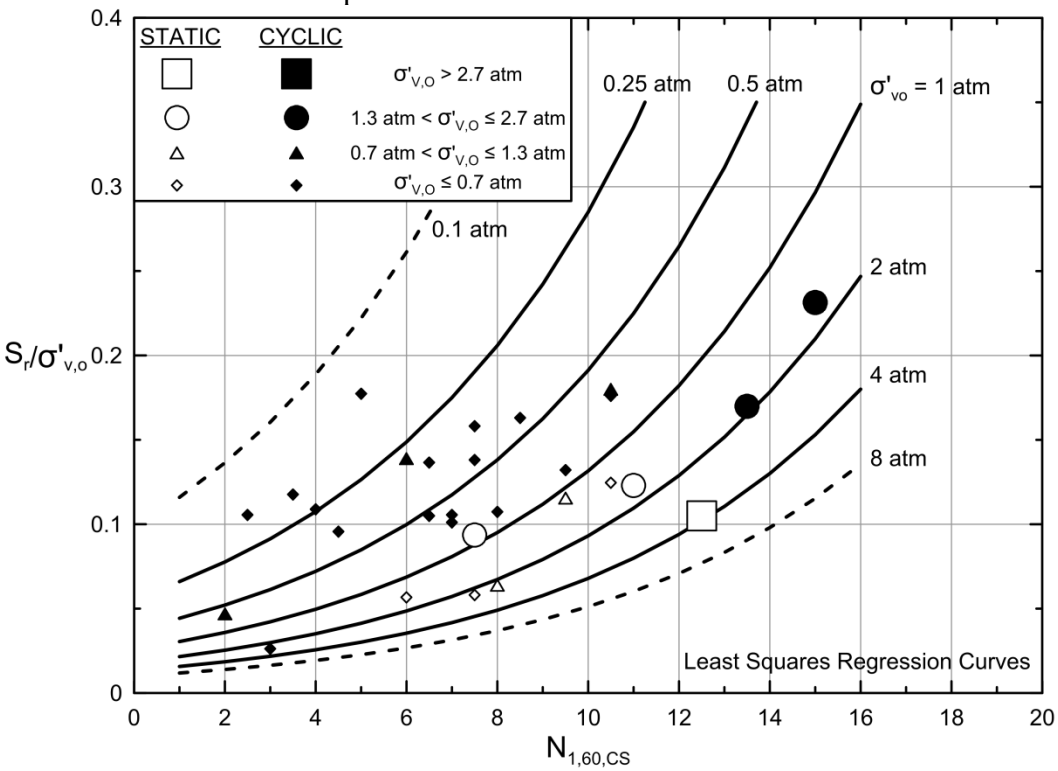

Figure 5.2(b): Results of deterministic regression showing post-liquefaction strength ratio (S_r/P) as a function of both penetration resistance and initial effective vertical stress.

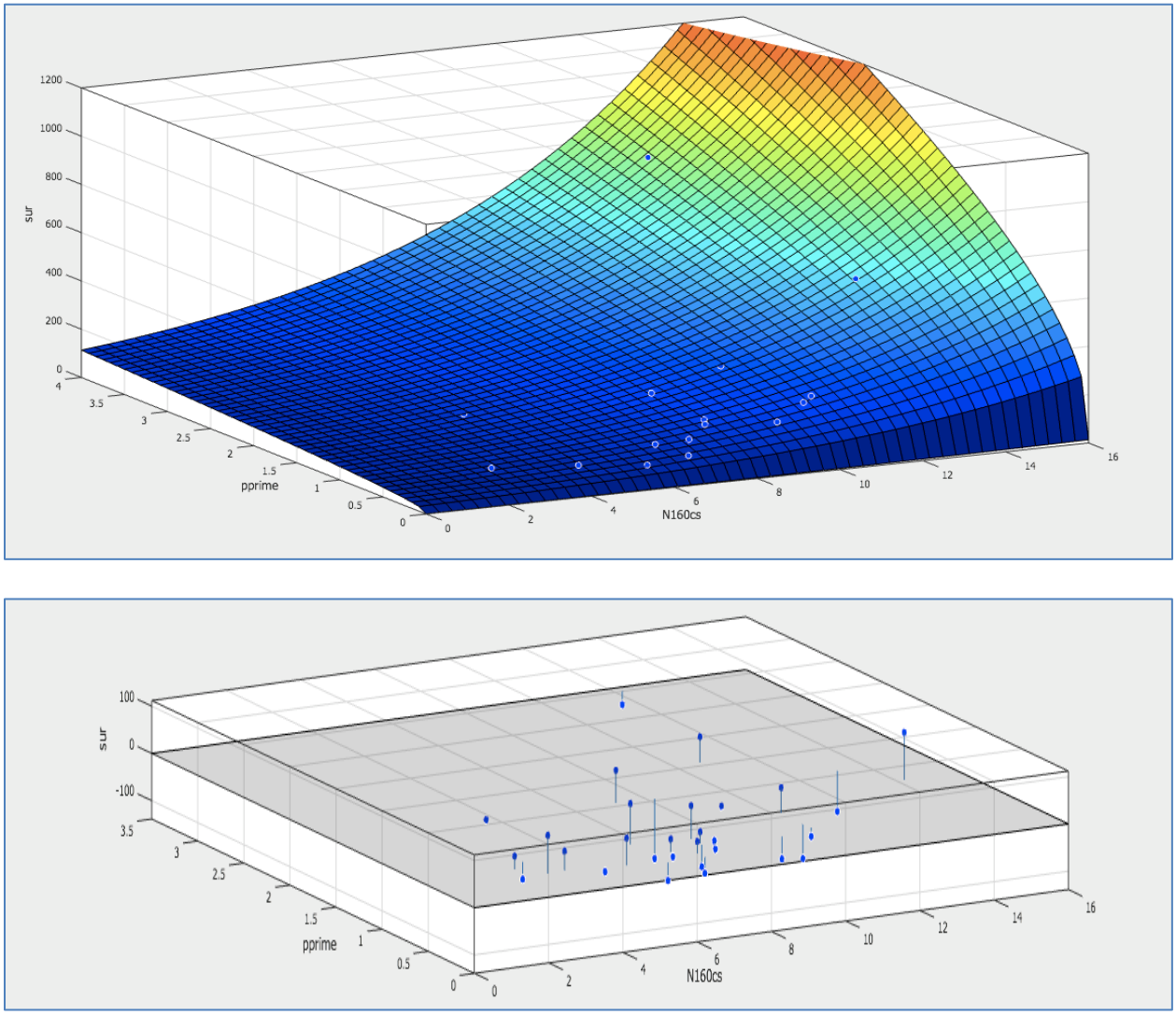

Figure 5.3: Results of probabilistic regression showing (a) the relationship for post-liquefaction strength ($\overline{S_r}$) as a function of both $\overline{N_{1,60,CS}}$ and $\overline{\sigma'_{vo}}$, and (b) residuals from the deterministic least squares regression in terms of predicted vs. observed $\overline{S_r}$ for each of the 29 liquefaction field case histories. [Note: Residuals in the lower figure are vertically exaggerated by a factor of 2 for clarity.]

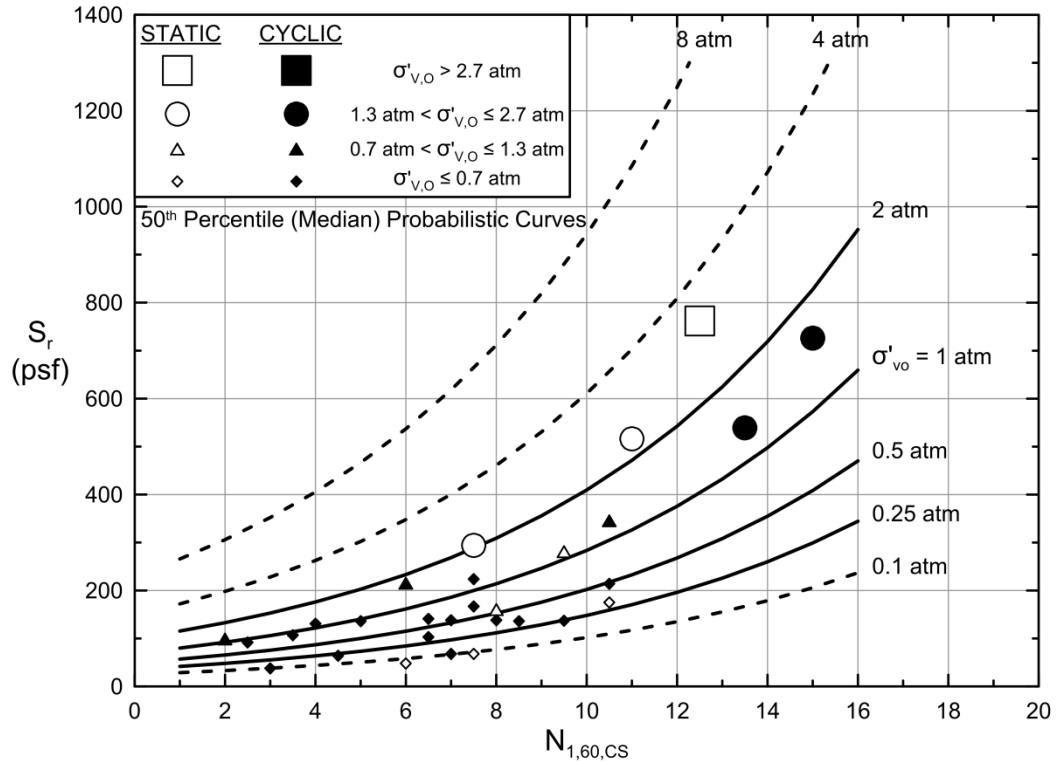

Figure 5.4(a): Results of probabilistic regression showing median values of S_r as a function of both penetration resistance and initial effective vertical stress.

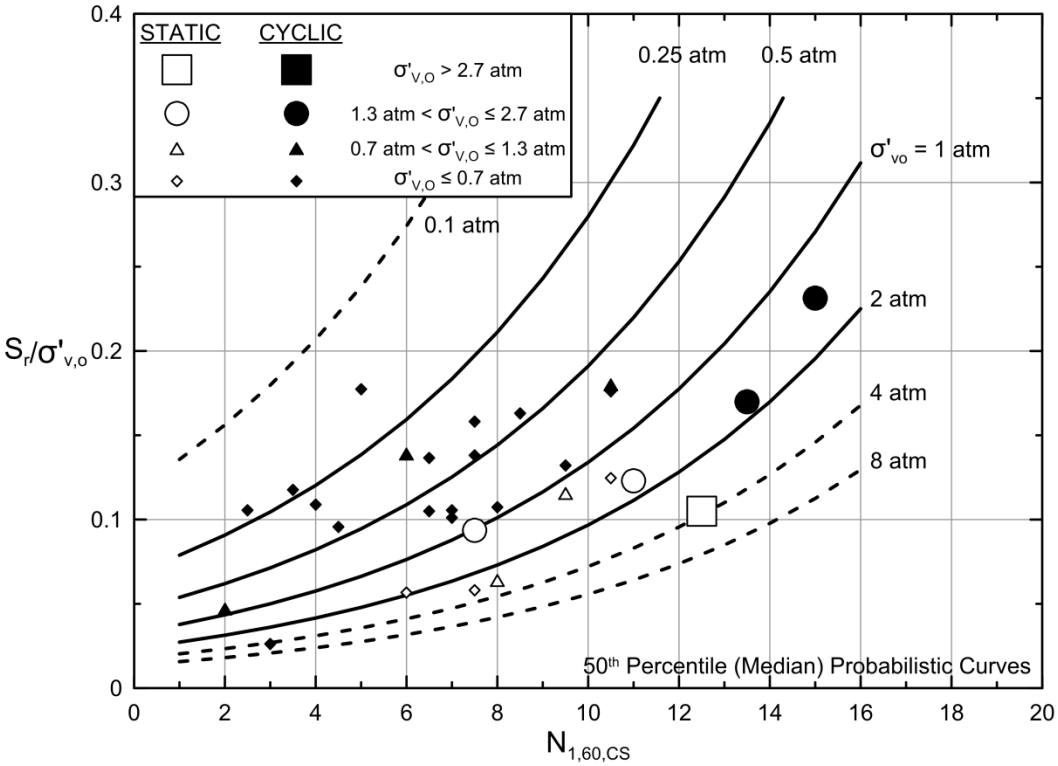

Figure 5.4(b): Results of probabilistic regression showing median values of S_r/P as a function of both penetration resistance and initial effective vertical stress.

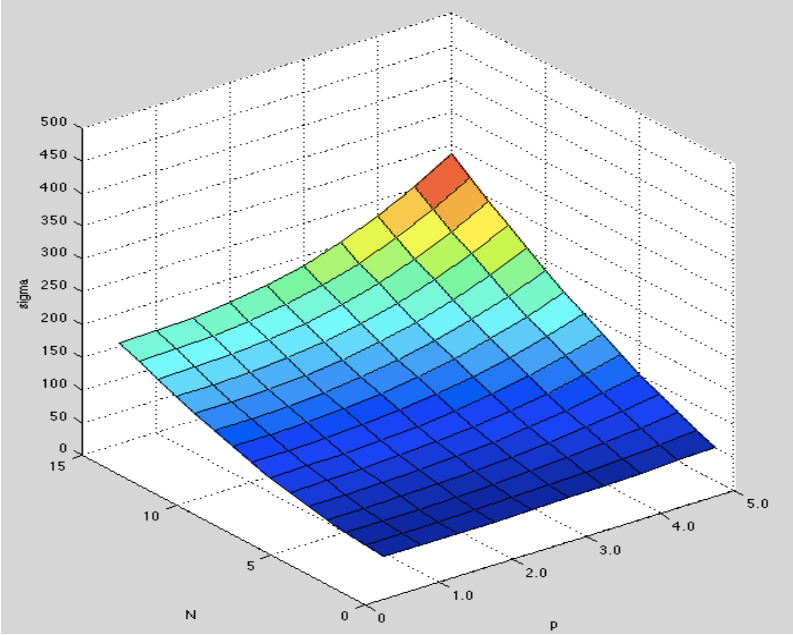

Figure 5.5: Three-dimensional surface showing values of standard deviation in S_r as a function of (1) $N_{1,60,CS}$ and (2) initial effective vertical effective stress based on the probabilistic method regression analyses.

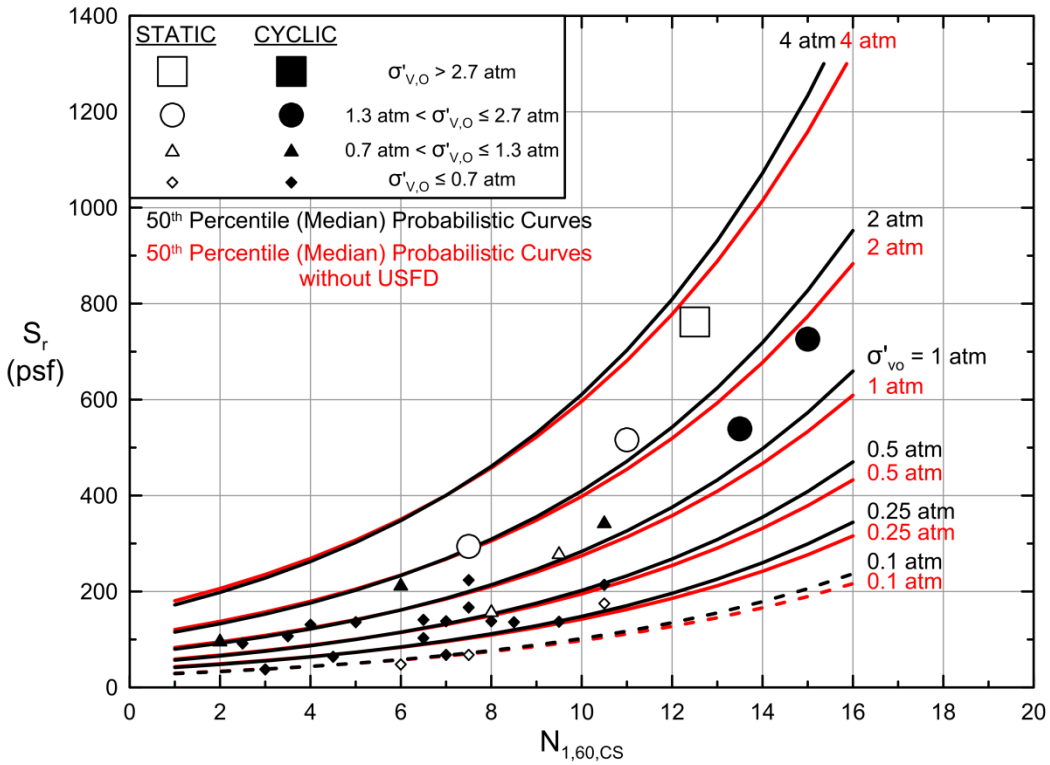

Figure 5.6: Figure 5.4(a) repeated (black lines) also showing the results of a probabilistic regression performed with the data point from the Upper San Fernando Dam case history deleted (red lines).

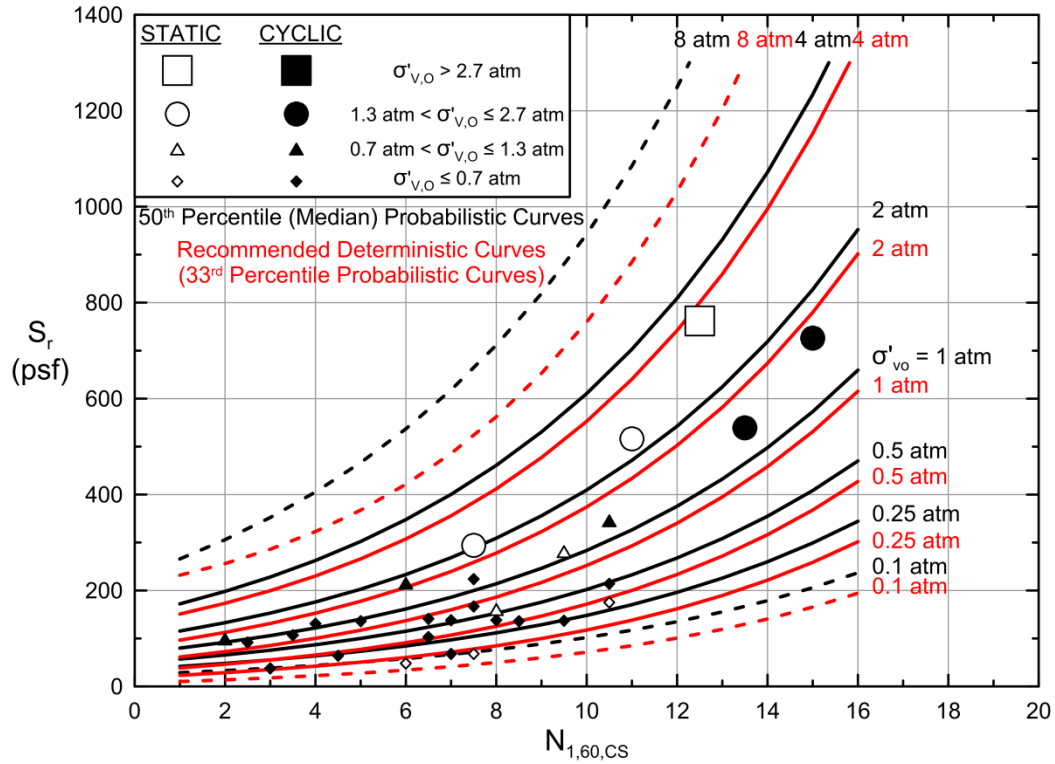

Figure 5.7(a): Comparison between 33rd percentile values of S_r (red lines) and 50th percentile values of S_r (black lines) from the probabilistic relationship of Equation 5-6.

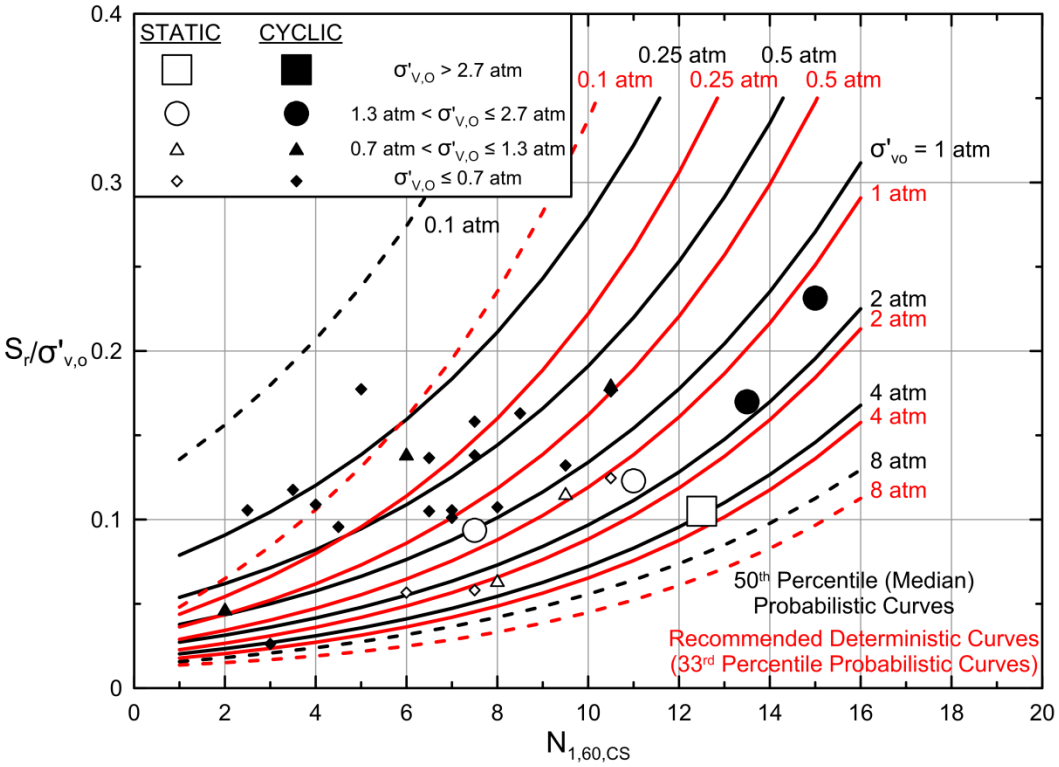

Figure 5.7(b): Comparison between 33rd percentile values of S_r/P (red lines) and 50th percentile values of S_r/P (black lines) from the probabilistic relationship of Equation 5-6.

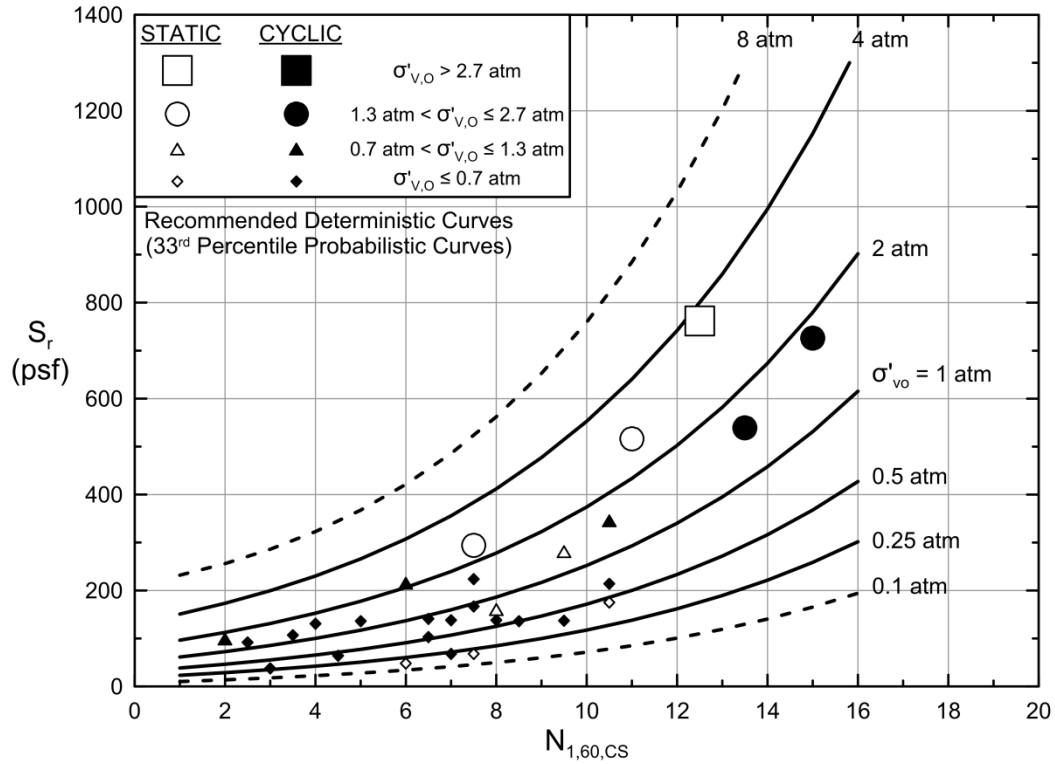

Figure 5.8(a): Recommended deterministic relationship (Equation 5-9); also the 33rd percentile values of S_r/P from the probabilistic relationship of Equation 5-6.

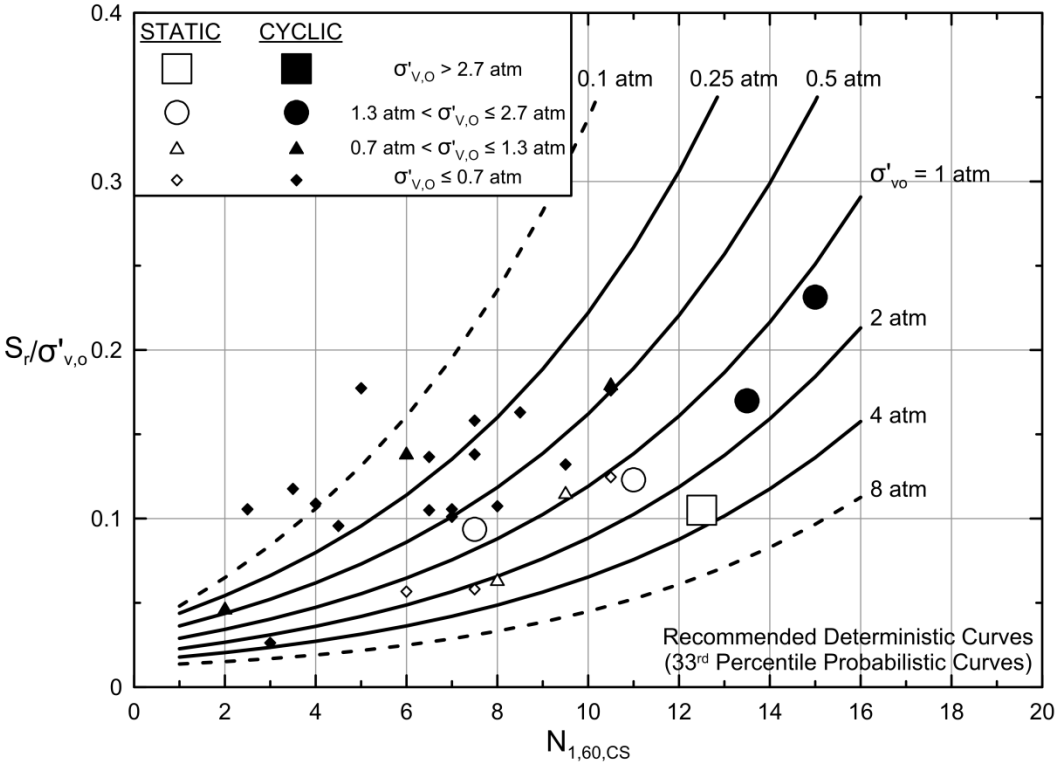

Figure 5.8(b): Recommended deterministic relationship (Equation 5-9); also the 33rd percentile values of S_r/P from the probabilistic relationship of Equation 5-6.

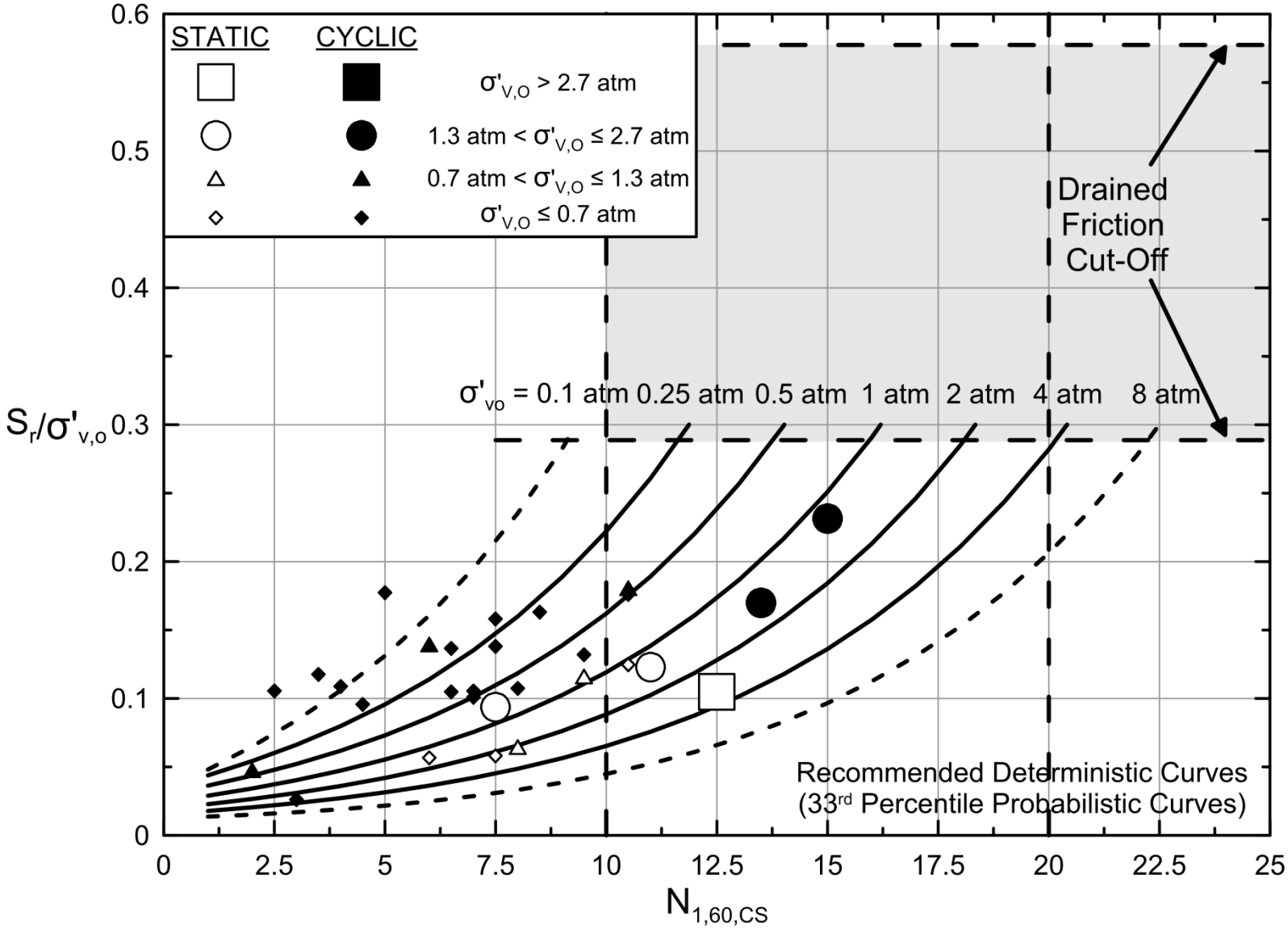

Figure 5.9: Extended view of 33rd percentile values of S_r/P from the probabilistic relationship of Equation 5-6, showing the approximate range of "fully drained cut-off" (shaded region).

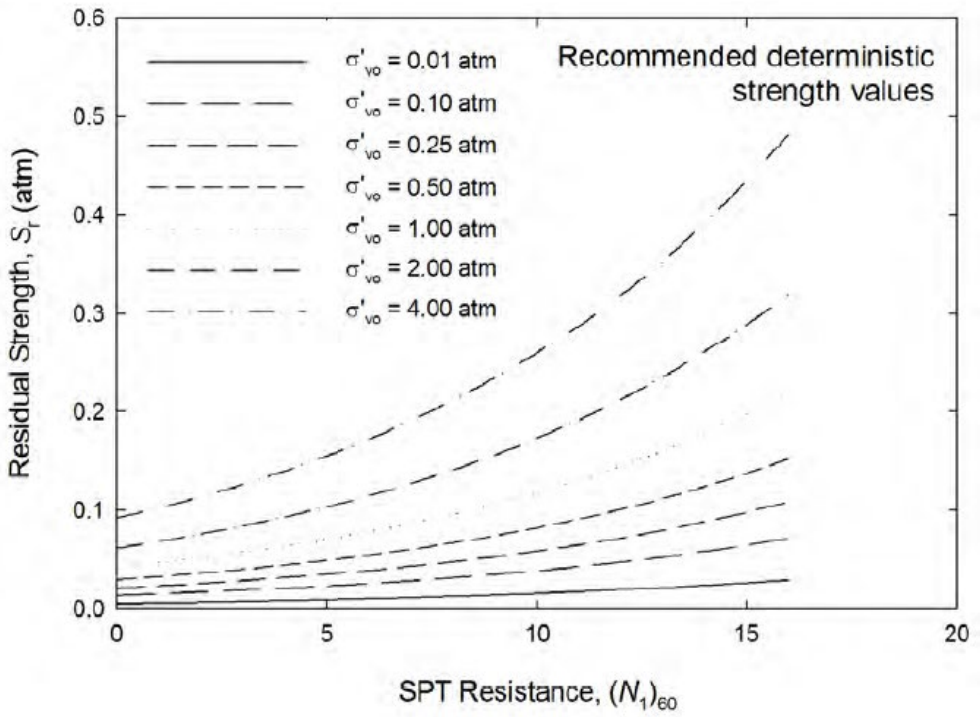

Figure 5.10: Recommended deterministic relationship of Kramer (2008) showing 40th percentile values of S_r as a function of (a) $N_{1,60,CS}$ and (b) initial effective vertical stress.

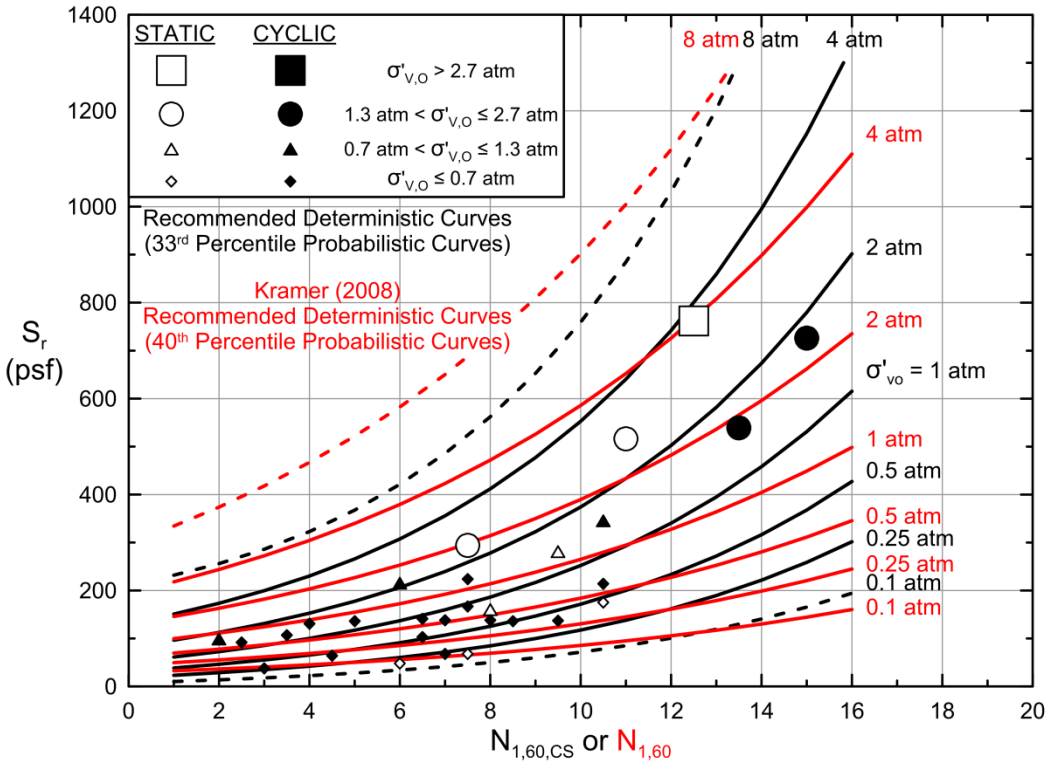

Figure 5.11: Comparison between the recommended deterministic relationship of these current studies from Figure 5.8(a) [33rd percentile; black lines] and the recommended deterministic relationship [40th percentile; red lines] of Kramer (2008).

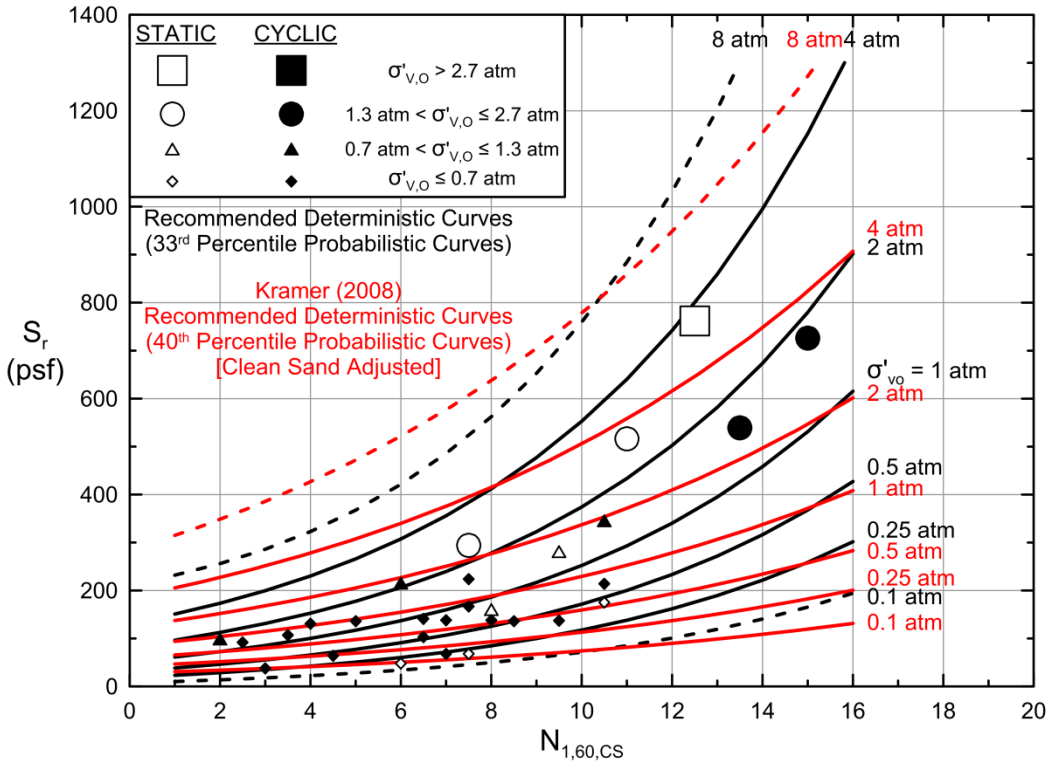

Figure 5.12: Comparison between the recommended deterministic relationship of these current studies from Figure 5.8(a) [33rd percentile; black lines] and the recommended deterministic relationship of Kramer (2008) [40th percentile; red lines, with approximate fines correction to clean sand basis].

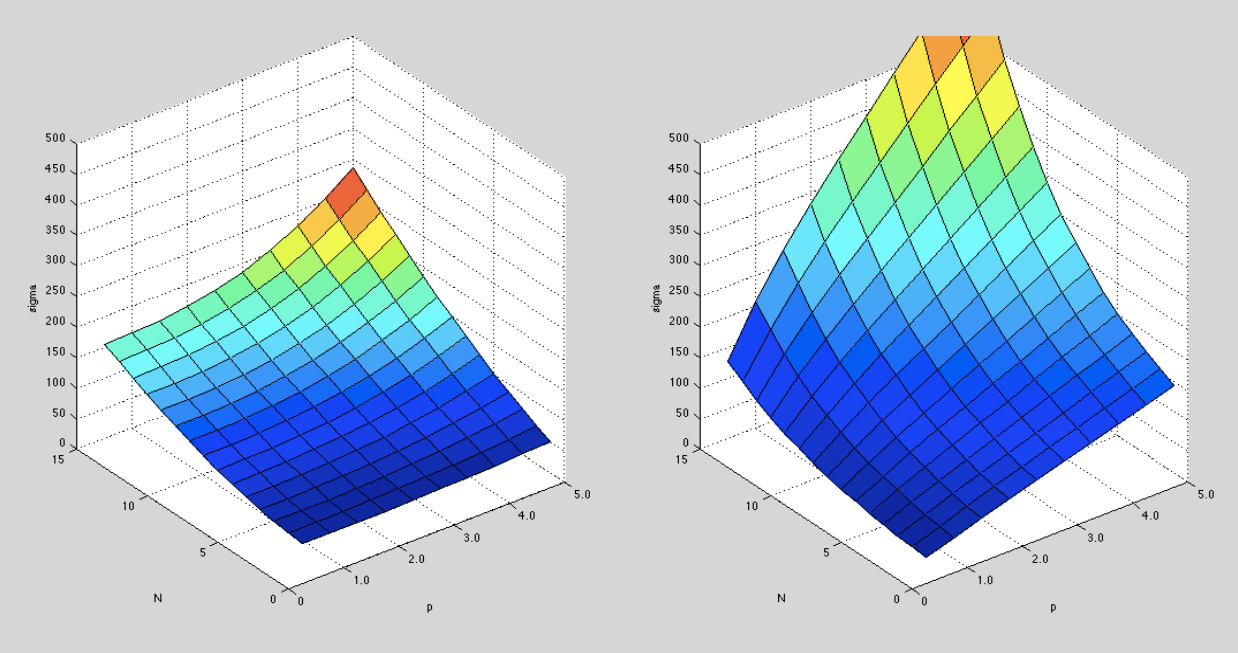

Figure 5.13: Surfaces showing standard deviation of S_r as a function of $N_{1,60,CS}$ and initial effective vertical stress from the probabilistic relationships developed (a) in these current studies, and (b) by Kramer (2008).

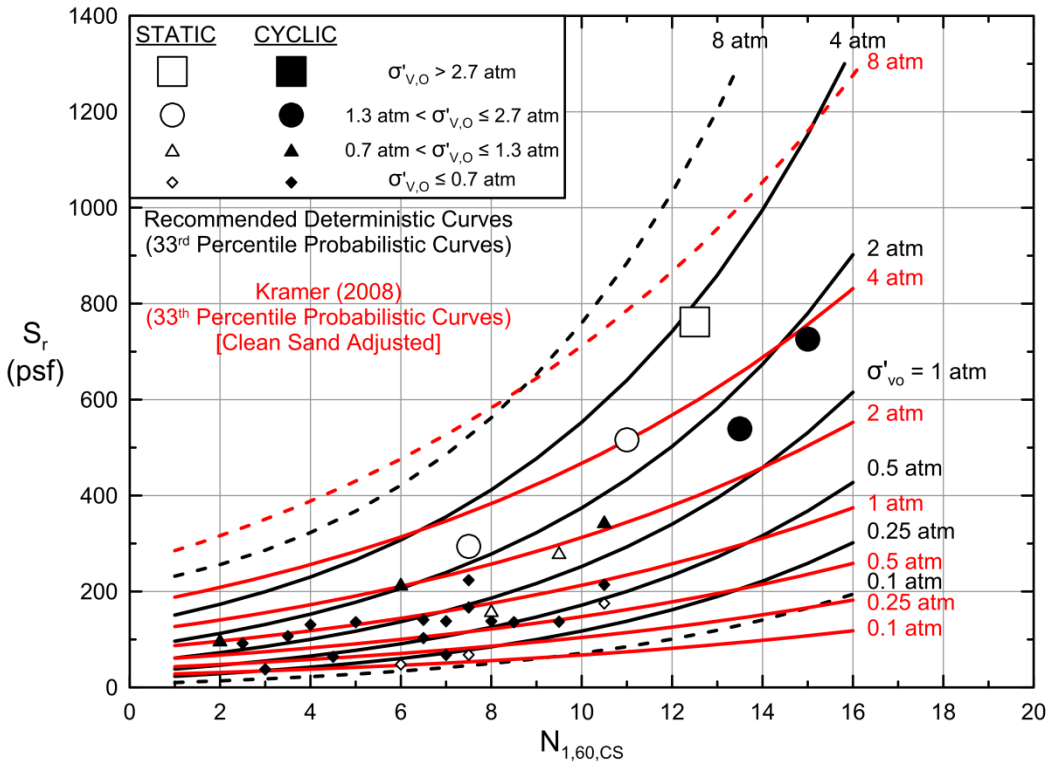

Figure 5.14: Comparison between 33rd percentile values of S_r from these current studies [black lines] and 33rd percentile values from Kramer (2008) [red lines, with approximate fines correction to clean sand basis].

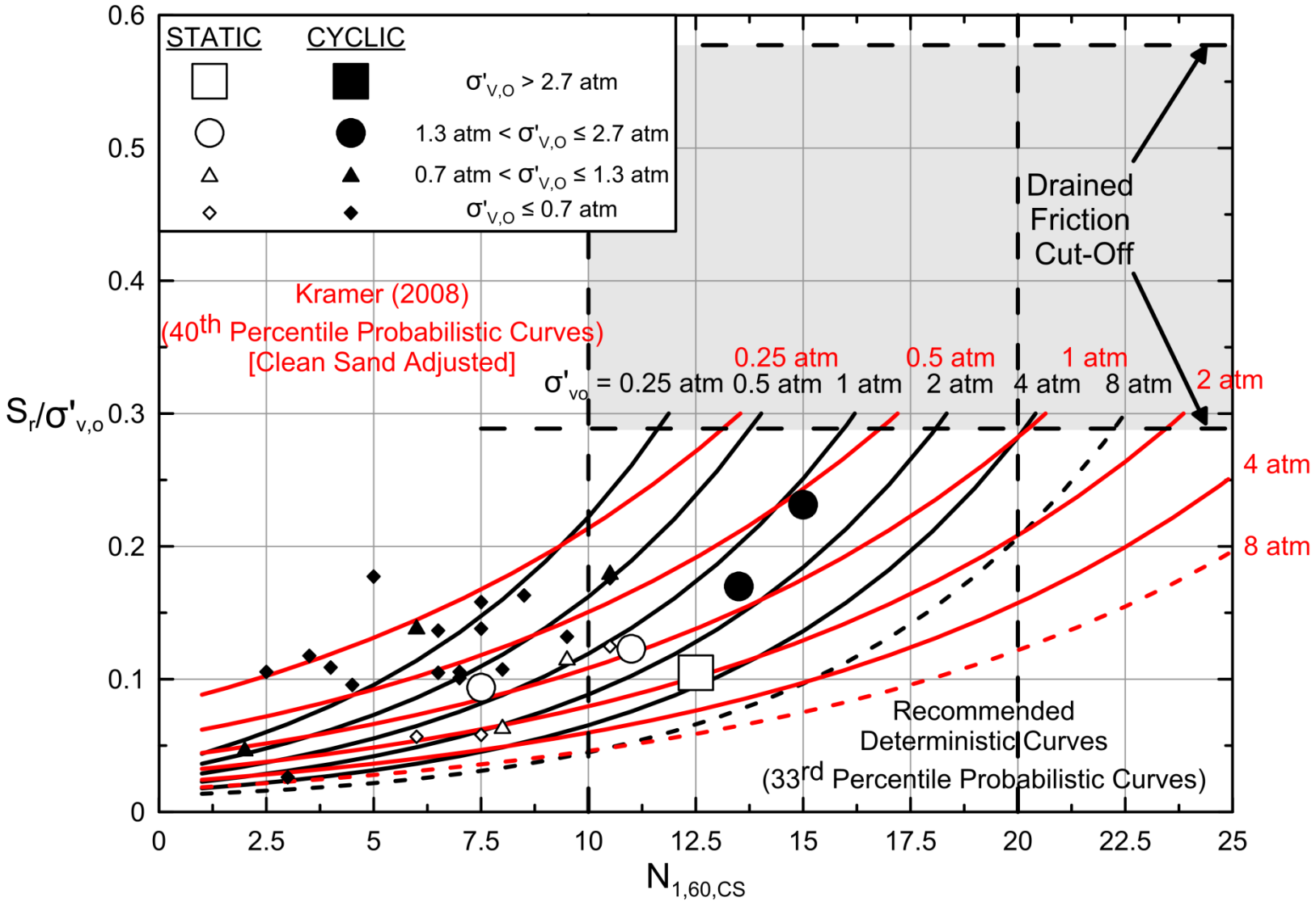

Figure 5.15: Comparison between the recommended deterministic relationships developed in these current studies [33rd percentile; black lines] and the recommended deterministic relationship of Kramer (2008) [40th percentile; red lines], extended to higher $N_{1,60,CS}$ values.

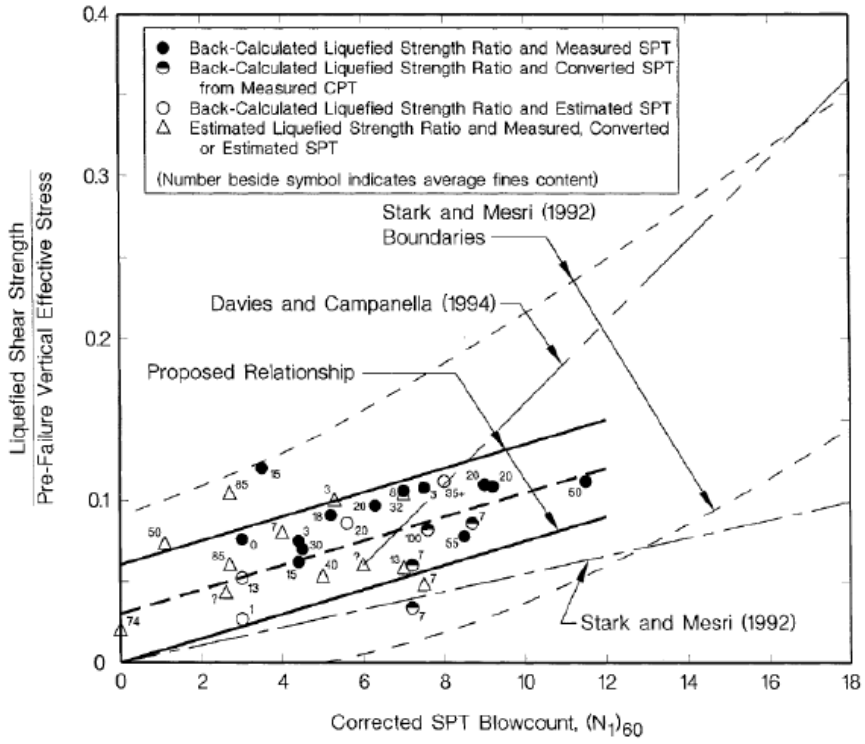

Figure 5.16: Recommended relationship between post-liquefaction strength ratio (S_r/P) and penetration resistance of Olson and Stark (2002).

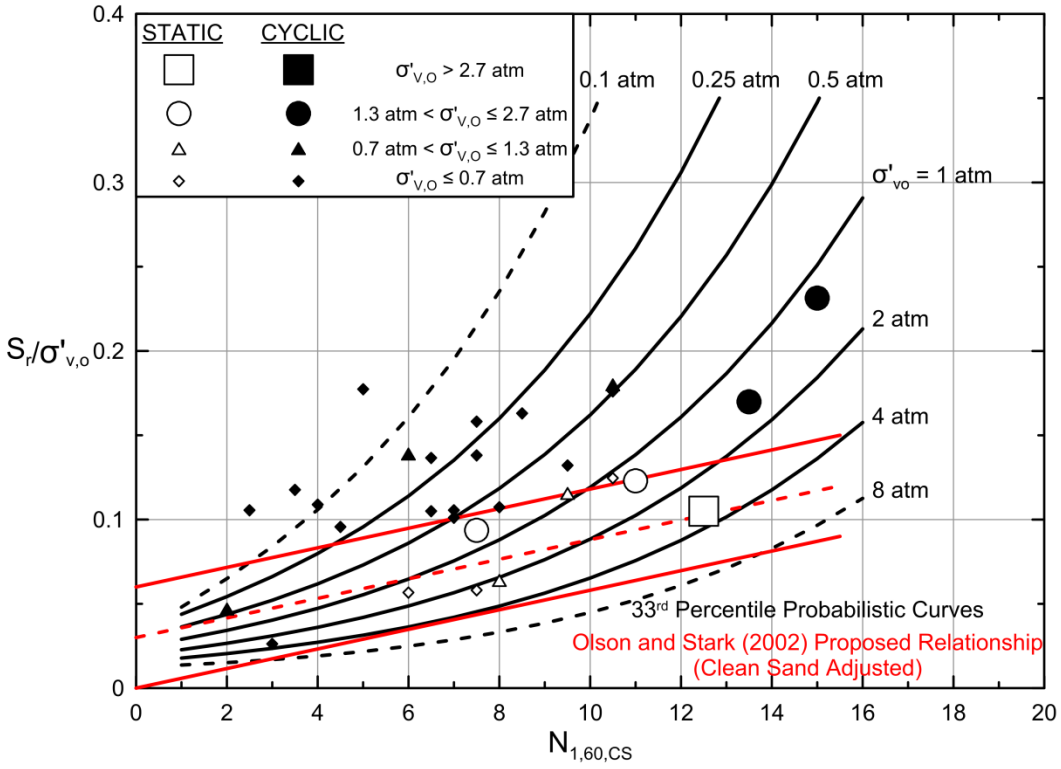

Figure 5.17: Comparison between the relationship of Olson and Stark (2002), and the recommended deterministic (33rd percentile) values of S_r based on these current studies.

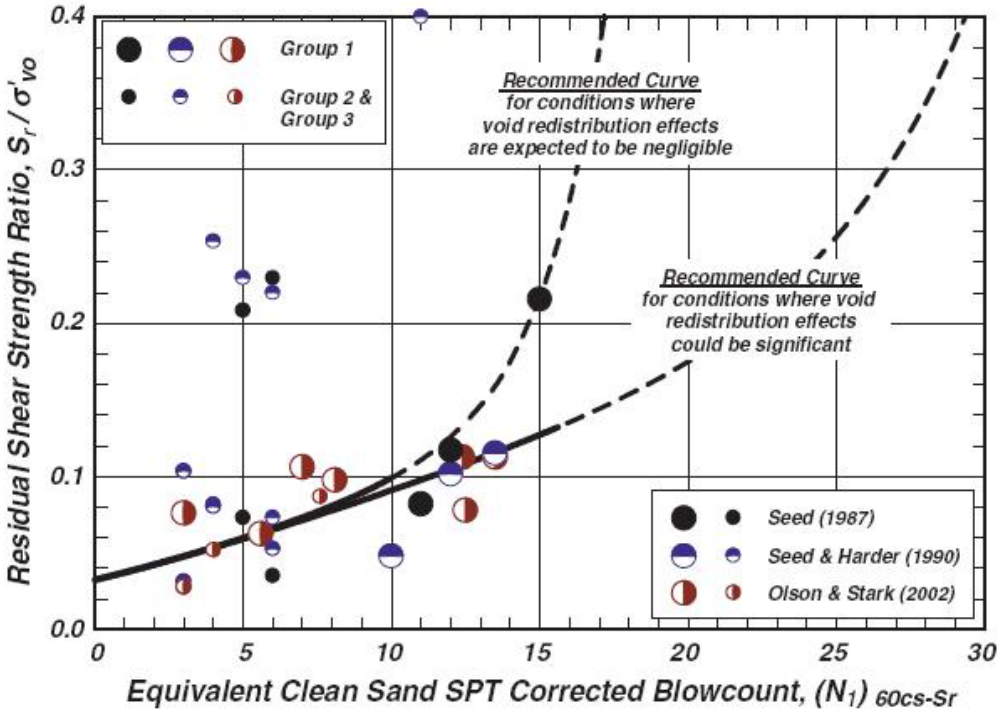

Figure 5.18: Recommended relationships between S_r/P and penetration resistance by Idriss and Boulanger (2008)

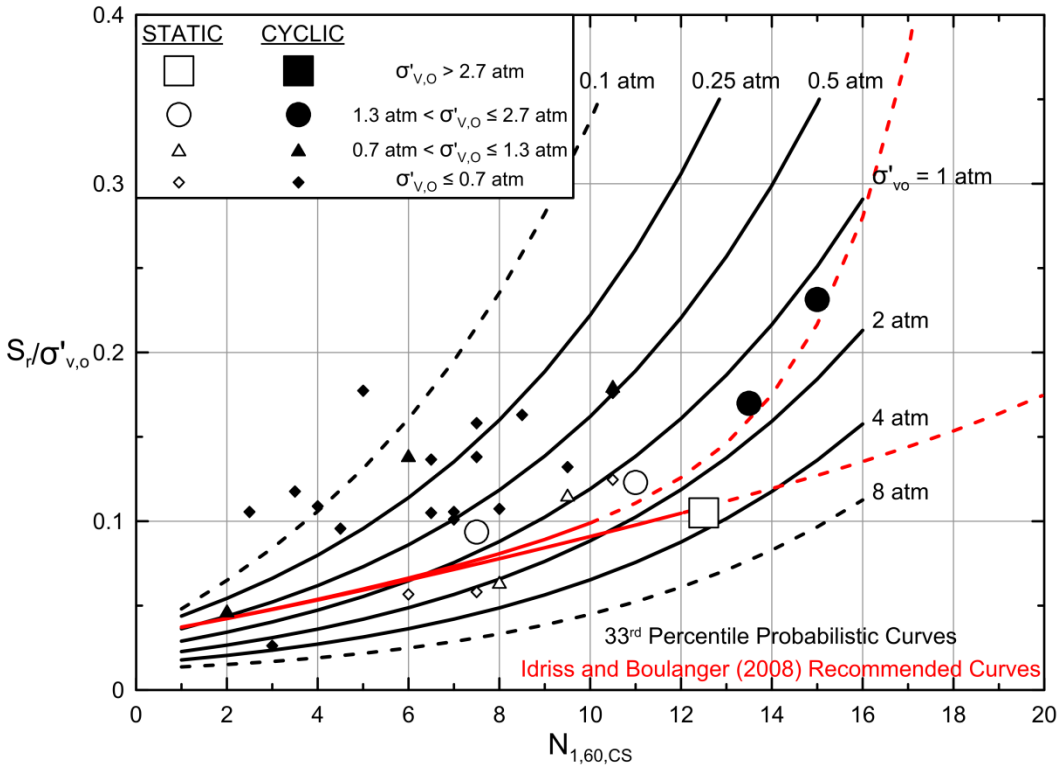

Figure 5.19: Comparison between the recommended relationships of Idriss and Boulanger (2008) from Figure 5.13 (red lines) with the recommended 33rd percentile relationship recommended in these current studies (black lines).

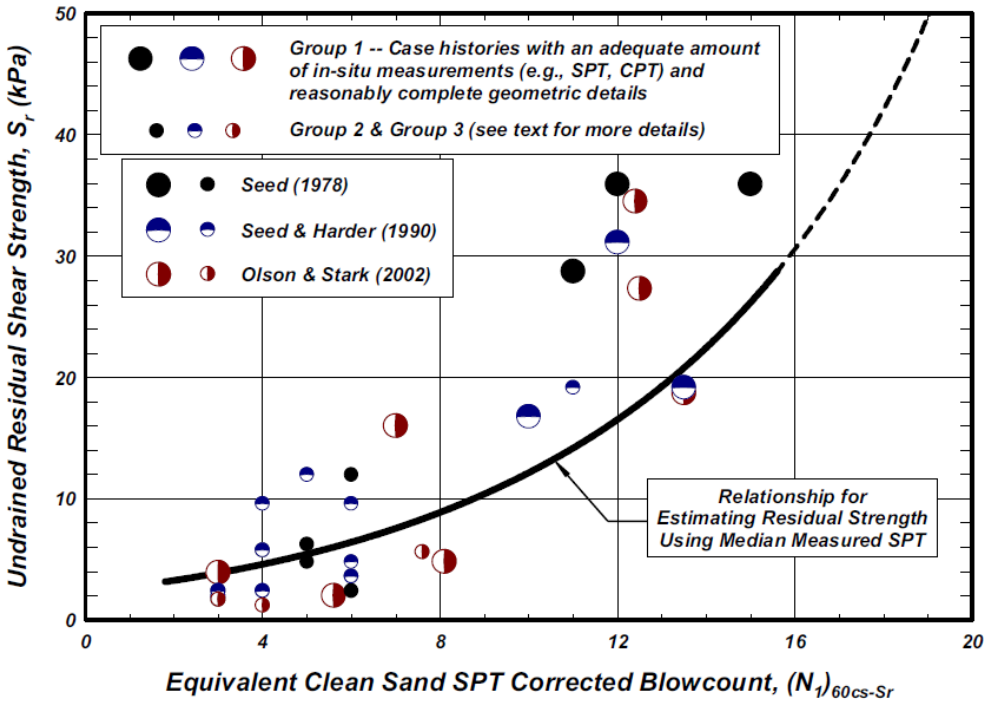

Figure 5.20: Recommended relationships between S_r and penetration resistance by Idriss and Boulanger (2008)

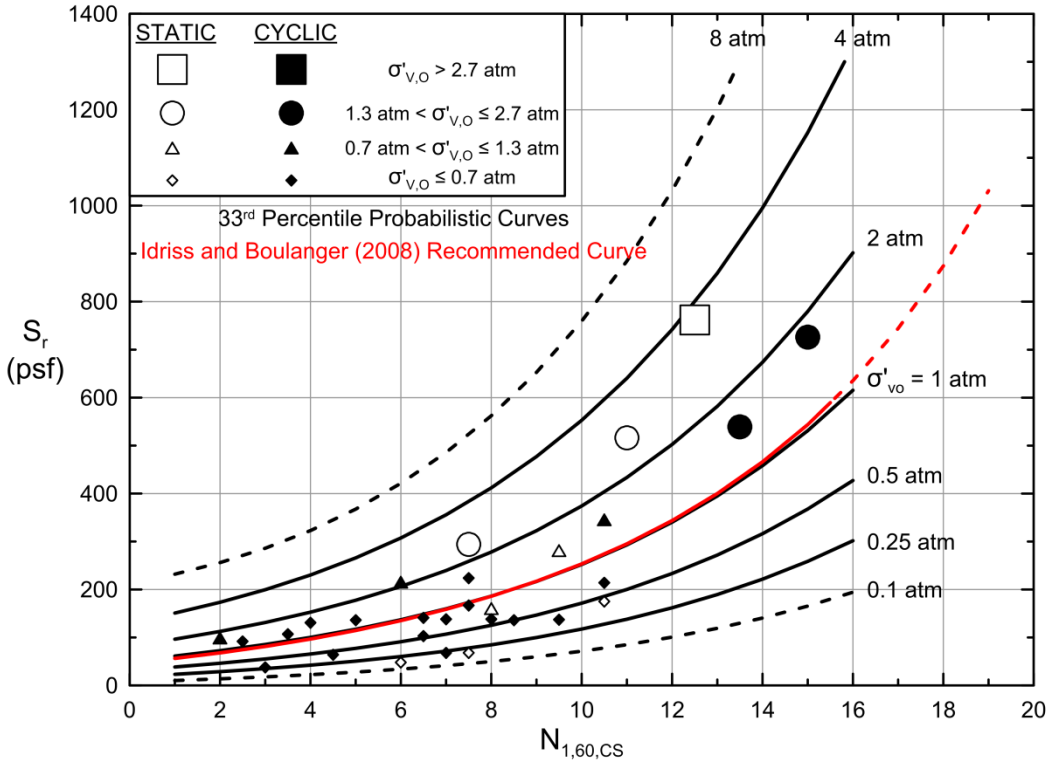

Figure 5.21: Comparison between the recommended relationship of Idriss and Boulanger (2008) from Figure 5.20 (red lines) with the recommended 33rd percentile relationship recommended in these current studies (black lines).

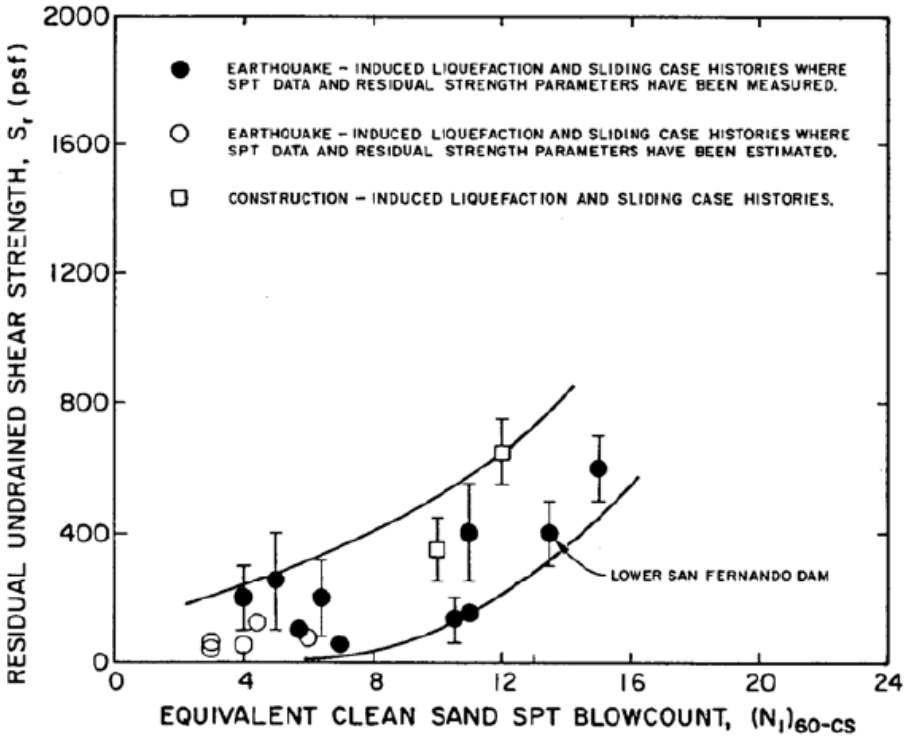

Figure 5.22: Recommended relationship between S_r and penetration resistance of Seed and Harder (1990).

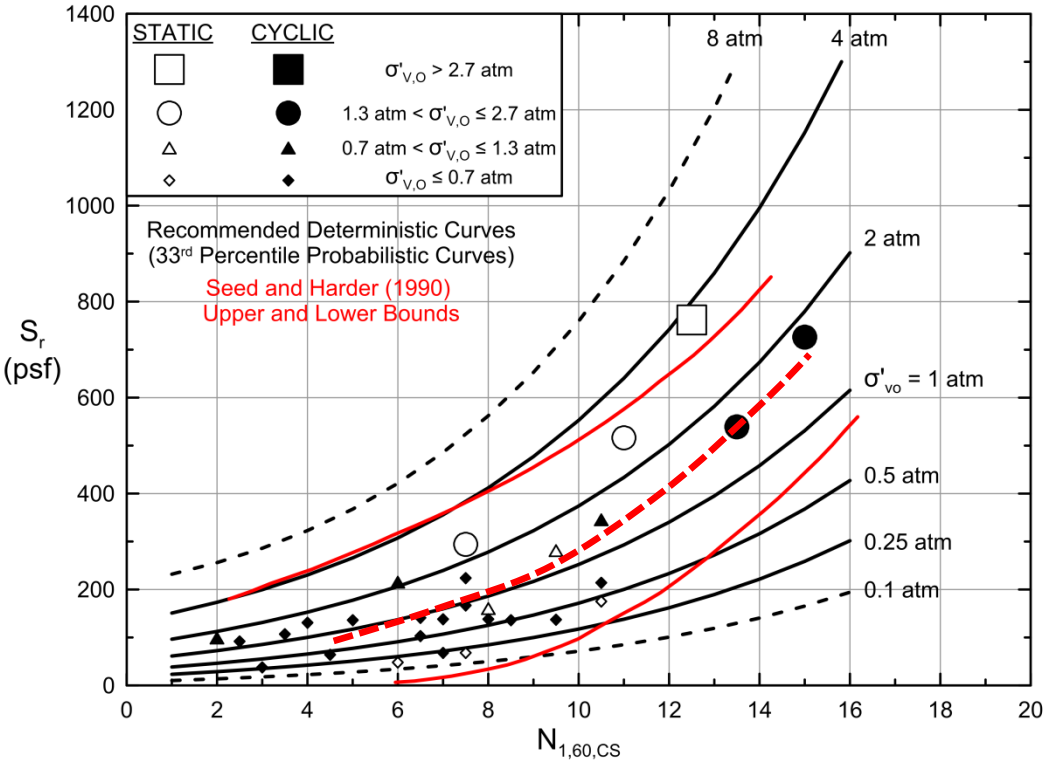

Figure 5.23: Comparison between the recommended relationship of Seed and Harder (1990) from Figure 5.17 (red lines) with the recommended 33rd percentile relationship recommended in these current studies (black lines).

Chapter Six

Summary and Conclusions

6.1 Summary and Findings

The issue of engineering evaluation of in situ post-liquefaction strengths has grown rapidly in importance over the past three decades, as engineers have increasingly been called upon to provide more refined evaluations of projected seismic performance for (1) risk evaluation studies of existing projects and facilities, (2) for analyses and design to mitigate existing risk, and (3) for seismic analysis and design of new projects and facilities.

The topic of assessment of post-liquefaction strengths has sometimes been fraught with disagreement, and a number of different recommendations have been developed by different teams of experts and researchers over the past three decades.

These current studies began with a technical review of previous efforts. That proved to be a valuable exercise. Evaluation of previous work, and recommendations, with emphasis on strengths and drawbacks of prior efforts, led to some important insights. It turns out that a number of previous efforts had developed important lessons, and in some cases important pieces of the overall puzzle. They also served to provide ideas and to inspire some of the new elements of these current studies. And they provided lessons with regard to mistakes to avoid.

These current studies have focused on the development of empirical methods for evaluation of in situ post-liquefaction strengths, largely because of issues and challenges involved in application of laboratory-based testing approaches to evaluation of post-liquefaction strengths for full-scale field conditions.

A suite of full-scale field liquefaction failure case histories were reviewed, vetted and selected for back-analyses. New methods were developed for performing these back-analyses, including methods that more accurately and reliably deal with momentum and inertia effects in liquefaction failures that experience large displacements. These new methods also appear to provide the first set of tools able to reasonably accurately back-analyze large displacement liquefaction-induced slope failures that develop either (1) monolithically, or (2) incrementally, on a slice by slice basis, retrogressing back towards the eventual back heel. And these new methods also provide increased ability to model changing conditions as slide movements progress from start to finish; which is important in back-analyses of many of the liquefaction failure case histories employed in these types of studies.

A suite of additional empirical relationships were developed specifically for cross-comparison of the results of back-analyses of large displacement liquefaction failures. These provided both a framework and a basis for cross-comparison of results of back-analyses of liquefaction failure case histories; both within this current study and with results from previous studies by others.

In the end, a suite of back-analysis results of unprecedented reliability were developed, based on (1) improved back-analysis procedures, (2) internal cross-checking within the framework of the new empirical relationships developed, and (3) external cross-checking against the results obtained by previous investigations, with an informed understanding of the strengths and drawbacks of the back-analysis methods and assumptions employed in those previous studies.

The resulting hard-earned back-analyzed field case history database was then used, in the context of probabilistic regressions that incorporated the best available evaluations of uncertainties, to perform probabilistic (Bayesian) regressions by the maximum likelihood estimation method, in order to develop new predictive relationships for engineering evaluation of post-liquefaction strength as a function of both (1) corrected SPT penetration resistance, and (2) initial in situ effective vertical stress.

These new empirical relationships were then compared with previous relationships and recommendations. Here, again, with understanding of the strengths and drawbacks of the procedures by which the previous relationships were developed, and of the back-analyses that provided the parameters for those earlier efforts, a coherent overall pattern emerged and the juxtaposition of the different values of post-liquefaction strengths provided by different proposed relationships can now be better understood.

The new predictive relationships developed in these current studies agree reasonably well with the recent recommendations of Wang (2003) and Kramer (2008) who executed a similar overall effort, but with significant differences in approaches, and judgments, at essentially every step of the way. Some elements of their work are poorly documented, and thus difficult to check and verify. And there are a number of errors in their processing of a number of their "secondary" field case histories. These errors tend to bias their predictive relationships in a slightly conservative manner. But with appropriate allowance for this moderate conservative bias, the level of agreement between their findings with the results of these current studies is generally pretty good.

Similarly, the levels of agreement of the current studies with the recommendations of Seed and Harder (1990), Olson and Stark (2002) and Idriss and Boulanger (2008) are also found to be reasonably good, but only over specific ranges of (1) initial in situ effective vertical stress, and (2) corrected SPT penetration resistance. In other ranges, these previous relationships can now be shown to be either conservative, or unconservative, and often to a significant degree. Moreover, the reasons for good agreement over specific ranges, and poorer agreement over other ranges, can now be understood.

The new predictive relationships for engineering evaluation of post-liquefaction strength are presented in a fully probabilistic form, and can be used for fully probabilistic risk studies and design of high-level projects. These are then also "simplified" to develop deterministic recommendations that are likely to be more broadly applicable to more routine projects.

These new relationships offer potentially significant advantages over previously available recommendations and relationships. They are based on back-analyses, and regressions, which provide insight into the underlying forms of the relationships between post-liquefaction strengths and both (1) penetration resistance and (2) effective vertical stress, over the ranges of conditions

well-represented in the 30 full-scale field liquefaction case histories back-analyzed. Because they provide insight as to the underlying forms of these relationships, they provide a better basis for extrapolation to higher ranges of penetration resistance, and to higher ranges of effective stress, than do previous recommendations. The currently available back-analyzed field case history database provides fair to good coverage for values of $N_{1,60,CS}$ up to approximately 15 blows/ft, and for representative effective overburden stresses of up to approximately 4 atmospheres. The range of principal engineering interest, however, is usually $N_{1,60,CS} \approx 10$ to 22 blows/ft as it is over that range that field behavior, and project performance, often transitions from unacceptable to acceptable. Similarly, for major earth and rockfill dams (and their foundations), ranges of effective overburden stress larger than 4 atmospheres are often of engineering importance.

In addition to the development of improved relationships for engineering evaluation of post-liquefactions strengths, the suite of new empirical relationships developed for use in cross-checking of back-analyses of liquefaction failure case histories will likely also have applications with regard to checking of forward engineering calculations and analyses of expected performance of actual engineering projects, including high-level analyses involving fully nonlinear seismic finite element or finite difference analyses for critical and/or high risk projects involving soil liquefaction hazard.

Finally, it should be noted that the relationships developed and presented herein do not fully resolve all issues. As discussed in Section 5.6, the currently available suite of reasonably well characterized large displacement liquefaction failure case histories has limits with regard to the ranges of conditions covered, and also with regard to the overall number of reliable case histories available. The 30 case histories back-analyzed in these current studies reflect failures that have occurred over slightly more than the past century (the earliest failure case history used in these current studies was the 1889 slope failure at Vietepolder, in Zeeland Province, the Netherlands). It must be assumed that suitable failures will continue to occur, further augmenting this liquefaction-induced failure case history database. But it is not possible simply to await further data. Accordingly, it is necessary to make best possible use of the data (and failure case histories) currently available.

It that regard, it is noted that the current suite of case histories include failures induced both by (1) monotonic loading, and (2) by cyclic loading. There are some potentially good arguments that can be made regarding the possibility that cyclic loading might result in greater amounts of void redistribution, and might thus produce lower post-liquefaction strengths than failures induced by monotonic loading; but the current failure case history data base does not provide good support for this.

Similarly, the back-analyses performed in these current studies, and in most previous studies, do not account for the effects of cyclic lurching as contributing to the overall liquefaction-induced displacements observed. A singular exception here is the Upper San Fernando Dam case history, but the treatment of cyclic lurching forces in back-analysis of this case in these current studies is deliberatively conservative given the uncertainties involved. As discussed in Section 5.5, it does not appear likely that cyclic lurching forces would contribute significantly to the displacements observed in most of the liquefaction failure case histories back-analyzed and then used in these current studies to develop the predictive relationships that result. Two main

reasons for this are: (1) nine of the thirty case histories back-analyzed in these current studies were statically (monotonically) triggered failures, and three more were cyclically-induced, but with essentially no significant cyclic lurching forces to drive large displacements, and (2) few of the remaining eighteen cyclically-induced liquefaction failures had strong enough cyclic lurching forces of sufficient duration (enough strong cycles) as to contribute significantly to the observed large displacements. Nonetheless, it is possible that the back-analyses of some of the liquefaction failure case histories may have conservatively underestimated, to some extent, the values of post-liquefaction for a limited number of the case histories due to inability to accurately assess cyclic lurching effects for cases in which statically driven displacements are very large.

A second source of potential conservatism, also discussed in Section 5.5, is the likelihood that the liquefaction-induced failure case histories back-analyzed in these current studies may represent some degree of "self-selection" as cases in which failures occurred, and these may represent some degree of conservatism with regard to enveloping of only "failure" case histories while not also capturing and considering near-failure situations in which similar conditions were present but failures did not occur. This is an issue that cannot be conclusively resolved at present, and the corollary potential for some undetermined degree of conservative bias in forward estimation of expected post-liquefaction strengths must simply be accepted for now.

For these two sets of reasons, it appears likely that the post-liquefaction strength assessment relationships developed and presented herein would likely be potentially biased in a somewhat conservative manner. Such bias appears unavoidable at this juncture, given the available data, and it is noted that (1) some degree of conservatism is to be preferred rather than an expected unconservative bias, and (2) the new relationships presented herein appear to provide for somewhat higher values of post-liquefaction strength (S_r) than do previously available relationships over most ranges of (a) penetration resistance, and (b) initial effective stress.

Overall, the relationships developed and presented herein appear to provide a flexibly adaptable set of tools suitable for engineering evaluation of post-liquefaction strengths on either a fully probabilistic or a more simplified deterministic basis. The underlying forms of the relationships developed are intended to optimize their extrapolation to ranges of higher penetration resistances, and higher effective stress ranges, than are currently represented in the available case history database. Given the lack of current alternatives, it must be expected that these relationships will be extrapolated for use in those ranges.

REFERENCES

Alarcon-Guzman, A., Leonards, G.A., and Chameau, J.L. (1988). “Undrained monotonic and cyclic strength of sands.” Journal of Geotechnical Engineering, ASCE, 114(10), 1089-1109.

Andresen, A. and Bjerrum, L. (1968). “Slides in subaqueous slopes in loose sand and silt.” Norwegian Geotechnical Institute Publication No. 81, 1-9.

Arulanandan, K., Seed, H.B., Yogachandran, C., Muraleetharan, K.K., Seed, R.B., and Kabilamany, K. (1993). “Centrifuge study on volume changes and dynamic stability of earth dams.” Journal of Geotechnical Engineering, ASCE, 119(11), 1717-1731.

Baziar, M.H. and Dobry, R. (1995). “Residual strength and large-deformation potential of loose silty sands.” Journal of Geotechnical Engineering, ASCE, 121(12), 896-906.

Been, K., Conlin, B.H., Crooks, J.H.A., Fitzpatrick, S.W., Jefferies, M.G., Rogers, B.T., & Shinde, S. (1987). “Back analysis of the Nerlerk berm liquefaction slides: Discussion.” Canadian Geotechnical Journal, 24(1), 170-179.

Been, K., Jefferies, M.G., and Hachey, J. (1991). “The critical state of sands.” Geotechnique, Volume 41, Number 3, pp. 365-381.

Bennett, M.J. (1989). “Liquefaction analysis of the 1971 ground failure at the San Fernando Valley Juvenile Hall, California.” Bulletin of Association of Engineering Geologists, 26(2), 209-226.

Bjerrum, L. (1971). “Subaqueous slope failures in Norwegian fjords.” Publication 88, Norwegian Geotechnical Institute, Oslo.

Boulanger, R. W., and Truman, S. P. (1996). "Void redistribution in sand under post-earthquake loading." Canadian Geotechnical Journal, 33, 829-834

Bray, J.D. and Rathje, E.M. (1998). “Earthquake-induced displacements of solid-waste landfills.” Journal of Geotechnical and Geoenvironmental Engineering, ASCE 124(3):242-253.

Bray, J. D., and Travasarou, T. (2007). “Simplified procedure for estimating earthquake-induced deviatoric slope displacements.” Journal of Geotechnical and Geoenvironmental Engineering, ASCE, 133(4), 381-392.

Bryant, S.M., Duncan, J.M., and Seed, H.B. (1983). “Application of tailings dam flow analyses to field conditions.” Report No. UCB/GT/83-03, Dept. of Civil Engineering, Univ. of California, Berkeley, CA.

California Dept. of Water Resources [CDWR] - (1975) “Final Geologic Report on Perris Dam and Lake Part I Foundation Conditions, Grouting, and Instrumentation” Project Geology Report C-94, October 1975

California Dept. of Water Resources [CDWR] - (1998) “Perris Dam Foundation Study, Results of Phase I Geologic Investigations.” Project Geology Section Report No. 58-11-15, May 1998

Casagrande, A. (1940). “Characteristics of cohesionless soils affecting the stability of slopes and earth fills.” Contributions to Soil Mechanics, 1925-1940, Boston Society of Civil Engineers, October, (Originally published in the Journal of the Boston Society of Civil Engineers, January, 1936), 257-276.

Casagrande, A. (1965). “Second Terzaghi Lecture: the role of "calculated risk" in earthwork and foundation engineering.” Journal of the Soil Mechanics and Foundations Division, ASCE, 91(SM4), 1-40.

Casagrande, A. (1976). “Liquefaction and cyclic deformation of sands: a critical review.” Harvard Soil Mechanics Series No. 88, Harvard University Cambridge, MA.

Castro, G. (1969). “Liquefaction of sands.” Ph.D. Thesis, Harvard University, Cambridge, Massachusetts.

Castro, G. (1995). “Empirical methods in liquefaction evaluation.” Proc., First Annual Leonardo Zeevaert International Conference, Vol. 1, 1-41.

Castro, G. and Poulos, S.J. (1977). “Factors affecting liquefaction and cyclic mobility.” Journal of Geotechnical Engineering Division, ASCE, 103(GT6), 501-516.

Castro, G., Poulos, S.J., and Leathers, F.D. (1985). “Re-examination of slide of Lower San Fernando Dam.” Journal of Geotechnical Engineering, ASCE, 111(9), 1093-1106.

Castro, G., Keller, T.O., and Boynton, S.S. (1989). “Re-evaluation of the Lower San Fernando Dam: Report 1, an investigation of the February 9, 1971 slide.” U.S. Army Corps of Engineers Contract Report GL-89-2, Vols. 1 and 2, U.S. Army Corps of Engineers Waterways Experiment Station, Vicksburg, Mississippi.

Castro, G., Seed, R.B., Keller, T.O., and Seed, H.B. (1992). “Steady-state strength analysis of Lower San Fernando Dam slide.” Journal of Geotechnical Engineering, ASCE, 118(3), 406-427.

Cetin, K. O. (2000). "Reliability-Based Assessment of Seismic Soil Liquefaction Initiation Hazard." Dissertation in partial fulfillment for the degree of doctor of philosophy, University of California, Berkeley.

Cetin, K. O., Seed, R. B., Der Kiureghian, A., Tokimatsu, K., Harder Jr, L. F., Kayen, R. E., and Moss, R. E. (2004).” Standard penetration test-based probabilistic and deterministic assessment of seismic soil liquefaction potential.” Journal of Geotechnical and Geoenvironmental Engineering, 130(12), 1314-1340.

Cetin, K. O., Seed, R. B., Kayen, R. E., Moss, R. E., Bilge, H.T., Ilgac, M., and Chowdhury, K. (2018a). "SPT-based probabilistic and deterministic assessment of seismic soil liquefaction triggering hazard." Soil Dynamics and Earthquake Engineering. 115 (2018), 698-709.

Cetin, K. O., Seed, R. B., Kayen, R. E., Moss, R. E., Bilge, H.T., Ilgac, M., and Chowdhury, K. (2018b). "The use of the PST-based seismic soil liquefaction triggering evaluation methodology in engineering hazard assessments." MethodsX (2018), 1556-1557.

Cleary, A.J. (1914). "The Calaveras dam, California, the highest earth dam." Engineering News, 72(14), 692-695.

Davies, M.P., Dawson, B.D., and Chin, B.G. (1998). "Static liquefaction slump mine tailings – a case history." Proceedings 51st Canadian Geotechnical Conference, Vol. 1,123-131.

Davis, A.P. Jr., Poulos, S.J., and Castro, G. (1988). "Strengths backfigured from liquefaction case histories." Proc., 2nd Int. Conf. on Case Histories in Geotechnical Engineering, June 1- 5, St. Louis, MO, 1693-1701.

de Alba, P.A., Seed, H.B., Retamal, E., and Seed, R.B. (1987). "Residual strength of sand from dam failures in the Chilean earthquake of March 3, 1985." Earthquake Engineering Research Center Report No. UCB/EERC-87-11, University of California, Berkeley, CA.

de Alba, P.A., Seed, H.B., Retamal, E., and Seed, R.B. (1988). "Analyses of dam failures in 1985 Chilean earthquake." Journal of Geotechnical Engineering, ASCE, 114(12), 1414-1434.

Deger, T.T. (2014). "Overburden stress normalization and rod length corrections for the standard penetration test (SPT)." Doctoral Dissertation, University of California.

Dennis, N.D. (1988). "Influence of specimen preparation techniques and testing procedures on undrained steady state shear strength." Advanced Triaxial Testing of Soil and Rock, ASTM STP 977, R.T. Donaghe, R.C. Chaney, and M.L. Silver, eds., American Society for Testing and Materials, Philadelphia, 642-654.

Dobry, R. and Alvarez, L. (1967). "Seismic failures of Chilean tailings dams." Journal of the Soil Mechanics and Foundations Division, ASCE, 93(SM6), 237-260.

Duke, C. M., Johnson, K. E., Larson, L.E., and Egman, D.C. (1972). "Effects of Site Classification and Distance on Instrumental Indices in the San Fernando Earthquake." Report, UCLA Eng. 7247, School of Engineering, UCLA.

Ekström, A., & Olofsson, T. (1985). "Water and frost-stability risks for embankments of fine-grained soils." In From Proceedings of the Symposium on Failures in Earthworks, organized by the Institution of Civil Engineers, held in London, March 6-7, 1985.

Engineering News Record (1925). "What happened to municipal utilities at Santa Barbara." Engineering News Record, 95(4), 146-149.

Faris, A. T. (2004). “Probabilistic models for engineering assessment of liquefaction-induced lateral spreading displacements.” Doctoral dissertation, University of California, Berkeley.

Fear, C.E. and Robertson, P.K. (1995). “Estimating the undrained strength of sand: a theoretical framework.” Canadian Geotechnical Journal, 32(4), 859-870.

Fiegel, G.F. and Kutter, B.L. (1994). “Liquefaction induced lateral spreading of mildly sloping ground.” Journal of Geotechnical Engineering, ASCE, 120(12), 2236-2243.

Gelman, A., and Hill, J. (2007). Data analysis using regression and multilevel/hierarchical models. Cambridge University Press, New York, 648 pp.

GEOSLOPE International Ltd. (2021). GeoStudio 2021.4.

Gilboy, G. (1942). Discussion of “Fort Peck slide.” by T.A. Middlebrooks, Transactions of the American Society of Civil Engineers, 107, 723-764.

Gillette, D.R. (2010). “On the use of empirical correlations for estimating the residual undrained shear strength of liquefied soil in dam foundations.” Fifth International Conference on Recent Advances in Geotechnical Earthquake Engineering and Soil Dynamics, San Diego, California, May.

Gu, W.H., Morgenstern, N.R., and Robertson, P.K. (1993). “Progressive failure of Lower San Fernando Dam.” Journal of Geotechnical Engineering, ASCE, 119(2), 333-349.

GZA GeoEnvironmental, Inc. (1991). “Wachusett Dam – Clinton, Massachusetts – North Dike Stability.” Stage I Report, Volume II, Report to the Commonwealth of Massachusetts, Metropolitan District Commission, Boston, Massachusetts.

Haley & Aldrich, Inc. (1984a). “Report on Phase II Investigation, Wachusett Reservoir Dam, Clinton, Massachusetts.” Prepared for the Commonwealth of Massachusetts, Metropolitan District Commission, Boston, Massachusetts, February.

Haley & Aldrich, Inc. (1984b). “Report on Phase II Investigation, Wachusett Reservoir, North Dike, South Dike, Clinton, Massachusetts.” Prepared for the Commonwealth of Massachusetts, Metropolitan District Commission, Boston, Massachusetts, February.

Harder, L. F. Jr. (1988). “Use of Penetration Tests to Determine the Cyclic Loading Resistance of Gravelly Soils During Earthquake Shaking.” Ph.D. Thesis, University of California, Berkeley.

Hazen, A. (1918). “A study of the slip in the Calaveras Dam.” Engineering News-Record, 81(26), 1158-1164.

Hazen, A. (1920). “Hydraulic-fill dams.” Transactions of the American Society of Civil Engineers, Paper No. 1458, 1713-1821 (including discussions).

Hazen, A. and Metcalf, L. (1918). “Middle section of upstream side of Calaveras dam slips into reservoir.” Engineering News-Record, 80(14), 679-681.

Holtz, W.G. and Gibbs, H.J. (1979). Discussion of “SPT and relative density in coarse sand.” Journal of the Geotechnical Engineering Division, ASCE, 105(GT3), 439-441.

Hryciw, R.D., Vitton, S., and Thomann, T.G. (1990). “Liquefaction and flow failure during seismic exploration.” Journal of Geotechnical Engineering, ASCE, 116(12), 1881-1899.

Hynes-Griffin, M.E., Franklin, A.G. (1984). “Rationalizing the seismic coefficient method.” Misc. Paper No. GL-84-13, U.S. Army Engr. WES, Vicksburg, MS

Idriss, I. M. (1998). “Evaluation of liquefaction potential, consequences and mitigation—An update.” Presentation Notes, Vancouver Geotechnical Society Meeting, Vancouver, Canada.

Idriss, I.M. and Boulanger, R.W. (2008). “Soil liquefaction during earthquakes.” EERI Monograph 12, Earthquake Engineering Research Institute, Oakland, California, 262 p.

Inada (1982). “Methods of in situ soil investigations.” Japanese Society of Soil Mechanics and Foundation Engineering, 217 p.

Ishihara, K. (1984). “Post-earthquake failure of a tailings dam due to liquefaction of the pond deposit.” Proc., Inter. Conf. on Case Histories in Geotechnical Engineering, Rolla, Missouri, May 6-11, Vol. 3, 1129-1143.

Ishihara, K. (1985). “Stability of natural deposits during earthquakes.” Proc., 11th International Conference on Soil Mechanics and Foundation Engineering, San Francisco, CA, Vol. 1, 321-376.

Ishihara, K. (1993). “Liquefaction and flow failure during earthquakes.” Geotechnique, 43(3), 351-415.

Ishihara, K., Yasuda, S., and Yoshida, Y. (1990). “Liquefaction-induced flow failure of embankments and residual strength of silty sands.” Soils and Foundations, 30(3), 69-80.

Ishihara, K., Okusa, S., Oyagi, N., and Ischuk, A. (1990). “Liquefaction-induced flow slide in the collapsible loess deposit in Soviet Tajik.” Soils and Foundations, 30(4), 73-89.

Iverson, R.M. and LaHusen, R.G. (1993). “Friction in debris flows: inferences from largescale flume experiments.” Proc., Hydraulic Engineering ’93, 1993 Conf. of the Hydraulics Division of the American Society of Civil Engineers, Vol. 2, 1604-1609.

Iverson, R.M., Reid, M.E., and LaHusen, R.G. (1997). “Debris-flow mobilization from landslides.” Annual Review of Earth Planetary Science, 25, 85-138.

Jefferies, M.G., Been, K., and Hachey, J.E. (1990). “Influence of scale on the constitutive behavior of sand.” Proceedings of the 43rd Canadian Geotechnical Engineering Conference, Laval University, Quebec, Vol. 1, p. 263-273.

Jefferies, M., & Been, K. (2006). “Soil liquefaction: a critical state approach.” CRC Press.

Jibson, R.W., Harp E.L., and Michael, J.A. (1998). “A method for producing digital probabilistic seismic landslide hazard maps: an example from the Los Angeles, California, Area.” USGS Open-File Report, 98–113.

Jitno, H. (1995). “Liquefaction induced deformation of earth structures.” Ph.D. Thesis, Civil Engineering Dept., Univ. of British Columbia, Vancouver, B.C.

Jitno, H. and Byrne, P.M. (1995). “Predicted and observed liquefaction response of Mochikoshi tailings dam.” Proc., 1st International Conf. on Earthquake Geotechnical Engineering, Nov. 14-16, Tokyo, Japan, Vol. 2, 1085-1090.

Kawasumi, H. (1968). “General report on the Niigata Earthquake of 1964.” Tokyo Electrical Engineering College Press, Tokyo, Japan.

Kokusho, T. (1999). “Water film in liquefied sand and its effect on lateral spread.” Journal of Geotechnical and Geoenvironmental Engineering, 125(10), 817-826.

Konrad, J.M. (1991). “The Nerlerk berm case history: some consideration for the design of hydraulic sand fills.” Canadian Geotechnical Journal, 28, 601-612.

Konrad, J.M. and Watts, B.D. (1995). “Undrained shear strength for liquefaction flow failure analysis.” Canadian Geotechnical Journal, 32, 783-794.

Koppejan, A.W., van Wamelen, B.M., and Weinberg, L.J.H. (1948). “Coastal flow slides in the Dutch province of Zeeland.” Proc., 2nd International Conf. Of Soil Mechanics and Foundation Engineering, Rotterdam, Netherlands, June 21-30, 89-96.

Kramer, S. L. (2008). “Evaluation of liquefaction hazards in Washington State (Rept. No. WA-RD 668.1).” Washington State Department of Transportation, Office of Research and Library Services.

Kramer, S.L. (2015). Personal communication, August 7, 2015.

Kramer, S.L. and Wang, C.H. (2015). “Empirical Model for Estimation of the Residual Strength of Liquefied Soil.” Journal of Geotechnical and Geoenvironmental Engineering, ASCE, 04015038(15).

Kulasingam, R., Malvick, E. J., Boulanger, R. W., and Kutter, B. L. (2004). "Strength loss and localization at silt interlayers in slopes of liquefied sand." Journal of Geotechnical and Geoenvironmental Engineering, ASCE, 130(11), 1192-1202.

Kulhawy, F.H. and Mayne, P.W. (1990). “Manual on estimating soil properties for foundation design.” Electric Power Research Institute EL-6800, Project 1493-6, August, 400 pp.

Kulhawy, F.H. and Mayne, P.W. (1991). “Relative density, SPT, and CPT interrelationships.” 1st International Symposium on Calibration Chamber Testing, June 28-29, Potsdam, New York, 197-211.

Lade, P.V. (1993). “Initiation of static instability in the submarine Nerlerk berm.” Canadian Geotechnical Journal, 30, 895-904.

Lee, K.L., Seed, H.B., Idriss, I.M., and Makdisi, F.I. (1975). “Properties of soil in the San Fernando hydraulic fill dams.” Journal of the Geotechnical Engineering Division, ASCE, 101(GT8), 801-821.

Lewis, M.R., Arango, I., McHood, M.D. (2009). “Site characterization philosophy and liquefaction evaluation of aged sands.” Bechtel Technology Journal, Bechtel Corporation, Vol. 2, No. 1.

Liao, S.C., and Whitman, R.V. (1986). “Overburden correction factors for SPT in sand.” Journal of Geotechnical Engineering, ASCE, 112(3), 373-377.

Ligtenberg-Mak, C.E., Krajicek, P.V.F.S., and Kuiter, C. (1990). “Geological study of flow slide sensitive sediments.” Proc., 6th International Congress, International Association of Engineering Geology, Amsterdam, Vol. 1, 691-695.

Liu, H., & Qiao, T. (1984). “Liquefaction potential of saturated sand deposits underlying foundation of structure.” In Proceedings of the 8th World Conference on Earthquake Engineering, San Francisco, Calif., 21-28.

Lucia, P.C. (1981). “Review of experiences with flow failures of tailings dams and waste impoundments.” Ph.D. Thesis, University of California, Berkeley, Calif.

Makdisi, F. I., and Seed, H. B. (1978). “Simplified procedure for estimating dam and embankment earthquake-induced deformations.” Journal of the Geotechnical Engineering Division, ASCE, 104(7), 849-867.

Malvick, E. J., Kutter, B. .L., Boulanger, R. W., & Kulasingam, R. (2006). “Shear localization due to liquefaction-induced void redistribution in a layered infinite slope.” Journal of Geotechnical and Geoenvironmental Engineering, ASCE, 132(10), 1293–1303.

Marcuson, W.F., III. (1979). “Visit to Japan to observe damage which occurred during the Near Izu Oshima earthquakes January 14 and 15, 1978.” Miscellaneous Paper GL-79-20, U.S. Army Corps of Engineers Waterways Experiment Station, Vicksburg, MS.

Marcuson, W.F., III, and Krinitzsky, E.L. (1976). “Dynamic analysis of Fort Peck dam.” Technical Report S-76-1, U.S. Army Engineer Waterways Experiment Station, Vicksburg, MS, March.

Marcuson, W.F., III, Ballard, R.F., Jr., and Cooper, S.S. (1978). “Comparison of penetration resistance values to in situ shear wave velocities.” Proc., 2nd International Conf. on Microzonation for Safer Construction – Research and Application, San Francisco, CA Nov., 26 – Dec. 1, Vol. 2, 1013-1023.

Marcuson, W.F., III, Ballard, R.F., Jr., and Ledbetter, R.H. (1979). “Liquefaction failure of tailings dams resulting from the Near Izu Oshima earthquake, 14 and 15 January, 1978.” Proc. 6th Pan-American Conf. on Soil Mechanics and Foundation Engineering, Lima Peru, Vol. 2, 69-80.

McRoberts, E.C. and Sladen, J.A. (1992). “Observations on static and cyclic sand liquefaction methodologies.” Canadian Geotechnical Journal, 29, 650-665.

Mesri, G., Feng, T.W., and Benak, J.M. (1990). “Post densification penetration resistance of clean sands.” Journal of Geotechnical Engineering, ASCE, 116(7), 1095-1115.

Meyerhof, G.G. (1957). “Discussion on sand density by spoon penetration.” Proc., 4th Intl. Conf. on Soil Mechanics and Foundation Engineering, Vol. 3, 110.

Meyerhof, G.G. (1957). Discussion of “Research on determining the density of sands by spoon penetration testing.” by H.J. Gibbs and W.G. Holtz, Proc., International Conf. on Soil Mechanics and Foundation Engineering, Vol. 3, 110.

Meyerhof, G.G. (1971). “The mechanism of flow slides in cohesive soils.” Geotechnique, 1, 41-49.

Middlebrooks, T.A. (1942). “Fort Peck slide.” Transactions of the American Society of Civil Engineers, 107, 723-764.

Mishima, S. and Kimura, H. (1970). “Characteristics of landslides and embankment failures during the Tokachioki earthquake.” Soils and Foundations, 10(2), 39-51.

Mitchell, D.E. (1984). “Liquefaction slides in hydraulically placed sands.” Proc., 4th International Symposium on Landslides, Toronto, Ontario, Vol. 1, 141-146.

Mittal, H.K. and Hardy, R.M. (1977). “Geotechnical aspects of a tar sand tailings dyke.” Proc., Conference on Geotechnical Practice for Disposal of Solid Waste Materials, ASCE Specialty Conference of the Geotechnical Engineering Division, Vol. 1, 327-347.

Miura, K., Yoshida, N., and Wakamatsu, K. (1995). “Damage to fill embankment during the 1993 Kushiro-oki earthquake.” Proc., 1st International Conf. on Earthquake Geotechnical Engineering, Nov. 14-16, Tokyo, Japan, Vol. 2, 1057-1062.

Miura, K., Yoshida, N., Nishimura, M., and Wakamatsu, K. (1998). “Stability analysis of the fill embankment damaged by recent two major earthquakes in Hokkaido, Japan.” Proc., 1998 Geotechnical Earthquake Engineering and Soil Dynamics Specialty Conference, ASCE Geo-Institute Geotechnical Special Publication No. 75, Vol. 2, August 3-6, Seattle, Washington, 926-937.

Morgano, C.M. and Laing, R. (1992). “Energy Transfer in SPT-Rod Length Effect.” Proc., 4th Int. Conference on the Application of Stress-Wave Theory to Piles, The Hague, The Neatherlands, A.A. Balkema Publishers, pp. 1211-127.

Mori, S. (1993). “Reconnaissance report on the liquefaction aspects of the Kushiro-oki earthquake, January 15, 1993.” Proc., 28th Japan National Conf. on Soil Mechanics and Foundation Engineering, 1091-1094.

Morrill, B.J. (1972). “Seismoscope Results – San Fernando Earthquake of 9 February 1971.” Chapter 3 of California Institute of Technology Report EERL, 72-02, 72-124.

Moss, R. E. S. (2009). “Reduced Uncertainty of Ground Motion Prediction Equations through Bayesian Variance Analysis.” PEER Report No. 2009/105, November.

Moss, R. E. S. (2011). “Reduced Sigma of Ground Motion Prediction Equations through Uncertainty Propagation.” Bulletin of Seismological Society of America, 101(1).

National Research Council (1985). “Liquefaction of soils during earthquakes.” Report No. CETS-EE-001, Committee on Earthquake Engineering, National Academy Press, Washington, D.C.

Newmark, N. (1965). “Effects of earthquakes on dams and embankments.” Geotechnique, 15(2), 139-160.

Norris, G., Siddharthan, R., Zafir, Z., and Madhu, R. (1997). “Liquefaction and residual strength of sands from drained triaxial tests.” Journal of Geotechnical and Geoenvironmental Engineering, ASCE, 123(3), 220-228.

Nunn, H. (1925). “Municipal problems of Santa Barbara.” Bulletin, Seismological Society of America, 15(4), 308-319.

Ohya, S., Iwasaki, T., and Wakamatsu, M. (1985). “Comparative study of various penetration tests in ground that underwent liquefaction during the 1983 Nihon-Kai-Chubu and 1964 Niigata earthquakes.” Proc., Workshop on In-Situ Testing Methods for Evaluation of Soil Liquefaction Susceptibility, San Francisco, California, Vol. 1, 56-88.

Okusa, S. and Anma, S. (1980). “Slope failures and tailings dam damage in the 1978 Izu-Ohshima-Kinkai earthquake.” Engineering Geology, 16, 195-224.

Okusa, S., Anma, S., and Maikuma, H. (1980). “Liquefaction of mine tailings in the 1978 Izu-Ohshima-Kinkai earthquake, central Japan.” Proc., 7th World Conf. on Earthquake Engineering, Sept. 8-13, Istanbul, Turkey, Vol. 3, 89-96.

Okusa, S., Anma, S., and Maikuma, M. (1984). “The propagation of liquefaction pressure and delayed failure of a tailings dam dike in the 1978 Izu-Oshima-Kinkai earthquake.” Proc., 8th World Conf. on Earthquake Engineering, July 21-28, San Francisco, CA, Vol. 1, 389-396.

Olivia Chen Consultants, Inc. (2003). “Report on the Seismic Stability of Calaveras Dam”, report prepared for the San Francisco Public Utilities Commission, Utilities Engineering Bureau.

Olson, S.M. (2001). “Liquefaction analysis of level and sloping ground using field case histories and penetration resistance.” Ph.D. thesis, University of Illinois at Urbana-Champaign, Urbana, Illinois.

Olson, S.M. and Johnson, C.I. (2008). “Analyzing liquefaction-induced lateral spreads using strength ratios.” Journal of Geotechnical and Geoenvironmental Engineering, ASCE, 134(8), 1035-1049.

Olson, S.M., Stark, T.D., Walton, W.H., and Castro, G. (2000). “Static liquefaction flow failure of the North Dike of Wachusett Dam.” Journal of Geotechnical and Geoenvironmental Engineering, ASCE, 126(12), 1184-1193.

Olson, S.M. and Stark, T.D. (2001). “Liquefaction analysis of Lower San Fernando Dam using strength ratios." Paper No. 4.05, Proc., 4th International Conf. on Recent Advances in Geotechnical Earthquake Engineering and Soil Dynamics, March 26-31, San Diego, CA.

Olson, S.M. and Stark, T.D. (2002). “Liquefied strength ratio from liquefaction flow failure case histories,” Canadian Geotechnical Journal, 39(5), 629-647.

Pillai, V.S. and Salgado, F.M. (1994). “Post-liquefaction stability and deformation analysis of Duncan Dam.” Candian Geotechnical Journal, 31, 967-978.

Plewes, H.D., O’Neil, G.D., McRoberts, E.C., and Chan, W.K. (1989), “Liquefaction considerations for Suncor tailings pond.” Proc., Dam Safety Seminar, Edmonton, Alberta, Sept., Vol 1, 61-89.

Popescu, R., Prevost, J.H., and Deodatis, G. (1997). “Effects of spatial variability on soil liquefaction: some design recommendations.” Geotechnique, 47(5), 1019-1036.

Poulos, S.J. (1981). “The steady state of deformation.” Journal of Geotechnical Engineering Division, ASCE, 17(GT5), 553-562.

Poulos, S.J. (1988). “Liquefaction and related phenomena.” in Advanced Dam Engineering for Design, Construction, and Rehabilitation, R.B. Jansen, ed., Van Nostrand Reinhold, New York, 292-320.

Poulos, S.J., Castro, G., and France, W. (1985). “Liquefaction evaluation procedure.” Journal of Geotechnical Engineering, ASCE, 111(6), 772-792.

Poulos, S.J., Robinsky, E.I., and Keller, T.O. (1985). “Liquefaction resistance of thickened tailings.” Journal of Geotechnical Engineering, ASCE, 111(12), 1380-1394.

Poulos, S.J. Castro, G., and France, W. (1988). Closure to discussion of “Liquefaction evaluation procedure.” Journal of Geotechnical Engineering, ASCE, 114(2), 251-259.

Riemer, M.F. and Seed, R.B. (1992). “Observed effects of testing conditions on the residual strength of loose, saturated sands at large strains.” Proc., 4th Japan-U.S. Workshop on Earthquake Resistant Design of Lifeline Facilities and Countermeasures for Soil Liquefaction, Tech. Rpt. No. NCEER-92-0019, M. Hamada and T.D. O’Rourke, eds., Vol. 1, 223-237.

Riemer, M.F. and Seed, R.B. (1997). “Factors affecting apparent position of steady-state line. Journal of Geotechnical and Geoenvironmental Engineering, ASCE, 123(3), 281-288.

Robertson, P.K. (2010). “Evaluation of flow liquefaction and liquefied strength using cone penetration test.” Journal of Geotechnical and Geoenvironmental Engineering, ASCE, 136(6), 842-853.

Robertson, P.K. (2014). Personal communication.

Robertson, P.K. and Campanella, R.G. (1983). “Interpretation of cone penetration tests. Part I: sand.” Canadian Geotechnical Journal, 20(4), 718-733.

Robertson, P.K., and Wride (Fear), C.E. (1998). “Evaluating cyclic liquefaction potential using the cone penetrometer test.” Canadian Geotechnical Journal, 35(3), 442-459.

Rogers, B.T., Been, K., Hardy, M.D., Johnson, G.J., and Hachey, J.E. (1990). “Re-analysis of Nerlerk B-67 berm failures.” Proc., 43rd Canadian Geotechnical Conf. - Prediction of Performance in Geotechnique, Quebec, Canada, Vol. 1, 227-237.

Ross, G.A. (1968). “Case studies of soil stability problems resulting from earthquakes.” Ph.D. Thesis, University of California, Berkeley, Calif.

Saito, K. and Ine, N. (1993). Private communication to K. Miura, reported in Miura et al. (1998).

Sasaki, Y., Oshiki, H., and Nishikawa, J. (1994). “Embankment failure caused by the Kushiro-Oki earthquake of January 15, 1993.” Proc., 13th International Conf. on Soil Mechanics and Foundation Engineering, New Delhi, India, Vol. 1, 61-68.

Sasaki, Y., Tamura, K., Yamamoto, M., and Ohbayashi, J. (1995). “Soil improvement work for river embankment damaged by the 1993 Kushiro-Oki earthquake.” Proc., Earthquake Geotechnical Engineering, Nov. 14-16, Tokyo, Japan, Vol. 1, 43-48.

Schmertmann, J.H. (1987). Discussion of "Time-dependent strength in freshly deposited or densified sand." by J.K. Mitchell and Z.V. Solymar, Journal of Geotechnical Engineering, ASCE, 113(2), 173-175.

Schmidt, J., and Moss, R. (2021). "Bayesian hierarchical and measurement uncertainty model building for liquefaction triggering assessment." Computers and Geotechnics, Volume 132, 103963.

Schofield, A.N. and Wroth, C.P. (1968). Critical State Soil Mechanics. McGraw-Hill, London.

Scott, R. F. (1972). "The calculation of horizontal accelerations from seismoscope records." Paper presented at a Seismological Society of America Conference in Hawaii.

Seed, H.B. and Lee, K.L. (1966). "Liquefaction of saturated sands during cyclic loading." Journal of the Soil Mechanics and Foundations Division, ASCE, SM6(11), 105-134.

Seed, H. B. and Martin, G. R. (1966). "The seismic coefficient in earth dam design." Journal of the Soil Mechanics and Foundations Division, 92(3), 25-58.

Seed, H.B. (1968). "Landslides during earthquakes due to soil liquefaction." Journal of the Soil Mechanics and Foundation Division, ASCE, 94(SM5), 1055-1122.

Seed, H.B. and Idriss, I.M. (1971). "Simplified procedure for evaluating soil liquefaction potential." Journal of the Soil Mechanics and Foundation Division, ASCE, 97(SM9), 1249-1273.

Seed, H.B., Lee, K.L., and Idriss, I.M. (1969). "Analysis of Sheffield Dam failure." Journal of the Soil Mechanics and Foundations Division, ASCE, 95(SM6), 1453-1490.

Seed, H.B., Lee, K.L., Idriss, I.M., and Makdisi, F. (1973). "Analysis of the slides in the San Fernando Dams during the earthquake of Feb. 9, 1971." Earthquake Engineering Research Center 73-2, University of California, Berkeley, Calif.

Seed, H.B., Lee, K.L., Idriss, I.M., and Makdisi, F. (1975). "Dynamic analysis of the slide in the Lower San Fernando Dam during the earthquake of February 9, 1971." Journal of the Geotechnical Engineering Division, ASCE, 101(GT9), 889-911.

Seed, H.B. (1979). "Considerations in the earthquake-resistant design of earth and rockfill dams." Geotechnique, 29(3), 215-263.

Seed, H.B., Tokimatsu, K., Harder, L.F., and Chung, R. (1984). "The influence of SPT procedures on soil liquefaction resistance evaluations." Report No. UCB/EERC-84/15, Earthquake Engineering Research Center, Univ. of California, Berkeley, CA, October.

Seed, H.B., Tokimatsu, K., Harder, L.F., and Chung, R. (1985). "Influence of SPT procedures in soil liquefaction resistance evaluations." Journal of Geotechnical Engineering Division, ASCE, 111(12), 861-878.

Seed, H.B. (1987). “Design problems in soil liquefaction.” Journal of Geotechnical Engineering Division, ASCE, 113(8), 827-845.

Seed, H.B., Seed, R.B., Harder, L.F., and Jong, H.-L. (1988). “Re-evaluation of the slide in the Lower San Fernando Dam in the earthquake of Feb. 9, 1971.” Report No. UCB/EERC-88/04, Earthquake Engineering Research Center, Univ. of California, Berkeley, CA, April.

Seed, H.B., Seed, R.B., Harder, L.F., and Jong, H.-L. (1989). “Re-evaluation of the Lower San Fernando Dam: Report 2, examination of the post-earthquake slide of February 9, 1971.” U.S. Army Corps of Engineers Contract Report GL-89-2, U.S. Army Corps of Engineers Waterways Experiment Station, Vicksburg, Mississippi.

Seed, R.B. and Harder, L.F. Jr. (1990). “SPT-based analysis of cyclic pore pressure generation and undrained residual strength.” Proc. H. Bolton Seed Memorial Symposium, Bi-Tech Publishing Ltd., Vol. 2, 351-376.

Seed, R. B., Cetin, K. O., Moss, R. E., Kammerer, A. M., Wu, J., Pestana, J. M., Reimer, M.F., Sancio, R. B., Bray, J.D., Kayen, R.E., and Faris, A. (2003). “Recent advances in soil liquefaction engineering: a unified and consistent framework.” In Proceedings of the 26th Annual ASCE Los Angeles Geotechnical Spring Seminar: Long Beach, CA.

Silvis, F. and de Groot, M.B. (1995). “Flow slides in the Netherlands: experience and engineering practice.” Canadian Geotechnical Journal, 32, 1086-1092.

Skempton, A.W. (1986). “Standard penetration test procedures and the effects in sand of overburden pressure, relative density, particle size, ageing, and overconsolidation.” Geotechnique, 36, 425-447.

Sladen, J.A., D'Hollander, R.D., and Krahn, J. (1985). “The liquefaction of sands, a collapse surface approach.” Canadian Geotechnical Journal, 22, 564-578.

Sladen, J.A., D'Hollander, R.D., Krahn, J., and Mitchell, D.E. (1985). “Back analysis of the Nerlerk berm liquefaction slides.” Canadian Geotechnical Journal, 22, 579-588.

Sladen, J.A., D'Hollander, R.D., Krahn, J., and Mitchell, D.E. (1987). “Back analysis of the Nerlerk berm liquefaction slides: Reply.” Canadian Geotechnical Journal, 24, 179-185.

Sladen, J.A. and Hewitt, K.J. (1989). “Influence of placement method on the in situ density of hydraulic sand fills.” Canadian Geotechnical Journal, 26, 453-466.

Spencer, E. (1967). “A method of analysis of the stability of embankments assuming parallel inter-slice forces.” Geotechnique, 17(1), 11-26.

Stark, T.D. and Mesri, G. (1992). “Undrained shear strength of liquefied sands for stability analysis.” Journal of Geotechnical Engineering, ASCE, 118(11), 1727-1747.

Stark, T.D., Olson, S.M., Kramer, S.L., and Youd, T.L. (1998). “Shear strength of liquefied soils.” Proc., Workshop on Post-Liquefaction Shear Strength of Granular Soils, April 17-18, 1997, University of Illinois at Urbana-Champaign, Urbana, Illinois, 288 p.

Sully, J.P., Fernandez, A., and Zalzman, S. (1995). “Backanalysis of deformations for case histories involving flow-type failures.” Proc., 3rd International Conf. on Recent Advances in Geotechnical Earthquake Engineering and Soil Dynamics, April 2-7, St. Louis, MO, Vol. 1, 499-502.

Terzaghi, K., Peck, R.B., and Mesri, G. (1996). Soil Mechanics in Engineering Practice, Third Edition. John Wiley & Sons, Inc., New York, 549 pp.

Tokimatsu, K. and Seed, H.B. (1987). “Evaluation of settlements in sands due to earthquake shaking.” Journal of Geotechnical Engineering, ASCE, 113(8), 861-878.

U.S. Army Corps of Engineers. (1939). “Report on the slide of a portion of the upstream face of the Fort Peck Dam, Fort Peck, Montana.” United States Government Printing Office, Washington, D.C.

U.S. Army Corps of Engineers. (1949). “Report on investigation of failure of Sheffield Dam, Santa Barbara, California.” Office of the District Engineer, Los Angeles, California, June.

Vaid, Y.P. and Chern, J.C. (1985). “Cyclic and monotonic undrained response of saturated sands.” in Advances in the Art of Testing Soils under Cyclic Conditions, V.Khosla, ed., ASCE, New York, 120-147.

Vaid, Y.P., Chung, E.F.K., and Kuerbis, R.H. (1990). “Stress path and steady state,” Canadian Geotechnical Journal, 27(1), 1-7.

Vaid, Y.P. and Thomas, J. (1995). “Liquefaction and post-liquefaction behavior of sand.” Journal of Geotechnical Engineering, ASCE, 121(2), 163-173.

Vaid, Y.P., Sivathayalam, S., and Stedman, D. (1999). “Influence of specimen reconstituting method on the undrained response of sand,” Geotechnical Testing Journal, ASTM, 22(3), 187-195.

Valiquette, M., Robinson, B., and Borden, R.H. (2010). “Energy Efficiency and Rod Length Effects in Standard Penetration Test Hammers.” Journal of the Transportation Research Board, No. 2186, pp. 47-56.

Vasquez-Herrera, A. and Dobry, R. (1989). “Re-evaluation of the Lower San Fernando Dam: Report 3, the behavior of undrained contractive sand and its effect on seismic liquefaction flow failures of earth structures.” U.S. Army Corps of Engineers Contract Report GL-89-2, U.S. Army Corps of Engineers Waterways Experiment Station, Vicksburg, Mississippi.

Verdugo, R. (1992). “Characterization of sandy soil behavior under large deformation.” Ph.D. Thesis, Dept. of Civil Engineering, University of Tokyo, Japan.

Verdugo, R. and Ishihara, K. (1996): "The steady state of sandy soils," Soils and Foundations, Vol. 36, No. 2, pp. 81-92.

Von Thun, J. L. (1986). “Analysis of dynamic compaction foundation treatment requirements, Stage 1, Jackson Lake Dam.” Technical memorandum No. TM-JL-230-26, Bureau of Reclamation, Engineering and Research Center, Division of Dam and Waterway Design, Embankment Dams Branch.

Wang, C. (2003). “Prediction of the residual strength of liquefied soils.” Ph.D. Dissertation, University of Washington.

Willis, B. (1925). “A study of the Santa Barbara earthquake of June 29, 1925.” Bulletin, Seismological Society of America, 15(4), 255-278.

Wride (Fear), C.E. (1996). “In situ testing for liquefaction evaluation of sandy soils.” Ph.D. Thesis, University of Alberta, Edmonton, Alberta.

Wride (Fear), C.E., McRoberts, E.C., and Robertson, P.K. (1999). “Reconsideration of case histories for estimating undrained shear strength in sandy soils.” Canadian Geotechnical Journal, 36, 907-933.

Wu, J. (2003). "Liquefaction Triggering and Post Liquefaction Deformations of Monterey 0/30 Sand Under Uni-Directional Cyclic Simple Shear Loading." Dissertation in partial fulfillment for the degree of doctor of philosophy, University of California, Berkeley.

Yamada, G. (1966). “Damage to earth structures and foundations by the Niigata earthquake June 16, 1964, in JNR.” Soils and Foundations, 6(1), 1-13.

Yamauro, J.A. and Convert, K. M. (2001). “Monotonic and cyclic liquefaction of very loose sands with high silt content.” Journal of Geotechnical and Geoenvironmental Engineering, ASCE, 127(4), 314-324.

Yashima, A., Oka, F., Konrad, J.M., Uzuoka, R., and Taguchi, Y. (1997). “Analysis of a progressive flow failure in an embankment of compacted till.” Proc., Deformation and Progressive Failure in Geomechanics, Vol. 1, 599-604.

Yasuda, S. et al. (1993). “Mechanical properties of soil where ground failure occurred during the Kushiro-oki earthquake.” Proc., 22nd JSCE Earthquake Engineering Symposium, 395-398.

Yegian, M.K., Ghahraman, V.G., and Harutinunyan, R.N. (1994). “Liquefaction and embankment failure case histories, 1988 Armenia earthquake.” Journal of Geotechnical Engineering, ASCE, 120(3), 581-596.

Yoshimine, M. and Ishihara, K. (1998). “Flow potential of sand during liquefaction.” Soils and Foundations, 38(3), 189-198.

Yoshimine, M., Robertson, P.K., and Wride (Fear), C.E. (1999). “Undrained shear strength of clean sands to trigger flow liquefaction.” Canadian Geotechnical Journal, 36(5), 891-906.

Yoshimine, M., Robertson, P.K. and Wride, C.E. (2001). “Undrained shear strength of clean sands to trigger flow liquefaction: Reply to discussion.” Canadian Geotechnical Journal, 38(3), 654-657.

Youd, T.L. (1995). “Liquefaction-induced lateral ground displacement.” Proc., 3rd International Conf. on Recent Advances in Geotechnical Earthquake Engineering and Soil Dynamics, April 2-7, St. Louis, MO, Vol. 2, 911-925.

Youd, T.L. and I.M. Idriss (1997). “Summary report.” Proc., NCEER Workshop on Evaluation of Liquefaction Resistance of Soils, NCEER-97-0022, 1-40.

Youd, T.L., I. M. Idriss, Ronald D. Andrus, Ignacio Arango, Gonzalo Castro, John T. Christian, Richardo Dobry, W. D. Liam Finn, Leslie F. Harder Jr., Mary Ellen Hynes, Kenji Ishihara, Joseph P. Koester, Sam S. C. Liao, William F. Marcuson III, Geoffrey R. Martin, James K. Mitchell, Yoshiharu Moriwaki, Maurice S. Power, Peter K. Robertson, Raymond B. Seed, and Kenneth H. Stokoe II. (2001). “Liquefaction Resistance of Soils: Summary Report from the 1996 NCEER and 1998 NCEER/NSF Workshops on Evaluation of Liquefaction Resistance of Soils.” Journal of Geotechnical and Geoenvironmental Engineering, ASCE, 124(10), pp. 817-833.

Youd, T. L., Hansen, C. M., and Bartlett, S. F. (2002). “Revised Multilinear Regression Equations for Prediction of Lateral Spread Displacement”, Journal of Geotechnical and Geoenvironmental Engineering, Vol. 128, No. 12, pp. 1007-1017.